Dynamo Action due to Turbulence in a Linear Shear Flow

A Thesis

Submitted For the Degree of

Doctor of Philosophy

in the Faculty of Science

by

Nishant Kumar Singh

Under the Supervision of

Prof. S. Sridhar
Raman Research Institute

Astronomy And Astrophysics
Indian Institute of Science
BANGALORE – 560 012

October 2012

Declaration

I hereby declare that the work presented in this thesis is entirely original and has been carried out by me at the Raman Research Institute under the auspices of the Joint Astronomy Programme of the Department of Physics, Indian Institute of Science. I further declare that this has not formed the basis for the award of any degree, diploma, membership, associateship or similar title of any University or Institution.

Department of Physics
Indian Institute of Science
Bangalore, 560012
INDIA

Nishant Kumar Singh
Date

Acknowledgements

It is a pleasure to thank many people who extended their support, in various forms, during my Ph.D. on the dynamo theory. I wish to thank few people in particular, although I realize that the list is inexhaustible.

Thanking my supervisor, Sridhar, appears more difficult to me than the problems studied in the thesis. I learnt a lot from him, particularly, most of the Physics I know, difficult issues related to dynamos & fluids, and more importantly, the attitude to pursue a problem. He has always been available for discussions and offered all the necessary support. I am grateful to him for his faith in me which helped me in getting more confidence to continue worrying about various topics we've discussed.

I thank Axel Brandenburg who completely supported my visit to NORDITA, taught me how to run numerical simulations by introducing me to the pencil code, provided me an encouraging atmosphere where I could work peacefully and put me in touch with many other interesting people from whom I learnt a lot. I am grateful to Axel for all his support and encouragements which he continued all along my Ph.D. It is due to his continued support that I could install the pencil code at RRI cluster and perform various numerical simulations. We've had many useful discussions on a number of outstanding issues, especially on incoherent alpha–shear dynamos.

Discussions with Karl–Heinz Rädler and Matthias Rheinhardt on the Galilean invariance of shear flows, in particular, and dynamos, in general, are memorable. I wish to thank them for their interests in our work.

It is a pleasure to thank Kandaswamy Subramanian whose suggestions and comments formed the basis for furthering our understanding of the shear dynamo problem. He encouraged us to estimate the fluctuations in "alpha" in our numerical simulations, which led to our analytical explorations of incoherent alpha–shear mechanism. I am grateful to him for his "short & crisp" suggestions and for supporting my visits to IUCAA which have been extremely beneficial.

My almost daily meetings with Desh, apart from some rare misses, added much fun to life. He has been a great company, a friend and a mentor. We've had extensive discussions on Science, and interesting talks on non–scientific issues, mostly at "the ashtray" or over many late night sittings. I thank Ranjana for many exotic dishes she offered while also being a patient listener of all the junks that I used to bug desh with.

Most of my non–scientific learning is derived from various endless "sessions" with many friends, especially, Chandrakant(h), Harsha, Mam(a)t(h)a, Giri, Habeeba, Ryuichi, Madhukar, Radhakrishnan, Aloks, Rohit, Prakhyat, Naveen and many others, which were always accompanied by "all states of matter" and occasionally flanked by apparently passive appearance of Mahavir, Yogesh and Jaya Kumar.

Chandrakant and I had a smooth sail through our PhDs due to Mamta, who always took care of exchange of all the important documents with the offices of RRI & IISc, ensured that our tuition fee to IISc is paid in time and so on, in short, she ensured our survival/salary in Bangalore. She is a wonderful friend and I am thankful to her for being so kind to many of us.

I thank all my collegues at Raman Research Institute with whom I've enjoyed my stay at RRI and have had enlightening discussions. Yogesh, Chaitra, Wasim, Prasad, Kanhaiya, Naveen, Mamta and Chandrakant thankfully involved me in many discussions which helped me to improve my understanding of some other subjects as well.

Thanks are due to my volleyball-friends, and music partners – Narayanaswamy, Ram, Chandreyee, Nipanjana and many others, who kept the atmosphere so alive.

I thank all my JAP teachers and instructors at ICTP school who've offered some excellent courses. Thanks are due to Sam, Supurna, Yashodhan, Ravi, Biswajit, Tarun,

Biman, Shiv, Dwaraka, Uday, Ramesh and Madhusudana for useful interactions at different times.

I've used cluster facilities of NORDITA, RRI and IUCAA for some of the works presented in this thesis, and I wish to thank all the supporting staff, especially Jacob, who was always so helpful.

Simulations pesented in this thesis are jointly done with Naveen, an interesting character with a sober tone and steady head, mostly found hanging between the "inner" and "outer" worlds.

Mahavir has been a great company with whom I've had some of the most interesting discussions. I thank Rabbi for being such a wonderful friend whose smiles, jokes and poems were missed after he went back to his college. Chandrakant, Madhukar and Jaya Kumar are excused from the embarrassment that they might otherwise feel, if thanked.

Most of my studies have happened in RRI Library and I thank all the library staff for their support all along, and for maintaining the Library so wonderfully. Their caring attitude is gratefully acknowledged.

I wish to thank all the drivers of RRI shuttle who have been carrying us back & forth from hostel to the institute. Thanks are due to the staff of Canteen and Computer section.

Krishna provided me the financial support when I needed it urgently within my first week at RRI. I am grateful to him for all his support. I thank all the administrative staff of RRI & IISc who have helped me whenever it was sought.

I thank Lakshmamma and Hanumantha for maintaining cleanlines on the Astro–floor and the pantry.

My inexpressible gratitute to Vidya for her motherly attitude who took care of all of us so well that we didn't even realize many troubles, which could have otherwise affected our general day–to–day life at RRI.

Finally I thank my family whose affection, encouragement and tolerance with me & my idiosyncracies have always provided a comfortable setting in which I could focus on my work and everything else that I wished.

Synopsis

Astrophysical systems such as, the Sun, disc galaxies, clusters of galaxies, accretion discs etc., possess ordered magnetic field in addition to a random component, which survives for time scales much larger than the diffusion time scales in those systems, and therefore are thought to be self–sustained by the *turbulent dynamo action*. The dynamo action may be stated as the conversion of kinetic energy into the magnetic energy *without any electric currents at infinity*. The mean differential rotation is common in these systems, e.g., the Sun, the disc galaxies, the accretion discs etc. The standard paradigm involves amplification of seed magnetic fields, due to non mirror–symmetric (i.e. helical) turbulent flows through the so called $\alpha-$effect (Moffatt, 1978; Parker, 1979). It may be noted that the magnetic field being a *pseudovector* is inherently non mirror–symmetric and therefore its generation at certain scale due to the dynamo action is a symmetry breaking process at that scale, which demands that the flow must host such a quantity which is also non mirror–symmetric. The quantity α is one such object which is a measure of *net* or *average* kinetic helicity in the flow and it is a *pseudoscalar*. Only recently the role of mean shear in the turbulent flow is beginning to be appreciated, as the breaking of mirror–symmetry, so necessary for large–scale dynamo action, may also come from the background shear flow. Dynamo action due to shear and turbulence received some attention in the astrophysical contexts of accretion discs (Vishniac & Brandenburg, 1997) and galactic discs (Blackman, 1998; Sur & Subramanian, 2009). The natural question to be addressed may be posed as: In the absence of usual $\alpha-$ effect, will it be possible to generate large–scale magnetic

field just due to the action of mirror–symmetric turbulence in background shear flow on the seed magnetic field ? This question just posed was simulated in the recent past by Yousef et al. (2008); Brandenburg et al. (2008). These simulations clearly demonstrated the growth of large–scale magnetic field due to non–helical stirring at small scale in the background linear shear flow. This forms the basic motivation for our interest in the study of *the shear dynamo problem* in the absence of usual $\alpha-$effect. In the problems studied in this thesis, we assume a *linear* shear flow, and throughout this thesis, we will deal with the shear parameter *non–perturbatively*.

Problems studied in the thesis:

Our primary interest is to study the growth of large–scale magnetic fields, due to small–scale, mirror–symmetric (i.e. non–helical) turbulence in a background linear shear flow. This problem of the shear dynamo, with no net value of α, turns out to be quite complicated for magnetic fields because they have a pseudovector character. Therefore we present our investigations by first studying the *free* and *non–helically forced* shearing waves in the background shear flow. Then we present a preliminary application of our techniques to understand the large–scale mixing of a passive scalar in a non–helical turbulent linear shear flow. The problems just described form part I of this thesis. We deal with magnetic fields in part II of the thesis. Below, we briefly state the different problems that were studied:

1. **Shearing waves:** Shear flows are common and seen in variety of astrophysical contexts; like differential rotation in disc galaxies, accretion discs around compact objects etc. The shearing waves are excited in such systems by some random stirring in the medium, e.g., in disc galaxies the random supernovae (SNe) events stir the differentially rotating disc and excite shearing waves. Our aim is to understand the large–scale dynamo action in systems which possess mean shear, and therefore a necessary understanding of waves in such shearing systems will be useful in our studies related to the large–scale dynamo action.

- Exact solutions of the Navier–Stokes equations: We studied the incompressible Navier–Stokes equations in a background linear shear flow *in the absence of any external forcing*. Plane shearing wave solutions were sought whose wave vectors were time dependent, and these solutions were found to be the *exact solutions* of the Navier–Stokes equations.

- Forced stochastic velocity dynamics: Here, we study the dynamics of an incompressible fluid in a background linear shear flow, by solving the *externally forced* Navier–Stokes equations in the limit of small fluid Reynolds number. The external forcing is assumed to be stochastic, as a response to which, the resulting velocity field is also expected to be stochastic. Our aim is to model non–helical (mirror–symmetric) turbulence in linear shear flows and therefore we specialize to the case when the fluid is stirred non–helically.

These shearing waves lead to the mixing of various active and passive variables[1] embedded in the medium. Our analysis of non–helically forced stochastic velocity dynamics will be extremely useful in determining the various transport coefficients of different transport phenomena (of magnetic fields or passive scalars), which in turn, enable us to comment on the large–scale dynamo action. As a preliminary application of the techniques developed here, we next study the problem of passive scalar mixing, before investigating the difficult problem of the growth of large–scale magnetic field.

2. **Passive scalar mixing in shear flows:** A passive scalar evolves according to an advection–diffusion equation, which is much simpler than the induction equation governing the evolution of magnetic field, and therefore provides a simpler situation where we can quickly apply our techniques to understand the large–scale mixing of the passive scalar. As we have developed stochastic forced shearing wave solutions which are non–helical, because of our ultimate interest in the shear dynamos, we apply the same solutions of non–helical turbulent flows in background linear shear flows to study the

[1]The passive variables do not act back on the flow whereas the active variables dynamically affect the flow.

mixing of passive scalars. The specific problem that we wish to address is: Under what conditions does the mean concentration of the passive scalar grow due to the mirror–symmetric turbulence at small scales, in the background linear shear flow ?

Now we are ready to study the problems related to the magnetic fields, which form part II of the thesis.

3. **The shear dynamo problem:** This problem may be viewed in the following way: In a given background mean shear flow, the kinetic energy is being supplied by stirring the electrically conducting incompressible fluid in a non–helical fashion, as a result of which, the magnetic energy at large–scale is seen to grow in time due to the large–scale dynamo action. This is clearly a process of inverse–cascade in which the energy is being transferred from small scale to large scale. Our aim is to understand the reason for this shear dynamo action in the absence of usual $\alpha-$effect.

The problem of the shear dynamo was first analytically studied in the limit of low Reynolds numbers and *the $\alpha-$effect was strictly absent*. These investigations motivated us to look for the dynamo action in such systems in the limit when at least the fluid Reynolds number be below unity, and we performed numerical simulations using the Pencil Code[2] in previously unexplored parameter regimes. Results of our numerical simulations and the simulations of Brandenburg et al. (2008) in different parameter regimes provided strong evidence for the non–trivial role of fluctuations in α, which have zero mean, in the presence of background linear shear flow. This led us to analytically study the shear dynamo problem where α could be considered as a fluctuating quantity with zero mean. As argued before by Kraichnan (1976), these fluctuations in α may be understood in terms of helicity fluctuations. We show analytically that the fluctuations in α with zero mean together with mean background shear can drive the large–scale dynamo action.

[2]See http://www.nordita.org/software/pencil-code.

Our approach to mean–field theory in shear flows:

Our analytical investigations of the problems discussed above are based on the framework of mean–field (two–scale), in which, the field variables (e.g. magnetic fields or the passive scalars) may be split into mean and fluctuating components, where the mean field varies over scales (spatial and temporal) much larger than the scale of the turbulence (Moffatt, 1978; Krause & Rädler, 1980). Following steps may be taken to study the mean–field theory in linear shear flows, which we applied to both, the magnetic field and the passive scalars, and present here the brief summary of the techniques by considering magnetic field as an example:

(i) **Reynolds averaging:** Using Reynolds averaging, we split the magnetic field into mean and fluctuating components. The mean magnetic field is driven by the Curl of the mean EMF, which is given by the correlation between random velocity field and the fluctuating magnetic field. To know the mean EMF, it is necessary to determine the magnetic fluctuations which may be expressed in terms of the mean magnetic field and the velocity fluctuations. So we develop the equation for the fluctuating components, which we solve using the shearing coordinate transformation.

(ii) **Shearing coordinate transformation:** Exploiting the shearing coordinate transformation, we write the Green's function solution for magnetic fluctuations. This transformation enable us to explicitly derive the *resistive Green's function for a linear shear flow*, and thus we could write an explicit expression for fluctuating magnetic field in terms of random velocity field and the mean magnetic field. Using the solution for the fluctuating magnetic field, we determine the mean EMF, and note that the transport coefficients are given in general form in terms of unequal–time two–point correlators of random velocity field.

(iii) **Galilean invariance:** The linear shear flow has a basic symmetry relating to measurements made by a special subset of all observers, which are termed as the *comoving observers* in Sridhar & Subramanian (2009). We prove a result on the Galilean invariant form of the unequal–time two–point velocity correlators in Fourier space,

and demonstrate that any general second order correlator of random velocity field, in terms of which various transport coefficients could be expressed, can entirely be written in terms of a single entity which we called the *velocity spectrum tensor*. We derive the Galilean–invariant expressions for the transport coefficients and the mean EMF, and express them in terms of the velocity spectrum tensor, which is the most fundamental quantity to be determined in order to explore various conditions for the dynamo action.

The knowledge of the velocity spectrum tensor is necessary for further progress leading to the exploration of conditions for the dynamo action in the parameter regimes that we worked in, and which will be described shortly. Our analysis of the forced stochastic velocity dynamics in linear shear flows, described before, enabled us to determine the desired velocity spectrum tensor in the limit of low fluid Reynolds numbers. It may be noted that all the analysis presented in this thesis is *always non–perturbative in the shear parameter*.

Numerical simulations of the shear dynamo:

We simulate, using the Pencil Code, the shear dynamo problem due to non–helical stirring at small scales, in a background linear shear flow. We note that all the earlier numerical experiments done so far have been carried out for both the fluid Reynolds number (Re) and the magnetic Reynolds number (Rm) above unity. Our analytical investigations in the limit of low Reynolds numbers motivated us to look for dynamo action when at least one of Re, Rm is below unity. Two main motivations are: first, to compare our analytical findings with the results of numerical simulations in similar parameter regimes; and second, to look for the growth of mean magnetic field in the limit when $\mathrm{Re} < 1$. The limit of low Re is particularly interesting, as seeing a dynamo action in this limit would provide enough motivation for further theoretical investigations, which may focus the attention to this analytically more tractable limit of $\mathrm{Re} < 1$, as compared to the more formidable limit of $\mathrm{Re} > 1$.

A brief summary of results obtained:

A short summary of salient results, obtained while studying different problems described above, is being given below:

• **Plane shearing waves:** We have constructed a plane shearing wave solution for the Navier–Stokes equations in linear shear flows. These solutions are also the *exact solutions* and we have presented explicit expressions for all three components of the velocity field in the real form. We demonstrate that, when these shearing modes, also known as the Kelvin modes, with parallel wavevectors are superposed, they remain exact solutions. We give, in explicit form, the most general plane transverse shearing wave solution, with any specified initial orientation, profile and polarization structure, with either unbounded or shear–periodic boundary conditions.

• **Forced stochastic velocity dynamics:** We study the dynamics of an incompressible fluid due to non–helical random stirring in a background linear shear flow in the absence of Lorentz forces, in the limit of low fluid Reynolds numbers, by solving the corresponding Navier–Stokes equations. Some of our findings are given below:

(i) We show that non–helical forcing gives rise to non–helical velocity field.

(ii) We determine the velocity spectrum tensor, which was argued above to be the most fundamental entity, and which needed to be known in order to study various transport processes of magnetic field & the passive scalars.

(iii) Various time–correlation properties of random velocity field are studied and it is found, by analyzing the different components of two–time random velocity correators, that the shear has non–trivial anisotropic effects on the velocity correlators, and hence is expected to lead to anisotropic transport of magnetic fields & passive scalars.

• **Passive scalar mixing in shear flows:** The analysis of passive scalar mixing due to non–helical stirring of an incompressible linear shear flow was done in the limit when both, the fluid Reynolds number and the Peclet number were below unity. We find the

possibility of transient amplification of mean concentration of the passive scalar. Just like everything else in the thesis, this result is non–perturbative in the shear parameter.

• **The shear dynamo problem:** The shear dynamo problem was analytically studied in two different ways; one, in which, the $\alpha-$effect was strictly absent, and the other, in which, the α was considered to be a fluctuating quantity with zero mean. We have also performed numerical simulations for this problem. The results may be given as follows:

(i) When $\alpha-$effect is strictly zero: Some earlier works on the similar problem proposed that the origin of the large–scale magnetic field in such systems may be explained by an effect known as the shear–current effect (Rogachevskii & Kleeorin 2003, 2004, 2008).

We formulated the problem of the shear dynamo in the limit of low Reynolds numbers and concluded that the shear–current effect cannot be responsible for dynamo action. Our theory is found to be in good agreement with some other works, esp., with Brandenburg et al. (2008) who computed the magnetic diffusivity tensor and concluded that the relevant component responsible for the shear–current effect (η_{21}^{∞}) is of wrong sign and hence cannot give rise to the dynamo action. This was the natural prediction of our theory.

Thus the main contribution of our studies, in which α was strictly zero, may be stated as follows: The mean magnetic field cannot grow due to mirror–symmetric turbulence in the background linear shear flow, at least in the limit when: (a) both fluid and magnetic Reynolds numbers are below unity; (b) $\alpha-$effect is strictly absent (without considering any fluctuations in α); but (c) the shear parameter can take arbitrary values.

This negative result of no dynamo action prompted us to carry out various numerical simulations when at least one of Re, Rm is below unity.

(ii) Results of numerical studies of the shear dynamo: We demonstrated the large–scale dynamo action in the limit when $\mathrm{Re} < 1$ and $\mathrm{Rm} > 1$. We performed simulations in the regime when both $(\mathrm{Re}, \mathrm{Rm}) < 1$ to compare the results with our analytical

calculations done in the similar regime and found a reasonably good agreement. We also estimated the dynamo number ($D_{\alpha S}$), which was empirically defined in Brandenburg et al. (2008) corresponding to the *incoherent alpha–shear mechanism*[3], for many simulations, and found that the dynamo number ($D_{\alpha S}$) is always *supercritical* for cases, in which, we see dynamo growth, a result which is in agreement with Brandenburg et al. (2008)[4]. This suggested that the incoherent alpha–shear mechanism could plausibly be the reason for observed shear dynamo due to non–helical random stirring in these simulations. Thus our numerical investigations, together with those of Brandenburg et al. (2008) in different parameter regime, motivated us to analytically study the problem of dynamo action by assuming fluctuations in α *with no net value* in the presence of background linear shear flow.

(iii) When α is a fluctuating quantity with zero mean: By considering temporal fluctuations in the quantity α, with its mean value zero, we demonstrated that *the fluctuations in α with zero mean in conjunction with background shear flow can give rise to the growth of large–scale magnetic field.* Some other conclusions of this analysis could be stated as:

(a) In the limit of zero shear, we find that only the diagonal components of the turbulent diffusivity tensor (β^{∞}_{mp}) survive, which are *negative*. This leads to the *negative turbulent diffusion* of mean magnetic field, which in case of sufficiently strong $\alpha-$fluctuations may give rise to the self–excited dynamo action. This result was first obtained by Kraichnan (1976) who did a similar analysis in the absence of shear.

(b) The shear leads to cross–coupling of different components of mean magnetic

[3]A mechanism by which the fluctuations in α with no net value in conjunction with mean shear might give rise to the large–scale dynamo action in such systems.

[4]Critical value of $D_{\alpha S}$ ($D^{\rm crit}_{\alpha S} \approx 2.3$), above which the dynamo is seen, was empirically determined in Brandenburg et al. (2008). We show by our analytical investigation of fluctuating α with background mean shear that this number 2.3 is not unique; we describe it later.

field with each other through the off–diagonal components of β^{∞}_{mp}. The diagonal components couple each component of mean magnetic field with itself. The shear makes one of the diagonal components β^{∞}_{22} more negative whereas β^{∞}_{11} is independent of the shear.

(c) By deriving the dispersion relation and putting it in a useful form in terms of three dimensionless parameters, we explored various conditions for the dynamo action, and found that the critical conditions could be given by a surface in three dimensional parameter space. Therefore, the critical value required by one of the parameters for dynamo action is a function of the remaining two dimensionless parameters (e.g., $D^{\rm crit}_{\alpha S}$ varies as a function of two other dimensionless parameters, and hence is not a unique number).

(d) We find that the shear helps in the generation of large–scale magnetic field in the presence of $\alpha-$fluctuations. If the fluctuations in α are extremely small, one can still find growing solutions for the mean magnetic field for sufficiently large values of shear.

(e) In most numerical simulations that we perform, the fluctuations in α are not too strong, and hence these alone may not give rise to the dynamo action, unless supported by the shear.

It is routinely found in the numerical simulations of the shear dynamo that the quantity α fluctuates in time without having any net value, even when the random forcing at small scales in these simulations was non–helical, therefore, it seems plausible that these observed $\alpha-$fluctuations together with background shear flow could have led to the growth of large–scale magnetic fields in these simulations, by the mechanisms described in our analytical calculations of fluctuating α discussed above. The natural scope for future works related to this problem could be to perform numerical experiments exploring conditions for the dynamo action, as predicted in our analytical calculation of $\alpha-$fluctuations, in which, we suggested that there are three dimensionless parameters, which, if tuned suitably, can always give rise to the dynamo action.

Contents

Chapter 1

Introduction

Magnetic fields are ubiquitous and seem to be one of the most pervasive features in the Universe. Investigations of the origins of magnetic fields in cosmic matter (e.g., the Earth, the Sun, the Galaxy etc.) started with the work of J. Larmor in 1919 who wondered about the Solar magnetic field, after the pioneering measurements by G. Hale in 1908, of Zeeman splittings of the sunspot spectral lines, suggesting the existence of magnetic field in sunspots (Hale, 1908; Larmor, 1919). From the classical electrodynamics, it is known that there could be following two possibilities which might give rise to the magnetic field: (i) the *permanent magnetization* of condensed matter; and (ii) the *electric currents* in electrically conducting fluids. The conditions in most of the astrophysical objects rule out the permanent magnetization as an option for the origin of associated magnetic field. Considering a particular example of the Earth, it is known that the temperature of the Earth's interior ($\sim 5500^\circ$ C) is well above the critical temperature, i.e., the Curie point ($\sim 700^\circ$ C), at which any ferromagnetic material loses its permanent magnetization. However, most of the baryonic matter in the Universe exists in the *plasma* state, which may be thought of as an electrically neutral fluid as a whole, whose constituents are ions, electrons and neutrals, in general. Motions in these electrically conducting fluids, which fill almost the entire Universe, drive electric currents giving rise to the magnetic fields, but it should be noted that the dynamo action, in which the kinetic energy of the flow gets converted into the magnetic energy due to the hydromagnetic interactions,

require some *seed magnetic field* to become operative. Many different mechanisms have been proposed for the origin of seed magnetic fields (see the reviews (Widrow, 2002; Brandenburg & Subramanian, 2005) and a recent work (Deshpande & Kumar, 2012) for the possible origins of the seed field), which lead to fields which are much weaker than the observed magnetic fields. It is thought that the observed cosmic magnetic fields could have arisen due to the dynamo amplification of these seed fields. Another possibility that was suggested to explain the observed magnetic field was the *primordial–field* hypothesis, in which, it was considered that the magnetic fields were already present in the matter which collapsed to form Galaxies, and thus the galaxies carried that signature (Widrow, 2002). This simple idea remained a promising candidate, as the other mechanisms for generation of magnetic fields were poorly understood at that time due to the non–linear nature of the hydromagnetic interactions, which are unavoidable in all the astrophysical systems. While it is possible that the primordial fields could have existed at the time of birth of the galaxies, it is now clear that no magnetic field could have survived over the life time of the galaxy due to *the turbulent magnetic diffusion*, and therefore a self–sustained dynamo action seems to be the reason behind the observed large and small scale magnetic fields (Shukurov & Sokoloff, 2008); see also § 1.4 given below.

Advances in the dynamo theory are relatively recent and slow due to the very nature of the problem being quite difficult, but there have been considerable progress in this area due to advancements of numerical simulations in the recent past. A detailed treatment on the subject of astrophysical dynamos can be found in the review by Brandenburg & Subramanian (2005), where the current topics of dynamos together with its historical developments and the outlook have been given in a rigorous fashion; see also Brandenburg, Sokoloff & Subramanian (2012) for relatively more recent review on current status of turbulent dynamos, where various technical issues related to the large–scale and the small–scale dynamo action have been discussed.

In this thesis, our primary interest is to study the growth of large–scale magnetic fields, due to small–scale, mirror–symmetric (i.e. non–helical) turbulence in a background linear shear flow. Before describing the specific problems that were studied in detail, we

briefly discuss the fundamental concepts of hydrodynamics, magnetohydrodynamics and mean–field theory, which will be used throughout the thesis.

1.1 Basics of hydrodynamics

Consider the lab frame in which the position vector is denoted as $\boldsymbol{x}$, and the time is denoted as t. The fluid (liquids and gases) is modelled as *continuum* in which all the *state variables* are smoothly varying functions of space. A *fluid particle* is assumed to be in *local thermodynamic equilibrium* and it is assigned with a *bulk* or *mass–weighted average* velocity, $\boldsymbol{v}'(\boldsymbol{x}, t)$, which is smoothly varying function. Thus the state of the fluid is mathematically described by the knowledge of the *flow*, i.e. $\boldsymbol{v}'(\boldsymbol{x}, t)$, together with any two thermodynamic variables, say, pressure ($p(\boldsymbol{x}, t)$) and density ($\rho(\boldsymbol{x}, t)$). The fundamentals of fluid dynamics are discussed in detail in a number of textbooks (see e.g., Landau & Lifshitz (1987); Pedlosky (1987); Acheson (1990); Choudhuri (1998)).

1.1.1 Basic equations of hydrodynamics

• **Relation between the Lagrangian and the Eulerian derivative :** Let $\mathcal{Q}(\boldsymbol{x}, t)$ be some quantity of interest whose variation with respect to time is to be determined. The rate of change of $\mathcal{Q}$ at a fixed position in space is called the *Eulerian* derivative, denoted by $\partial\mathcal{Q}/\partial t$. The *Lagrangian* (or the *material* or the *convective*) derivative of $\mathcal{Q}$, which we denote by $d\mathcal{Q}/dt$, may be described by imagining the time derivative of $\mathcal{Q}$ as seen by the one moving with the fluid element with the fluid velocity $\boldsymbol{v}'(\boldsymbol{x}, t)$. The relation between the two is given by,

$$\frac{d\mathcal{Q}}{dt} = \frac{\partial\mathcal{Q}}{\partial t} + (\boldsymbol{v}' \cdot \boldsymbol{\nabla})\,\mathcal{Q} \tag{1.1}$$

• **Mass conservation or the continuity equation :** For a fluid of density $\rho(\boldsymbol{x}, t)$, the

continuity equation is written as,

$$\frac{\partial \rho}{\partial t} \; + \; \boldsymbol{\nabla \cdot} \; (\rho \, \boldsymbol{v}') \; = \; 0 \, , \tag{1.2}$$

which using Eqn. (1.1) may be expressed as,

$$\frac{d \rho}{d t} \; = \; -\rho \, (\boldsymbol{\nabla \cdot} \, \boldsymbol{v}') \tag{1.3}$$

• **Momentum balance or the Navier–Stokes equation :** In this thesis, we will be concerned only with the *Newtonian* fluids, for which, the viscous stress is proportional to the rate of change of strain within the fluid, i.e., the velocity gradient. It is due to the Galilean invariance that the viscous stress can depend only on the gradients of the velocity field, and not on the velocity field itself. The basic equation of motion governing the dynamics of a Newtonian viscous fluid is given by the Navier–Stokes equation:

$$\frac{\partial \boldsymbol{v}'}{\partial t} \; + \; (\boldsymbol{v}' \boldsymbol{\cdot} \boldsymbol{\nabla}) \, \boldsymbol{v}' \; = \; -\frac{1}{\rho} \boldsymbol{\nabla} p + \boldsymbol{F}_b + \nu \nabla^2 \boldsymbol{v}' + \left(\frac{\nu}{3} + \frac{\zeta}{\rho} \right) \boldsymbol{\nabla} (\boldsymbol{\nabla \cdot} \, \boldsymbol{v}') \tag{1.4}$$

where p, $\boldsymbol{F}_b$, ν and ζ represent the pressure, the body force, the coefficient of kinematic viscosity and the coefficient of bulk viscosity.

• **Incompressible (or the isochoric) fluids :** Our aim in this thesis will be to understand the behaviour of *incompressible fluids* (except when we perform numerical simulations presented in Ch. 7, in which case, a weakly compressible fluid has been modelled). The density of an incompressible fluid does not change, and therefore we can write from Eqn. (1.3)

$$\boldsymbol{\nabla \cdot} \, \boldsymbol{v}' \; = \; 0 \tag{1.5}$$

as the condition for incompressibility of the fluid. We note that $\boldsymbol{\nabla \cdot} \, \boldsymbol{v}'$ represents the rate of change of volume element of a fluid element, which is why the incompressible fluid are also sometimes referred to as the isochoric fluids. The flows, in which, the typical velocities of fluid elements are much smaller than the local sound speed, are known as the *subsonic* flows, whereas for *supersonic* flows, typical velocities of fluid elements are much

larger as compared to the local sound speed. The subsonic flows could be approximately considered as incompressible. Thus, using Eqn. (1.5) in Eqn. (1.4), the Navier–Stokes equation for an incompressible fluid can be written as,

$$\frac{\partial \boldsymbol{v}'}{\partial t} + (\boldsymbol{v}' \cdot \boldsymbol{\nabla})\, \boldsymbol{v}' = -\frac{1}{\rho}\boldsymbol{\nabla} p + \boldsymbol{F}_b + \nu \nabla^2 \boldsymbol{v}' \tag{1.6}$$

We note that the pressure (p) appearing in Eqn. (1.6) can be determined using the incompressibility condition given in Eqn. (1.5) (by taking the divergence of Eqn. (1.6) and then solving the resulting Poisson's equation for the pressure). Therefore, Eqns. (1.6) and (1.5) are adequate to study the evolution of all the independent dynamical variables or the unknowns, forming a closed system.

1.2 Basics of magnetohydrodynamics (MHD)

Magnetohydrodynamics (MHD) is a *model* of the plasma in which we try to understand the interaction of the magnetic field and the plasma. MHD model is valid under the following assumptions:

- The plasma is assumed to be sufficiently *collisional*, so that it can be treated as a *continuum* (i.e. fluid-like).
- The plasma is treated as a *single fluid* in which, any charge imbalance (due to, for example, thermal fluctuations) within the plasma is ignored. This assumption will be true if we consider the macroscopic length scales to be much larger than the *Debye shielding length*[1] and the time scales be much larger than the inverse of the *plasma frequency*[2].

[1]The Debye length (λ_D) is characterized by a length scale above which any charge imbalance is almost completely screened due to presence of opposite charges. Thus, the plasma can be treated as charge-neutral when distances larger than λ_D are considered.

[2]The plasma frequency (ω_P) describes the frequency of rapid oscillations (known as the Langmuir waves) of the charge density in the plasma. Thus, considering the time scales much larger than the ω_P^{-1}, we can safely ignore the charge separations in the plasma.

- If $\boldsymbol{v}'$ be the bulk velocity of a *plasma particle* at some space–time point and c be the speed of light, the terms of order v'^2/c^2, or higher, are ignored, while the terms of order v'/c are retained in MHD model. Thus, MHD is a non-relativistic reduction of the plasma dynamics.

1.2.1 Basic equations of MHD

The plasma can carry electric currents due to motions, which produce magnetic fields. The magnetic fields thus generated exert Lorentz force on the plasma. Therefore, the Maxwell's equations of electrodynamics together with the fluid equations, in which we include the Lorentz forces due to electromagnetic fields, describe the plasma processes under the simplified MHD model described above.

• **Maxwell's equations :** We write below the Maxwell's equations in Gaussian cgs units,

$$\begin{aligned} \frac{1}{c}\frac{\partial \boldsymbol{B}'}{\partial t} &= -\boldsymbol{\nabla}\times\boldsymbol{E}' \; ; \qquad & \boldsymbol{\nabla}\cdot\boldsymbol{B}' = 0 \\ \frac{1}{c}\frac{\partial \boldsymbol{E}'}{\partial t} &= \boldsymbol{\nabla}\times\boldsymbol{B}' - \frac{4\pi}{c}\boldsymbol{J}' \; ; \qquad & \boldsymbol{\nabla}\cdot\boldsymbol{E}' = 4\pi\rho_e \end{aligned} \tag{1.7}$$

where $\boldsymbol{E}'$, $\boldsymbol{B}'$, $\boldsymbol{J}'$ and ρ_e are the electric field, the magnetic field, the current density and charge density, respectively, all seen in the lab frame.

• **Lorentz transformation of electromagnetic fields (non-relativistic approximation) :** Let $\boldsymbol{E}'^{\mathrm{R}}$ and $\boldsymbol{B}'^{\mathrm{R}}$ be the electromagnetic fields in the *rest frame of the plasma*, which is moving with velocity $\boldsymbol{v}'(\boldsymbol{x},t)$, as seen in the laboratory frame. $\boldsymbol{E}'^{\mathrm{R}}$ and $\boldsymbol{B}'^{\mathrm{R}}$ are related to $\boldsymbol{E}'$ and $\boldsymbol{B}'$ (the electromagnetic fields in the laboratory frame) by Lorentz transformation,

$$\begin{aligned} E'^{\mathrm{R}}_{\parallel} &= E'_{\parallel} \; ; \qquad & B'^{\mathrm{R}}_{\parallel} = B'_{\parallel} \\ \boldsymbol{E}'^{\mathrm{R}}_{\perp} &= \gamma\left(\boldsymbol{E}'_{\perp} + \frac{\boldsymbol{v}'}{c}\times\boldsymbol{B}'_{\perp}\right) \; ; \qquad & \boldsymbol{B}'^{\mathrm{R}}_{\perp} = \gamma\left(\boldsymbol{B}'_{\perp} - \frac{\boldsymbol{v}'}{c}\times\boldsymbol{E}'_{\perp}\right) \end{aligned} \tag{1.8}$$

where $\gamma = 1/\sqrt{1 - v'^2/c^2}$ is the Lorentz factor, and the subscripts $\parallel$ and $\perp$ refer to the directions parallel and perpendicular to $\boldsymbol{v}'$, respectively. In the MHD model, as described before, γ approaches unity, and we can write from Eqn. (1.8),

$$\boldsymbol{E}'^{\mathrm{R}} \;=\; \boldsymbol{E}' + \frac{\boldsymbol{v}'\times\boldsymbol{B}'}{c} \tag{1.9}$$

• **Ohm's law and the induction equation :** Ohm's law is a model relating, *linearly*, the current density with the electromagnetic fields. In the laboratory frame, for non-relativistic velocities of the plasma, it is expressed as,

$$\boldsymbol{J}' = \sigma\left(\boldsymbol{E}' + \frac{\boldsymbol{v}'\times\boldsymbol{B}'}{c}\right) \tag{1.10}$$

where σ is the electrical conductivity of the plasma. From Eqns. (1.8) and (1.10), we can write,

$$\boldsymbol{J}' \;=\; \sigma\,\boldsymbol{E}'^{\mathrm{R}} \;=\; \boldsymbol{J}'^{\mathrm{R}} \tag{1.11}$$

Thus we see that, to order v'/c, the current density remains the same when transformed from one frame to another. In the *high electrical conductivity limit* (i.e., $\sigma \to \infty$), it may be seen from Eqns. (1.10) and (1.11) that, for a finite $\boldsymbol{J}'$, $\boldsymbol{E}'^{\mathrm{R}} \to 0$, implying,

$$|\boldsymbol{E}'| \;\approx\; \frac{|\boldsymbol{v}'|}{c}|\boldsymbol{B}'| \tag{1.12}$$

Therefore the electric field in the plasma rest frame approximately vanishes due to high electrical conductivity, and in the laboratory frame, the electric field is given by Eqn. (1.12), which is a small quantity as compared to the magnetic field. This is the reason that we usually talk about cosmic *magnetic* field, and the cosmic *electric* fields are not so much discussed due to electrical conductivity of the astrophysical plasma being usually very high.

Eliminating $\boldsymbol{J}'$ using Eqn. (1.10) from one of the Eqns. (1.7), we get

$$\frac{\eta}{c^2}\frac{\partial \boldsymbol{E}'}{\partial t} + \boldsymbol{E}' = \frac{\eta}{c}\boldsymbol{\nabla}\times\boldsymbol{B}' - \frac{\boldsymbol{v}'\times\boldsymbol{B}'}{c} \tag{1.13}$$

where $\eta = c^2/(4\pi\sigma)$ is called the magnetic resistivity. The time derivative term (which is called the *displacement current* term) may be safely ignored if the relevant time scale over which the electric field varies is larger than the *Faraday time scale*, $\tau_f = \eta/c^2$. For the ionized plasma, the Faraday time scale may be estimated from, $\tau_f \sim 10^{-14}\, T_4^{-3/2}$ s, where T_4 is the temperature of the plasma in units of 10^4 K. For conditions in astrophysical systems, τ_f is extremely small quantity, and therefore the displacement current term can be ignored from the above equations. Under these conditions, we can write the following:

$$\boldsymbol{E}' = \frac{\eta}{c}\boldsymbol{\nabla}\times\boldsymbol{B}' - \frac{\boldsymbol{v}'\times\boldsymbol{B}'}{c}\ ; \qquad \boldsymbol{\nabla}\times\boldsymbol{B}' = \frac{4\pi}{c}\boldsymbol{J}' \quad \text{(Ampère's law)} \tag{1.14}$$

Using expression for $\boldsymbol{E}'$ as given in Eqn. (1.14) in one of the Maxwell's equations (Eqn. (1.7)), which involves the time derivative of the magnetic field, we get

$$\frac{\partial \boldsymbol{B}'}{\partial t} = \boldsymbol{\nabla}\times(\boldsymbol{v}'\times\boldsymbol{B}' - \eta\boldsymbol{\nabla}\times\boldsymbol{B}') \tag{1.15}$$

Equation (1.15) is known as *the induction equation* which describes the evolution of magnetic fields in the plasma *for a given velocity field* ($\boldsymbol{v}'$). Taking the divergence of both sides of Eqn. (1.15), we find that $\partial(\boldsymbol{\nabla}\cdot\boldsymbol{B}')/\partial t = 0$, and therefore the magnetic field remains divergence–free at all times, as it must be.

It is important to realize at this point that the magnetic field, which evolves according to the Eqn. (1.15), acts back on the plasma modifying its velocity field ($\boldsymbol{v}'$), and therefore, for a complete description of the plasma, one needs to simultaneously study the evolutions of both, the magnetic field and the velocity field. If the magnetic resistivity (η) is a homogeneous quantity, then Eqn. (1.15) may be expressed as

$$\frac{\partial \boldsymbol{B}'}{\partial t} = \boldsymbol{\nabla}\times(\boldsymbol{v}'\times\boldsymbol{B}') + \eta\nabla^2\boldsymbol{B}' \tag{1.16}$$

• **The momentum equation with the Lorentz force :** As mentioned above that the magnetic field influences the charges in the plasma by exerting the Lorentz forces. Considering a single charged particle having charge q, we know that the Lorentz force

on the charge due to the electromagnetic field is $\boldsymbol{F}_L = q[\boldsymbol{E}' + (\boldsymbol{v}' \times \boldsymbol{B}')/c]$. Let n_i be the number density of ions, each with charge q_i, and n_e be the number density of electrons. Let $\boldsymbol{v}_i'$ and $\boldsymbol{v}_e'$ be the bulk velocities of ions and electrons respectively, then the Lorentz force per unit volume $\boldsymbol{f}_L = \rho_e \boldsymbol{E}' + (\boldsymbol{J}' \times \boldsymbol{B}')/c$, where $\rho_e = (q_i n_i - e n_e)$ is the net charge density and $\boldsymbol{J}' = (q_i n_i \boldsymbol{v}_i' - e n_e \boldsymbol{v}_e')$ is the current density in the conducting fluid. Any charge imbalance in the plasma decays shorting out the electric field over a time scale of the order of the Faraday time scale (τ_f) discussed above, which is usually very small for higly conducting fluid. Thus the electric part of the Lorentz is ignored as compared to the magnetic part. This can also be seen as follows: Consider the Gauss's law relating $\boldsymbol{E}'$ with ρ_e and the Ampère's law relating $\boldsymbol{B}'$ with $\boldsymbol{J}'$ (ignoring the displacement current term), and let the scale of variation of both $\boldsymbol{E}'$ and $\boldsymbol{B}'$ be the same, which we denote as ℓ_{EM}, we can write,

$$\frac{|\rho_e \boldsymbol{E}'|}{|(\boldsymbol{J}' \times \boldsymbol{B}')/c|} \;=\; \frac{|E'^2/\ell_{EM}|}{|B'^2/\ell_{EM}|} \;=\; \frac{|E'^2|}{|B'^2|} \;=\; \frac{v'^2}{c^2} \ll 1 \tag{1.17}$$

where we have used Eqn. (1.12). Thus we can safely ignore the electric part of the Lorentz force as compared to the magnetic part in the non–relativistic limit we are interested in. Thus the momentum balance equation for the fluid element in the presence of Lorentz force may be written by adding the Lorentz force term on the right hand side of the Navier–Stokes equation given in Eqn. (1.6):

$$\frac{\partial \boldsymbol{v}'}{\partial t} \;+\; (\boldsymbol{v}' \cdot \boldsymbol{\nabla})\, \boldsymbol{v}' \;=\; -\frac{1}{\rho}\boldsymbol{\nabla} p + \boldsymbol{F}_b + \frac{\boldsymbol{J}' \times \boldsymbol{B}'}{\rho\, c} + \nu \nabla^2 \boldsymbol{v}' \tag{1.18}$$

where ρ in Eqn. (1.18) is the mass density of the fluid (which is assumed to be constant here due to incompressibility) and $\boldsymbol{J}' = c\,(\boldsymbol{\nabla} \times \boldsymbol{B}')/4\pi$.

1.2.2 Few comments on the induction equation

Considering the induction equation given in Eqn. (1.16), we briefly mention few comments below:

- $\eta = 0$ **(Ideal MHD) :** In this limit the magnetic flux is *frozen* into the plasma.

- $\boldsymbol{v}' = \mathbf{0}$ **:** In this limit the *inductive* term is absent from the induction equation and the magnetic field monotonously decays due to microscopic (or the Ohmic) diffusion.

- The finite $\boldsymbol{v}'$ may act as a *dynamo* whose formal definition may be stated as : it is the conversion of kinetic energy into the magnetic energy *without any electric currents at infinity.*

- $\boldsymbol{B}' = \mathbf{0}$ **:** The zero magnetic field is a *solution* of the induction equation and therefore the existence of finite *seed magnetic field* is necessary for dynamo to operate.

1.3 Mean–field theory and turbulent dynamos

Mean–field theory provides a framework in which one can study the evolution of magnetic field (or other variables) over scales which are separated by the scales of the turbulence (Moffatt, 1978; Krause & Rädler, 1980). This provides a natural setting for the evolutionary studies of fields which have definite spatial ordering together with a random component at the scale of random flow, and this framework is also called a *two–scale approach.* In mean–field theory, we will solve the Reynolds–averaged equations by suitably defining ensembles (see, Monin & Yaglom (1971, 1975) for rigorous treatments of statistical concepts in fluid mechanics.)

1.3.1 Rules of Reynolds averaging

In a medium, in which the velocity field has a stochastic component at some (small) scale, all the field variables (e.g., the magnetic field or the passive scalars) will also show irregular variations in space and time at a similar scale, although they might also have 'definite ordering' at some different (large) scale. The stochastic velocity field may be assumed as a model representing the turbulence. Consider an ensemble of identical systems, in which, different members of the ensemble correspond to different realizations

of fluctuating velocity field. The 'mean' of any field variable is defined by taking its average over the ensemble. Thus any variable can be split into mean and fluctuating components. Let $\boldsymbol{v}'$ and $\boldsymbol{B}'$ be the *total* velocity and the magnetic field respectively, both having well–defined *mean* (denoted by $\boldsymbol{V}$ and $\boldsymbol{B}$ respectively) and *fluctuating* (denoted by $\boldsymbol{v}$ and $\boldsymbol{b}$ respectively) components. Denoting by $\langle\ \rangle$ the ensemble averaging in the sense of Reynolds, we write below all the Reynolds rules which will be used for averaging procedures, whenever needed :

$$\begin{aligned}
\boldsymbol{v}' &= \boldsymbol{V} + \boldsymbol{v}\ ; \qquad \langle \boldsymbol{v}' \rangle = \boldsymbol{V}\ ; \qquad \langle \boldsymbol{v} \rangle = \boldsymbol{0} \\
\boldsymbol{B}' &= \boldsymbol{B} + \boldsymbol{b}\ ; \qquad \langle \boldsymbol{B}' \rangle = \boldsymbol{B}\ ; \qquad \langle \boldsymbol{b} \rangle = \boldsymbol{0} \\
\langle \langle \boldsymbol{B}' \rangle \rangle &= \boldsymbol{B}\ ; \quad \langle B_1' + B_2' \rangle = \langle B_1' \rangle + \langle B_2' \rangle = B_1 + B_2 \\
\langle\ \langle B_1' \rangle\, \langle B_2' \rangle\ \rangle &= B_1\, B_2\ ; \quad \langle B\, b \rangle = 0\ ; \quad \left\langle \frac{\partial \boldsymbol{B}'}{\partial t} \right\rangle = \frac{\partial \boldsymbol{B}}{\partial t}
\end{aligned} \tag{1.19}$$

We note that the operator $\langle\ \rangle$ commutes with the differentiation and the integration operators; example of commutation with time derivative is shown in Eqn. (1.19).

1.3.2 Equations for 'mean' and 'fluctuating' magnetic field

Applying the averaging techniques given in Eqn. (1.19) on the induction equation, Eqn. (1.15), and working out

$$\langle \boldsymbol{v}' \times \boldsymbol{B}' \rangle = \langle (\boldsymbol{V} + \boldsymbol{v}) \times (\boldsymbol{B} + \boldsymbol{b}) \rangle = \boldsymbol{V} \times \boldsymbol{B} + \langle \boldsymbol{v} \times \boldsymbol{b} \rangle$$

we can write the following two equations describing the evolutions of the mean and the fluctuating magnetic fields :

$$\frac{\partial \boldsymbol{B}}{\partial t} = \boldsymbol{\nabla} \times (\boldsymbol{V} \times \boldsymbol{B} + \boldsymbol{\mathcal{E}} - \eta \boldsymbol{\nabla} \times \boldsymbol{B}) \tag{1.20}$$

$$\frac{\partial \boldsymbol{b}}{\partial t} = \boldsymbol{\nabla} \times (\boldsymbol{V} \times \boldsymbol{b} + \boldsymbol{v} \times \boldsymbol{B} - \eta \boldsymbol{\nabla} \times \boldsymbol{b}) + \boldsymbol{\nabla} \times (\boldsymbol{v} \times \boldsymbol{b} - \boldsymbol{\mathcal{E}}) \tag{1.21}$$

where $\boldsymbol{\mathcal{E}} = \langle \boldsymbol{v} \times \boldsymbol{b} \rangle$ is known as the mean electromotive force (EMF), or the *turbulent EMF*. As may be seen from Eqn. (1.20) that the mean EMF ($\boldsymbol{\mathcal{E}}$) drives the mean–field, which depends on the fluctuating components of the velocity and the magnetic fields. Thus the correlation between the fluctuations give rise to the mean EMF, which ultimately decides the evolution of mean magnetic field. In order to determine $\boldsymbol{\mathcal{E}}$, *for a given velocity field*, we need to solve Eqn. (1.21) for fluctuating magnetic field.

We noted before that the magnetic field affects the dynamics of the flow through the action of Lorentz forces in the momentum balance equation, Eqn. (1.18). The momentum balance equation must also be split into the mean and fluctuations by applying Reynolds rules, and for a full dynamical treatment of the problem of magnetic field generation, one must study the simultaneous evolution of the magnetic and the velocity field, a task which is difficult due to presence of nonlinearities, and is mostly studied by numerical simulations.

Here, we simplify the problem by assuming that the velocity is *given*, and study the mean–field and fluctuating field induction equations, Eqns. (1.20) and (1.21), for specific velocity fields, $\boldsymbol{V}$ and $\boldsymbol{v}$. This is called the *kinematic* study of dynamo action.

1.3.3 First order smoothing approximation (FOSA)

Let τ_v and ℓ be the correlation time and the correlation length of fluctuating velocity field (with root–mean–squared value $v_{\rm rms}$), which may be defined as the characteristic temporal and spatial scales respectively, over which, the fluctuating velocity field does not vary appreciably. Imagining that the dominant source of $\boldsymbol{b}$ is due to the action of $\boldsymbol{v}$ on mean–field $\boldsymbol{B}$ (see Eqn. (1.21)), we can assume that the correlation time and length of $\boldsymbol{b}$ is same as that of $\boldsymbol{v}$. Considering Eqn. (1.21), we find that the ratio of the terms $\boldsymbol{\nabla} \times (\boldsymbol{v} \times \boldsymbol{b} - \boldsymbol{\mathcal{E}})$ and $\partial \boldsymbol{b}/\partial t$ is of order ${\rm St} = v_{\rm rms}\tau_v/\ell$, and ratio of the term $\boldsymbol{\nabla} \times (\boldsymbol{v} \times \boldsymbol{b} - \boldsymbol{\mathcal{E}})$ and the resistive term $\eta \nabla^2 \boldsymbol{b}$ is of order ${\rm Rm} = \ell v_{\rm rms}/\eta$, where St and Rm are Strouhal number and the magnetic Reynolds number respectively.

The last term on the right hand side of Eqn. (1.21) poses the problem of *closure*, and is generally ignored under what is known as the "first–order smoothing approximation"

(FOSA), also known as the "second–order correlation approximation" (SOCA) or the "quasi–linear approximation, which is valid in the limit when $\min(\mathrm{St}, \mathrm{Rm}) \ll 1$ (Moffatt, 1978; Krause & Rädler, 1980; Brandenburg & Subramanian, 2005). In the astrophysically interesting limit of high magnetic Reynolds numbers, $\mathrm{Rm} \gg 1$, the term $\boldsymbol{\nabla}\times(\boldsymbol{v}\times\boldsymbol{b}-\boldsymbol{\mathcal{E}})$ in Eqn. (1.21) can still be ignored in the limit when $\mathrm{St} \ll 1$, and therefore, under FOSA, we can write from Eqn. (1.21) by ignoring the mean flow ($\boldsymbol{V}$) for simplicity,

$$\frac{\partial \boldsymbol{b}}{\partial t} \;=\; \boldsymbol{\nabla}\times\left(\boldsymbol{v}\times\boldsymbol{B}\right) \tag{1.22}$$

This equation may also understood to be derived in the limit of sufficiently small magnitudes of $\boldsymbol{b}$ by noting that all the terms except $\boldsymbol{\nabla}\times\left(\boldsymbol{v}\times\boldsymbol{B}\right)$ on the right hand side of Eqn. (1.21) are linear in $\boldsymbol{b}$; this argument may be found in Choudhuri (1998). Now the system of equations are closed and the expression for the mean EMF can be determined by,

$$\boldsymbol{\mathcal{E}}(\boldsymbol{x},t) \;=\; \langle \boldsymbol{v}\times\boldsymbol{b}\rangle \;=\; \left\langle \boldsymbol{v}(\boldsymbol{x},t)\times\int_0^t \mathrm{d}t'\;\boldsymbol{\nabla}\times\left[\boldsymbol{v}(\boldsymbol{x},t')\times\boldsymbol{B}(\boldsymbol{x},t')\right]\right\rangle \tag{1.23}$$

which can be expressed in component form, by using the divergence–free condition for the magnetic field together with the condition of incompressibility for the fluid, as

$$\mathcal{E}_i(\boldsymbol{x},t) \;=\; \int_0^t \mathrm{d}t' \;\left[\alpha_{ij}(\boldsymbol{x},t,t')\;B_j(\boldsymbol{x},t') \;-\; \eta_{ikj}(\boldsymbol{x},t,t')\;\frac{\partial B_j(\boldsymbol{x},t')}{\partial x_k}\right] \tag{1.24}$$

where $\alpha_{ij}(\boldsymbol{x},t,t')$ and $\eta_{ikj}(\boldsymbol{x},t,t')$ are the *turbulent transport coefficients*, which control the evolution of the mean–magnetic field, and are given by

$$\alpha_{ij}(\boldsymbol{x},t,t') \;=\; \epsilon_{ilk}\left\langle v_l(\boldsymbol{x},t)\;\frac{\partial v_k(\boldsymbol{x},t')}{\partial x_j}\right\rangle \;;\;\; \eta_{ikj}(\boldsymbol{x},t,t') \;=\; \epsilon_{ilj}\;\langle v_l(\boldsymbol{x},t)\,v_k(\boldsymbol{x},t')\rangle \tag{1.25}$$

where ϵ_{ijk} is the Levi–Civita symbol. In the statistically steady state, and assuming the isotropy of the transport coefficients, i.e., by taking $\alpha_{ij}(\boldsymbol{x},t,t') = \delta_{ij}\hat{\alpha}(\boldsymbol{x},t-t')$ and $\eta_{ikj}(\boldsymbol{x},t,t') = \epsilon_{ikj}\hat{\eta}_t(\boldsymbol{x},t-t')$, it can be shown (Choudhuri, 1998; Brandenburg &

Subramanian, 2005),

$$\boldsymbol{\mathcal{E}}(\boldsymbol{x},t) \;=\; \alpha(\boldsymbol{x},t)\,\boldsymbol{B}(\boldsymbol{x},t) \;-\; \eta_t(\boldsymbol{x},t)\,\boldsymbol{J}(\boldsymbol{x},t) \tag{1.26}$$

where $\boldsymbol{J} = \boldsymbol{\nabla}\times\boldsymbol{B}$, and α and η_t are given by,

$$\begin{aligned}
\alpha &= -\frac{1}{3}\int_0^t \mathrm{d}t' \;\langle \boldsymbol{v}\cdot(\boldsymbol{\nabla}\times\boldsymbol{v})\rangle \;\approx\; -\frac{1}{3}\,\tau_v\;\langle \boldsymbol{v}\cdot(\boldsymbol{\nabla}\times\boldsymbol{v})\rangle \\
\eta_t &= \frac{1}{3}\int_0^t \mathrm{d}t' \;\langle \boldsymbol{v}\cdot\boldsymbol{v}\rangle \;\approx\; \frac{1}{3}\,\tau_v\;\langle \boldsymbol{v}\cdot\boldsymbol{v}\rangle
\end{aligned} \tag{1.27}$$

It may be noted from Eqn. (1.27) that α is a measure of *average kinetic helicity* and is a *pseudoscalar*, and η_t is a measure of average energy density of the fluctuating velocity field. Using Eqns. (1.26) and (1.27) in Eqn. (1.20), assuming α and η_t to be homogeneous, and choosing the mean velocity field to be of the form $\boldsymbol{V} = Sx\hat{\mathbf{e}}_y$ (where we assume for the moment that (x,y,z) denote the position vector, t denotes the time, and $(\hat{\mathbf{e}}_x,\hat{\mathbf{e}}_y,\hat{\mathbf{e}}_z)$ denote the unit vectors in a Cartesian coordinate system), we write the evolution equation for each component of mean magnetic field in explicit form,

$$\begin{aligned}
\left(\frac{\partial}{\partial t} + Sx\frac{\partial}{\partial y}\right)B_x &= \alpha\left(\frac{\partial B_z}{\partial y} - \frac{\partial B_y}{\partial z}\right) + (\eta+\eta_t)\nabla^2 B_x \\
\left(\frac{\partial}{\partial t} + Sx\frac{\partial}{\partial y}\right)B_y &= SB_x\hat{\mathbf{e}}_y + \alpha\left(\frac{\partial B_x}{\partial z} - \frac{\partial B_z}{\partial x}\right) + (\eta+\eta_t)\nabla^2 B_y \\
\left(\frac{\partial}{\partial t} + Sx\frac{\partial}{\partial y}\right)B_z &= \alpha\left(\frac{\partial B_y}{\partial x} - \frac{\partial B_x}{\partial y}\right) + (\eta+\eta_t)\nabla^2 B_z
\end{aligned} \tag{1.28}$$

Few general comments on Eqn. (1.28):

- The equation for any component of mean–field depends on other components through the $\alpha-$term, thus the presence of α may lead to the *cross-coupling* dynamo, in which, any component of mean–field evolves due to the other components of mean–field.

- The η_t-term mimics the role of diffusion and therefore η_t is called *the turbulent magnetic diffusivity.*
- Thus, even in the simplest case of isotropic transport coefficients, various components can feed each other through the $\alpha-$effect, and a *self–sustained* dynamo action may be achieved.
- The finiteness of α (which is a pseudoscalar) ensures the presence of non mirror–symmetric property in the flow at certain scale, which is necessary for the generation of a *pseudovector* (e.g. the magnetic field).

The generation of magnetic field *in the absence of* α (i.e., in the non–helical turbulence) is quite a difficult problem, and one has to consider situations in which the mirror–symmetry be naturally broken, even without α. Shear flows break the mirror–symmetry and could provide settings, necessary for the generation of magnetic fields in the absence of usual $\alpha-$effect. Dynamo action in the absence of $\alpha-$effect are called non–helical dynamos, and our primary interest in this thesis will be to understand non–helical dynamo action in background shear flows.

1.4 Necessity of dynamo action

Astrophysical objects usually have very large magnetic Reynolds numbers and the ohmic resistivity (η) of the plasma in such systems are negligible. In such *ideal MHD* limit, the magnetic flux will be frozen to the plasma and will not suffer decay *due to Ohmic diffusion.* As shown in Eqn. (1.28) that the turbulent magnetic diffusivity, η_t, adds to η and it has a similar role to play, i.e., it leads to the *turbulent diffusion of the magnetic field.* Astrophysical systems are highly turbulent and therefore η_t is expected to be dominant, which can be estimated using Eqn. (1.27) (Brandenburg & Subramanian, 2005; Shukurov & Sokoloff, 2008). It is found that most astrophysical systems have survived for time scales much larger than the turbulent magnetic diffusion time scale, over which, any initial magnetic field would have decayed due to the action of the turbulence, hence,

any magnetic field observed today must have been supported by the dynamo action, say e.g., by the action of $\alpha-$effect through which various components of large–scale magnetic field are coupled leading to the self–sustained scenario of magnetic field generation. We demonstrate this by considering the interstellar medium (ISM) of Milky Way as an illustrative example:

Supernovae (SNe) are the main source of turbulence in the interstellar medium (ISM) and inject energy in the ISM with a typical stirring scale of order, $\ell_{\rm stir} \sim 100\,{\rm pc}$; the turbulent velocity field caused due to SNe stirring is typically of order, $v_{\rm turb} \sim 10\,{\rm km/s}$ at the disc mid–plane; a typical scale over which the mean magnetic field varies (L_B) may be taken to be of the order of the scale height of the ionized gas, thus $L_B \sim 500\,{\rm pc}$. The correlation time of random velocity field may be estimated as $\tau_v \sim \ell_{\rm stir}/v_{\rm turb}$, which may be used in Eqn. (1.27) to find, $\eta_t \sim (v_{\rm turb}\ell_{\rm stir})/3$. Using the parameter values just mentioned, it can be obtained that, (i) the turbulent diffusivity, $\eta_t \sim 10^{26}\,{\rm cm}^2/{\rm s}$; and (ii) the turbulent diffusion time scale (or the decay time scale) of the "large–scale" magnetic field, $t_{\rm decay} \sim L_B^2/\eta_t \sim 5 \times 10^8\,{\rm yr}$. Comparing $t_{\rm decay}$ with the galactic lifetime, $t_{\rm galaxy} \sim 10^{10}\,{\rm yr}$, we see that $t_{\rm galaxy} \sim 20\,t_{\rm decay}$.

This suggests that any initial magnetic field in the galaxy would have decayed due to the turbulent diffusion, and the observed magnetic field must have been supported by the turbulent dynamo action. By doing similar calculations for variety of astrophysical systems, we conclude that almost all the astrophysical bodies must host a turbulent dynamo.

1.5 Motivation, aim and the structure of the Thesis

As could be shown in Eqn. (1.28) that the quantity α may naturally lead to the generation of large–scale magnetic field, and has been the main quantity of interest for mean–field generation in the standard dynamo theory. It may be noted that the magnetic field being a *pseudovector* is inherently non mirror–symmetric and therefore its generation at certain scale due to the dynamo action is a symmetry breaking process at that scale, which

demands that the flow must host such a quantity which is also non mirror–symmetric. The quantity α is one such object which is a measure of *net* or *average* kinetic helicity in the flow and it is a *pseudoscalar*. Only recently the role of mean shear in the turbulent flow is beginning to be appreciated, as the breaking of mirror–symmetry, so necessary for large–scale dynamo action, may also come from the background shear flow. Dynamo action due to shear and turbulence received some attention in the astrophysical contexts of accretion discs (Vishniac & Brandenburg, 1997) and galactic discs (Blackman, 1998; Sur & Subramanian, 2009). The natural question to be addressed may be posed as: In the absence of usual $\alpha-$ effect, will it be possible to generate large–scale magnetic field just due to the action of mirror–symmetric turbulence in background shear flow on the seed magnetic field ? This question just posed was simulated in the recent past by Yousef et al. (2008a,b); Brandenburg et al. (2008). These simulations clearly demonstrated the growth of large–scale magnetic field due to non–helical stirring at small scale in the background linear shear flow.

This forms the basic motivation for our interest in the study of *the shear dynamo problem* in the absence of usual $\alpha-$effect. In the problems studied in this thesis, we assume a *linear* shear flow, and throughout this thesis, we will deal with the shear parameter non–perturbatively. Our primary interest is to study the growth of large–scale magnetic fields, due to small–scale, mirror–symmetric (i.e. non–helical) turbulence in a background linear shear flow. This problem of the shear dynamo, with no net value of α, turns out to be quite complicated for magnetic fields because they have a pseudovector character.

As the main aim is to understand the large–scale dynamo action in systems which possess mean shear, a necessary understanding of waves in such shearing systems will be useful in our studies related to the large–scale dynamo action. These shearing waves, which could be excited in such systems by some random stirring in the medium, e.g., in disc galaxies the random supernovae (SNe) events stir the differentially rotating disc and excite shearing waves, tend to mix the magnetic fields in the medium and might lead to the large–scale dynamo action in suitable conditions. Thus, while our main focus

has always been on the study of the growth of mean magnetic field in such systems, we studied some other problems as well, which were useful to pursue the shear dynamo problem. We present our investigations in the following way:

In Ch. 2 we study the incompressible Navier–Stokes equation in a background linear shear flow *in the absence of any external forcing*. Plane shearing wave solutions are sought whose wave vectors are time dependent, and these solutions are found to be the *exact solutions* of the Navier–Stokes equations.

Non–helically forced incompressible Navier–Stokes equations in background linear shear flows are studied in Ch. 3. The forcing is assumed to be stochastic and the forced shearing wave solutions are obtained by using the shearing coordinate transformation which are time–dependent, and have close connection with the time–dependent wave vectors discussed in Ch. 2, which were given in the lab frame. Using the concept of Galilean invariance in linear shear flow, which is a statement of homogeneity in the sheared coordinate frame, we study various correlation properties of the random velocity field. We prove a result on the Galilean invariant form of the unequal–time two–point velocity correlators in Fourier space, and demonstrate that any general second order correlator of random velocity field can entirely be written in terms of a single entity which we call the *velocity spectrum tensor*. We determine this quantity in this chapter. It is shown in later chapters that all the transport coefficients of magnetic fields or the passive scalar could be expressed in terms of this velocity spectrum tensor, and thus the calculations of this chapter find ready applications in later chapters.

As a preliminary application of our techniques, we try to understand the large–scale mixing of a passive scalar in a non–helical turbulent linear shear flow. A passive scalar evolves according to an advection–diffusion equation, which is much simpler than the induction equation governing the evolution of magnetic field, and therefore provides a simpler situation where we can quickly apply our techniques to understand the large–scale mixing of the passive scalar. As we have developed forced shearing wave solutions which are non–helical, because of our ultimate interest in the shear dynamo problem, we apply the same solutions of non–helical turbulent flows in background linear shear

flows to study the mixing of passive scalars. We study this problem in the framework of mean–field theory, and determine the transport coefficients, which could be expressed in terms of the velocity spectrum tensor derived in Ch. 3, using which we finally study the implications for the growth of mean concentration of the passive scalar. This work is presented in Ch. 4.

Chs. 2, 3 and 4 form the part I of the thesis. Part II, consisting of Chs. 5, 6, 7 and 8, deals only with the problems related to the magnetic fields. We use various techniques developed in part I of the thesis to study the evolution of magnetic fields in background linear shear flow in the absence of usual $\alpha-$effect.

In Ch. 5 we formulate the kinematic shear dynamo problem, in the limit of small magnetic Reynolds numbers (Rm) but arbitrary fluid Reynolds number (Re). This may be thought of as FOSA *with finite resistivity*. Using the Reynolds averaging, shearing coordinate transformation and the Galilean invariance, we write the Galilean invariant expressions for the mean EMF and the turbulent transport coefficients. We find that the evolution of mean magnetic field is governed by a set of coupled integro–differential equations. We discuss some important properties of the evolution equation of the mean magnetic field and demonstrate that our theory reduces to the quasilinear theory of Sridhar & Subramanian (2009a,b) in the formal limit of zero resistivity. We show that the natural setting for the integro–differential equation governing mean–field equation is in sheared Fourier space. Using the result on the form of Galilean–invariant Fourier–space unequal–time two–point velocity correlators, which is given in the Appendix B, we express all the integral kernels in terms of a single entity, the velocity spectrum tensor, which is the fundamental dynamical quantity that needs to be specified, and is pursued in Ch. 6.

Building on the formulation developed in Ch. 5, we present, in Ch. 6, a theory of the shear dynamo problem for small magnetic and fluid Reynolds numbers, but for arbitrary values of the shear parameter. We consider the case when the mean magnetic field is a slowly varying function of time and derive the Galilean invariant expressions for the mean EMF and the transport coefficients for slowly varying mean field. We make use of

the results of Ch. 3, where we studied the stochastic velocity dynamics due to non–helical random stirring of an incompressible fluid in a background linear shear flow in the limit of low fluid Reynolds number. We prove that when the velocity field is non–helical, the transport coefficient α_{il}, which characterizes the usual $\alpha-$effect, vanishes. Specializing to the case when the mean magnetic field is a function only of the spatial coordinate X_3 and time τ, we derive explicit expressions for all components of the magnetic diffusivity tensor, and discuss the implications for the dynamo action by deriving the dispersion relation. We demonstrate that the shear–current effect cannot be responsible for dynamo action at small Reynolds numbers, but for all values of the shear parameter.

In Ch. 7 we simulate, using the Pencil Code, the shear dynamo problem due to non–helical stirring at small scales, in a background linear shear flow. We note that all the earlier numerical experiments done so far have been carried out for both the fluid Reynolds number (Re) and the magnetic Reynolds number (Rm) above unity. Our analytical investigations in the limit of low Reynolds numbers motivated us to look for dynamo action when at least one of Re, Rm is below unity. Two main motivations are: first, to compare our analytical findings with the results of numerical simulations in similar parameter regimes; and second, to look for the growth of mean magnetic field in the limit when $\mathrm{Re} < 1$. The limit of low Re is particularly interesting, as seeing a dynamo action in this limit would provide enough motivation for further theoretical investigations, which may focus the attention to this analytically more tractable limit of $\mathrm{Re} < 1$, as compared to the more formidable limit of $\mathrm{Re} > 1$. We demonstrate the large–scale dynamo action in the limit when $\mathrm{Re} < 1$ and $\mathrm{Rm} > 1$. We find a reasonably good agreement between our analytical findings of Ch. 6 and results of our simulations done in the limit when $(\mathrm{Re}, \mathrm{Rm}) < 1$. Temporal variations in α were observed in numerical simulations of the shear dynamo, even when the fluid is stirred non–helically (Brandenburg et al., 2008). We estimate the dynamo number ($D_{\alpha S}$), which was empirically defined in Brandenburg et al. (2008) corresponding to the *incoherent alpha–shear mechanism*[3], for

[3]A mechanism by which the fluctuations in α with no net value in conjunction with mean shear might give rise to the large–scale dynamo action in such systems.

many simulations, and found that the dynamo number ($D_{\alpha S}$) is always *supercritical* for cases, in which, we see dynamo growth, a result which is in agreement with Brandenburg et al. (2008). This suggested that the incoherent alpha–shear mechanism could plausibly be the reason for observed shear dynamo due to non–helical random stirring in these simulations.

In Ch. 8 we formulate the shear dynamo problem by considering temporal fluctuations in α, which have zero mean. Following the arguments of Kraichnan (1976); Sokolov (1997), we study this problem using the concept of double averaging. Starting with the usual α^2-Ω equation and treating α as a stochastic variable, we develop the equations for the mean and fluctuating magnetic fields. We derive explicit expressions for mean EMF and transport coefficients due to $\alpha-$fluctuations. Considering the case of slowly varying mean field, we derive expressions for mean EMF and magnetic diffusivity tensor. We then specialize to the case when the mean–field is a function only of the spatial coordinate X_3 and time τ. This reduction is useful for comparisons with earlier works. All components of the magnetic diffusivity tensor are derived which could be written in terms of the two–time correlator of fluctuating α. We derive the general expression for the dispersion relation which could be written in terms of three dimensionless parameters. Implications for dynamo action are discussed and we show analytically that the fluctuations in α with zero mean together with mean background shear can drive the large–scale dynamo action.

Part I

Navier-Stokes Equations: Free and Forced solutions & Passive Scalar Mixing

Chapter 2

Exact Solutions of The Navier-Stokes Equation: Plane Shearing Waves

2.1 Introduction

The Navier–Stokes equations are the fundamental equations governing the dynamics of the *Newtonian fluids*[1]. These are a set of inherently nonlinear partial differential equations, for which, no general solution is known. Exact solutions of the Navier–Stokes equations have been found only for a few specific problems of the fluid dynamics. Large number of important and apparently simple fluid dynamical problems, with variety of boundary conditions, continue to be the central topic of research due to the unavailability of the exact solutions. Finding any class of 'new' exact solutions, for any kind of fluid dynamical situation, is always extremely useful, and worth pursuing. Although any such solution must indeed satisfy the Navier–Stokes equations, the phrase "exact solution" has been given a special meaning in the literature (Wang, 1991; Drazin & Riley, 2006). It is usually described as following: it must be valid for all spacetime points, and for

[1]The Newtonian fluids are the ones for which the viscous stress is proportional to the rate of change of strain, i.e., the velocity gradient, within the fluid.

all values of viscosity; it should be expressible as finite terms of simple, elementary functions, i.e., it should be an explicit closed–form solution. Infinite–series solutions are often excluded from the definition of the exact solutions. The exact solutions describe the fundamental flows and are invaluable, as they usually offer a better understanding and physical insight, which may be obscured in the approximate or the numerical results. In the modern era of computational fluid dynamics, when we aim to study complicated problems using numerical techniques, it is legitimate to question the validity of such results obtained numerically. The exact solutions, thus, serve as a benchmark to test the accuracy of various numerical codes and approximate solutions.

In 1986 Craik and Criminale (Craik & Criminale, 1986) presented a class of exact solutions of the Navier–Stokes equations which were wavelike disturbances in background shear flows. Since then these solutions have proved extremely useful in the study of astrophysical and atmospheric fluid dynamics; a very useful collection of exact solutions can be found in Drazin & Riley (2006). The approach taken in Craik & Criminale (1986) was a generalization of a century–old method invented by Kelvin (Kelvin, 1887) to study linearized perturbations of Couette flows; see also Marcus & Press (1977). These shearing wave solutions, also referred to as *Kelvin modes*, have time–dependent wave vectors and amplitudes. This feature makes them extremely useful in local stability analysis (Lifschitz & Hameiri, 1991; Eckhardt & Yao, 1995). Although a single Kelvin mode is an exact solution of the full Navier–Stokes (NS) equations, it has been remarked (Craik & Criminale, 1986) that until about 1965 there seems to be no evidence that this was so recognized; in fact, the first published mention is as late as 1983 (Tung, 1983). Moreover, an explicit formula has been published (Kelvin, 1887; Craik & Criminale, 1986) for only one of the three components of the disturbance.

In this chapter, we have studied the incompressible Navier–Stokes equation in a background linear shear flow, which is unbounded. In § 2.2, we describe the set of equations being considered. In § 2.3, we construct shearing wave solutions of the Navier–Stokes equations for all three components of the velocity field of a Kelvin mode, in closed form using only elementary mathematical functions. These solutions are also the exact

solutions to the Navier–Stokes equations. We identify a subset of these modes whose wave vectors — though time–dependent — remain parallel to each other for all time. These are used to synthesize the most general plane transverse shearing wave, which can have any specified initial orientation, profile and polarization structure, with either unbounded or shear–periodic boundary conditions. We present our conclusions in § 2.3.

2.2 The model system

Let $(\boldsymbol{e}_1, \boldsymbol{e}_2, \boldsymbol{e}_3)$ be the unit basis vectors of a Cartesian coordinate system in the laboratory frame. Using notation, $\boldsymbol{x} = (x_1, x_2, x_3)$ for the position vector and t for time, we write the fluid velocity as $(Sx_1\boldsymbol{e}_2 + \boldsymbol{v})$, where S is the rate of shear parameter and $\boldsymbol{v}(\boldsymbol{x}, t)$ is an incompressible velocity field (i.e. $\boldsymbol{\nabla}\cdot\boldsymbol{v} = 0$), which is assumed to obey the Navier–Stokes equation expressed below for a fluid of unit mass density without any external forcing:

$$\left(\frac{\partial}{\partial t} + Sx_1\frac{\partial}{\partial x_2}\right)\boldsymbol{v} + Sv_1\boldsymbol{e}_2 + (\boldsymbol{v}\cdot\boldsymbol{\nabla})\,\boldsymbol{v} = -\boldsymbol{\nabla}p + \nu\nabla^2\boldsymbol{v} \tag{2.1}$$

The pressure, $p(\boldsymbol{x}, t)$, is determined by requiring that Eqn. (2.1) preserve the incompressibility of the flow. Then p satisfies the Poisson equation,

$$\nabla^2 p = -\boldsymbol{\nabla}\cdot[(\boldsymbol{v}\cdot\boldsymbol{\nabla})\,\boldsymbol{v}] - 2S\frac{\partial v_1}{\partial x_2} \tag{2.2}$$

2.3 Construction of the exact solutions

2.3.1 Sheared plane wave solutions

We seek a *single plane wave* solution to Eqns. (2.1) and (2.2) of the form,

$$\begin{aligned} \boldsymbol{v}_{\boldsymbol{k}}(\boldsymbol{x}, t) &= \mathrm{Re}\,\{\boldsymbol{A}(\boldsymbol{k}, t)\,\exp[\mathrm{i}\,\boldsymbol{K}(\boldsymbol{k}, t)\cdot\boldsymbol{x}]\}\ , \\ p_{\boldsymbol{k}}(\boldsymbol{x}, t) &= \mathrm{Re}\,\{\psi(\boldsymbol{k}, t)\,\exp[\mathrm{i}\,\boldsymbol{K}(\boldsymbol{k}, t)\cdot\boldsymbol{x}]\}\ , \end{aligned} \tag{2.3}$$

These single plane waves are also known as *single Kelvin modes*. The wavenumber ($\boldsymbol{K}$) and the amplitudes in the Eqn. (2.3) are explicit functions of time which depend on the rate of shear. The meaning of $\boldsymbol{k}$ will be made clear in some time. Incompressibility requires that

$$\boldsymbol{K}(\boldsymbol{k},t)\cdot\boldsymbol{A}(\boldsymbol{k},t) \;=\; 0 \tag{2.4}$$

The nonlinear term, $(\boldsymbol{v}\cdot\boldsymbol{\nabla})\boldsymbol{v}$, in Eqn. (2.1) vanishes identically due to the form of the plane waves given in Eqn. (2.3) and the incompressibility condition, Eqn. (2.4), as may be seen from the following:

$$(\boldsymbol{A}\cdot\boldsymbol{\nabla})\,\exp\left[\mathrm{i}\,\boldsymbol{K}(t)\cdot\boldsymbol{x}\right] \;=\; (\mathrm{i}\,\boldsymbol{K}\cdot\boldsymbol{A})\,\exp\left[\mathrm{i}\,\boldsymbol{K}(t)\cdot\boldsymbol{x}\right] \;=\; 0 \tag{2.5}$$

Using Eqn. (2.3) in Eqns. (2.1) and (2.2), we get

$$\frac{\partial\boldsymbol{A}}{\partial t} + \mathrm{i}\boldsymbol{A}\left(\boldsymbol{x}\cdot\frac{\partial\boldsymbol{K}}{\partial t} + Sx_1K_2\right) + SA_1\boldsymbol{e}_2 \;=\; -\mathrm{i}\boldsymbol{K}\psi - \nu K^2\boldsymbol{A} \tag{2.6}$$

$$-K^2\psi \;=\; -\mathrm{i}2SA_1K_2 \tag{2.7}$$

Only the terms inside the parentheses in Eqn. (2.6) are $\boldsymbol{x}$–dependent and hence they should vanish. This leads to the following form for the *time–dependent sheared wavevector* $\boldsymbol{K}$:

$$K_1 \;=\; k_1 - Stk_2, \qquad K_2 \;=\; k_2, \qquad K_3 \;=\; k_3 \tag{2.8}$$

where $\boldsymbol{k} = (k_1, k_2, k_3)$ is a constant wavevector[2]. Eliminating ψ using Eqn. (2.7) and following the argument leading to Eqn. (2.8), we find that $\boldsymbol{A}$ satisfies,

$$\frac{\partial\boldsymbol{A}}{\partial t} + SA_1\boldsymbol{e}_2 \;=\; 2SA_1\left(\frac{K_2\boldsymbol{K}}{K^2}\right) - \nu K^2\boldsymbol{A} \tag{2.9}$$

[2]We note that k_1, k_2 and k_3 are constant in time but they can in general be assigned any value and so they exhaust $k_1 - k_2 - k_3$ axes. Therefore we write $\boldsymbol{K} = \boldsymbol{K}(\boldsymbol{k},t)$

where $K^2 = |\boldsymbol{K}|^2 = \left[(k_1 - Stk_2)^2 + k_2^2 + k_3^2\right]$. Our aim now is to obtain explicit solutions for $\boldsymbol{A}$. To do this, we define a new amplitude variable, $\boldsymbol{a}(\boldsymbol{k}, t)$, by

$$\boldsymbol{A}(\boldsymbol{k}, t) \;=\; \widetilde{G}_\nu(\boldsymbol{k}, t)\, \boldsymbol{a}(\boldsymbol{k}, t)\,, \tag{2.10}$$

where $\widetilde{G}_\nu(\boldsymbol{k}, t)$ is a Fourier–space *viscous Green's function*[3],

$$\widetilde{G}_\nu(\boldsymbol{k}, t) \;=\; \exp\left[-\nu \int_0^t \mathrm{d}s\, K^2(s)\right] \;=\; \exp\left[-\nu \left(k^2 t \;-\; S k_1 k_2 t^2 \;+\; \frac{S^2}{3} k_2^2 t^3\right)\right]. \tag{2.11}$$

where $k^2 = (k_1^2 + k_2^2 + k_3^2)$. It may be noted from Eqn. (2.11) that $\widetilde{G}_\nu(\boldsymbol{k}, t)$ is an *even* function of $\boldsymbol{k}$ and k_3, and it is bounded between 0 and 1. When Eqns. (2.10) and (2.11) are substituted in Eqn. (2.9), we obtain the following equation for the new velocity variable, $a_i(\boldsymbol{k}, t)$, which may be written compactly as:

$$\frac{\partial a_i}{\partial t} \;-\; 2S \left(\frac{K_2 K_i}{K^2} - \frac{\delta_{i2}}{2}\right) a_1 \;=\; 0 \tag{2.12}$$

where $K_i = k_i - \delta_{i1} S t k_2$. It may be noted that the dependence of $\boldsymbol{A}(t)$ on the viscosity, ν, arises solely through the Fourier–space Green's function. It is helpful to display, in explicit form, all three components of Eqn. (2.12):

$$\frac{\partial a_1}{\partial t} \;-\; 2S \left[\frac{(k_1 - Stk_2)\, k_2}{(k_1 - Stk_2)^2 + k_2^2 + k_3^2}\right] a_1 \;=\; 0\,, \tag{2.13}$$

$$\frac{\partial a_2}{\partial t} \;-\; 2S \left[\frac{k_2^2}{(k_1 - Stk_2)^2 + k_2^2 + k_3^2} - \frac{1}{2}\right] a_1 \;=\; 0\,, \tag{2.14}$$

$$\frac{\partial a_3}{\partial t} \;-\; 2S \left[\frac{k_2 k_3}{(k_1 - Stk_2)^2 + k_2^2 + k_3^2}\right] a_1 \;=\; 0\,. \tag{2.15}$$

[3]See the Appendix A for the most general form of the resistive Green's function for linear shear flows, the expression for which has been explicitly given for both, the real space and the Fourier space. Compare, for instance, Eqns. (2.11) and (A.10).

Eqn. (2.13) can be solved to get an explicit expression for $a_1(\boldsymbol{k},t)$:

$$a_1(\boldsymbol{k},t) \;=\; \frac{k^2}{\left(k_1 - Stk_2\right)^2 + k_2^2 + k_3^2}\, a_1(\boldsymbol{k},0)\,, \tag{2.16}$$

which expression is given in Kelvin (1887). When this is substituted in Eqns. (2.14) and (2.15), the latter can be integrated to obtain expressions for $a_2(\boldsymbol{k},t)$ and $a_3(\boldsymbol{k},t)$. However, neither Kelvin nor anyone else, to the best of our knowledge, have published explicit formulae for these two components.[4] Below, we present the solutions for $a_2(\boldsymbol{k},t)$ and $a_3(\boldsymbol{k},t)$, which could be expressed entirely in terms of elementary functions:

$$\begin{aligned} a_2(\boldsymbol{k},t) \;=\; a_2(\boldsymbol{k},0) \;+\; \Bigg\{ & \frac{k^2 k_3^2}{k_2\left(k_2^2+k_3^2\right)^{3/2}} \left[\arctan\left(\frac{k_1 - Stk_2}{\sqrt{k_2^2+k_3^2}}\right) \;-\; \arctan\left(\frac{k_1}{\sqrt{k_2^2+k_3^2}}\right)\right] \\ & -\; \frac{k^2 k_2}{k_2^2+k_3^2}\left[\frac{k_1 - Stk_2}{\left(k_1-Stk_2\right)^2 + k_2^2 + k_3^2} \;-\; \frac{k_1}{k^2}\right]\Bigg\}\, a_1(\boldsymbol{k},0)\,, \end{aligned} \tag{2.17}$$

$$\begin{aligned} a_3(\boldsymbol{k},t) \;=\; a_3(\boldsymbol{k},0) \;-\; \Bigg\{ & \frac{k^2 k_3}{\left(k_2^2+k_3^2\right)^{3/2}} \left[\arctan\left(\frac{k_1 - Stk_2}{\sqrt{k_2^2+k_3^2}}\right) \;-\; \arctan\left(\frac{k_1}{\sqrt{k_2^2+k_3^2}}\right)\right] \\ & +\; \frac{k^2 k_3}{k_2^2+k_3^2}\left[\frac{k_1 - Stk_2}{\left(k_1-Stk_2\right)^2 + k_2^2 + k_3^2} \;-\; \frac{k_1}{k^2}\right]\Bigg\}\, a_1(\boldsymbol{k},0)\,. \end{aligned} \tag{2.18}$$

Incompressibility requires that $\boldsymbol{K}(\boldsymbol{k},t)\cdot\boldsymbol{a}(\boldsymbol{k},t) \;=\; 0$, which is guaranteed if the initial conditions are chosen such that $\boldsymbol{k}\cdot\boldsymbol{a}(\boldsymbol{k},0) \;=\; 0$. Note that $\boldsymbol{K}(\boldsymbol{k},0) = \boldsymbol{k}$. Thus, choosing $\boldsymbol{a}(t=0)$ and $\boldsymbol{k}$ to be orthogonal to each other at initial time, ensures that the condition of incompressibility is preserved for all time, i.e., $K_i(\boldsymbol{k},t)a_i(\boldsymbol{k},t) = k_i a_i(\boldsymbol{k},0) = 0$. From Eqns. (2.16)—(2.18), we can see that, at late times, $a_1(\boldsymbol{k},t) \to 0$, whereas both $a_2(\boldsymbol{k},t)$ and $a_3(\boldsymbol{k},t)$ saturate at non zero values. This happens because the background flow shears out the a_1 component, and generates the a_2 and a_3 components.

[4] Marcus & Press (1977) study perturbations of plane Couette flow using Kelvin waves. However, their analysis is limited to two dimensional perturbations, whereas the shearing waves we consider are fully three dimensional.

2.3.2 Velocity field in real form

When Eqns. (2.10), (2.11), (2.16)—(2.18) are substituted in Eqn. (2.3), we obtain the full velocity field of a single Kelvin mode. Our aim is to express the velocity field in its explicit *real* form. To do that, we use the arguments familiar from the discussion of the polarization of monochromatic plane electromagnetic waves (see, e.g., § 48 of Landau & Lifshitz (1975)).

Let us define the dimensionless and scale–invariant functions, $F_i(\boldsymbol{Q})$, as

$$F_i(\boldsymbol{Q}) \;=\; \frac{Q_3}{\sqrt{Q_2^2+Q_3^2}}\left[\frac{Q_3}{Q_2}\,\delta_{i2} \;-\; \delta_{i3}\right]\arctan\left(\frac{Q_1}{\sqrt{Q_2^2+Q_3^2}}\right) \;-\; \frac{Q_1 Q_i}{Q^2} \tag{2.19}$$

From Eqns. (2.10), (2.11), (2.16)—(2.18) and (2.19), we can compactly write the expression for $\boldsymbol{A}$ in component form as,

$$A_i(\boldsymbol{k},t) \;=\; \widetilde{G}_\nu(\boldsymbol{k},t)\left\{a_i(\boldsymbol{k},0) + \frac{k^2}{k_2^2+k_3^2}\left[F_i(\boldsymbol{K}(\boldsymbol{k},t)) - F_i(\boldsymbol{k})\right]\, a_1(\boldsymbol{k},0)\right\} \tag{2.20}$$

$\boldsymbol{A}$ (or $\boldsymbol{a}$) in the Eqn. (2.3) or (2.20) is, in general, a complex vector. It's square is (in general) a complex number. All the terms on the right hand side of Eqn. (2.20) are real, except $a_i(\boldsymbol{k},0)$, which is a complex quantity. Let us assume that the square of $\boldsymbol{a}(\boldsymbol{k},0)$ has argument equal to 2ϕ (i.e. $(a(\boldsymbol{k},0))^2 = \boldsymbol{a}(\boldsymbol{k},0)\cdot\boldsymbol{a}(\boldsymbol{k},0) = |(a(\boldsymbol{k},0))^2|e^{2\mathrm{i}\phi}$), then we define a complex vector $\boldsymbol{e}$ as

$$\boldsymbol{a}(\boldsymbol{k},0) \;=\; \boldsymbol{e}\exp\left[\mathrm{i}\phi\right]; \qquad\qquad \boldsymbol{k}\cdot\boldsymbol{e} \;=\; 0\,, \tag{2.21}$$

whose square, $e^2 = \boldsymbol{e}\cdot\boldsymbol{e} = |(a(\boldsymbol{k},0))^2|$, is a real quantity. We now express $\boldsymbol{e}$ in explicit form as,

$$\boldsymbol{e} \;=\; \boldsymbol{b} - \mathrm{i}\boldsymbol{c}\,; \qquad\qquad \boldsymbol{k}\cdot\boldsymbol{b} = 0\,; \qquad\qquad \boldsymbol{k}\cdot\boldsymbol{c} = 0\,, \tag{2.22}$$

where $\boldsymbol{b}$ and $\boldsymbol{c}$ are real vectors orthogonal to $\boldsymbol{k}$. Since $e^2 = (b^2 - c^2 - 2\mathrm{i}\boldsymbol{b}\cdot\boldsymbol{c})$ has been chosen to be a real quantity, we must have $\boldsymbol{b}\cdot\boldsymbol{c} = 0$. In other words, $\boldsymbol{b}$ and $\boldsymbol{c}$ are mutually orthogonal vectors lying in the plane perpendicular to $\boldsymbol{k}$. Using Eqns. (2.21) and (2.22),

we can write the Eqn. (2.20) as,

$$A_i(\boldsymbol{k},t) \;=\; \widetilde{G}_\nu(\boldsymbol{k},t)\left\{(b_i - \mathrm{i}\,c_i) + \frac{k^2}{k_2^2+k_3^2}\left[F_i(\boldsymbol{K}(\boldsymbol{k},t)) - F_i(\boldsymbol{k})\right]\,(b_1 - \mathrm{i}\,c_1)\right\} \qquad (2.23)$$

Thus the explicit real form of the velocity field of Eqn. (2.3) can be written in component form as,

$$\begin{aligned} v_i(\boldsymbol{x},\tau) \;\;=\;\; \widetilde{G}_\nu(\boldsymbol{k},t)\Bigg\{&\left[b_i + \frac{k^2}{k_2^2+k_3^2}\left[F_i(\boldsymbol{K}(\boldsymbol{k},t)) - F_i(\boldsymbol{k})\right]\,b_1\right]\cos\left[\boldsymbol{K}(\boldsymbol{k},t)\cdot\boldsymbol{x}+\phi\right] + \\ &+\left[c_i + \frac{k^2}{k_2^2+k_3^2}\left[F_i(\boldsymbol{K}(\boldsymbol{k},t)) - F_i(\boldsymbol{k})\right]\,c_1\right]\sin\left[\boldsymbol{K}(\boldsymbol{k},t)\cdot\boldsymbol{x}+\phi\right]\Bigg\} \end{aligned} \qquad (2.24)$$

We choose the directions of $\boldsymbol{b}$, $\boldsymbol{c}$ and $\boldsymbol{k}$ in such a way that they satisfy the following

$$\boldsymbol{k}\cdot\boldsymbol{c} = 0\,; \qquad\qquad \boldsymbol{e}_b = \boldsymbol{e}_k \times \boldsymbol{e}_c, \qquad (2.25)$$

where $\boldsymbol{e}_c$, $\boldsymbol{e}_b$ and $\boldsymbol{e}_k$ are unit vectors along the directions of $\boldsymbol{c}$, $\boldsymbol{b}$ and $\boldsymbol{k}$.
It may be verified that the structure of the mode depends on the dimensionless variable, St, and the dimensionless parameter, $(\nu k^2/S)$. The spatio–temporal behavior of these modes is briefly explored through Figs. (2.1) and (2.2). In order to understand its time variation, it is convenient to measure the velocity components at the origin (i.e., $\boldsymbol{x}=0$), as is done in Fig. (2.1). Fig. (2.1a) corresponds to the case of zero viscosity, $(\nu k^2/S)=0$. In this case $\widetilde{G}_\nu = 1$, and the plots give $\boldsymbol{v}(\boldsymbol{0},t) = \mathrm{Re}\{\boldsymbol{a}(\boldsymbol{k},t)\}$, where we can see the decay of a_1 and the saturation of a_2 and a_3 discussed above. In Fig. (2.1b), we have chosen $(\nu k^2/S) = -0.1$, so that all three components of $\boldsymbol{v}(\boldsymbol{0},t)$ ultimately suffer viscous decay. It can be seen that, before this decay, there is transient amplification of v_2 and v_3, due to competition between shear and viscosity. For larger values of viscosity (not shown here), this transient amplification may be absent because the damping can overwhelm shear.

Until now we have considered an unbounded flow. However, in numerical simulations of the local dynamics of differentially rotating discs in astrophysical systems (Binney & Tremaine, 2008; Balbus & Hawley, 1998), it is customary to employ "shear–periodic"

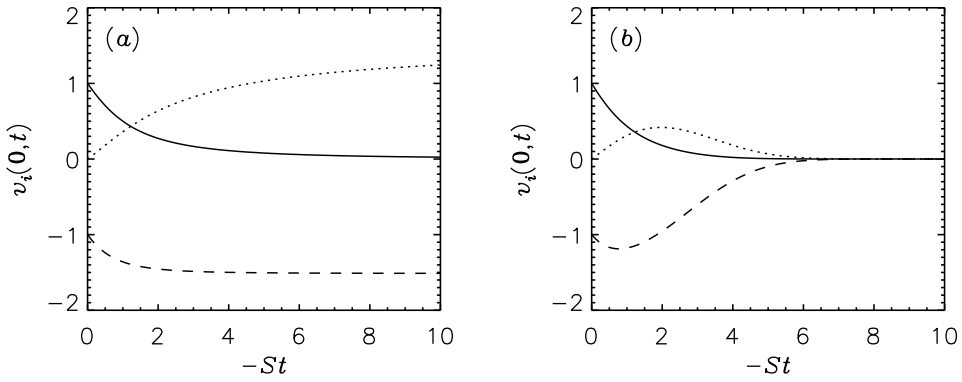

Figure 2.1: Plots of the three components of the velocity field, measured at the origin, as functions of St. We have chosen $\boldsymbol{k} = (1,1,1)$ and $\boldsymbol{a}(\boldsymbol{k},0) = (1,0,-1)$. The bold lines are for $v_1(\mathbf{0},t)$, the dotted for $v_2(\mathbf{0},t)$, and the dashed for $v_3(\mathbf{0},t)$. Panel (a) is for the non viscous case, $\nu = 0$, so the velocity components are identical to the amplitudes, $\boldsymbol{a}(\boldsymbol{k},t)$, of Eqns. (2.16)—(2.18). Panel (b) corresponds to $(\nu k^2/S) = -0.1$, and all three components ultimately suffer viscous decay.

boundary conditions. Let us define *sheared coordinates* by

$$x_1^{\rm sh} = x_1\,, \qquad x_2^{\rm sh} = x_2 - Stx_1\,, \qquad x_3^{\rm sh} = x_3\,. \tag{2.26}$$

These may be thought of as the Lagrangian coordinates of fluid elements that are carried along by the background shear flow. A function is said to be *shear–periodic* when it is a periodic function of $(x_1^{\rm sh}, x_2^{\rm sh}, x_3^{\rm sh})$ with periodicities (L_1, L_2, L_3), respectively. The phase of the function $\boldsymbol{v}_{\boldsymbol{k}}$ can be written as $\boldsymbol{K}(\boldsymbol{k},t)\cdot\boldsymbol{x} = \boldsymbol{k}\cdot\boldsymbol{x}^{\rm sh}$. Therefore, a shear–periodic Kelvin mode has wave vectors $\boldsymbol{k} \in (2\pi m_1/L_1, 2\pi m_2/L_2, 2\pi m_3/L_3)$, where the m_i take any integer values.

2.3.3 Superposition of Kelvin modes

We now use the explicit expressions obtained for the Kelvin modes to construct the most general plane transverse shearing wave. Let us consider two Kelvin modes, $\boldsymbol{v}_{\boldsymbol{k}}(\boldsymbol{x},t)$ and

$\boldsymbol{v}_{\boldsymbol{k}'}(\boldsymbol{x},t)$ corresponding to wave vectors $\boldsymbol{k}$ and $\boldsymbol{k}'$, which are parallel to each other but could differ in magnitudes. Using Eqns. (2.8), we see that the corresponding sheared wave vectors, $\boldsymbol{K}(\boldsymbol{k},t)$ and $\boldsymbol{K}(\boldsymbol{k}',t)$, are also parallel to each other for all time. Incompressibility implies that $\boldsymbol{v}_{\boldsymbol{k}}(\boldsymbol{x},t)$ and $\boldsymbol{v}_{\boldsymbol{k}'}(\boldsymbol{x},t)$ are perpendicular to $\boldsymbol{K}(\boldsymbol{k},t)$ and $\boldsymbol{K}(\boldsymbol{k}',t)$ for all time. So, if we superpose $\boldsymbol{v}_{\boldsymbol{k}}(\boldsymbol{x},t)$ and $\boldsymbol{v}_{\boldsymbol{k}'}(\boldsymbol{x},t)$, the nonlinear term in the Navier–Stokes equations vanishes, because the superposed velocity field remains parallel to the wavefronts. Thus *the superposition of an arbitrary number of Kelvin modes, all with wave vectors parallel to each other, is an exact solution of the Navier–Stokes equations.*

Let us choose a unit vector $\hat{\boldsymbol{n}} = (n_1, n_2, n_3)$, and define the sheared (non–unit) vector $\boldsymbol{n}^{\rm sh}(t)$ by

$$n_1^{\rm sh} \;=\; (n_1 - Stn_2)\;, \qquad n_2^{\rm sh} \;=\; n_2\,, \qquad n_3^{\rm sh} \;=\; n_3\,. \tag{2.27}$$

Superposing all Kelvin modes with wave vectors $\boldsymbol{q} = q\hat{\boldsymbol{n}}$, where $-\infty < q < \infty$, we obtain an exact plane–wave solution of the Navier–Stokes equations with wavefronts perpendicular to $\boldsymbol{n}^{\rm sh}(t)$:

$$\begin{aligned} v_i(\boldsymbol{x},t) \;\;=\;\; & \int_{-\infty}^{\infty} \frac{{\rm d}q}{2\pi}\, \widetilde{G}_\nu(q\hat{\boldsymbol{n}},t)\, \widetilde{W}_i(q)\, \exp\left[{\rm i}q\boldsymbol{n}^{\rm sh}(t)\boldsymbol{\cdot}\,\boldsymbol{x}\right] \;+ \\ & + \left[\frac{F_i\left(\boldsymbol{n}^{\rm sh}(t)\right) - F_i(\hat{\boldsymbol{n}})}{n_2^2+n_3^2}\right] \int_{-\infty}^{\infty} \frac{{\rm d}q}{2\pi}\, \widetilde{G}_\nu(q\hat{\boldsymbol{n}},t)\, \widetilde{W}_1(q)\, \exp\left[{\rm i}q\boldsymbol{n}^{\rm sh}(t)\boldsymbol{\cdot}\,\boldsymbol{x}\right] \end{aligned} \tag{2.28}$$

where the dimensionless and scale–invariant functions, $F_i(\boldsymbol{Q})$, are defined by Eqn. (2.19). For shear–periodic boundary conditions, the integral over q in Eqn. (2.28) should be replaced by an appropriate sum. The $\widetilde{\boldsymbol{W}}(q)$ are Fourier–space initial conditions corresponding to the $\boldsymbol{a}(\boldsymbol{k},0)$ of eqns. (2.16)—(2.18), and must satisfy the incompressibility condition, $\hat{\boldsymbol{n}}\boldsymbol{\cdot}\,\widetilde{\boldsymbol{W}}(q) \;=\; 0\,$. They are determined by the initial profile and polarization structure of the plane wave. At $t = 0$, the wavefronts are perpendicular to $\hat{\boldsymbol{n}}$, so we write $\boldsymbol{v}(\boldsymbol{x},0) \;=\; \boldsymbol{W}(\hat{\boldsymbol{n}}\boldsymbol{\cdot}\,\boldsymbol{x})$, where $\hat{\boldsymbol{n}}\boldsymbol{\cdot}\,\boldsymbol{W} \;=\; 0$. Note that the only constraint on the initial condition, $\boldsymbol{W}$, is that it is a vector field that is perpendicular everywhere to the unit vector $\hat{\boldsymbol{n}}$; otherwise it is a quite arbitrary function of its one argument. Thus, no

restriction need be placed on the initial profile and polarization structure of the initial conditions. Given $\boldsymbol{W}(y)$, we can determine $\widetilde{\boldsymbol{W}}(q) = \int_{-\infty}^{\infty} \mathrm{d}y\, \boldsymbol{W}(y) \exp\left[-\mathrm{i}qy\right]$, and use this in Eqn. (2.28) to calculate $\boldsymbol{v}(\boldsymbol{x}, t)$.

Eqn. (2.28) is a complete solution for a general plane shearing wave, expressed in terms of a Fourier integral. However, it is physically more transparent to rewrite the right side in terms of real–space quantities. To do this, we must introduce the real–space viscous Green's function, whose natural definition is with respect to the sheared coordinates[5]:

$$G_\nu\left(\boldsymbol{x}^{\mathrm{sh}}, t\right) \;=\; \int \frac{\mathrm{d}\boldsymbol{k}}{(2\pi)^3}\, \widetilde{G}_\nu(\boldsymbol{k}, t)\, \exp\left[\mathrm{i}\boldsymbol{k}\cdot\, \boldsymbol{x}^{\mathrm{sh}}\right]. \tag{2.29}$$

Noting that $\boldsymbol{n}^{\mathrm{sh}}(t)\cdot\, \boldsymbol{x} \;=\; \hat{\boldsymbol{n}}\cdot\, \boldsymbol{x}^{\mathrm{sh}}$, we can write the general form of the plane shearing wave as

$$\begin{aligned} v_i(\boldsymbol{x}, t) \quad &= \quad \int \mathrm{d}^3\xi\, G_\nu(\boldsymbol{\xi}, t)\, W_i\left(\hat{\boldsymbol{n}}\cdot\, [\boldsymbol{x}^{\mathrm{sh}}(t) - \boldsymbol{\xi}]\right) \;+ \\ &+ \quad \left[\frac{F_i\left(\boldsymbol{n}^{\mathrm{sh}}(t)\right) - F_i(\hat{\boldsymbol{n}})}{n_2^2 + n_3^2}\right] \int \mathrm{d}^3\xi\, G_\nu(\boldsymbol{\xi}, t)\, W_1\left(\hat{\boldsymbol{n}}\cdot\, [\boldsymbol{x}^{\mathrm{sh}}(t) - \boldsymbol{\xi}]\right) \end{aligned} \tag{2.30}$$

As an illustrative example let us consider the following initial condition, corresponding to a polarized wavepacket with wave vector pointing along the x_2–axis: $\hat{\boldsymbol{n}} = \boldsymbol{e}_2$, $W_1(x_2) = W_0 \exp\left[-x_2^2/2\sigma^2\right] \sin kx_2$, $W_2 \,=\, 0$, $W_3(x_2) \,=\, hW_0 \exp\left[-x_2^2/2\sigma^2\right] \cos kx_2$, where $-1 \,\leq\, h \,\leq\, 1$. The wavepacket is linearly polarized when $h \,=\, 0$, and right/left circularly polarized when $h \,=\, \pm 1$; other values of h correspond to different degrees of elliptical polarizations. At a later time, the wave vector has components $n_1^{\mathrm{sh}} \,=\, -St$, $n_2^{\mathrm{sh}} \,=\, 1$, $n_3^{\mathrm{sh}} = 0$. Since both W_i and $G_\nu(\boldsymbol{\xi}, t)$ are Gaussian functions, the integrals in Eqn. (2.30) can be performed analytically and $\boldsymbol{v}(\boldsymbol{x}, t)$ evaluated explicitly. We present the results

[5]The properties of this function are discussed in the Appendix A, where it is shown that it takes the form of a sheared heat kernel, which is an anisotropic Gaussian function of $\boldsymbol{x}^{\mathrm{sh}}$ with time–dependent coefficients; all the principal axes increase without bound and rotate against the direction of the background shear.

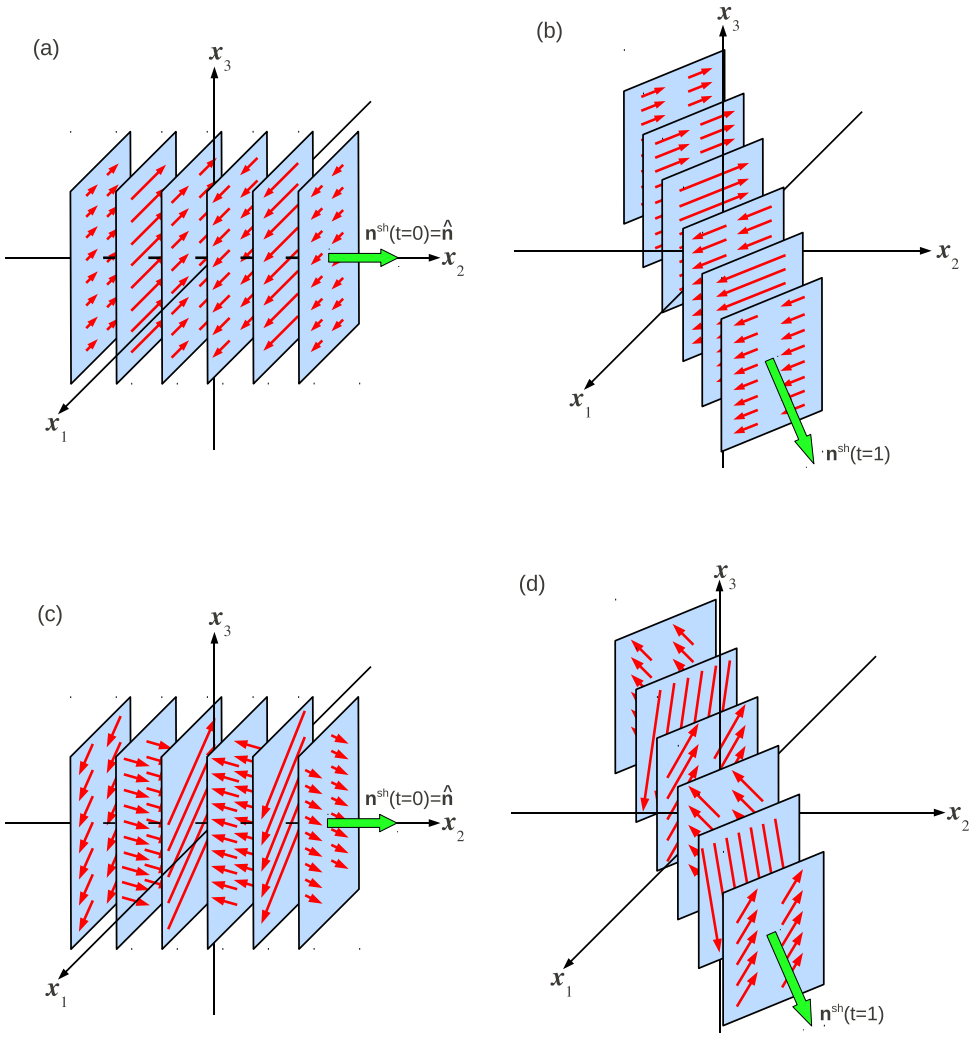

Figure 2.2: Evolution of plane transverse shearing wavepackets. The polarization structure of the velocity field is indicated on some sections of the plane wavefronts. The parameters values used are $S = -1$, $\nu = 1$, $W_0 = 1$, $\sigma = 10$ and $k = 1$. (a) and (b) show Linearly polarized ($h = 0$) wavepackets at times $t = 0$ and $t = 1$. (c) and (d) show Right circularly polarized ($h = 1$) at times $t = 0$ and $t = 1$.

graphically in Fig.(2.2) for two cases, one linearly polarized and the other right circularly polarized. As the wavepackets are sheared, they undergo transient amplification due to the combined action of shear and viscosity, and at late times suffer viscous damping.

2.4 Conclusion

We have constructed exact solutions of the Navier–Stokes equations with a background linear shear flow. All three components of the velocity field of the Kelvin modes are given in closed form using only elementary mathematical functions. An explicit real form of the velocity field was obtained. It was demonstrated that, when Kelvin modes with parallel wave vectors are superposed, they remain exact solutions. We give, in explicit form, the most general plane transverse shearing waves, with any specified initial orientation, profile and polarization structure, with either unbounded or shear–periodic boundary conditions. As an illustrative example, we show in Fig. (2.2) the evolution of plane transverse shearing wavepackets by considering linearly and right circularly polarized wavepackets. Such solutions represent the local structure of any disturbance in general shear flows, and can therefore be expected to find many applications in the theory and simulations of astrophysical and atmospheric flows.

Chapter 3

Forced Stochastic Velocity Dynamics

3.1 Introduction

Shear flows are common and seen in variety of astrophysical contexts; differential rotation in disc galaxies, accretion discs around compact objects etc. The study of waves and instabilities in astrophysical shear flows is complex but extremely useful. The shearing waves are excited in such systems by some random stirring in the medium, e.g., in disc galaxies the random supernovae (SNe) events stir the differentially rotating disc and excite shearing waves. These shearing waves lead to the mixing of various active and passive variables[1] embedded in the medium. It will be shown in later chapters that the shearing waves, which are excited by some random events in shear flows (due to, for example, SNe in disc galaxies), interact passively with the embedded seed magnetic field (without spatial ordering) of very small magnitude, and lead to the generation and growth of ordered magnetic fields by what is known as the dynamo action. Therefore the study of stochastically forced shear flows is itself an important problem and will be the focus of the present chapter. Shearing wave solutions for Navier–Stokes equations

[1]The passive variables do not act back on the flow whereas the active variables dynamically affect the flow.

without any external forcing were constructed in the last chapter, which were also the exact solutions.

In this chapter, we study the dynamics of an incompressible fluid in a background linear shear flow, by solving the *externally forced* Navier–Stokes equations in the limit of small fluid Reynolds number. The external forcing is assumed to be stochastic, as a response to which, the resulting velocity field is also expected to be stochastic, due to the linear nature of the Navier–Stokes equations in the limit of small fluid Reynolds number. Our aim is to model non–helical (mirror–symmetric) turbulence in linear shear flows and therefore we specialize to the case when the fluid is stirred non–helically. There is no *a priori* reason to guess that the resulting random velocity field due to non–helical random forcing will be non–helical. This important issue will also be addressed in this chapter. As will be seen in subsequent chapters that the transport phenomena of passive scalars or magnetic fields may be studied by solving the advection–diffusion equation or the induction equation, and the most fundamental quantities to be determined in order to compute various transport coefficients are unequal–time two–point velocity correlators. We study time correlation properties of such a turbulent flow.

In § 3.2, we solve the Navier–Stokes equations in background linear shear flow due to non–helical forcing in the limit of low fluid Reynolds number. An explicit solution for the velocity field is presented. Galilean invariance is a basic symmetry of the problem, which has been discussed in detail in Appendix B. Various two–point unequal time velocity correlators could be expressed in terms of a single entity, which is called the velocity spectrum tensor. In § 3.3, we derive the expression for velocity spectrum tensor in terms of Galilean–invariant forcing statistics. We demonstrate that the non–helical forcing gives rise to a non–helical velocity field. Various time correlation properties of the velocity field are discussed in § 3.4. We conclude in § 3.5.

3.2 Forced velocity dynamics for small Re

Let $(\boldsymbol{e}_1, \boldsymbol{e}_2, \boldsymbol{e}_3)$ be the unit basis vectors of a Cartesian coordinate system in the laboratory frame. Using notation, $\boldsymbol{X} = (X_1, X_2, X_3)$ for the position vector and τ for time, we write the fluid velocity as $(SX_1\boldsymbol{e}_2 + \boldsymbol{v})$, where S is the rate of shear parameter and $\boldsymbol{v}(\boldsymbol{X}, \tau)$ is an incompressible velocity deviation from the background linear shear flow. We consider the simplest of dynamics for the velocity field by ignoring Lorentz forces, and assuming that the fluid is stirred randomly by some external means. If the velocity fluctuations have root–mean–squared (rms) amplitude $v_{\rm rms}$ on some typical spatial scale ℓ, the fluid Reynolds number may be defined as ${\rm Re} = (v_{\rm rms}\ell/\nu)$, where ν is the kinematic viscosity; note that Re has been defined with respect to the fluctuation velocity field, not the background shear velocity field. In the limit of small Reynolds number (${\rm Re} \ll 1$), the nonlinear term in the Navier–Stokes equations may be ignored. Then the dynamics of the velocity field, $\boldsymbol{v}(\boldsymbol{X}, \tau)$, with unit mass density is governed by the randomly forced, linearized Navier–Stokes equations,

$$\left(\frac{\partial}{\partial\tau} \; + \; SX_1\frac{\partial}{\partial X_2}\right)\boldsymbol{v} \; + \; Sv_1\boldsymbol{e}_2 \; = \; -\boldsymbol{\nabla}p \; + \; \nu\nabla^2\boldsymbol{v} \; + \; \boldsymbol{f} \tag{3.1}$$

$\boldsymbol{f}(\boldsymbol{X}, \tau)$ is the random stirring force per unit mass which is assumed to be divergence–free with zero mean: $\boldsymbol{\nabla}\cdot\boldsymbol{f} = 0$ and $\langle\boldsymbol{f}\rangle = \boldsymbol{0}$.[2] The pressure variable, p, is determined by requiring that Eqn. (3.1) preserves the condition, $\boldsymbol{\nabla}\cdot\boldsymbol{v} = 0$. Then p satisfies the Poisson equation,

$$\nabla^2 p \; = \; -2S\frac{\partial v_1}{\partial X_2} \tag{3.2}$$

It should be noted that the linearity of the Eqns. (3.1) and (3.2) implies that the velocity fluctuations have zero mean, $\langle\boldsymbol{v}\rangle = \boldsymbol{0}$. It is clear from Eqn. (3.2) that p is a non local function of the velocity field, so it is best to work in Fourier–space.

[2] $\langle\ \rangle$ denotes ensemble averaging in the sense of Reynolds.

3.2.1 The Fourier space shearing transformation

Let $\tilde{\boldsymbol{v}}(\boldsymbol{K},\tau)$ be the spatial Fourier transform of $\boldsymbol{v}(\boldsymbol{X},\tau)$, defined by

$$\tilde{\boldsymbol{v}}(\boldsymbol{K},\tau) \;=\; \int \mathrm{d}^3X\, \boldsymbol{v}(\boldsymbol{X},\tau)\, \exp\left[-\mathrm{i}\boldsymbol{K}\boldsymbol{\cdot}\,\boldsymbol{X}\right]; \qquad\qquad [\boldsymbol{K}\boldsymbol{\cdot}\,\tilde{\boldsymbol{v}}(\boldsymbol{K},\tau)] \;=\; 0 \tag{3.3}$$

Using Eqn. (3.3) and taking the spatial Fourier transform of Eqn. (3.1), we can see that the Fourier transform of the velocity field, $\tilde{\boldsymbol{v}}(\boldsymbol{K},\tau)$, obeys,

$$\left(\frac{\partial}{\partial\tau} \;-\; SK_2\frac{\partial}{\partial K_1} \;+\; \nu K^2\right)\tilde{v}_i \;-\; 2S\left(\frac{K_2K_i}{K^2} \;-\; \frac{\delta_{i2}}{2}\right)\tilde{v}_1 \;=\; \tilde{f}_i \tag{3.4}$$

where $\tilde{f}_i(\boldsymbol{K},\tau)$ is the spatial Fourier transform of f_i. We can get rid of the inhomogeneous term, $(K_2\partial/\partial K_1)$, in Eqn. (3.4) by transforming from the old variables $(\boldsymbol{K},\tau)$ to new variables $(\boldsymbol{k},t)$, through the Fourier–space *shearing transformation*,

$$k_1 \;=\; K_1 \;+\; S\tau K_2, \qquad k_2 \;=\; K_2, \qquad k_3 \;=\; K_3, \qquad t \;=\; \tau \tag{3.5}$$

It may be verified using Eqn. (3.5) that the Eqn. (3.4) preserves the incompressibility condition $K_m\tilde{v}_m \;=\; 0$. We define new velocity and forcing variables, $a_i(\boldsymbol{k},t)$ and $g_i(\boldsymbol{k},t)$, respectively, by

$$\tilde{v}_i(\boldsymbol{K},\tau) \;=\; \widetilde{G}_\nu(\boldsymbol{k},t,0)\, a_i(\boldsymbol{k},t) \tag{3.6}$$

$$\tilde{f}_i(\boldsymbol{K},\tau) \;=\; \widetilde{G}_\nu(\boldsymbol{k},t,0)\, g_i(\boldsymbol{k},t) \tag{3.7}$$

where $\widetilde{G}_\nu(\boldsymbol{k},t,0)$ is the Fourier–space *viscous Green's function*, defined by[3]

$$\widetilde{G}_\nu(\boldsymbol{k},t,t') \;=\; \exp\left[-\nu\int_{t'}^{t}\mathrm{d}s\, K^2(\boldsymbol{k},s)\right] \tag{3.8}$$

[3]See the Appendix A for a general discussion on the resistive Green's function, which is given in both, the real space and the Fourier space. Some general properties have also been discussed.

Noting the fact that $\boldsymbol{K}(\boldsymbol{k},s) = (k_1 - Ssk_2, k_2, k_3)$ and $K^2(\boldsymbol{k},s) = |\boldsymbol{K}(\boldsymbol{k},s)|^2$, the viscous Green's function can be calculated in explicit form as

$$\widetilde{G}_\nu(\boldsymbol{k},t,t') = \exp\left[-\nu\left(k^2(t-t') - S\,k_1\,k_2\,(t^2-t'^2) + \frac{S^2}{3}k_2^2(t^3-t'^3)\right)\right] \tag{3.9}$$

We note that $\widetilde{G}_\nu(\boldsymbol{k},t,t')$ is a positive quantity which takes values between 0 and 1, and that it is an even function of $\boldsymbol{k}$ and k_3. Also, $\widetilde{G}_\nu(\boldsymbol{k},t,t') = \widetilde{G}_\nu(\boldsymbol{k},t,s) \times \widetilde{G}_\nu(\boldsymbol{k},s,t')$, for any s. The inverse of the Fourier–space shearing transformation is given as,

$$K_1 = k_1 - Stk_2, \qquad K_2 = k_2, \qquad K_3 = k_3, \qquad \tau = t \tag{3.10}$$

The partial derivatives transform as,

$$\frac{\partial}{\partial K_j} = \frac{\partial}{\partial k_j} + St\delta_{j2}\frac{\partial}{\partial k_1}; \qquad \frac{\partial}{\partial \tau} = \frac{\partial}{\partial t} + Sk_2\frac{\partial}{\partial k_1} \tag{3.11}$$

Evolution equation for the new velocity variable $a_i(\boldsymbol{k},t)$ may be written by using Eqns. (3.6), (3.7), (3.10) and (3.11) in the Eqn. (3.4):

$$\frac{\partial a_i}{\partial t} - 2S\left(\frac{K_2K_i}{K^2} - \frac{\delta_{i2}}{2}\right)a_1 = g_i \tag{3.12}$$

where $\boldsymbol{K}(\boldsymbol{k},t) = (k_1 - Stk_2, k_2, k_3)$ and $K^2(\boldsymbol{k},t) = |\boldsymbol{K}(\boldsymbol{k},t)|^2$ as given by Eqn. (3.10). It can be verified that Eqn. (3.12) preserves the dot product, $K_i a_i = 0$. We also note that the dependence of the velocities, $\tilde{v}_i(\boldsymbol{K},\tau)$ on the viscosity ν arises solely through the Fourier–space Green's function given by Eqn. (3.9).

3.2.2 Explicit solution for $\boldsymbol{a}(\boldsymbol{k}, t)$

It is helpful to display, in explicit form, all three components of Eqn. (3.12):

$$\frac{\partial a_1}{\partial t} \; - \; 2S \left(\frac{K_1 K_2}{K^2} \right) a_1 \quad = \quad g_1 \tag{3.13}$$

$$\frac{\partial a_2}{\partial t} \; - \; 2S \left(\frac{K_2^2}{K^2} - \frac{1}{2} \right) a_1 \quad = \quad g_2 \tag{3.14}$$

$$\frac{\partial a_3}{\partial t} \; - \; 2S \left(\frac{K_2 K_3}{K^2} \right) a_1 \quad = \quad g_3 \tag{3.15}$$

Then Eqn. (3.13) can be solved to get an explicit expression for $a_1(\boldsymbol{k}, t)$. When this is substituted in Eqns. (3.14) and (3.15), they can be integrated directly to obtain expressions for $a_2(\boldsymbol{k}, t)$ and $a_3(\boldsymbol{k}, t)$. The *forced* (or particular) solution, with initial condition $a_i(\boldsymbol{k}, 0) \; = \; 0$ is

$$a_i(\boldsymbol{k}, t) \quad = \quad \int_0^t \mathrm{d}s \, g_i(\boldsymbol{k}, s) \; + \; \int_0^t \mathrm{d}s \, \left[\Lambda_i(\boldsymbol{K}(\boldsymbol{k}, t)) \; - \; \Lambda_i(\boldsymbol{K}(\boldsymbol{k}, s)) \right] \frac{K^2(\boldsymbol{k}, s)}{K_\perp^2} \, g_1(\boldsymbol{k}, s) \tag{3.16}$$

where $K_\perp^2 \; \equiv \; K_2^2 + K_3^2 \; = \; k_2^2 + k_3^2 \; \equiv \; k_\perp^2$, and the function, Λ_i, is defined as

$$\Lambda_i(\boldsymbol{K}) \quad = \quad - \, \frac{K_1 K_i}{K^2} \; + \; \frac{K_3}{K_\perp} \left[\frac{K_3}{K_2} \, \delta_{i2} \; - \; \delta_{i3} \right] \arctan \left(\frac{K_1}{K_\perp} \right) \tag{3.17}$$

Eqn. (3.16), together with Eqns. (3.17), (3.6) and (3.7), completely specifies the velocity field in the Fourier space, $\tilde{v}_i(\boldsymbol{K}, \tau)$. Taking inverse Fourier transform of $\tilde{v}_i(\boldsymbol{K}, \tau)$ gives us the expression for the velocity field in real space.

3.3 The velocity spectrum tensor

We wish to determine the unequal–time, two–point velocity correlator, which may be given by,

$$\langle v_i(\boldsymbol{X},\tau)\, v_j(\boldsymbol{X}',\tau')\rangle = \int \frac{\mathrm{d}^3K}{(2\pi)^3}\,\frac{\mathrm{d}^3K'}{(2\pi)^3}\,\exp\left[\mathrm{i}\,(\boldsymbol{K}\boldsymbol{\cdot}\boldsymbol{X}-\boldsymbol{K}'\boldsymbol{\cdot}\boldsymbol{X}')\right]\left\langle \tilde{v}_i\,(\boldsymbol{K},t)\,\tilde{v}_j^*\,(\boldsymbol{K}',t')\right\rangle \tag{3.18}$$

Also, we wish to work out the correlation between the velocity field and its gradient, which will be useful for our later purposes. This may be given by,

$$\begin{aligned}\langle v_i(\boldsymbol{X},\tau)\, v_{jl}(\boldsymbol{X}',\tau')\rangle &= \frac{\partial}{\partial X_l'}\langle v_i(\boldsymbol{X},\tau)\, v_j(\boldsymbol{X}',\tau')\rangle \\ &= \int \frac{\mathrm{d}^3K}{(2\pi)^3}\,\frac{\mathrm{d}^3K'}{(2\pi)^3}\,(-\mathrm{i}\,K_l')\,\exp\left[\mathrm{i}\,(\boldsymbol{K}\boldsymbol{\cdot}\boldsymbol{X}-\boldsymbol{K}'\boldsymbol{\cdot}\boldsymbol{X}')\right]\times \\ &\qquad \times\left\langle \tilde{v}_i\,(\boldsymbol{K},t)\,\tilde{v}_j^*\,(\boldsymbol{K}',t')\right\rangle \end{aligned} \tag{3.19}$$

where $v_{jl}(\boldsymbol{X}',\tau') = (\partial v_j/\partial X_l')$. As may be seen from Eqns. (3.18) and (3.19) that the quantity to be determined, in order to find various real–space correlators between velocities and their gradients, is Fourier–space two–point unequal–time velocity correlator, $\left\langle \tilde{v}_i\,(\boldsymbol{K},t)\,\tilde{v}_j^*\,(\boldsymbol{K}',t')\right\rangle$. Our interest is in developing a *Galilean invariant* statistics of the stochastic velocity field in the background linear shear flow, which has been discussed in detail in the Appendix B. It is proved in the Appendix B that a G–invariant Fourier–space two–point velocity correlator must be of the form given by Eqn. (B.7), which suggests that the most fundamental object, which needs to be determined in order to find various velocity correlators, is the *velocity spectrum tensor*, $\Pi_{ij}(\boldsymbol{k},t,t')$[4]. Below we wish to determine $\Pi_{ij}(\boldsymbol{k},t,t')$ in terms of the forcing.

[4]See Eqn. (B.8) of the Appendix B for the properties of $\Pi_{ij}(\boldsymbol{k},t,t')$.

3.3.1 $\Pi_{jm}(\boldsymbol{k}, t, t')$ expressed in terms of the forcing

Our goal is to express the velocity spectrum tensor in terms of the statistical properties of the forcing. If the forcing is Galilean–invariant, then its two–point correlator should possess the same general properties (see Eqns. B.7 and B.8 given in the Appendix B) as the two–point velocity correlator. In other words, we must have,

$$\left\langle \tilde{f}_j(\boldsymbol{K}, \tau)\, \tilde{f}^*_m(\boldsymbol{K}', \tau') \right\rangle \;=\; (2\pi)^6\, \delta(\boldsymbol{k} - \boldsymbol{k}')\Phi_{jm}(\boldsymbol{k}, t, t') \tag{3.20}$$

where the *forcing spectrum tensor*, $\Phi_{jm}(\boldsymbol{k}, t, t')$, must satisfy,

$$\begin{aligned}
\Phi_{jm}(\boldsymbol{k}, t, t') &= \Phi^*_{jm}(-\boldsymbol{k}, t, t') \;=\; \Phi_{mj}(-\boldsymbol{k}, t', t) \\
K_j \Phi_{jm}(\boldsymbol{k}, t, st') &= [k_j - St\, \delta_{j1} k_2]\; \Phi_{jm}(\boldsymbol{k}, t, t') \;=\; 0 \\
K'_m \Phi_{jm}(\boldsymbol{k}, t, t') &= [k_m - St'\, \delta_{m1} k_2]\; \Phi_{jm}(\boldsymbol{k}, t, t') \;=\; 0
\end{aligned} \tag{3.21}$$

We are now ready to use the dynamical solution obtained in § 3.2. Using Eqns. (3.6) and (3.16), Fourier–space, unequal–time, two–point velocity correlator is given by,

$$
\begin{aligned}
\langle \tilde{v}_j(\boldsymbol{K},\tau)\,\tilde{v}^*_m(\boldsymbol{K}',\tau')\rangle &= \widetilde{G}_\nu(\boldsymbol{k},t,0)\,\widetilde{G}_\nu(\boldsymbol{k}',t',0)\,\langle \tilde{a}_j(\boldsymbol{k},t)\,\tilde{a}^*_m(\boldsymbol{k}',t')\rangle \\
&= \widetilde{G}_\nu(\boldsymbol{k},t,0)\,\widetilde{G}_\nu(\boldsymbol{k}',t',0)\int_0^t \mathrm{d}s \int_0^{t'} \mathrm{d}s' \;\times \\
&\quad \times\Bigg\{ \langle g_j(\boldsymbol{k},s)\,g^*_m(\boldsymbol{k}',s')\rangle \;+ \\
&+ \left[\Lambda_j(\boldsymbol{K}(\boldsymbol{k},t)) - \Lambda_j(\boldsymbol{K}(\boldsymbol{k},s))\right]\frac{K^2(\boldsymbol{k},s)}{K_\perp^2}\,\langle g_1(\boldsymbol{k},s)\,g^*_m(\boldsymbol{k}',s')\rangle + \\
&+ \left[\Lambda_m(\boldsymbol{K}(\boldsymbol{k}',t')) - \Lambda_m(\boldsymbol{K}(\boldsymbol{k}',s'))\right]\frac{K^2(\boldsymbol{k}',s')}{K_\perp'^2}\,\langle g_j(\boldsymbol{k},s)\,g^*_1(\boldsymbol{k}',s')\rangle + \\
&+ \left[\Lambda_j(\boldsymbol{K}(\boldsymbol{k},t)) - \Lambda_j(\boldsymbol{K}(\boldsymbol{k},s))\right]\left[\Lambda_m(\boldsymbol{K}(\boldsymbol{k}',t')) - \Lambda_m(\boldsymbol{K}(\boldsymbol{k}',s'))\right]\times \\
&\qquad \times \frac{K^2(\boldsymbol{k},s)K^2(\boldsymbol{k}',s')}{K_\perp^2 K_\perp'^2}\,\langle g_1(\boldsymbol{k},s)\,g^*_1(\boldsymbol{k}',s')\rangle\Bigg\} \qquad (3.22)
\end{aligned}
$$

Using Eqns. (3.7) and (3.20), we write

$$
\begin{aligned}
\langle g_j(\boldsymbol{k},s)\,g^*_m(\boldsymbol{k}',s')\rangle &= \frac{1}{\widetilde{G}_\nu(\boldsymbol{k},s,0)\,\widetilde{G}_\nu(\boldsymbol{k}',s',0)}\left\langle \tilde{f}_j(\boldsymbol{K}(\boldsymbol{k},s),s)\,\tilde{f}^*_m(\boldsymbol{K}(\boldsymbol{k}',s'),s')\right\rangle \\
&= \frac{1}{\widetilde{G}_\nu(\boldsymbol{k},s,0)\,\widetilde{G}_\nu(\boldsymbol{k}',s',0)}(2\pi)^6\,\delta(\boldsymbol{k}-\boldsymbol{k}')\Phi_{jm}(\boldsymbol{k},t,t') \qquad (3.23)
\end{aligned}
$$

Using $\widetilde{G}_\nu(\boldsymbol{k},t,0)(\widetilde{G}_\nu(\boldsymbol{k},s,0))^{-1}=\widetilde{G}_\nu(\boldsymbol{k},t,s)$, Eqns. (3.22), (3.23) and (B.7) give,

$$\begin{aligned}
\Pi_{jm}(\boldsymbol{k},t,t') &= \int_0^t \mathrm{d}s \int_0^{t'} \mathrm{d}s'\, \widetilde{G}_\nu(\boldsymbol{k},t,s)\,\widetilde{G}_\nu(\boldsymbol{k},t',s')\times \\
&\quad \times\Bigg\{\Phi_{jm}(\boldsymbol{k},s,s') \;+ \\
&+ \left[\Lambda_j(\boldsymbol{K}(\boldsymbol{k},t)) - \Lambda_j(\boldsymbol{K}(\boldsymbol{k},s))\right]\frac{K^2(\boldsymbol{k},s)}{K_\perp^2}\Phi_{1m}(\boldsymbol{k},s,s') \;+ \\
&+ \left[\Lambda_m(\boldsymbol{K}(\boldsymbol{k},t')) - \Lambda_m(\boldsymbol{K}(\boldsymbol{k},s'))\right]\frac{K^2(\boldsymbol{k},s')}{K_\perp^2}\Phi_{j1}(\boldsymbol{k},s,s') \;+ \\
&+ \left[\Lambda_j(\boldsymbol{K}(\boldsymbol{k},t)) - \Lambda_j(\boldsymbol{K}(\boldsymbol{k},s))\right]\left[\Lambda_m(\boldsymbol{K}(\boldsymbol{k},t')) - \Lambda_m(\boldsymbol{K}(\boldsymbol{k},s'))\right]\times \\
&\qquad \times\frac{K^2(\boldsymbol{k},s)K^2(\boldsymbol{k},s')}{K_\perp^4}\,\Phi_{11}(\boldsymbol{k},s,s')\Bigg\}
\end{aligned} \tag{3.24}$$

When $\Phi_{jm}(\boldsymbol{k},t,t')$ is real, the forcing may be called non helical. Then Eqn. (3.24) proves that the velocity spectrum tensor, $\Pi_{jm}(\boldsymbol{k},t,t')$ is also a real quantity.

The *correlation helicity* may be defined as,

$$H_{\rm cor}(t,t') \;=\; \epsilon_{jlm}\,\langle v_j(\boldsymbol{0},t)\,v_{ml}(\boldsymbol{0},t')\rangle \;=\; \mathrm{i}\int \mathrm{d}^3k\;[k_l - St'\delta_{l1}k_2]\,\epsilon_{ljm}\Pi_{jm}(\boldsymbol{k},t,t') \tag{3.25}$$

where we have used Eqns. (3.10) and (3.19). From the first of Eqns. (B.8), it is clear that the real part of $\Pi_{jm}(\boldsymbol{k},t,t')$ is an even function of $\boldsymbol{k}$, whereas the imaginary part is an odd function of $\boldsymbol{k}$. Hence only the imaginary part of $\Pi_{jm}(\boldsymbol{k},t,t')$ contributes to the correlation helicity. Therefore, for non–helical forcing, for which $\Phi_{jm}(\boldsymbol{k},t,t')$ is real, implying that $\Pi_{jm}(\boldsymbol{k},t,t')$ is also a real quantity, we see from Eqn. (3.25) that the correlation helicity, $H_{\rm cor}(t,t')$, vanishes. In other words, *non helical forcing of an incompressible fluid at low* Re*, in the absence of Lorentz forces, gives rise to a non helical velocity field.* This may not seem like a particularly surprising conclusion, but it is by no means an obvious one, because at high Re it may happen that $\Pi_{jm}(\boldsymbol{k},t,t')$ is complex even when $\Phi_{jm}(\boldsymbol{k},t,t')$ is real.

We now specialize to the case when the forcing is not only *non helical*, but *isotropic* and *delta–correlated–in–time* as well; in this case,

$$\Phi_{jm}(\boldsymbol{k}, s, s') \;=\; \delta(s - s')\, P_{jm}(\boldsymbol{K}(\boldsymbol{k}, s))\, F\left(\frac{K(\boldsymbol{k}, s)}{K_F}\right) \tag{3.26}$$

where $K(\boldsymbol{k}, s) = |\boldsymbol{K}(\boldsymbol{k}, s)|$, $K_F = \ell^{-1}$ is the wavenumber at which the fluid is stirred, $P_{jm}(\boldsymbol{K}) = (\delta_{jm} - K_j K_m / K^2)$ is a projection operator, and $F(K/K_F) \geq 0$ is the *forcing power spectrum*. We substitute Eqn. (3.26) in (3.24), and reduce the double–time integrals to a single–time integral using,

$$\int_0^t \mathrm{d}s \int_0^{t'} \mathrm{d}s'\, \delta(s - s')\, w(\boldsymbol{k}, s, s') \;=\; \int_0^{t_<} \mathrm{d}s\, w(\boldsymbol{k}, s, s) \tag{3.27}$$

where $t_< = \mathrm{Min}\,(t, t')$. Then the velocity spectrum tensor takes the form,

$$\begin{aligned}
\Pi_{jm}(\boldsymbol{k}, t, t') \;=\; & \int_0^{t_<} \mathrm{d}s\; \widetilde{G}_\nu(\boldsymbol{k}, t, s)\, \widetilde{G}_\nu(\boldsymbol{k}, t', s)\, F\left(\frac{K(\boldsymbol{k}, s)}{K_F}\right) \times \\
& \times \Bigg\{ P_{jm}(\boldsymbol{K}(\boldsymbol{k}, s)) \;+ \\
& + \;\left[\Lambda_j(\boldsymbol{K}(\boldsymbol{k}, t)) \;-\; \Lambda_j(\boldsymbol{K}(\boldsymbol{k}, s))\right] \frac{K^2(\boldsymbol{k}, s)}{K_\perp^2} P_{1m}(\boldsymbol{K}(\boldsymbol{k}, s)) \;+ \\
& + \;\left[\Lambda_m(\boldsymbol{K}(\boldsymbol{k}, t')) \;-\; \Lambda_m(\boldsymbol{K}(\boldsymbol{k}, s))\right] \frac{K^2(\boldsymbol{k}, s)}{K_\perp^2} P_{j1}(\boldsymbol{K}(\boldsymbol{k}, s)) \;+ \\
& + \;\left[\Lambda_j(\boldsymbol{K}(\boldsymbol{k}, t)) \;-\; \Lambda_j(\boldsymbol{K}(\boldsymbol{k}, s))\right] \left[\Lambda_m(\boldsymbol{K}(\boldsymbol{k}, t')) \;-\; \Lambda_m(\boldsymbol{K}(\boldsymbol{k}, s))\right] \times \\
& \qquad \times \frac{K^4(\boldsymbol{k}, s)}{K_\perp^4}\, P_{11}(\boldsymbol{K}(\boldsymbol{k}, s)) \Bigg\}
\end{aligned} \tag{3.28}$$

which can be completely determined when the forcing power spectrum, $F(K/K_F)$, be specified. Also note that although Φ_{jm} is delta–correlated–in–time, the velocity spectrum tensor, Π_{jm}, and hence the resulting velocity field is *not* delta–correlated–in–time. This may be attributed to the inertia of the fluid particles.

3.4 Time correlation properties of the fluid velocity

We now discuss some of the simplest statistical properties of the random velocity field. Let an observer located at the origin of the laboratory frame correlate fluid velocities at time $\tau = t$ and at time $\tau' = t'$. The two–point function that measures this quantity may be written by setting $\boldsymbol{X} = \boldsymbol{X}' = \boldsymbol{0}$ in Eqn. (3.18) and using Eqn. (B.7),

$$\langle v_j(\boldsymbol{0},\tau) v_m(\boldsymbol{0},\tau')\rangle \;=\; R_{jm}(\boldsymbol{0},t,t') \;=\; \int \mathrm{d}^3k\; \Pi_{jm}(\boldsymbol{k},t,t') \tag{3.29}$$

where we used $\mathrm{d}^3K\,\mathrm{d}^3K' = \mathrm{d}^3k\,\mathrm{d}^3k'$, as the Jacobian of transformation from $K-$variables to $k-$variables is unity. It can be proved that, in the long time limit when $t \to \infty$ and $t' \to \infty$, $R_{jm}(\boldsymbol{0},t,t')$ is a function only of the difference, $(t-t')$. To do this, we need to manipulate the $\boldsymbol{k}$–space integral in Eqn. (3.29), and make use of properties of the viscous Green's function noted earlier, which are given in detail in the Appendix A. First, we change from the integration variable, $\boldsymbol{k}$ to $\boldsymbol{K}(\boldsymbol{k},s)$, which we now write simply as $\boldsymbol{K}$. In other words, given $\boldsymbol{K}$ and s, the variable $\boldsymbol{k}$ is given by

$$\boldsymbol{k} \;=\; \boldsymbol{k}(\boldsymbol{K},s) \;=\; (K_1 + SsK_2, K_2, K_3)$$

Then

$$\int \mathrm{d}^3k \int_0^{t_<} \mathrm{d}s \;\equiv\; \int \mathrm{d}^3K \int_0^{t_<} \mathrm{d}s$$

$$\boldsymbol{K}(\boldsymbol{k},t) \;=\; (k_1 - Stk_2, k_2, k_3) \;=\; (K_1 + S(s-t)K_2, K_2, K_3) \;=\; \boldsymbol{k}(\boldsymbol{K}, s-t)$$

$$\boldsymbol{K}(\boldsymbol{k},t') \;=\; \boldsymbol{k}(\boldsymbol{K}, s-t')$$

Working out the exponent of the viscous Green's function

$$k^2(t-s) - Sk_1k_2(t^2-s^2) + \frac{S^2}{3}k_2^2(t^3-s^3) \;=\; K^2(t-s) - SK_1K_2(t-s)^2 + \frac{S^2}{3}K_2^2(t-s)^3$$

which implies that

$$\widetilde{G}_\nu(\boldsymbol{k},t,s) \;=\; \widetilde{G}_\nu(\boldsymbol{K}(\boldsymbol{k},s),t-s,0) \;=\; \widetilde{G}_\nu(\boldsymbol{K},t-s,0)$$

$$\widetilde{G}_\nu(\boldsymbol{k},t',s) \;=\; \widetilde{G}_\nu(\boldsymbol{K},t'-s,0)$$

Then

$$\begin{aligned} R_{jm}(\mathbf{0},t,t') \;=\; & \int \mathrm{d}^3K\; F\left(\frac{K}{K_F}\right) \int_0^{t_<} \mathrm{d}s\; \widetilde{G}_\nu(\boldsymbol{K},t-s,0)\, \widetilde{G}_\nu(\boldsymbol{K},t'-s,0) \Bigg\{ P_{jm}(\boldsymbol{K}) \;+ \\ & + \;\left[\Lambda_j(\boldsymbol{k}(\boldsymbol{K},s-t)) \;-\; \Lambda_j(\boldsymbol{K})\right] \frac{K^2}{K_\perp^2} P_{1m}(\boldsymbol{K}) \;+ \\ & + \;\left[\Lambda_m(\boldsymbol{k}(\boldsymbol{K},s-t')) \;-\; \Lambda_m(\boldsymbol{K})\right] \frac{K^2}{K_\perp^2} P_{j1}(\boldsymbol{K}) \;+ \\ & + \;\left[\Lambda_j(\boldsymbol{k}(\boldsymbol{K},s-t)) \;-\; \Lambda_j(\boldsymbol{K})\right] \left[\Lambda_m(\boldsymbol{k}(\boldsymbol{K},s-t')) \;-\; \Lambda_m(\boldsymbol{K})\right] \times \\ & \qquad \times \frac{K^4}{K_\perp^4}\, P_{11}(\boldsymbol{K}) \Bigg\} \end{aligned} \tag{3.30}$$

We now discuss some important properties of the velocity correlator $R_{jm}(\mathbf{0},t,t')$:

1. We can come to some general conclusions about the functional dependence of $R_{jm}(\mathbf{0},t,t')$. Let F_0 be a typical value of the forcing function, $F(K/K_F)$. Then it can be verified from Eqn. (3.30) that

$$R_{jm}(\mathbf{0},t,t') \;=\; R^{ZS} \;\times\; \widehat{R}_{jm}\left(\nu K_F^2 t\,,\; \nu K_F^2 t'\,;\; \frac{S}{\nu K_F^2}\right) \tag{3.31}$$

where the constant

$$R^{ZS} \;=\; \frac{4\pi}{3}\left(\frac{F_0 K_F}{\nu}\right) \tag{3.32}$$

is a typical value of R_{jm} in the absence of shear (see Eqn. 3.37 below). The function, $\widehat{R}_{jm}$, is a dimensionless function of the two dimensionless variables, $(\nu K_F^2 t)$ and $(\nu K_F^2 t')$, as well as the dimensionless parameter, $(S/\nu K_F^2)$.

2. The components $R_{13}(\mathbf{0},t,t')$, $R_{31}(\mathbf{0},t,t')$, $R_{23}(\mathbf{0},t,t')$ and $R_{32}(\mathbf{0},t,t')$ are all zero. This happens because, for these values of the indices (j,m), the integrand in Eqn. (3.30) is an odd function of K_3 .

3. It is of interest to look at the behavior of the *equal–time* correlator, $R_{jm}(\mathbf{0},t,t)$, as a function of t. By definition, this is symmetric, $R_{jm}(\mathbf{0},t,t) = R_{mj}(\mathbf{0},t,t)$. A related quantity is the root–mean–squared velocity, $v_{\rm rms}(t)$, defined by

$$v^2_{\rm rms}(t) \;=\; R_{11}(\mathbf{0},t,t) \;+\; R_{22}(\mathbf{0},t,t) \;+\; R_{33}(\mathbf{0},t,t) \tag{3.33}$$

In the long–time limit, we expect both $R_{jm}(\mathbf{0},t,t)$ and $v_{\rm rms}(t)$ to saturate due to the balance reached between forcing and viscous dissipation; see Figs. (3.1a–e). Let $v^\infty_{\rm rms} = \lim_{t\to\infty} v_{\rm rms}(t)$. We now define useful dimensionless quantities:

$$\begin{aligned} {\rm Re} \;&=\; \frac{v^\infty_{\rm rms}}{\nu K_F}\,; \qquad \textit{Fluid Reynolds number} \\ {\rm Sh} \;&=\; \frac{S}{v^\infty_{\rm rms} K_F}\,; \qquad \textit{Dimensionless Shear parameter} \end{aligned} \tag{3.34}$$

For numerical computations, it is necessary to choose a form for the forcing power spectrum. A quite common choice, used especially in numerical simulations, is forcing which is confined to a spherical shell of magnitude K_F. Therefore, whenever we need to choose a form for the forcing power spectrum, we take it to be,

$$F\left(\frac{K}{K_F}\right) \;=\; F_0\,\delta\left(\frac{K}{K_F}-1\right) \tag{3.35}$$

For this forcing, in the case of *zero shear*, Eqn. (3.30) gives,

$$\lim_{S\to 0} R_{jm}(\mathbf{0},t,t') \;=\; \delta_{jm}\,R^{ZS}\left[\exp\left[-\nu K_F^2(t-t')\right] \;-\; \exp\left[-\nu K_F^2(t+t')\right]\right] \tag{3.36}$$

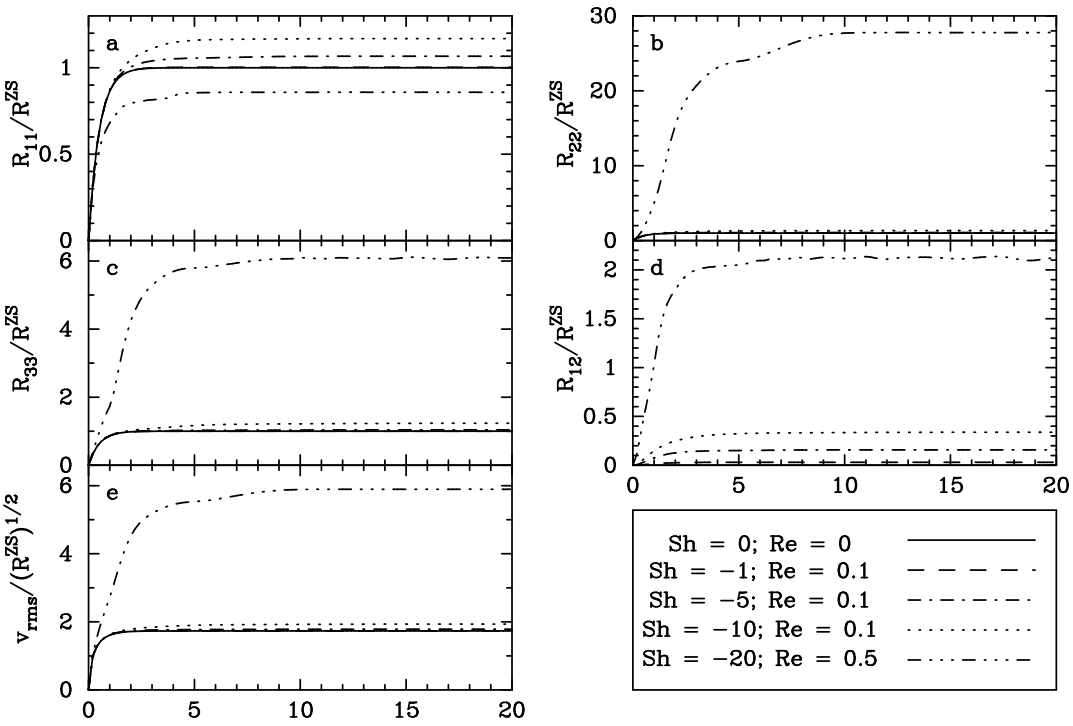

Figure 3.1: Plots of $R_{jm}(\mathbf{0},t,t)$ scaled with respect to R^{ZS}, and $v_{\rm rms}(t)$ scaled with respect to $\sqrt{R^{ZS}}$. The abscissa in all figures is the dimensionless time variable $(\nu K_F^2\, t)$.

and the equal–time quantities are,

$$\begin{aligned}\lim_{S\to 0} R_{jm}(\mathbf{0},t,t) &= \delta_{jm}\, R^{ZS}\left[1 \;-\; \exp\left(-2\nu K_F^2 t\right)\right] \\ \lim_{S\to 0} v_{\rm rms}(t) &= \sqrt{3R^{ZS}\left[1 \;-\; \exp\left(-2\nu K_F^2 t\right)\right]}\end{aligned} \tag{3.37}$$

Figs. (3.1a–d) display plots of $R_{jm}(\mathbf{0},t,t)$ versus t, and Fig. (3.1e) displays $v_{\rm rms}(t)$ versus t. Some of the noteworthy properties are as follows:

(i) Only the non vanishing components of R_{jm}, namely $R_{11}(\mathbf{0},t,t)$, $R_{22}(\mathbf{0},t,t)$, $R_{33}(\mathbf{0},t,t)$, $R_{12}(\mathbf{0},t,t) = R_{21}(\mathbf{0},t,t)$, are plotted. R_{jm} has been scaled with respect to R^{ZS} of Eqn. (3.32), and $v_{\rm rms}$ has been scaled with respect to $\sqrt{R^{ZS}}$.

(ii) From item (1) above and Eqns. (3.34), we can see that $R_{jm}(\mathbf{0},t,t)$ and $v_{\rm rms}(t)$ depend on the dimensionless time variable, $(\nu K_F^2 t)$, and the dimensionless

parameter, $(S/\nu K_F^2) = \mathrm{Sh} \times \mathrm{Re}$. We choose $\mathrm{Sh} \leq 0$, i.e., the sign of the rate of shear (S) is assumed to be negative. For comparison, the expressions in Eqn. (3.37), giving $R_{jm}(\mathbf{0}, t, t)$ and $v_{\mathrm{rms}}(t)$ for the case of zero shear ($\mathrm{Sh} = 0$), are shown in bold lines in Fig. (3.1).

(iii) All the components of $R_{jm}(\mathbf{0}, t, t)$ are zero at time equal to zero; they grow and saturate at late times.

(iv) As the control parameter $|\mathrm{Sh}|\,\mathrm{Re}$ increases, R_{11} begins saturating at values above that for the case of zero shear (i.e. R^{ZS}) and somewhere in the range, $1 < |\mathrm{Sh}|\,\mathrm{Re} < 10$, the saturation value starts decreasing, dropping below R^{ZS}.

(v) As $|\mathrm{Sh}|\,\mathrm{Re}$ increases, both R_{22} and R_{33} saturate at values above R^{ZS}. Of the three diagonal components, R_{22} is the largest, R_{33} is the next largest, and R_{11} is the smallest component.

(vi) R_{12} vanishes for the case of zero shear, and saturates at larger positive values which increase with increasing $|\mathrm{Sh}|\,\mathrm{Re}$.

(vii) The contribution to v_{rms} is dominated by R_{22}.

4. Another property of interest is the long–time behavior of the *two–time* correlator $R_{jm}(\mathbf{0}, t, t')$. Without loss of generality, we assume that $t \geq t'$. Changing the integration variable from s to $\xi = t' - s$ in Eqn. (3.30),

$$
\begin{aligned}
R_{jm}(\mathbf{0}, t, t') \;=\; & \int \mathrm{d}^3K\; F\left(\frac{K}{K_F}\right) \int_0^{t'} \mathrm{d}\xi\; \widetilde{G}_\nu(\boldsymbol{K}, t - t' + \xi, 0)\, \widetilde{G}_\nu(\boldsymbol{K}, \xi, 0) \Bigg\{ P_{jm}(\boldsymbol{K}) \;+ \\
& + \; [\Lambda_j(\boldsymbol{k}(\boldsymbol{K}, -(t - t' + \xi))) \;-\; \Lambda_j(\boldsymbol{K})]\, \frac{K^2}{K_\perp^2} P_{1m}(\boldsymbol{K}) \;+ \\
& + \; [\Lambda_m(\boldsymbol{k}(\boldsymbol{K}, -\xi)) \;-\; \Lambda_m(\boldsymbol{K})]\, \frac{K^2}{K_\perp^2} P_{j1}(\boldsymbol{K}) \;+ \\
& + \; [\Lambda_j(\boldsymbol{k}(\boldsymbol{K}, -(t - t' + \xi))) \;-\; \Lambda_j(\boldsymbol{K})]\, [\Lambda_m(\boldsymbol{k}(\boldsymbol{K}, -\xi)) \;-\; \Lambda_m(\boldsymbol{K})] \times \\
& \qquad \times \frac{K^4}{K_\perp^4}\, P_{11}(\boldsymbol{K}) \Bigg\}
\end{aligned}
$$

On the right side, the variables t and t' occur only in the combination $(t-t')$, except in the upper limit of the ξ–integral. So, in the long time limit when $t \to \infty$ and $t' \to \infty$, but $(t-t')$ is held constant at some finite value, the right side is a function only of $(t-t')$. i.e.

$$\begin{aligned}
R^{\infty}_{jm}(t-t') \;&\equiv\; \lim_{t \geq t' \to \infty} R_{jm}(\mathbf{0}, t, t') \\
&= \int \mathrm{d}^3K \; F\left(\frac{K}{K_F}\right) \int_0^{\infty} \mathrm{d}\xi \; \widetilde{G}_{\nu}(\boldsymbol{K}, t-t'+\xi, 0)\, \widetilde{G}_{\nu}(\boldsymbol{K}, \xi, 0) \Bigg\{ P_{jm}(\boldsymbol{K}) \; + \\
&+ \; [\Lambda_j(\boldsymbol{k}(\boldsymbol{K}, -(t-t'+\xi))) \; - \; \Lambda_j(\boldsymbol{K})] \, \frac{K^2}{K_{\perp}^2} P_{1m}(\boldsymbol{K}) \; + \\
&+ \; [\Lambda_m(\boldsymbol{k}(\boldsymbol{K}, -\xi)) \; - \; \Lambda_m(\boldsymbol{K})] \, \frac{K^2}{K_{\perp}^2} P_{j1}(\boldsymbol{K}) \; + \\
&+ \; [\Lambda_j(\boldsymbol{k}(\boldsymbol{K}, -(t-t'+\xi))) - \Lambda_j(\boldsymbol{K})] \times \\
&\qquad \times [\Lambda_m(\boldsymbol{k}(\boldsymbol{K}, -\xi)) - \Lambda_m(\boldsymbol{K})] \, \frac{K^4}{K_{\perp}^4} P_{11}(\boldsymbol{K}) \Bigg\}
\end{aligned} \tag{3.38}$$

Thus the two–time velocity correlator becomes *stationary* in the limit of long times, when a balance has been achieved between stirring and viscous dissipation; as Figs. (3.2a-e) show, they decay with the time difference, $(t-t')$. For the case of zero shear, Eqn. (3.36) gives,

$$\lim_{S \to 0} R^{\infty}_{jm}(t-t') \;=\; \delta_{jm} \, R^{ZS} \, \exp\left[-\nu K_F^2 (t-t')\right] \tag{3.39}$$

Figs. (3.2a–e) display the five independent components of $R^{\infty}_{jm}(t-t')$ versus $(t-t')$; all of them decay with increasing $|t-t'|$. For comparison, we have plotted in bold lines the case of zero shear given in Eqn. (3.39). Of the three diagonal components, R^{∞}_{11} is the least affected by shear, whereas R^{∞}_{22} is the most affected by shear. Note that R^{∞}_{12} and R^{∞}_{21} look symmetric for small shear, but for large shear they are seen to be highly antisymmetric.

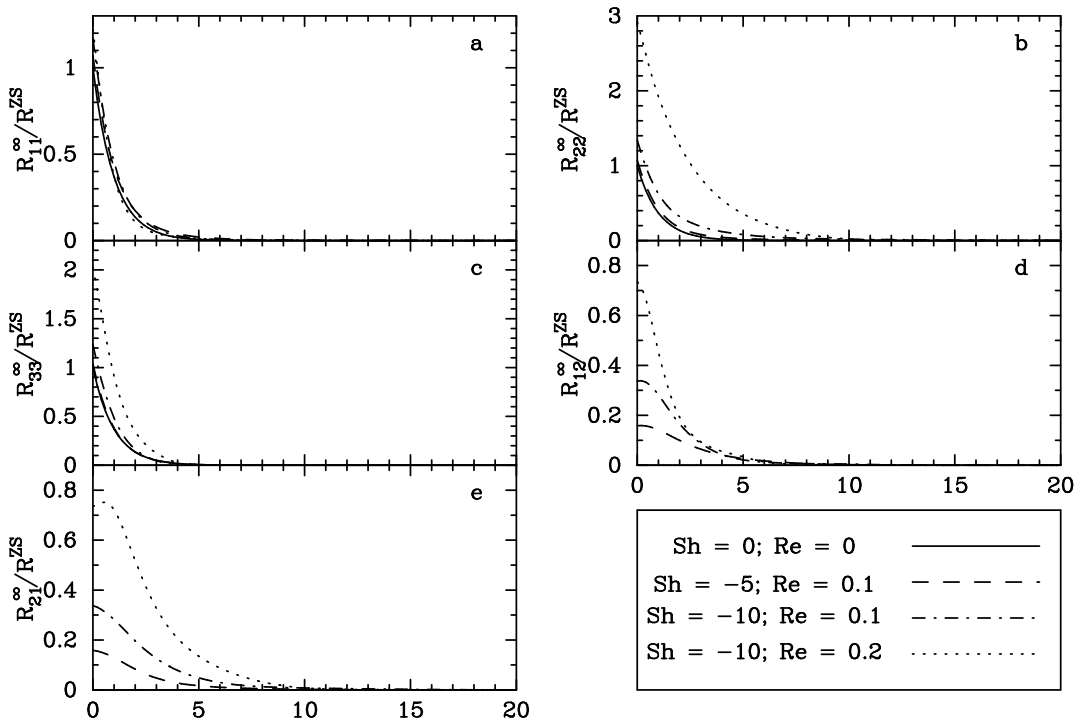

Figure 3.2: Plots of $R^{\infty}_{jm}(t-t')$ scaled with respect to R^{ZS}. The abcissa in all figures is the dimensionless time variable $[\nu K_F^2\,(t-t')]$.

3.5 Conclusions

Stochastically forced incompressible shear flows were studied by solving the Navier–Stokes equations in the absence of Lorentz forces with a background linear shear flow with external forcing in the limit of small fluid Reynolds numbers. The forcing is assumed to be non–helical (mirror–symmetric), as our aim is to model the non–helical random flow in linear shear flows. Taking the Fourier transform of the Navier–Stokes equations and using the Fourier–space *shearing transformation*, we develop the Green's function solutions for the velocity field. Using the result presented in the Appendix B on the Galilean invariant Fourier–space two–point velocity correlator, we show that the unequal–time two–point velocity correlator, and the correlation between the velocity and its gradient, may be expressed in terms of a single entity, Π_{jm}, which is called the *velocity spectrum tensor*. Velocity correlators could be expressed in terms of the forcing correlators, and noting the fact that the Galilean invariant forcing must also possess the same general

properties given in the Appendix B for the velocity correlators, we could express the velocity spectrum tensor in terms of the forcing spectrum tensor, Φ_{jm}. We note that the forcing is non–helical when Φ_{jm} is real, and for such a forcing, Π_{jm} is also a real quantity. Therefore we conclude that non helical forcing of an incompressible fluid at low Re, in the absence of Lorentz forces, gives rise to a non helical velocity field. We then specialize to the case when Φ_{jm} is not only non–helical, but also isotropic and delta–correlated–in–time. We show that the resulting velocity field is not delta–correlated–in–time. This may be attributed to the inertia of the fluid particles. We study some of the simplest statistical properties of the random flow by deriving expressions for the velocity correlators measured from the origin of the laboratory frame at two different times. Such two–point functions were denoted as $R_{jm}(\mathbf{0}, t, t')$. The root–mean–squared velocity could be defined by the trace of the *equal–time* correlator $R_{jm}(\mathbf{0}, t, t)$. We also note that the equal–time correlator is symmetric in the indices j and m. Then it is shown that the *two–time* velocity correlator becomes *stationary* in the long–time limit, which is expected once a balance has been achieved between stirring and viscous dissipation. We summarize some of the key results below:

1. The non helical forcing of an incompressible fluid at low Re, in the absence of Lorentz forces, gives rise to a non helical velocity field.

2. For the delta–correlated–in–time forcing, the resulting velocity field is *not* delta–correlated–in–time. This may be attributed to the inertia of the fluid particles.

3. Only the diagonal components of $R_{jm}(\mathbf{0}, t, t')$ are non–zero in the limit of zero shear, and for equal–time correlator we find $R_{jm}(\mathbf{0}, t, t) = R_{mj}(\mathbf{0}, t, t)$.

4. $R_{jm}(\mathbf{0}, t, t)$ and $v_{\rm rms}(t)$ depend only on two dimensionless variables, $(\nu K_F^2 t)$ and $(S/\nu K_F^2) = {\rm Sh} \times {\rm Re}$. The contribution to $v_{\rm rms}$ is dominated by R_{22}.

5. All the components of $R_{jm}(\mathbf{0}, t, t)$ are zero at time equal to zero; they grow and saturate at late times. The non–zero components of $R_{jm}(\mathbf{0}, t, t)$ are $R_{11}(\mathbf{0}, t, t)$, $R_{22}(\mathbf{0}, t, t)$, $R_{33}(\mathbf{0}, t, t)$ and $R_{12}(\mathbf{0}, t, t) = R_{21}(\mathbf{0}, t, t)$.

6. The *two–time* velocity correlator becomes *stationary* in the long–time limit (denoted by $R^{\infty}_{jm}(t-t')$), which is expected once a balance has been achieved between stirring and viscous dissipation.

7. The non–trivial effects of the shear may be seen from Figs. (3.1) and (3.2).

Chapter 4

Passive Scalar Mixing due to Turbulence in a Linear Shear Flow

4.1 Introduction

A passive scalar is a substance mixed with the fluid in such a low concentration that it does not affect the dynamics of the fluid; few examples could be the smoke in the air, chemicals in the atmosphere, dye diffusing in the turbulent flow etc. The passive scalar is advected by the flow and exhibits complex dynamical behaviour if the flow be turbulent. The study of the mixing of a "passive scalar field" due to a turbulent flow is important in various areas of natural sciences, esp. astrophysics, atmospheric science, engineering physics, biophysics etc; see the reviews by Shraiman & Siggia (2000); Warhaft (2000); Falkovich, Gawedzki & Vergassola (2001). It is known that turbulence leads to more effective mixing of such substances. It has been argued in Shraiman & Siggia (2000) that the phenomenon of turbulent transport of the passive scalar is closely related to the 'turbulence' itself, which is still an unsolved problem. Whereas the formulation and the study of the problem of the passive scalar mixing is much simpler, its better understanding could prove to be insightful for the problems of pure turbulence.

In this chapter, our aim is to understand the evolution of the *mean* concentration of the passive scalar, which is "ordered" over larger spatial scales than that of the random

flow, where the background shear flow is assumed to be given. We study this problem under the framework of "mean–field" theory (Moffatt, 1978; Krause & Rädler, 1980). Such studies have recently been carried out numerically by Madarassy & Brandenburg (2010) in which, the transport of the passive scalar was studied in linear shear flow which was stirred both helically and non–helically. All the components of the turbulent diffusivity tensor were numerically determined by test–field method[1] and it was found that: shear leads to anisotropic diffusion of the passive scalar significantly modifying its turbulent transport; and the transport properties are unaffected by the presence of helicity. There have been previous studies on the evolution of mean concentration of passive scalar in the absence of background shear (Elperin et al., 2000; Blackman & Field, 2003).

The shearing waves, excited due to the random stirring of the background shear flow, were studied in the last chapter. We will show that these shearing waves tend to effectively mix the embedded passive scalars (and the magnetic fields, which will be studied in detail in part II of this thesis). In § 4.2 we formulate the problem of mean–field theory of passive scalar mixing for small Peclet numbers (Pe). Our theory is non–perturbative in the shear parameter. Using Reynolds averaging, we split the total concentration into mean and fluctuating components. The equation for fluctuations is expanded perturbatively in the small parameter, Pe. Using the shearing coordinate transformation, we write the Green's function solution for the fluctuating component. We use the properties of the resistive Green's function and its Fourier transform, which has been derived in the Appendix A, to write the explicit expressions for the fluctuations and the turbulent flux at low Pe. Galilean invariance is a fundamental symmetry of the problem and is discussed in the Appendix B. In § 4.3 we provide the Galilean invariant expressions for the turbulent flux at low Pe. In § 4.4 we write the mean–field advection–diffusion equation in sheared coordinates and note that its evolution is governed by an integro–differential equation. We then take the limit of slowly varying mean–field, for which, the integro–differential equation simplifies to the partial differential equation. The

[1]see Brandenburg et al. (2008) or Ch. 7 of this thesis for a brief discussion on the test–field method.

transport coefficients are given in general form in terms of the two–point correlators of the fluctuating velocity field. An explicit expression for the transport coefficients in terms of the velocity spectrum tensor is given. The velocity spectrum tensor is the fundamental object which has been determined in Ch. 2. All components of the transport coefficient, κ_{jm}, are evaluated and presented in § 4.5. In § 4.6 we discuss the implications for the amplification of the mean concentration due to non–helical flows. We then conclude in § 4.7.

4.2 Mean–field theory of passive scalar mixing in a linear shear flow

4.2.1 The limit of small Peclet number Pe

Let $(\boldsymbol{e}_1, \boldsymbol{e}_2, \boldsymbol{e}_3)$ be the unit vectors of a Cartesian coordinate system in the lab frame, $\boldsymbol{X} = (X_1, X_2, X_3)$ the position vector, and τ the time. The fluid velocity is given by $(SX_1\boldsymbol{e}_2 + \boldsymbol{v})$, where S is the rate of shear parameter and $\boldsymbol{v}(\boldsymbol{X}, \tau)$ is a randomly fluctuating velocity field which is incompressible, $\boldsymbol{\nabla \cdot v} = 0$. Our goal is to develop a mean–field theory of the mixing of a passive scalar added to the fluid.

We assume that the total concentration, $\mathcal{C}(\boldsymbol{X}, \tau)$, of the passive scalar obeys the *advection–diffusion equation*:

$$\left(\frac{\partial}{\partial \tau} + SX_1 \frac{\partial}{\partial X_2}\right)\mathcal{C} + \boldsymbol{v \cdot \nabla}\mathcal{C} = \kappa \boldsymbol{\nabla}^2 \mathcal{C} \tag{4.1}$$

where κ is the molecular diffusivity of the passive scalar. The velocity fluctuations could be deterministic or turbulent, freely generated by instabilities or forced externally. We assume that the randomly varying fluctuations have zero mean, $\langle \boldsymbol{v} \rangle = \boldsymbol{0}$, with root–mean–squared amplitude $v_{\rm rms}$ on some typical spatial scale ℓ. $\langle\ \rangle$ denotes ensemble averaging in the sense of Reynolds. The dimensionless parameter *Peclet number* may be defined as $\mathrm{Pe} = (v_{\rm rms}\ell/\kappa)$; note that Pe has been defined with respect to the fluctuation

velocity field, not the background shear velocity field.

The passive scalar is mixed by the velocity field; we write $\mathcal{C}$ as the sum of a *mean*, $C(\boldsymbol{X},\tau)$, and a *fluctuating* part, $c(\boldsymbol{X},\tau)$:

$$\mathcal{C} \;=\; C \;+\; c\,, \qquad \langle\mathcal{C}\rangle \;=\; C\,, \qquad \langle c\rangle \;=\; 0 \tag{4.2}$$

Applying Reynolds averaging to the Eqn. (4.1), we obtain the following equations governing the dynamics of the mean and fluctuating components:

$$\left(\frac{\partial}{\partial\tau} \;+\; SX_1\frac{\partial}{\partial X_2}\right)C \quad=\quad -\boldsymbol{\nabla\cdot F} \;+\; \kappa\boldsymbol{\nabla}^2 C \tag{4.3}$$

$$\left(\frac{\partial}{\partial\tau} \;+\; SX_1\frac{\partial}{\partial X_2}\right)c \quad=\quad -\boldsymbol{v\cdot\nabla}C \;+\; \kappa\boldsymbol{\nabla}^2 c \;-\; \boldsymbol{\nabla\cdot}\left[c\boldsymbol{v}-\boldsymbol{F}\right] \tag{4.4}$$

where $\boldsymbol{F}=\langle c\boldsymbol{v}\rangle$ is the mean flux density of the passive scalar due to random advection; we refer to $\boldsymbol{F}$ simply as the *turbulent flux*. The first step toward solving the problem is to calculate $\boldsymbol{F}$ and obtain a closed equation for the mean–field, $C(\boldsymbol{X},\tau)$.

When $\mathrm{Pe}\ll 1$, we can expand c in a series,

$$c \;=\; c^{(0)} \;+\; c^{(1)} \;+\; c^{(2)} \;+\; \ldots \tag{4.5}$$

where $c^{(n)}$ is of order $c^{(n-1)}$ multiplied by the small quantity Pe. The equations governing the time evolution of these quantities are

$$\left(\frac{\partial}{\partial\tau} \;+\; SX_1\frac{\partial}{\partial X_2}\right)c^{(0)} \quad=\quad -\boldsymbol{v\cdot\nabla}C \;+\; \kappa\boldsymbol{\nabla}^2 c^{(0)} \tag{4.6}$$

$$\left(\frac{\partial}{\partial\tau} \;+\; SX_1\frac{\partial}{\partial X_2}\right)c^{(n)} \quad=\quad \kappa\boldsymbol{\nabla}^2 c^{(n)} \;-\; \boldsymbol{\nabla\cdot}\left[c^{(n-1)}\boldsymbol{v}-\left\langle c^{(n-1)}\boldsymbol{v}\right\rangle\right]$$
$$\text{for } n \;=\; 1,2,\ldots \tag{4.7}$$

Note that $-\boldsymbol{v}\cdot\boldsymbol{\nabla}C$ acts as a source term for $c^{(0)}$, whereas the source term for $c^{(n)}$ is $-\boldsymbol{\nabla}\cdot\left[c^{(n-1)}\boldsymbol{v}-\left\langle c^{(n-1)}\boldsymbol{v}\right\rangle\right]$. Once the $c^{(n)}$ have been determined, the mean flux density can be calculated directly by

$$\boldsymbol{F} \;=\; \langle c\boldsymbol{v}\rangle \;=\; \left\langle \left(c^{(0)} \;+\; c^{(1)} \;+\; c^{(2)} \;+\; \ldots\right)\boldsymbol{v}\right\rangle \tag{4.8}$$

Here, we focus on the determination of the lowest order term, $c^{(0)}$. It should be understood as the *First Order Smoothing Approximation*, (FOSA). The evolution of $c^{(0)}$ is governed by Eqn. (4.6) which we will solve and determine the mean flux density. General methods of solving equations such as Eqn. (4.6) are presented in Krause & Rädler (1980), but we prefer to employ *the shearing coordinate transformation* because it is directly adapted to the problem at hand and greatly simplifies the task of writing down the Green's function solution. The $(X_1\partial/\partial X_2)$ term makes Eqn. (4.6) inhomogeneous in the coordinate X_1. This term can be eliminated through a shearing transformation to new spacetime variables, given in Eqn. (A.2) of Appendix A. Thus, using Eqns. (A.2) and (A.3), given in the Appendix A, and defining the new variables:

$$\Psi(\boldsymbol{x},t) \;=\; C(\boldsymbol{X},\tau)\,, \qquad \psi(\boldsymbol{x},t) \;=\; c^{(0)}(\boldsymbol{X},\tau)\,, \qquad \boldsymbol{u}(\boldsymbol{x},t) \;=\; \boldsymbol{v}(\boldsymbol{X},\tau) \tag{4.9}$$

we can write Eqn. (4.6) as,

$$\left(\frac{\partial}{\partial t} \;-\; \kappa\boldsymbol{\nabla}^2\right)\psi(\boldsymbol{x},t) \;=\; -\left[u_m \;-\; St\delta_{m2}\,u_1\right]\Psi_m \tag{4.10}$$

where $\boldsymbol{\nabla}^2$ is given by Eqn. (A.4), and $\Psi_m = (\partial\Psi/\partial x_m)$. It is important to note that the new velocities are expanded in the same fixed Cartesian basis of the lab frame: $\boldsymbol{u} = u_1\boldsymbol{e}_1 + u_2\boldsymbol{e}_2 + u_3\boldsymbol{e}_3$, where $u_i(\boldsymbol{x},t) = v_i(\boldsymbol{X},\tau)$ are component–wise equal to the old velocities. The Green's function for an equation of the form of Eqn. (4.10) has been constructed in the Appendix A. We can write the particular solution of Eqn. (4.10) which

vanishes at $t = 0$:

$$\psi(\boldsymbol{x},t) \;=\; -\int_0^t dt' \int d^3x'\, G_\kappa(\boldsymbol{x}-\boldsymbol{x}',t,t')\; [u'_m - St'\delta_{m2}u'_1]\,\Psi'_m \tag{4.11}$$

where primes denote evaluation at the spacetime point $(\boldsymbol{x}', t')$ and the Green's function $G_\kappa(\boldsymbol{x}-\boldsymbol{x}', t, t')$ has been given in explicit form in the Appendix A. In the present context, the quantity μ of the Appendix A takes the role of the molecular diffusivity (κ) of the passive scalar. Below, we mention some of the properties of the Green's function which are discussed in detail in the Appendix A:

$$G_\kappa(\boldsymbol{x},t,t') \quad \text{is non–zero only when} \quad 0 \le t' < t. \tag{4.12a}$$

$$\lim_{t'\to t_-}\; G_\kappa(\boldsymbol{x},t,t') \;=\; \delta^3(\boldsymbol{x}) \tag{4.12b}$$

$$\left(\frac{\partial}{\partial t} - \kappa\boldsymbol{\nabla}^2\right) G_\kappa(\boldsymbol{x},t,t') \;=\; 0 \tag{4.12c}$$

We also note that G_κ has the "reproducibility" property

$$G_\kappa(\boldsymbol{x}-\boldsymbol{x}',t,t_0) \;=\; \int \mathrm{d}^3x''\, G_\kappa(\boldsymbol{x}-\boldsymbol{x}'',t,s)\, G_\kappa(\boldsymbol{x}''-\boldsymbol{x}',s,t_0)\,; \quad \text{for } t_0 < s < t\,. \tag{4.12d}$$

Defining the spatial Fourier transform of the Green's function as given in Eqn. (A.8), we find from Eqns. (4.12a)–(4.12d),

$$\widetilde{G}_\kappa(\boldsymbol{k},t,t') \quad \text{is non–zero only when} \quad 0 \le t' < t. \tag{4.13a}$$

$$\lim_{t'\to t_-}\; \widetilde{G}_\kappa(\boldsymbol{k},t,t') \;=\; 1 \tag{4.13b}$$

$$\frac{\partial\, \widetilde{G}_\kappa}{\partial t} \;+\; \kappa\, K^2(\boldsymbol{k},t)\, \widetilde{G}_\kappa \;=\; 0 \tag{4.13c}$$

$$\widetilde{G}_\kappa(\boldsymbol{k},t,t_0) \;=\; \widetilde{G}_\kappa(\boldsymbol{k},t,s)\, \widetilde{G}_\kappa(\boldsymbol{k},s,t_0)\,; \quad \text{for } t_0 < s < t\,. \tag{4.13d}$$

where, in Eqn. (4.13c), $K^2(\boldsymbol{k},t) = (k_1 - Stk_2)^2 + k_2^2 + k_3^2$. Also $\boldsymbol{k}$, being conjugate to the sheared coordinate vector $\boldsymbol{x}$, can be regarded as a *sheared wavevector*. It is now

straightforward to write down the solution, which is also given in the Appendix A:

$$\begin{aligned}\widetilde{G}_\kappa(\boldsymbol{k},t,t') &= \exp\left[-\kappa\int_{t'}^{t}\mathrm{d}s\,K^2(\boldsymbol{k},s)\right] \\ &= \exp\left[-\kappa\left(k^2(t-t')-S\,k_1\,k_2(t^2-t'^2)+\frac{1}{3}S^2\,k_2^2(t^3-t'^3)\right)\right] \quad (4.14)\end{aligned}$$

We note that $\widetilde{G}_\eta(\boldsymbol{k},t,t')$ is a positive quantity which takes values between 0 and 1, and that it is an even function of $\boldsymbol{k}$ and k_3. The real space Green's function $G_\kappa(\boldsymbol{x},t,t')$, which is equivalent to the one derived earlier by Krause & Rädler (1971), can be written explicitly by taking the inverse Fourier transform of Eqn. (4.14), and is being provided in the Appendix A. Following Appendix A and the related discussion given in Ch. 5, we note that it takes the form of an anisotropic, rotated Gaussian in $\boldsymbol{x}$–space, which may be referred to as a *sheared heat kernel*.

4.2.2 The turbulent flux at small Pe

To lowest order in Pe, the mean flux density (or the turbulent flux) is given by $\boldsymbol{F} = \left\langle c^{(0)}\boldsymbol{v}\right\rangle = \langle\psi\boldsymbol{u}\rangle$ where Eqn. (4.11) for ψ should be substituted. Following standard procedure, we allow $\langle\ \rangle$ to act only on the velocity variables but not the mean field; symbolically, it is assumed that $\langle\boldsymbol{u}\boldsymbol{u}\Psi\rangle = \langle\boldsymbol{u}\boldsymbol{u}\rangle\,\Psi$. Then the FOSA expression for the turbulent flux is

$$\begin{aligned}F_j &= \langle\psi\,u_j\rangle \\ &= -\int_0^t dt'\int d^3x'\,G_\kappa(\boldsymbol{x}-\boldsymbol{x}',t,t')\,\left[R_{jm}(\boldsymbol{x},\boldsymbol{x}',t,t')\;-\;St'\delta_{m2}R_{j1}(\boldsymbol{x},\boldsymbol{x}',t,t')\right]\Psi'_m\end{aligned} \quad (4.15)$$

where R_{jm} is the *transport coefficient* which is the two–point unequal–time velocity correlator defined by

$$R_{jm}\,(\boldsymbol{x},\boldsymbol{x}',t,t') \;=\; \langle u_j(\boldsymbol{x},t)\,u_m(\boldsymbol{x}',t')\rangle \tag{4.16}$$

To obtain more specific expressions for the transport coefficients, we need to provide information on the $\boldsymbol{uu}$ velocity correlators. However, it is physically more transparent to consider velocity statistics in terms of $\boldsymbol{vv}$ velocity correlators, because this is referred to the lab frame instead of the sheared coordinates. By definition, from Eqn. (4.9),

$$u_m(\boldsymbol{x},t) \;=\; v_m(\boldsymbol{X}(\boldsymbol{x},t),t) \tag{4.17}$$

where

$$X_1 \;=\; x_1\,, \qquad X_2 \;=\; x_2 + Stx_1\,, \qquad X_3 \;=\; x_3\,, \qquad \tau \;=\; t \tag{4.18}$$

is the inverse of the shearing transformation given in Eqn. (A.2). Thus we can write

$$R_{jm}\,(\boldsymbol{x},\boldsymbol{x}',t,t') \;=\; \langle v_j(\boldsymbol{X},t)\,v_m(\boldsymbol{X}',t')\rangle \tag{4.19}$$

where $\boldsymbol{X}$ and $\boldsymbol{X}'$ are shorthand for

$$\boldsymbol{X} \;=\; (x_1\,, x_2 + Stx_1\,, x_3)\;, \qquad \boldsymbol{X}' \;=\; (x_1'\,, x_2' + St'x_1'\,, x_3') \tag{4.20}$$

Eqn. (4.15), together with (4.16) or (4.19), gives the turbulent flux in general form. $\boldsymbol{X}$ can be thought of as the coordinates of the origin at time t of an observer *comoving* with the background shear flow, who was at $\boldsymbol{x}$ at time equal to zero. Similarly, $\boldsymbol{X}'$ can be thought of as the coordinates of the origin at time t' of an observer *comoving* with the background shear flow, who was at $\boldsymbol{x}'$ at time equal to zero. Therefore the transport properties depend only on the velocity correlators measured by such observers at the origin of their coordinate system. This fact will have profound consequences for turbulent mixing when we consider G–invariant velocity correlators in the next section.

Before discussing the Galilean invariance of the linear shear flow, we derive the form of turbulent flux for a special case, when the velocity field is "delta–correlated–in–time".

4.2.3 Delta–correlated–in–time velocity correlator

Although somewhat artificial, it is not uncommon to study dynamo action due to velocity fields whose correlation times are considered so small that the two–point correlator taken between spacetime points $(\boldsymbol{R}, \tau)$ and $(\boldsymbol{R}', \tau')$ is assumed to be

$$\langle v_i(\boldsymbol{R}, \tau)\, v_j(\boldsymbol{R}', \tau')\rangle \;=\; \delta(\tau - \tau')\, T_{ij}(\boldsymbol{R}, \boldsymbol{R}', \tau) \tag{4.21}$$

Incompressibility implies that

$$\frac{\partial T_{ij}}{\partial R_i} \;=\; 0\,; \qquad \frac{\partial T_{ij}}{\partial R'_j} \;=\; 0 \tag{4.22}$$

Then velocity correlator

$$\langle v_i(\boldsymbol{X}, t)\, v_j(\boldsymbol{X}', t')\rangle \;=\; \delta(t - t')\, T_{ij}(\boldsymbol{X}, \boldsymbol{X}', t) \tag{4.23}$$

where $\boldsymbol{X}$ and $\boldsymbol{X}'$ can be written in this case as

$$\boldsymbol{X} = \boldsymbol{X}(\boldsymbol{x}, t) = (x_1\,, x_2 + St x_1\,, x_3)\;, \qquad \boldsymbol{X}' = \boldsymbol{X}(\boldsymbol{x}', t) = (x'_1\,, x'_2 + St x'_1\,, x'_3) \tag{4.24}$$

Putting Eqns. (4.19) and (4.24) in the Eqn. (4.15) and using the property (4.12b) we can write

$$F_j \;=\; -\Psi_m(\boldsymbol{x}, t)\,[T_{jm}(\boldsymbol{X}, \boldsymbol{X}, t) - St\delta_{m2} T_{j1}(\boldsymbol{X}, \boldsymbol{X}, t)] \tag{4.25}$$

Using

$$\frac{\partial}{\partial x_m} \;=\; \frac{\partial}{\partial X_m} \;+\; S\tau\, \delta_{m1}\, \frac{\partial}{\partial X_2} \tag{4.26}$$

we write the turbulent flux in terms of the original variables and lab frame coordinates as

$$F_j(\boldsymbol{X},\tau) \;=\; -T_{jm}(\boldsymbol{X},\tau)\, C_m(\boldsymbol{X},\tau) \tag{4.27}$$

where $C_m = (\partial C/\partial X_m)$. Thus the turbulent flux F_j does not depend explicitly on the shear parameter S. Equation (4.27) is identical to the familiar expression in the absence of background shear. *Therefore we conclude that the shear needs time to produce non trivial effects and it is necessary to consider velocity correlators with non zero correlation times.* Henceforth we shall consider the general case of finite velocity correlation times.

4.3 Galilean invariant velocity statistics

The basic concepts of the Galilean invariance have been given in the Appendix B. Here, we wish to derive the Galilean invariant expressions for the transport coefficients and the turbulent flux.

4.3.1 Galilean invariance of the advection–diffusion equation

Let $\left[\tilde{\mathcal{C}}(\tilde{\boldsymbol{X}},\tilde{\tau}),\tilde{C}(\tilde{\boldsymbol{X}},\tilde{\tau}),\tilde{c}(\tilde{\boldsymbol{X}},\tilde{\tau}),\tilde{\boldsymbol{v}}(\tilde{\boldsymbol{X}},\tilde{\tau})\right]$ denote the total, the mean, the fluctuating components of the concentration of the passive scalar and the fluctuating velocity field, respectively, as measured by the comoving observer[2]. These are all equal to the respective quantities measured in the lab frame:

$$\left[\tilde{\mathcal{C}}(\tilde{\boldsymbol{X}},\tilde{\tau}),\tilde{C}(\tilde{\boldsymbol{X}},\tilde{\tau}),\tilde{c}(\tilde{\boldsymbol{X}},\tilde{\tau}),\tilde{\boldsymbol{v}}(\tilde{\boldsymbol{X}},\tilde{\tau})\right] \;=\; \left[\mathcal{C}(\boldsymbol{X},\tau),C(\boldsymbol{X},\tau),c(\boldsymbol{X},\tau),\boldsymbol{v}(\boldsymbol{X},\tau)\right] \tag{4.28}$$

Invariance of the total, the mean and the fluctuating components of the passive scalar in the two frames (i.e. in the lab frame and the comoving frame) is obvious. To see that the fluctuating velocity fields must be the same, we note from the discussions of the Appendix B that the total fluid velocity measured by the comoving observer is, by

[2]See the Appendix B for the concept of the comoving observer, in particular, and the Galilean invariance, in general.

definition, equal to $\left(S\tilde{X}_1\boldsymbol{e}_2 + \tilde{\boldsymbol{v}}(\tilde{\boldsymbol{X}},\tilde{\tau})\right)$. This must be equal to the difference between the velocity in the lab frame, $(SX_1\boldsymbol{e}_2 + \boldsymbol{v}(\boldsymbol{X},\tau))$, and $(S\xi_1\boldsymbol{e}_2)$, which is the velocity of the comoving observer with respect to the lab frame. Using $\tilde{X}_1 = X_1 - \xi_1$, we see that $\tilde{\boldsymbol{v}}(\tilde{\boldsymbol{X}},\tilde{\tau}) = \boldsymbol{v}(\boldsymbol{X},\tau)$.

Using Eqns. (B.2) and (B.3) of the Appendix B, we find that Eqns. (4.1), (4.3) and (4.4) are invariant under the simultaneous transformations given in Eqns. (B.2) and (4.28). We note that this symmetry property is actually an invariance under a subset of the full ten–parameter Galilean group, parametrized by the five quantities $(\xi_1, \xi_2, \xi_3, \tau_0, S)$; for brevity we will refer to this restricted symmetry as Galilean invariance, or simply GI.

It is important to note that the lab and comoving frames need not constitute inertial coordinate systems. The only requirement is that the passive scalar field satisfies the advection–diffusion Eqn. (4.1).

4.3.2 Galilean–invariant velocity correlators

We derive a Galilean–invariant expression for the transport coefficient, $R_{jm}(\boldsymbol{x},\boldsymbol{x}',t,t')$, given by Eqn. (4.19). We follow the basic ideas of G–invariant velocity correlators discussed in the Appendix B, and rewrite below the statement of Galilean–invariance of unequal time two–point velocity correlator:

$$\langle v_i(\boldsymbol{R},\tau)\, v_j(\boldsymbol{R}',\tau')\rangle \;=\; \langle v_i(\boldsymbol{R}+\boldsymbol{X}_c(\boldsymbol{\xi},\tau),\tau)\, v_j(\boldsymbol{R}'+\boldsymbol{X}_c(\boldsymbol{\xi},\tau'),\tau')\rangle \tag{4.29}$$

for all $(\boldsymbol{R},\boldsymbol{R}',\tau,\tau',\boldsymbol{\xi})$. We want to choose $(\boldsymbol{R},\boldsymbol{R}',\tau,\tau',\boldsymbol{\xi})$ as functions of $(\boldsymbol{x},\boldsymbol{x}',t,t')$ such that we can use Eqn. (4.29) to simplify the velocity correlators in Eqn. (4.19). We note that Eqns. (4.20) and (B.1) give

$$\boldsymbol{X} \;=\; \boldsymbol{X}_c(\boldsymbol{x},t)\,, \qquad \boldsymbol{X}' \;=\; \boldsymbol{X}_c(\boldsymbol{x}',t') \tag{4.30}$$

It is therefore natural to choose

$$\tau = t\,, \qquad \tau' = t' \tag{4.31}$$

Thus the velocity correlator we require can now be written as

$$\langle v_i(\boldsymbol{X},t)\, v_j(\boldsymbol{X}',t')\rangle \;=\; \langle v_i(\boldsymbol{X}_c(\boldsymbol{x},t),t)\, v_j(\boldsymbol{X}_c(\boldsymbol{x}',t'),t')\rangle \tag{4.32}$$

Comparing Eqn. (4.32) with Eqn. (4.29), we see that if we choose

$$\boldsymbol{R} = \boldsymbol{X}_c(\boldsymbol{x},t), \qquad \boldsymbol{R}' = \boldsymbol{X}_c(\boldsymbol{x}',t') \tag{4.33}$$

then Eqn. (4.32), together with Eqns. (B.1) and (4.29) implies that

$$\begin{aligned}
\langle v_i(\boldsymbol{X},t)v_j(\boldsymbol{X}',t')\rangle &= \langle v_i(\boldsymbol{R},\tau)v_j(\boldsymbol{R}',\tau')\rangle \\
&= \langle v_i(\boldsymbol{R}+\boldsymbol{X}_c(\boldsymbol{\xi},\tau),\tau)v_j(\boldsymbol{R}'+\boldsymbol{X}_c(\boldsymbol{\xi},\tau'),\tau')\rangle \\
&= \langle v_i(\boldsymbol{X}_c(\boldsymbol{x}+\boldsymbol{\xi},t),t)v_j(\boldsymbol{X}_c(\boldsymbol{x}'+\boldsymbol{\xi},t'),t')\rangle
\end{aligned}$$

Now it is natural to choose

$$\boldsymbol{\xi} = -\frac{1}{2}(\boldsymbol{x}+\boldsymbol{x}') \tag{4.34}$$

Then

$$\begin{aligned}
\langle v_i(\boldsymbol{X},\tau)v_j(\boldsymbol{X}',\tau')\rangle &= \left\langle v_i\left(\boldsymbol{X}_c\left(\frac{\boldsymbol{x}-\boldsymbol{x}'}{2}\right),t\right) v_j\left(\boldsymbol{X}_c\left(\frac{\boldsymbol{x}'-\boldsymbol{x}}{2},t'\right),t'\right)\right\rangle \\
&= R_{ij}(\boldsymbol{x}-\boldsymbol{x}',t,t')
\end{aligned} \tag{4.35}$$

where the transport coefficient R_{ij} is defined in Eqn. (4.16) (or (4.19)). We note that

$$R_{ij}(\boldsymbol{x},t,t') \;=\; R_{ji}(-\boldsymbol{x},t,t') \tag{4.36}$$

4.3.3 Galilean–invariant turbulent flux

As can be seen from Eqn. (4.35) that R_{ij} depend on $\boldsymbol{x}$ and $\boldsymbol{x}'$ only through the combination, $(\boldsymbol{x}-\boldsymbol{x}')$, which arises because of Galilean invariance. We change the integration variable in Eqn. (4.15) to $\boldsymbol{r} = \boldsymbol{x}-\boldsymbol{x}'$ and using Eqn. (4.35) in the Eqn. (4.15), the expression for the turbulent flux can be written as

$$F_j = -\frac{\partial}{\partial x_m}\int_0^t dt' \int d^3r\, G_\kappa(\boldsymbol{r},t,t')\,\left[R_{jm}(\boldsymbol{r},t,t') \;-\; St'\delta_{m2}R_{j1}(\boldsymbol{r},t,t')\right]\Psi(\boldsymbol{x}-\boldsymbol{r},t') \tag{4.37}$$

where we have used

$$\frac{\partial\Psi(\boldsymbol{x}',t')}{\partial x'_m} \;=\; \frac{\partial\Psi(\boldsymbol{x}-\boldsymbol{r},t')}{\partial x_m}$$

Using Eqn. (4.26) and arranging the terms in Eqn. (4.37), we can write the Galilean–invariant expression for the turbulent flux as

$$F_j = -\frac{\partial}{\partial X_m}\int_0^t dt' \int d^3r\, G_\kappa(\boldsymbol{r},t,t')\, T_{jm}(\boldsymbol{r},t,t')\Psi(\boldsymbol{x}-\boldsymbol{r},t') \tag{4.38}$$

where

$$T_{jm}(\boldsymbol{r},t,t') \;=\; R_{jm}(\boldsymbol{r},t,t') \;+\; S(t-t')\delta_{m2}R_{j1}(\boldsymbol{r},t,t') \tag{4.39}$$

4.4 Mean–field advection–diffusion equation

Applying the shearing transformation given in Eqns. (A.2) and (A.3) to the mean–field Eqn. (4.3), we see that the mean–field, $\Psi(\boldsymbol{x},t)$, obeys

$$\frac{\partial\Psi}{\partial t} \;=\; -\boldsymbol{\nabla}\cdot\boldsymbol{F} \;+\; \kappa\boldsymbol{\nabla}^2\Psi \tag{4.40}$$

where

$$(\boldsymbol{\nabla})_p \;\equiv\; \frac{\partial}{\partial X_p} \;=\; \frac{\partial}{\partial x_p} \;-\; St\,\delta_{p1}\frac{\partial}{\partial x_2} \tag{4.41}$$

We now use Eqns. (4.38) and (4.41) to evaluate $\boldsymbol{\nabla\cdot F}$.

$$\boldsymbol{\nabla\cdot F} \;=\; \frac{\partial F_j}{\partial X_j} \;=\; -\frac{\partial^2}{\partial X_j \partial X_m}\int_0^t dt' \int d^3r\, G_\kappa(\boldsymbol{r},t,t')\, T_{jm}(\boldsymbol{r},t,t')\Psi(\boldsymbol{x}-\boldsymbol{r},t') \qquad (4.42)$$

The differential operator outside the integral in Eqn. (4.42) operates only on the mean–field, $\Psi(\boldsymbol{x}-\boldsymbol{r},t')$, inside the integral. Also, as the differential operator, $\partial^2/(\partial X_j \partial X_m)$, is symmetric in the dummy indices j and m, the quantity T_{jm} should also be a symmetric tensor in the indices j and m. Therefore we symmetrize T_{jm} by defining the symmetric tensor $\widetilde{T}_{jm}$ as

$$\widetilde{T}_{jm} \;=\; \frac{T_{jm}\,+\,T_{mj}}{2} \;=\; \frac{1}{2}\left[R_{jm}+R_{mj}+S(t-t')\{\delta_{m2}R_{j1}+\delta_{j2}R_{m1}\}\right] \qquad (4.43)$$

Thus the correct expression for $\boldsymbol{\nabla\cdot F}$ should contain $\widetilde{T}_{jm}$ inside the integral and we write it explicitly below

$$\boldsymbol{\nabla\cdot F} \;=\; \frac{\partial F_j}{\partial X_j} \;=\; -\frac{\partial^2}{\partial X_j \partial X_m}\int_0^t dt' \int d^3r\, G_\kappa(\boldsymbol{r},t,t')\, \widetilde{T}_{jm}(\boldsymbol{r},t,t')\Psi(\boldsymbol{x}-\boldsymbol{r},t') \qquad (4.44)$$

Substituting the Eqn. (4.44) in Eqn. (4.40), we obtain an integro–differential equation governing the evolution of mean–field, $\Psi(\boldsymbol{x},t)$, valid for arbitrary values of the shear strength S:

$$\frac{\partial\Psi}{\partial t} \;=\; \kappa\boldsymbol{\nabla}^2\Psi \;+\; \frac{\partial^2}{\partial X_j \partial X_m}\int_0^t dt' \int d^3r\, G_\kappa(\boldsymbol{r},t,t')\, \widetilde{T}_{jm}(\boldsymbol{r},t,t')\Psi(\boldsymbol{x}-\boldsymbol{r},t') \qquad (4.45)$$

4.4.1 Advection–diffusion equation for slowly varying mean field

The turbulent flux given in Eqn. (4.38) is a *functional* of Ψ. When the mean–field is slowly varying compared to velocity correlation times, we expect to be able to approximate $\boldsymbol{F}$ as a *function* of Ψ. In this case, the mean–field advection–diffusion equation would reduce to a partial differential equation, instead of the more formidable integro-differential equation given by (4.45). Sheared coordinates are essential for the calculations, but physical interpretation is simplest in the laboratory frame; hence we derive an

expression for the turbulent flux in terms of $C(\boldsymbol{X},\tau)$.

The first step involves the Taylor expansion of the quantity Ψ occurring in Eqn. (4.38). We neglect spacetime derivatives higher than the first order ones in the expression for the turbulent flux (Eqn. (4.38)). As the factor $\partial/\partial X_m$ appears outside the integral in Eqn. (4.38), Taylor expansion of Ψ to the desired order becomes

$$\Psi(\boldsymbol{x}-\boldsymbol{r},t') \;=\; \Psi(\boldsymbol{x},t) \;-\; (t-t')\frac{\partial\Psi}{\partial t} \;+\; \ldots \tag{4.46}$$

We now use the mean–field Eqn. (4.40) to express $(\partial\Psi/\partial t)$ in terms of spatial derivatives. The diffusion term can be dropped because it involves second order spatial derivatives. Let us introduce an ordering parameter, $\varepsilon \ll 1$, and consider $\boldsymbol{F}$ to be $\mathcal{O}(\varepsilon)$. Then,

$$\frac{\partial\Psi}{\partial t} \;=\; \mathcal{O}(\varepsilon) \tag{4.47}$$

and Eqn. (4.46) becomes

$$\Psi(\boldsymbol{x}-\boldsymbol{r},t') \;=\; \Psi(\boldsymbol{x},t) \;+\; \mathcal{O}(\varepsilon) \tag{4.48}$$

We substitute Eqn. (4.48) in (4.38) and write $\widetilde{T}_{jm}$ instead of T_{jm} due to the reason discussed above,

$$F_j(\boldsymbol{X},\tau) \;=\; -\kappa_{jm}\,\frac{\partial C(\boldsymbol{X},\tau)}{\partial X_m} \tag{4.49}$$

where we have used $\Psi(\boldsymbol{x},t) = C(\boldsymbol{X},\tau)$ in order to write the expression in terms of lab–frame variables. Equation (4.49) provides us the Galilean–invariant expression for the turbulent flux when the mean–field $C(\boldsymbol{X},\tau)$ is a slowly varying function. The *transport coefficient* $\kappa_{jm}(\tau)$ is given by,

$$\kappa_{jm}(\tau) \;=\; \int_0^\tau dt' \int d^3r\, G_\kappa(\boldsymbol{r},t,t')\,\widetilde{T}_{jm}(\boldsymbol{r},t,t') \tag{4.50}$$

Thus the mean–field Eqn. (4.3), which is repeated below,

$$\left(\frac{\partial}{\partial\tau} \; + \; SX_1\frac{\partial}{\partial X_2}\right)C \; = \; -\frac{\partial F_j}{\partial X_j} \; + \; \kappa\boldsymbol{\nabla}^2 C$$

together with Eqns. (4.49) and (4.50), is a closed partial differential equation (which is first order in temporal and second order in spatial derivatives).

4.4.2 Velocity correlators expressed in terms of the velocity spectrum tensor

Our aim is to express the velocity correlators, $R_{jm}(\boldsymbol{r},t,t')$ and $\widetilde{T}_{jm}(\boldsymbol{r},t,t')$, in terms of the velocity spectrum tensor, $\Pi_{jm}(\boldsymbol{k},t,t')$, which was derived in Ch. 3. To do this, we use the results derived in the Appendix B, where we show that the G–invariant expression for Fourier–space two–point velocity correlator is given by Eqn. (B.7). Thus making use of the Appendix B and Eqns. (4.35) & (3.18), we can write

$$\begin{aligned} R_{jm}(\boldsymbol{r},t,t') \; &= \; \int \mathrm{d}^3k\,\Pi_{jm}(\boldsymbol{k},t,t')\,\exp\left[\mathrm{i}\,\boldsymbol{k}\cdot\boldsymbol{r}\right] \\ \widetilde{T}_{jm}(\boldsymbol{r},t,t') \; &= \; \frac{1}{2}\int \mathrm{d}^3k\,\left[\Pi_{jm}+\Pi_{mj}+S(t-t')\{\delta_{m2}\Pi_{j1}+\delta_{j2}\Pi_{m1}\}\right]\exp\left[\mathrm{i}\,\boldsymbol{k}\cdot\boldsymbol{r}\right] \end{aligned} \tag{4.51}$$

where we noted that $\boldsymbol{K}\cdot\boldsymbol{X} = \boldsymbol{k}\cdot\boldsymbol{x}$ and $\boldsymbol{K}'\cdot\boldsymbol{X}' = \boldsymbol{k}'\cdot\boldsymbol{x}'$. Using the above expressions for R_{jm} and $\widetilde{T}_{jm}$ in Eqn. (4.50), the transport coefficient $\kappa_{jm}(\tau)$ can also be written in terms of the velocity spectrum tensor.

We note from the analysis of Ch. 3 that the velocity spectrum tensor, Π_{jm}, is given in terms of the forcing spectrum tensor, Φ_{jm}, which requires the knowledge of the forcing power spectrum, $F(K/K_F)$; see Eqns. (3.24) and (3.28). For computation of the transport coefficients, we always choose the form for $F(K/K_F)$ as given in Eqn. (3.35). Few useful dimensionless variables could be defined as: The *fluid Reynolds number*,

$\mathrm{Re} = v^{\infty}_{\mathrm{rms}}/(\nu K_F)$; the *peclet number*, $\mathrm{Pe} = v^{\infty}_{\mathrm{rms}}/(\kappa K_F)$; the *Schmidt number*, $\mathrm{Sc} = \nu/\kappa$; the dimensionless *Shear parameter*, $\mathrm{S_h} = S/(v^{\infty}_{\mathrm{rms}} K_F)$. The definition of $v^{\infty}_{\mathrm{rms}}$ may be seen from the discussion following Eqn. (3.33) of Ch. 3, and K_F is the wavenumber at which the fluid is stirred.

4.5 Evaluation of κ_{jm} for a slowly varying mean–field

It is useful to display the expression for $\kappa_{jm}(\tau)$ given by Eqn. (4.50) in terms of velocity spectrum tensor Π_{jm}. Using Eqn. (4.51) in the Eqn. (4.50) and noting the fact that $G_\kappa(\boldsymbol{r}, t, t')$ (or $\widetilde{G}_\kappa(\boldsymbol{k}, t, t')$) is an even function of $\boldsymbol{r}$ (or $\boldsymbol{k}$), we can write,

$$\kappa_{jm}(\tau) = \frac{1}{2}\int_0^\tau \mathrm{d}t' \int \mathrm{d}^3k\, \widetilde{G}_\kappa(\boldsymbol{k}, t, t')\, [\Pi_{jm} + \Pi_{mj} + S(t-t')\{\delta_{m2}\Pi_{j1} + \delta_{j2}\Pi_{m1}\}] \quad (4.52)$$

where $\Pi_{lm} = \Pi_{lm}(\boldsymbol{k}, t, t')$, and the indices (i, j) run over values 1 and 2. Here $\widetilde{G}_\kappa(\boldsymbol{k}, t, t')$ is the Fourier–space resistive Green's function defined in Eqn. (4.14). The final step in computing $\kappa_{jm}(\tau)$ is to use Eqns. (3.28) and (3.35) for Π_{jm} and $F(K/K_F)$, respectively. Below we discuss some important properties of $\kappa_{jm}(\tau)$:

(i) The tensor $\kappa_{jm}(\tau)$ is symmetric in the indices (j, m).

(ii) The components κ_{13} and κ_{23} vanish because, for these values of the indices (j, m), the integrand in Eqn. (4.52) is an *odd* function of K_3 (or k_3). Thus there are only four non–zero independent components of $\kappa_{jm}(\tau)$, namely κ_{11}, κ_{22}, κ_{33} and κ_{12}, that we need to compute.

(iii) The $\kappa_{jm}(\tau)$ saturate at some constant values at late times; let us denote these constant values by $\kappa^{\infty}_{jm} = \kappa_{jm}(\tau \to \infty)$. If the mean field changes over times that are longer than the saturation time, we may use κ^{∞}_{jm} instead of the time–varying quantities $\kappa_{jm}(\tau)$ for our purposes.

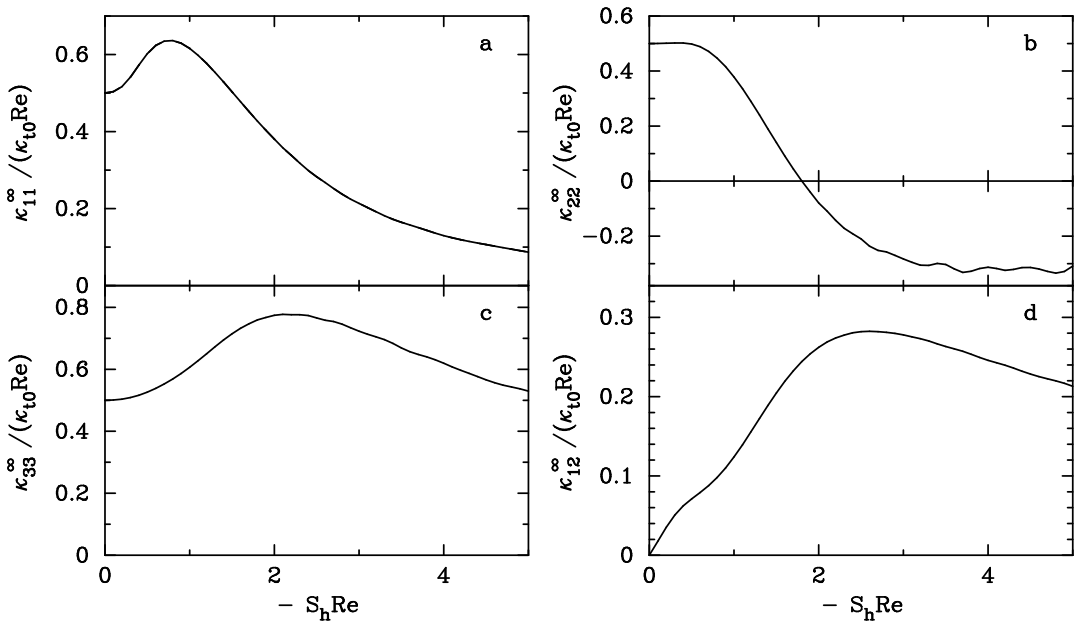

Figure 4.1: Plots of the saturated quantities κ_{11}^{∞}, κ_{22}^{∞}, κ_{33}^{∞} and κ_{12}^{∞} for Re = Pe = 0.1 and Re = Pe = 0.5, corresponding to Sc = 1, versus the dimensionless parameter $(-\mathrm{S_h} \times \mathrm{Re})$. The two plots have collapsed on each other due to scaling of the functions as given in Eqn. (4.53).

From Eqns. (4.52), (4.14), (3.28) and (3.35), it can be verified that the saturated values of the transport coefficients, κ_{jm}^{∞}, have the following general functional form:

$$\kappa_{jm}^{\infty} \;=\; \kappa_{t0}\,\mathrm{Re}\, f_{jm}(\mathrm{S_h Re}\,,\mathrm{Sc}) \tag{4.53}$$

where the f_{ij} are dimensionless functions of two variables and $\kappa_{t0} = (v_{\mathrm{rms}}^{\infty}/3K_F)$. Figs. (4.1–4.3) display plots of the saturated values of the transport coefficients, κ_{11}^{∞}, κ_{22}^{∞}, κ_{33}^{∞} and κ_{12}^{∞}, versus the dimensionless parameter $(-\mathrm{S_h} \times \mathrm{Re})$. The scalings of the ordinates have been chosen for compatibility with the functional form displayed in Eqn. (4.53) above. The plots in Fig. (4.1a–d) are for Sc = 1, but for two sets of values of the Reynolds number and Peclet number; Re = Pe = 0.1, and Re = Pe = 0.5. Fig. (4.2a–d) are for Re = 0.1 and Pe = 0.5, corresponding to Sc = 5. Fig. (4.3a–d) are for Re = 0.5 and Pe = 0.1, corresponding to Sc = 0.2. Some noteworthy properties are as follows:

(i) κ_{11}^{∞}, κ_{33}^{∞} and κ_{12}^{∞} are always positive.

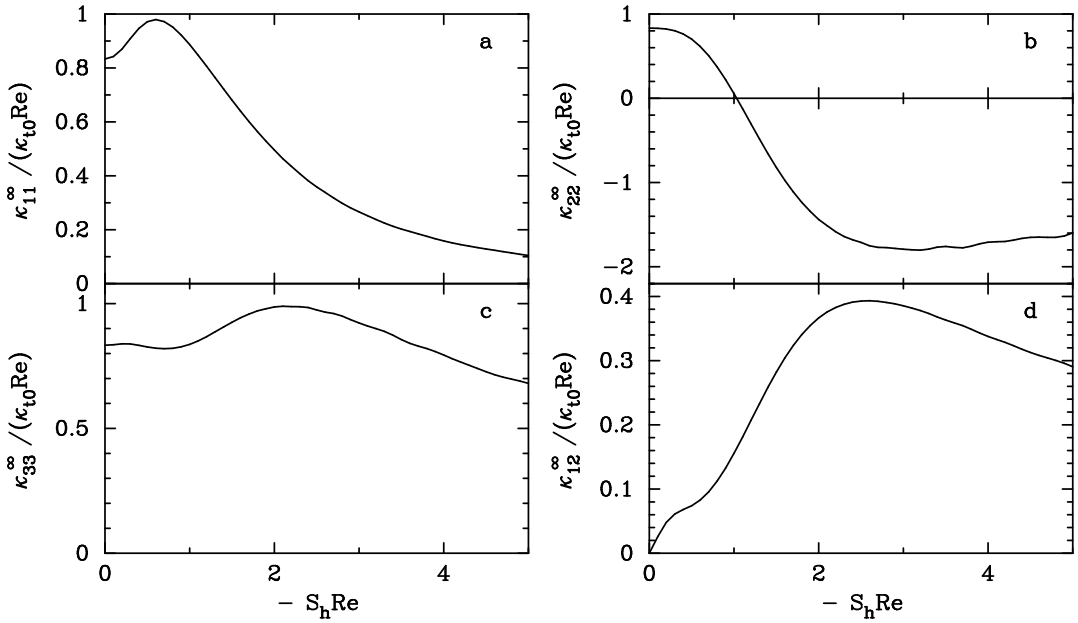

Figure 4.2: Plots of the saturated quantities κ_{11}^{∞}, κ_{22}^{∞}, κ_{33}^{∞} and κ_{12}^{∞} for Re = 0.1 and Pe = 0.5, corresponding to Sc = 5, versus the dimensionless parameter $(-\mathrm{S_h} \times \mathrm{Re})$.

(ii) κ_{22}^{∞} changes sign with $|\mathrm{S_h}|$. It starts with positive value at $\mathrm{S_h} = 0$, increases slightly with increasing values of $|\mathrm{S_h}|$, attains maximum quickly, it then becomes a decreasing function of $|\mathrm{S_h}|$ and becomes negative for large values of $|\mathrm{S_h}|$.

4.6 Slowly varying mean–field dynamics for non–helical flows

Transport properties of the passive scalar in the presence of background shear flow, in which the velocity fluctuations are non–helical, have been studied for small Peclet numbers by explicitly evaluating the transport coefficients. The evolution of the mean–field, assuming that it changes over times that are longer than the saturation time so that we can use κ_{jm}^{∞} instead of the time–varying quantities $\kappa_{jm}(\tau)$, is given by

$$\left(\frac{\partial}{\partial\tau} + SX_1\frac{\partial}{\partial X_2}\right)C = \kappa_{jm}^{\infty}\frac{\partial^2 C}{\partial X_j \partial X_m} + \kappa\boldsymbol{\nabla}^2 C \tag{4.54}$$

Equation (4.54) is inhomogeneous in the spatial coordinates so, as before, we find it

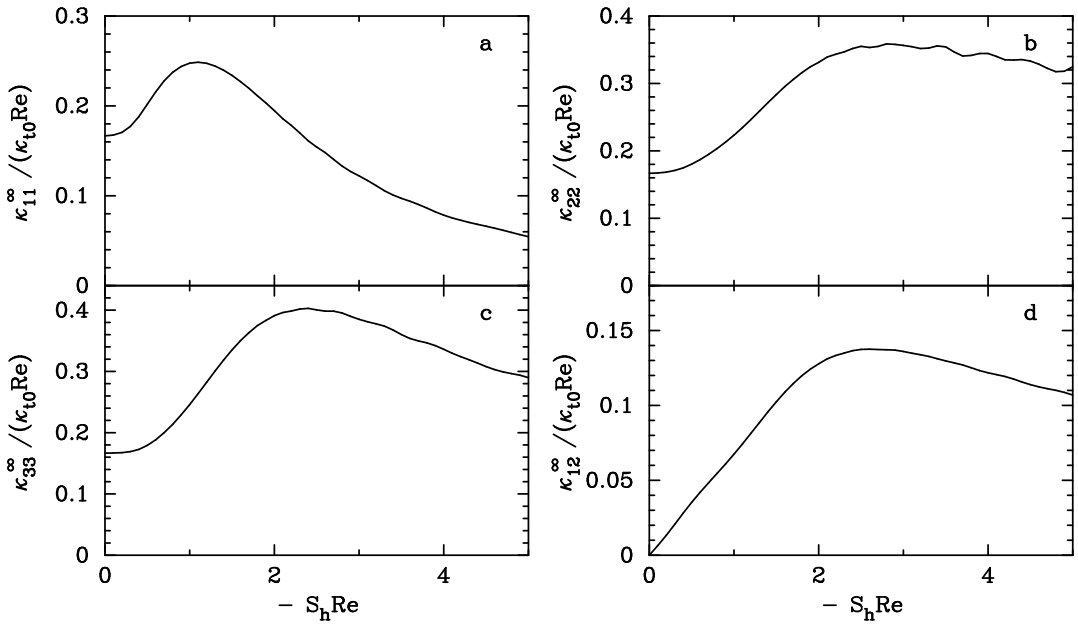

Figure 4.3: Plots of the saturated quantities κ_{11}^{∞}, κ_{22}^{∞}, κ_{33}^{∞} and κ_{12}^{∞} for Re = 0.5 and Pe = 0.1, corresponding to Pr = 0.2, versus the dimensionless parameter $(-\mathrm{S_h} \times \mathrm{Re})$.

convenient to work with new variable, $\Psi(\boldsymbol{x}, t)$, and transform Eqn. (4.54) to the shearing coordinates $(\boldsymbol{x}, t)$:

$$\frac{\partial \Psi}{\partial t} \;=\; \kappa_{jm}^{\infty} \frac{\partial^2 \Psi}{\partial X_j \partial X_m} \;+\; \kappa \boldsymbol{\nabla}^2 \Psi \tag{4.55}$$

where

$$\frac{\partial^2}{\partial X_j \partial X_m} \;=\; \frac{\partial^2}{\partial x_j \partial x_m} - \delta_{m1} St \frac{\partial^2}{\partial x_j \partial x_2} - \delta_{j1} St \frac{\partial^2}{\partial x_2 \partial x_m} + \delta_{j1}\delta_{m1} S^2 t^2 \frac{\partial^2}{\partial x_2^2} \tag{4.56}$$

and $\boldsymbol{\nabla}^2$ has been defined in Eqn. (A.4) of the Appendix A. Equation (4.55) is homogeneous in $\boldsymbol{x}$ but not in t, so we take a spatial Fourier transform of Eqn. (4.55). Let $\widetilde{\Psi}(\boldsymbol{k}, t)$ be the spatial Fourier transform of $\Psi(\boldsymbol{x}, t)$, defined by

$$\widetilde{\Psi}(\boldsymbol{k}, t) \;=\; \int \mathrm{d}^3 x \, \Psi(\boldsymbol{x}, t) \, \exp\left[-\mathrm{i}\boldsymbol{k}\cdot\boldsymbol{x}\right] \tag{4.57}$$

Then $\widetilde{\Psi}(\boldsymbol{k}, t)$ satisfies

$$\frac{\partial\widetilde{\Psi}}{\partial t} \;=\; -\left[\kappa^{\infty}_{jm}K_jK_m + \kappa K^2\right]\widetilde{\Psi} \tag{4.58}$$

where the vector $\boldsymbol{K}(\boldsymbol{k},t) = (k_1 - St\,k_2,\; k_2,\; k_3)$ and $K^2 = |\boldsymbol{K}|^2 = (k_1 - Stk_2)^2 + k_2^2 + k_3^2$, as before. The solution of Eqn. (4.58) can be readily written as

$$\widetilde{\Psi}(\boldsymbol{k},t) \;=\; \widetilde{\Psi}(\boldsymbol{k},0)\,\widetilde{\mathcal{G}}(\boldsymbol{k},t,0) \tag{4.59}$$

where $\widetilde{\Psi}(\boldsymbol{k},0)$ is assumed to be given as an initial condition and $\widetilde{\mathcal{G}}(\boldsymbol{k},t,0)$ is the Green's function which is zero for $t<0$ and is defined for $t \geq 0$ by

$$\widetilde{\mathcal{G}}(\boldsymbol{k},t,0) \;=\; \exp\left[-\int_0^t ds\;\left(\kappa^{\infty}_{jm}K_jK_m + \kappa K^2\right)\right] \tag{4.60}$$

In the integrand, $K_j = k_j - Ss\delta_{j1}k_2$ should be regarded as a function of $\boldsymbol{k}$ and s, and the s–integral performed at fixed $\boldsymbol{k}$. Then $\widetilde{\mathcal{G}}(\boldsymbol{k},t,0)$ can be written as the product of a *microscopic* Green's function, $\widetilde{G}_{\kappa}(\boldsymbol{k},t,0)$, and a *turbulent* Green's function, $\widetilde{G}_{\rm turb}(\boldsymbol{k},t,0)$:

$$\begin{aligned}
\widetilde{\mathcal{G}}(\boldsymbol{k},t,0) &= \widetilde{G}_{\rm turb}(\boldsymbol{k},t,0)\widetilde{G}_{\kappa}(\boldsymbol{k},t,0) \\
\widetilde{G}_{\rm turb}(\boldsymbol{k},t,0) &= \exp\left[-\mathcal{T}_{jm}(t)k_jk_m\right] \\
\widetilde{G}_{\kappa}(\boldsymbol{k},t,0) &= \exp\left[-\kappa\left(k^2t - S\,k_1\,k_2t^2 + \frac{S^2}{3}\,k_2^2t^3\right)\right]
\end{aligned} \tag{4.61}$$

where $\mathcal{T}_{jm}(t)$ is a time–dependent symmetric matrix and depends on κ^{∞}_{jm} which are known quantities. It is easy to see that

$$-\mathcal{T}_{jm}(t)k_jk_m \;=\; -t\left[\kappa^{\infty}_{11}k_1^2 + \kappa^{\infty}_{22}k_2^2 + 2\kappa^{\infty}_{12}k_1k_2 + \kappa^{\infty}_{33}k_3^2\right] + St^2\left[\kappa^{\infty}_{11}k_1k_2 + \kappa^{\infty}_{12}k_2^2\right] - \frac{S^2}{3}t^3\left[\kappa^{\infty}_{11}k_2^2\right] \tag{4.62}$$

The solution in the original variables, $C(\boldsymbol{X},\tau)$, can be recovered by using the shearing transformation, Eqn. (A.2), to write $(\boldsymbol{x},t)$ in terms of the laboratory frame coordinates

$(\boldsymbol{X}, \tau)$:

$$C(\boldsymbol{X},\tau) \;=\; \Psi(\boldsymbol{x},t) \;=\; \int \frac{\mathrm{d}^3k}{(2\pi)^3}\,\widetilde{\Psi}(\boldsymbol{k},t)\exp\left(\mathrm{i}\boldsymbol{k}\cdot\boldsymbol{x}\right)$$

$$= \int \frac{\mathrm{d}^3k}{(2\pi)^3}\,\widetilde{\Psi}(\boldsymbol{k},\tau)\exp\left(\mathrm{i}\boldsymbol{K}(\boldsymbol{k},\tau)\cdot\boldsymbol{X}\right) \tag{4.63}$$

Using Eqn. (4.59) and writing $\widetilde{\Psi}(\boldsymbol{k},0) = \widetilde{C}(\boldsymbol{k},0)$, we get

$$C(\boldsymbol{X},\tau) \;=\; \int \frac{\mathrm{d}^3k}{(2\pi)^3}\,\widetilde{C}(\boldsymbol{k},0)\widetilde{\mathcal{G}}(\boldsymbol{k},\tau,0)\exp\left(\mathrm{i}\boldsymbol{K}(\boldsymbol{k},\tau)\cdot\boldsymbol{X}\right) \tag{4.64}$$

Below we discuss some useful properties of the analysis done in this section:

1. The above solution for $C(\boldsymbol{X},\tau)$ is a linear superposition of *shearing waves*, of the form $\exp\left(\mathrm{i}\boldsymbol{K}(\boldsymbol{k},\tau)\cdot\boldsymbol{X}\right) \;=\; \exp\left[\mathrm{i}(k_1 - S\tau k_2)X_1 + \mathrm{i}k_2X_2 + \mathrm{i}k_3X_3\right]$, indexed by the triplet of numbers (k_1, k_2, k_3).

2. Whether the waves grow or decay depends on the time dependence of the Green's function, $\widetilde{\mathcal{G}}(\boldsymbol{k},t,0) = \widetilde{G}_{\mathrm{turb}}(\boldsymbol{k},t,0)\widetilde{G}_{\kappa}(\boldsymbol{k},t,0)$.

3. $\widetilde{G}_{\kappa}(\boldsymbol{k},t,0)$ is known explicitly and describes the ultimate decay of the shearing waves (on the long diffusive timescale), although these could be transiently amplified.

4. $\widetilde{G}_{\mathrm{turb}}(\boldsymbol{k},t,0)$ depends on the behavior of Eqn. (4.62). The term linear in t will dominate at early times while the term proportional to t^3 will dominate eventually. Thus at early times we need one of the eigenvalues of the matrix

$$\begin{pmatrix} \kappa_{11}^{\infty} & \kappa_{12}^{\infty} & 0 \\ \kappa_{12}^{\infty} & \kappa_{22}^{\infty} & 0 \\ 0 & 0 & \kappa_{33}^{\infty} \end{pmatrix}$$

to be negative for the growth of mean concentration. These eigenvalues are

$$\lambda_{\pm} = \frac{(\kappa_{11}^{\infty} + \kappa_{22}^{\infty})}{2} \pm \frac{|\kappa_{11}^{\infty} - \kappa_{22}^{\infty}|}{2} \left[1 + 4\frac{(\kappa_{12}^{\infty})^2}{(\kappa_{11}^{\infty} - \kappa_{22}^{\infty})^2}\right]^{1/2}; \qquad \lambda_3 = \kappa_{33}^{\infty} \qquad (4.65)$$

It is evident that the nonzero values of κ_{12}^{∞} or negative values of the diagonal elements of the turbulent diffusion tensor favour growth at early times. Our analysis of § 4.5 suggests that the quantity κ_{22}^{∞} indeed becomes negative for large enough shear whereas κ_{11}^{∞} and κ_{33}^{∞} remain positive; this happens because the turbulence is strongly affected by the background shear and the velocity correlators are not isotropic. Thus a non-zero k_2 seems to be required for growth initially.

At intermediate times, when the t^2 term dominates we can always choose shearing waves with an appropriate sign and magnitude of $k_1 k_2$ such that $St^2\,(\kappa_{11}^{\infty} k_1 k_2 + \kappa_{12}^{\infty} k_2^2)$ is positive, and there is growth of the mean field. On the other hand, all shearing waves with non-zero k_2 will eventually decay, in the long time limit $t \to \infty$, if $\kappa_{11}^{\infty} > 0$, as then the t^3 term is negative definite. Thus it seems likely that the mean concentration of the passive scalar in the presence of background shear can have a shearing wave solutions which grow for some time if they have non-zero X_2 dependence, but which will eventually decay.

4.7 Conclusion

We have formulated the problem of the evolution of mean concentration of passive scalars which is being evolved by the action of non–helical random flows in the presence of the background linear shear flow. Our theory is valid for small Peclet numbers and small fluid Reynolds numbers, but it is non–perturbative in the shear parameter, i.e., it is valid for arbitrary values of the shear parameter. We make systematic use of the shearing coordinate transformation and the Galilean invariance of the linear shear flows. Using Reynolds averaging, we split the total concentration into mean and fluctuating components. The mean concentration is driven by the divergence of the turbulent flux of

the passive scalars, which in turn is determined by the statistics of the random velocity field. To determine the turbulent flux, we first need to solve for the fluctuating component of the concentration which may be expressed in terms of the mean concentration and the fluctuating velocity field. Therefore we develop the equation for the fluctuating component of the concentration perturbatively in the small parameter, Pe. We use the shearing coordinate transformation and the resistive Green's function for the linear shear flow derived in the Appendix A, to write the formal solution for the fluctuating field. Then we write explicit expression for the turbulent flux which is given in terms of unequal–time two–point velocity correlator. As a simple example, we first consider the case of delta–correlated–in–time velocity correlator and show that the turbulent flux does not depend on the shear parameter, and the expression thus found is a familiar expression in the absence of background shear flow. Therefore we conclude that the shear needs time to produce non trivial effects and it is necessary to consider velocity correlators with non zero correlation times. To study the effects of the shear on the transport properties of the passive scalar, we focussed again on the general case of finite velocity correlation times. The transport coefficients are given in general form in terms of the unequal–time two–point correlators of velocity fluctuations. Now we make use of the Galilean invariance, which is a fundamental symmetry of the problem. Making use of the result on Galilean invariant velocity correlators given in the Appendix B, we write explicit formula for the Galilean invariant turbulent flux.

Taking the divergence of the G–invariant turbulent flux, we write the evolution equation, which is an advection–diffusion equation, for the mean–field. We show that the evolution of mean–field is governed by an integro–differential equation. The advective term depends on the second order spatial derivative of mean–field and thus exhibits the properties of the diffusion which is anisotropic. To make further progress, we consider the limit in which the mean–field is a slowly varying function of both the space and the time. In this case, the mean–field evolves by the partial differential equation, instead of more formidable integro–differential equation. We then derive an explicit expression for the transport coefficient κ_{jm}, also known as the turbulent diffusivity tensor, in terms of

the velocity spectrum tensor which is the fundamental object and has been determined in Ch. 2. Some important properties of κ_{jm} are as follows:

1. κ_{jm} is symmetric in the indices (j, m) and has only four non–zero independent components, which are κ_{11}, κ_{22}, κ_{33} and κ_{12}. Other components vanish.

2. All the non–zero components of κ_{jm} are zero at time $\tau = 0$, and saturate at finite values at late times, which we denote by κ^{∞}_{jm}.

3. A general functional form for κ^{∞}_{jm} was derived and it was shown that it depends only on two dimensionless variables, $\mathrm{S_h Re}$ and Sc. This general functional form is verified in the Fig. (4.1).

4. The behaviour of all components of κ^{∞}_{jm} as a function of $|\mathrm{S_h}|$ are quite different. This is due to the effect of the shear which make the diffusion highly anisotropic.

5. In the limit of zero shear, all the diagonal components of κ^{∞}_{jm} approach non–zero values, whereas κ^{∞}_{12} becomes zero.

6. κ^{∞}_{11}, κ^{∞}_{33} and κ^{∞}_{12} are always positive, whereas κ^{∞}_{22} changes sign with $|\mathrm{S_h}|$. It starts with positive value at $\mathrm{S_h} = 0$, increases slightly with increasing values of $|\mathrm{S_h}|$, attains maximum quickly, it then becomes a decreasing function of $|\mathrm{S_h}|$ and becomes negative for large values of $|\mathrm{S_h}|$; see Figs. (4.1–4.3).

The negative sign of κ^{∞}_{22} has a noticeable effect on the evolution of the mean concentration of the passive scalar. As noted in § 4.6 the negative values of κ^{∞}_{22} and finite κ^{∞}_{12} favour growth of mean concentration of passive scalar at initial times; the growth at intermediate times can always be guaranteed. At late times the mean concentration will eventually decay due to positive sign of κ^{∞}_{11}. Thus we report a possibility of transient amplification of mean concentration of the passive scalar.

Part II

The Shear Dynamo Problem

An introduction to the shear dynamo problem

Astrophysical systems like planets, galaxies and clusters of galaxies possess magnetic fields which exhibit definite spatial ordering, in addition to a random component. The ordered (or "large–scale") components are thought to originate from turbulent dynamo action in the electrically conducting fluids in these objects. The standard paradigm involves amplification of seed magnetic fields, due to non mirror–symmetric (i.e. helical) turbulent flows, through the α–effect (Moffatt, 1978; Parker, 1979). Only recently the role of the mean shear in the turbulent flows is beginning to be appreciated. Dynamo action due to shear and turbulence has received some attention in the astrophysical contexts of accretion disks (Vishniac & Brandenburg, 1997) and galactic disks (Blackman, 1998). It has also been demonstrated that shear, in conjunction with rotating turbulent convection, can drive a large–scale dynamo (Käpylä, Korpi & Brandenburg, 2008; Hughes & Proctor, 2009).

We are interested in the more specific problem of large–scale dynamo action due to "non–helical" turbulence with mean shear. Direct numerical simulations now provide strong support for such a *shear dynamo*. Yousef et al. (2008a) demonstrated that forced small-scale non–helical turbulence in non–rotating linear shear flows leads to exponential growth of large–scale magnetic fields. These findings were later generalized by Yousef et al. (2008b) to a shearing sheet model of a differentially rotating disk with a Keplerian rotation profile. The investigations of Brandenburg et al. (2008) demonstrated the shear dynamo effect for a range of values of the Reynolds numbers and the shear parameter, and measured all components of the magnetic diffusivity tensor. While the shear dynamo has been conclusively demonstrated to function, it is not yet clear what makes it work. This outstanding, unsolved problem has been the focus of our investigations, which is being presented in chapters 5, 6, 7 and 8.

One possibility that has been suggested is dynamo action due to a "fluctuating α–effect" in turbulent flows which have zero mean helicities. In this proposal, large–scale dynamo action derives from the interaction of mean shear with fluctuations of helicity (Vishniac & Brandenburg, 1997; Sokolov, 1997; Proctor, 2007; Brandenburg et al., 2008;

Rogachevskii & Kleeorin, 2008; Heinemann, McWilliams & Schekochihin, 2011; Mitra & Brandenburg, 2012). Another suggestion is that, if even transient growth makes non axisymmetric mean magnetic fields strong enough, they themselves might drive motions which could lead to subcritical dynamo action (Rincon et al., 2008). Yet another possibility that has been suggested is "the shear–current effect" (Rogachevskii & Kleeorin, 2003, 2004, 2008). In this mechanism, it is thought that the mean shear gives rise to anisotropic turbulence, which causes an extra component of the mean electromotive force (EMF), leading to the generation of the cross–shear component of the mean magnetic field from the component parallel to the shear flow. However, there is no agreement yet whether the sign of such a coupling is favourable to the operation of a dynamo. Some analytic calculations (Rädler & Stepanov, 2006; Rüdiger & Kitchatinov, 2006) and numerical experiments (Brandenburg et al., 2008) find that the sign of the shear–current term is unfavourable for dynamo action. A quasilinear theory of dynamo action in a linear shear flow of an incompressible fluid which has random velocity fluctuations was presented in Sridhar & Subramanian (2009a,b). Unlike earlier analytic work which treated shear as a small perturbation, this work did not place any restriction on the strength of the shear. They arrived at an integro–differential equation for the evolution of the mean magnetic field and argued that the shear–current assisted dynamo is essentially absent. It should be noted that the quasilinear theory of Sridhar & Subramanian (2009a,b) assumes *zero resistivity*, and is valid in the limit of small velocity correlation times when the "first order smoothing approximation" (FOSA) holds.

Chapter 5

The Shear Dynamo Problem for Small Magnetic Reynolds Numbers: Kinematic Theory

5.1 Introduction

In this chapter we present a kinematic theory of the shear dynamo that is non perturbative in the shear strength, but perturbative in the magnetic Reynolds number (Rm); this may be thought of as FOSA *with finite resistivity*. Thus we are not limited to the quasi-linear limit of small velocity correlation times, and our conclusions are rigorously valid for velocity fluctuations which have small Rm but arbitrary fluid Reynolds number. In § 5.2 we formulate the shear dynamo problem for small Rm. Using Reynolds averaging, we split the magnetic field into mean and fluctuating components. The equation for the fluctuations is expanded perturbatively in the small parameter, Rm. Using the shearing coordinate transformation, we make an explicit calculation of the resistive Green's function for the linear shear flow. In § 5.3, the magnetic fluctuations and the mean electromotive force (EMF) are determined to lowest order in Rm. The transport coefficients are given in general form in terms of the two–point correlators of the velocity fluctuations. Galilean invariance is a basic symmetry in the problem and is the focus of § 5.4.

For Galilean invariant (G–invariant) velocity fluctuations, it is proved that the transport coefficients, although space-dependent, possess the property of translational invariance in sheared coordinate space. An explicit expression for the Galilean–invariant mean EMF is derived. We put together all the results in § 5.5 by deriving the integro–differential equation governing the time evolution of the mean magnetic field. Some important properties of this equation are discussed. In particular, it is shown that, in the formal limit of zero resistivity, the quasilinear results of Sridhar & Subramanian (2009a,b) are recovered. We also show that the natural setting for the integro–differential equation governing mean–field evolution is in sheared Fourier space. We prove a result on the form of the two–point velocity correlator in Fourier space, the derivation of which has been deferred to the Appendix B; the velocity spectrum tensor and its general properties are discussed. We then express all the integral kernels in terms of the velocity spectrum tensor, which is the fundamental dynamical quantity that needs to be specified. Summary and conclusions are presented in § 5.6.

5.2 The shear dynamo problem

5.2.1 The small Rm limit

Consider a Cartesian coordinate system with unit vectors $(\boldsymbol{e}_1, \boldsymbol{e}_2, \boldsymbol{e}_3)$ erected on a comoving patch of a differentially rotating disk. Henceforth this will be referred to as the lab frame and we will use notation $\boldsymbol{X} = (X_1, X_2, X_3)$ for the position vector, and τ for time. The fluid velocity is given by $(SX_1\boldsymbol{e}_2 + \boldsymbol{v})$, where S is the rate of shear parameter and $\boldsymbol{v}(\boldsymbol{X}, \tau)$ is a randomly fluctuating velocity field. The total magnetic field, $\boldsymbol{B}^{\rm tot}(\boldsymbol{X}, \tau)$, obeys the induction equation.

$$\left(\frac{\partial}{\partial\tau} \,+\, SX_1\frac{\partial}{\partial X_2}\right)\boldsymbol{B}^{\rm tot} \,-\, SB_1^{\rm tot}\boldsymbol{e}_2 \,=\, \boldsymbol{\nabla}\times\left(\boldsymbol{v}\times\boldsymbol{B}^{\rm tot}\right) \,+\, \eta\boldsymbol{\nabla}^2\boldsymbol{B}^{\rm tot} \qquad (5.1)$$

It is useful to note that the induction equation is unaffected by a uniform rotation of the frame of reference. So our coordinate system can refer to an inertial frame, or to

a comoving patch of a differentially rotating disk. We study a kinematic problem in this chapter, so will assume that the velocity field is prescribed. We also assume that the velocity fluctuations have zero mean ($\langle \boldsymbol{v} \rangle = \boldsymbol{0}$), with root–mean–squared amplitude $v_{\rm rms}$ on some typical spatial scale ℓ. The *magnetic Reynolds number* may be defined as ${\rm Rm} = (v_{\rm rms}\ell/\eta)$; note that Rm has been defined with respect to the fluctuating velocity field, not the background shear velocity field. To address the dynamo problem, we will use the approach of the theory of mean–field electrodynamics (Moffatt, 1978; Krause & Rädler, 1980; Brandenburg & Subramanian, 2005). Here, the action of the velocity fluctuations on some seed magnetic field is assumed to produce a total magnetic field with a well–defined *mean–field* ($\boldsymbol{B}$) and a *fluctuating–field* ($\boldsymbol{b}$):

$$\boldsymbol{B}^{\rm tot} \; = \; \boldsymbol{B} \; + \; \boldsymbol{b} \, , \qquad \left\langle \boldsymbol{B}^{\rm tot} \right\rangle \; = \; \boldsymbol{B} \, , \qquad \langle \boldsymbol{b} \rangle \; = \; \boldsymbol{0} \tag{5.2}$$

where $\langle \; \rangle$ denotes ensemble averaging in the sense of Reynolds. Applying Reynolds averaging to the induction Eqn. (5.1), we obtain the following equations governing the dynamics of the mean and fluctuating magnetic fields:

$$\left(\frac{\partial}{\partial \tau} \; + \; S X_1 \frac{\partial}{\partial X_2} \right) \boldsymbol{B} \; - \; S B_1 \boldsymbol{e}_2 \quad = \quad \boldsymbol{\nabla} \times \boldsymbol{\mathcal{E}} \; + \; \eta \boldsymbol{\nabla}^2 \boldsymbol{B} \tag{5.3}$$

$$\left(\frac{\partial}{\partial \tau} \; + \; S X_1 \frac{\partial}{\partial X_2} \right) \boldsymbol{b} \; - \; S b_1 \boldsymbol{e}_2 \quad = \quad \boldsymbol{\nabla} \times \left(\boldsymbol{v} \times \boldsymbol{B} \right) \; + \; \boldsymbol{\nabla} \times \left(\boldsymbol{v} \times \boldsymbol{b} - \langle \boldsymbol{v} \times \boldsymbol{b} \rangle \right) \; + \; \eta \boldsymbol{\nabla}^2 \boldsymbol{b} \tag{5.4}$$

where $\boldsymbol{\mathcal{E}} = \langle \boldsymbol{v} \times \boldsymbol{b} \rangle$ is the mean electromotive force (EMF). The first step towards solving the problem is to solve Eqn. (5.4) for $\boldsymbol{b}$, then calculate $\boldsymbol{\mathcal{E}}$ and obtain a closed equation for the mean–field, $\boldsymbol{B}(\boldsymbol{X}, \tau)$. In the framework of the above mean–field theory, the *shear dynamo problem* may be posed as follows: under what conditions does the equation for $\boldsymbol{B}(\boldsymbol{X}, \tau)$ admit growing solutions ? In particular, are growing solutions possible when the velocity field is non–helical (i.e. when the velocity field is mirror symmetric) ?

The problem is, in general, a difficult one, but it can be approached perturbatively

in the limit of small Rm. When $\mathrm{Rm} \ll 1$, we can expand $\boldsymbol{b}$ in a series,

$$\boldsymbol{b} \;=\; \boldsymbol{b}^{(0)} \;+\; \boldsymbol{b}^{(1)} \;+\; \boldsymbol{b}^{(2)} \;+\; \ldots \tag{5.5}$$

where $\boldsymbol{b}^{(n)}$ is of order $\boldsymbol{b}^{(n-1)}$ multiplied by the small quantity Rm. The equations governing the time evolution of these quantitites are

$$\left(\frac{\partial}{\partial\tau} \;+\; SX_1\frac{\partial}{\partial X_2}\right)\boldsymbol{b}^{(0)} \;-\; Sb_1^{(0)}\boldsymbol{e}_2 \;=\; \boldsymbol{\nabla}\times(\boldsymbol{v}\times\boldsymbol{B}) \;+\; \eta\boldsymbol{\nabla}^2\boldsymbol{b}^{(0)} \tag{5.6}$$

$$\left(\frac{\partial}{\partial\tau} \;+\; SX_1\frac{\partial}{\partial X_2}\right)\boldsymbol{b}^{(n)} \;-\; Sb_1^{(n)}\boldsymbol{e}_2 \;=\; \boldsymbol{\nabla}\times\left(\boldsymbol{v}\times\boldsymbol{b}^{(n-1)} - \left\langle\boldsymbol{v}\times\boldsymbol{b}^{(n-1)}\right\rangle\right) \;+\; \eta\boldsymbol{\nabla}^2\boldsymbol{b}^{(n)}$$
$$\text{for } n \;=\; 1, 2, \ldots \tag{5.7}$$

Note that $\boldsymbol{\nabla}\times(\boldsymbol{v}\times\boldsymbol{B})$ acts as a source term for $\boldsymbol{b}^{(0)}$, whereas the source term for $\boldsymbol{b}^{(n)}$ is $\boldsymbol{\nabla}\times\left(\boldsymbol{v}\times\boldsymbol{b}^{(n-1)} - \left\langle\boldsymbol{v}\times\boldsymbol{b}^{(n-1)}\right\rangle\right)$. Once the $\boldsymbol{b}^{(n)}$ have been determined, the mean EMF can be calculated directly by

$$\boldsymbol{\mathcal{E}} \;=\; \langle\boldsymbol{v}\times\boldsymbol{b}\rangle \;=\; \left\langle\boldsymbol{v}\times\left(\boldsymbol{b}^{(0)} \;+\; \boldsymbol{b}^{(1)} \;+\; \boldsymbol{b}^{(2)} \;+\; \ldots\right)\right\rangle \tag{5.8}$$

In this chapter, we work to lowest order in Rm, so we need to work out only $\boldsymbol{b}^{(0)}$; Eqn. (5.7) will not be used.

5.2.2 The shearing coordinate transformation

In this chapter we will focus on the determination of the lowest order term, $\boldsymbol{b}^{(0)}$. We also assume that the fluctuating velocity field is incompressible; i.e. $\boldsymbol{\nabla}\cdot\boldsymbol{v} \;=\; 0$. Then the evolution of $\boldsymbol{b}^{(0)}$ is governed by,

$$\left(\frac{\partial}{\partial\tau} \;+\; SX_1\frac{\partial}{\partial X_2}\right)\boldsymbol{b}^{(0)} \;-\; Sb_1^{(0)}\boldsymbol{e}_2 \;=\; (\boldsymbol{B}\cdot\boldsymbol{\nabla})\,\boldsymbol{v} \;-\; (\boldsymbol{v}\cdot\boldsymbol{\nabla})\,\boldsymbol{B} \;+\; \eta\boldsymbol{\nabla}^2\boldsymbol{b}^{(0)} \tag{5.9}$$

We will now solve this equation for $\boldsymbol{b}^{(0)}$ and determine the mean EMF. General methods of solving equations such as Eqn. (5.9) are presented in Krause & Rädler (1980), but we prefer to employ the shearing coordinate transformation because it is directly adapted to the problem at hand and greatly simplifies the task of writing down the Green's function solution. The $(X_1\partial/\partial X_2)$ term makes Eqn. (5.9) inhomogeneous in the coordinate X_1. This term can be eliminated through a shearing transformation to new spacetime variables, given in Eqn. (A.2) of Appendix A. Thus, using Eqns. (A.2) and (A.3), given in the Appendix A, and defining the new variables, which are component–wise equal to the old variables:

$$\boldsymbol{H}(\boldsymbol{x},t) \;=\; \boldsymbol{B}(\boldsymbol{X},\tau)\,, \qquad \boldsymbol{h}(\boldsymbol{x},t) \;=\; \boldsymbol{b}^{(0)}(\boldsymbol{X},\tau)\,, \qquad \boldsymbol{u}(\boldsymbol{x},t) \;=\; \boldsymbol{v}(\boldsymbol{X},\tau) \tag{5.10}$$

Note that, just like the old variables, the new variables are expanded in the fixed Cartesian basis of the lab frame. For example, $\boldsymbol{H} = H_1\boldsymbol{e}_1 + H_2\boldsymbol{e}_2 + H_3\boldsymbol{e}_3$, where $H_i(\boldsymbol{x},t) = B_i(\boldsymbol{X},\tau)$, and similarly for the other variables. In the new variables, Eqn. (5.9) becomes,

$$\frac{\partial \boldsymbol{h}}{\partial t} \;-\; Sh_1\boldsymbol{e}_2 \;=\; \left(\boldsymbol{H}\boldsymbol{\cdot}\,\frac{\partial}{\partial \boldsymbol{x}} - StH_1\frac{\partial}{\partial x_2}\right)\boldsymbol{u} \;-\; \left(\boldsymbol{u}\boldsymbol{\cdot}\,\frac{\partial}{\partial \boldsymbol{x}} - Stu_1\frac{\partial}{\partial x_2}\right)\boldsymbol{H} \;+\; \eta\boldsymbol{\nabla}^2\boldsymbol{h} \tag{5.11}$$

which can be expressed in component form as

$$\left(\frac{\partial}{\partial t} \;-\; \eta\boldsymbol{\nabla}^2\right) h_m(\boldsymbol{x},t) \;=\; q_m(\boldsymbol{x},t) \tag{5.12}$$

where $\boldsymbol{\nabla}^2$ is given by Eqn. (A.4), and

$$q_m(\boldsymbol{x},t) \;=\; \left[H_l - St\delta_{l2}H_1\right]u_{ml} \;-\; \left[u_l - St\delta_{l2}u_1\right]H_{ml} \;+\; S\delta_{m2}h_1 \tag{5.13}$$

We have used notation $u_{ml} = (\partial u_m/\partial x_l)$ and $H_{ml} = (\partial H_m/\partial x_l)$. Below we discuss the Green's function for Eqn. (5.12).

5.2.3 The resistive Green's function for a linear shear flow

Equation (5.12) is linear, homogeneous in $\boldsymbol{x}$ and inhomogeneous in t and is similar to Eqn. (A.1) of the Appendix A for which the general expressions for the Green's function, both, in the Fourier and the real space, have been constructed. The general solution of Eqn. (5.12) can be written in the form,

$$\begin{aligned} h_m(\boldsymbol{x},t) \;=\; & \int \mathrm{d}^3x'\, G_\eta(\boldsymbol{x}-\boldsymbol{x}',t,s)\; h_m(\boldsymbol{x}',s) \\ & + \int_s^t \mathrm{d}t' \int \mathrm{d}^3x'\, G_\eta(\boldsymbol{x}-\boldsymbol{x}',t,t')\; q_m(\boldsymbol{x}',t')\;; \qquad \text{for any } s<t\,, \end{aligned} \tag{5.14}$$

where $G_\eta(\boldsymbol{x},t,t')$ is the *resistive Green's function* for the linear shear flow, which satisfies,

$$\left(\frac{\partial}{\partial t} - \eta\boldsymbol{\nabla}^2\right) G_\eta(\boldsymbol{x},t,t') \;=\; 0 \tag{5.15a}$$

$$\lim_{t'\to t_-}\; G_\eta(\boldsymbol{x},t,t') \;=\; \delta^3(\boldsymbol{x}) \tag{5.15b}$$

$$G_\eta(\boldsymbol{x},t,t') \quad \text{is non–zero only when} \quad 0\le t'<t. \tag{5.15c}$$

$$G_\eta(\boldsymbol{x}-\boldsymbol{x}',t,t_0) \;=\; \int \mathrm{d}^3x''\, G_\eta(\boldsymbol{x}-\boldsymbol{x}'',t,s)\, G_\eta(\boldsymbol{x}''-\boldsymbol{x}',s,t_0)\,; \quad \text{for } t_0<s<t\,. \tag{5.15d}$$

The method of construction of the resistive Green's function and some of its general properties are given in detail in the Appendix A. Following the derivation given in the Appendix A, the spatial Fourier transform of the Green's function may be written as,

$$\begin{aligned} \widetilde{G}_\eta(\boldsymbol{k},t,t') \;&=\; \exp\left[-\eta\int_{t'}^{t}\mathrm{d}s\, K^2(\boldsymbol{k},s)\right] \\ &=\; \exp\left[-\eta\left(k^2(t-t') - S\,k_1\,k_2(t^2-t'^2) + \frac{S^2}{3}\,k_2^2(t^3-t'^3)\right)\right] \end{aligned} \tag{5.16}$$

where, as per Eqn. (5.15c) above, $t>t'$; $K^2(\boldsymbol{k},t) = (k_1 - Stk_2)^2 + k_2^2 + k_3^2$; and $\boldsymbol{k}$, being conjugate to the sheared coordinate vector $\boldsymbol{x}$, can be regarded as a *sheared wavevector*.

Note also that $\widetilde{G}_\eta(\boldsymbol{k}, t, t')$ is a positive quantity which takes values between 0 and 1, and that it is an even function of $\boldsymbol{k}$ and k_3.

The inverse Fourier transform of Eqn. (5.16) gives the expression for $G_\eta(\boldsymbol{x}, t, t')$, which may be thought of as a *sheared heat kernel* given by,

$$G_\eta(\boldsymbol{x}, t, t') = [4\pi\eta(t-t')]^{-3/2}\left[1 + \frac{S^2}{12}(t-t')^2\right]^{-1/2} \times \\ \times \exp\left[-\frac{1}{4\eta(t-t')}\left(\frac{\overline{x}_1^2}{\sigma_1^2} + \frac{\overline{x}_2^2}{\sigma_2^2} + \overline{x}_3^2\right)\right], \tag{5.17}$$

which is equivalent to the one first derived in Krause & Rädler (1971). For full derivation of Eqn. (5.17) and meanings of various terms, please refer to the Appendix A.

We now note some properties of the Green's function. For convenience we choose the shear parameter, S, to be negative: then the quantities, $f \geq 0$, $0 \leq \theta \leq \pi/2$, $\sigma_1 \geq 1$ and $0 \leq \sigma_2 \leq 1$ (see Appendix A for the meaning). At fixed t and t', the Green's function is a Gaussian with *long axis* along $\overline{x}_1$, *short axis* along $\overline{x}_2$, and the *intermediate axis* along $\overline{x}_3$ (see Appendix A for the meaning). To obtain some idea of the behaviour of the Green's function, it is useful to plot isocontours in the sheared coordinate space (x_1, x_2, x_3) at different values of t and t'. Figure (5.1) displays isocontours in the x_1–x_2 plane at four different values of t for $t' = 0$; we have chosen $x_3 = 0$ and $t' = 0$ in the interests of brevity of presentation. The figure is plotted in shearing coordinates, with respect to which diffusion is anisotropic and there is no advection. It may be noted that the Green's function shows a shearing motion *against* the direction of the actual shear. As t increases from zero to infinity, θ (which is the angle the long axis makes with the x_1–axis) increases from 45° to 90°, and all the principal axes increase without bound.

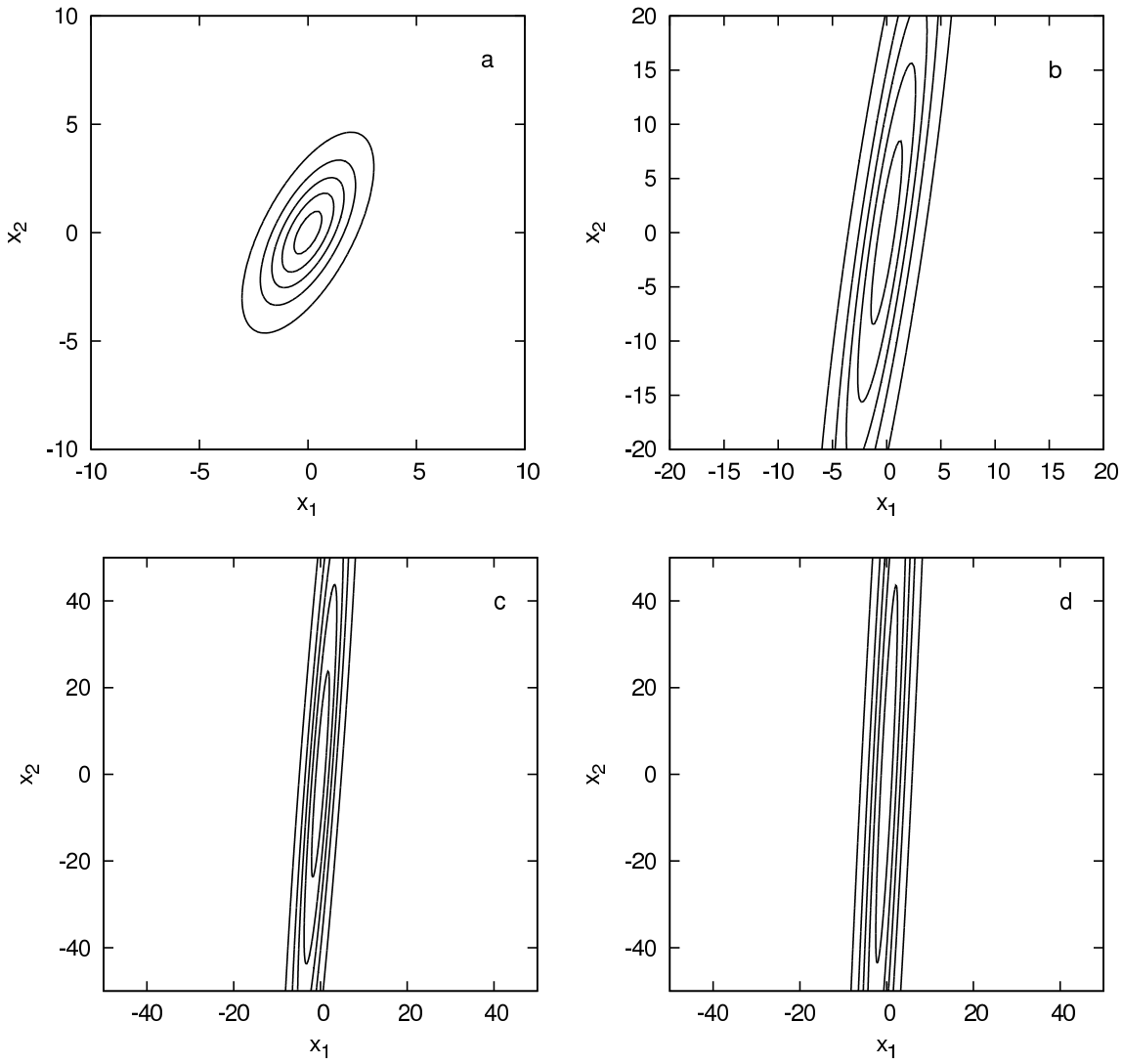

Figure 5.1: Isocontours of the resistive Green's function $G_\eta(\boldsymbol{x}, t, t')$ plotted in the x_1–x_2 plane of the shearing coordinate system, for $t' = 0$ at four different values of t. Units are such that $S = -2\,; \eta = 1$. Five isocontours at 90%, 70%, 50%, 30% and 10% of the maximum value are displayed. Panels (a), (b), (c) and (d) correspond to times $t = 1$, $t = 5$, $t = 10$ and $t = 15$.

5.3 Magnetic fluctuations & mean EMF at small Rm

5.3.1 Explicit solution for $\boldsymbol{h}(\boldsymbol{x}, t)$

We are interested in the particular solution to Eqn. (5.12) (i.e. the *forced solution*) which vanishes at $t = 0$. This can be written as

$$h_m(\boldsymbol{x}, t) \;=\; \int_0^t \mathrm{d}t' \int \mathrm{d}^3x'\, G_\eta(\boldsymbol{x} - \boldsymbol{x}', t, t')\; q_m(\boldsymbol{x}', t') \tag{5.18}$$

Substituting the expression for q_m from Eqn. (5.13) in Eqn. (5.18), we have

$$\begin{aligned} h_m(\boldsymbol{x}, t) \;=\; & \int_0^t \mathrm{d}t' \int \mathrm{d}^3x'\, G_\eta(\boldsymbol{x} - \boldsymbol{x}', t, t') \times \\ & \qquad \times \left\{ \left[H'_l - St' \delta_{l2} H'_1 \right] u'_{ml} \;-\; \left[u'_l - St' \delta_{l2} u'_1 \right] H'_{ml} \right\} \\ & + S\delta_{m2} \int_0^t \mathrm{d}t' \int \mathrm{d}^3x'\, G_\eta(\boldsymbol{x} - \boldsymbol{x}', t, t')\; h_1(\boldsymbol{x}', t') \end{aligned} \tag{5.19}$$

where primes denote evaluation at spacetime point $(\boldsymbol{x}', t')$. The solution is not yet in explicit form because the last term on the right side contains the unknown quantity $h_1(\boldsymbol{x}', t')$. Thus we need to work out the integral

$$\begin{aligned} \int_0^t \mathrm{d}t' \int \mathrm{d}^3x'\, G_\eta(\boldsymbol{x} - \boldsymbol{x}', t, t')\, h_1(\boldsymbol{x}', t') \;=\; & \int_0^t \mathrm{d}t' \int \mathrm{d}^3x'\, G_\eta(\boldsymbol{x} - \boldsymbol{x}', t, t') \times \\ & \times \int_0^{t'} \mathrm{d}t'' \int \mathrm{d}^3x''\, G_\eta(\boldsymbol{x}' - \boldsymbol{x}'', t', t'') \times \\ \times \;\; & \left\{ \left[H''_l - St'' \delta_{l2} H''_1 \right] u''_{1l} - \left[u''_l - St'' \delta_{l2} u''_1 \right] H''_{1l} \right\} \end{aligned}$$

where $''$ means evaluation at spacetime point $(\boldsymbol{x}'', t'')$. Note that, on the right side, $\boldsymbol{x}'$ occurs only in the Green's functions. So, by using the property given in Eqn. (5.15d),

the integral over $\boldsymbol{x}'$ can be performed. Then

$$\begin{aligned}\int_0^t \mathrm{d}t' \int \mathrm{d}^3x'\, G_\eta(\boldsymbol{x}-\boldsymbol{x}',t,t')\, h_1(\boldsymbol{x}',t') &= \int_0^t \mathrm{d}t' \int_0^{t'} \mathrm{d}t'' \int \mathrm{d}^3x''\, G_\eta(\boldsymbol{x}-\boldsymbol{x}'',t,t'') \times \\ &\times \left\{ \left[H_l'' - St''\delta_{l2} H_1'' \right] u_{1l}'' - \left[u_l'' - St''\delta_{l2} u_1'' \right] H_{1l}'' \right\}\end{aligned}$$

The double–time integrals can be reduced to single–time integrals because of the following simple identity. For any function $f(\boldsymbol{x},t)$, we have

$$\begin{aligned}\int_0^t \mathrm{d}t' \int_0^{t'} \mathrm{d}t'' \int \mathrm{d}^3x''\, f(\boldsymbol{x}'',t'') &= \int_0^t \mathrm{d}t'' \int \mathrm{d}^3x''\, f(\boldsymbol{x}'',t'') \int_{t''}^t \mathrm{d}t' \\ &= \int_0^t \mathrm{d}t''\, (t-t'') \int \mathrm{d}^3x''\, f(\boldsymbol{x}'',t'') \\ &= \int_0^t \mathrm{d}t'\, (t-t') \int \mathrm{d}^3x'\, f(\boldsymbol{x}',t')\end{aligned}$$

where in the last equality we have merely replaced the dummy integration variables $(\boldsymbol{x}'',t'')$ by $(\boldsymbol{x}',t')$. Then we have

$$\begin{aligned}\int_0^t \mathrm{d}t' \int \mathrm{d}^3x'\, G_\eta(\boldsymbol{x}-\boldsymbol{x}',t,t')\, h_1(\boldsymbol{x}',t') &= \int_0^t \mathrm{d}t'\, (t-t') \int \mathrm{d}^3x'\, G_\eta(\boldsymbol{x}-\boldsymbol{x}'',t,t'') \times \\ &\times \left\{ \left[H_l' - St'\delta_{l2} H_1' \right] u_{1l}' - \left[u_l' - St'\delta_{l2} u_1' \right] H_{1l}' \right\}\end{aligned}$$

Therefore the forced solution to Eqn. (5.12) can finally be written in explicit form as

$$\begin{aligned}h_m(\boldsymbol{x},t) &= \int_0^t \mathrm{d}t' \int \mathrm{d}^3x'\, G_\eta(\boldsymbol{x}-\boldsymbol{x}',t,t')\, \left[u_{ml}' + S(t-t')\delta_{m2} u_{1l}' \right] \times \\ &\qquad \times \left[H_l' - St'\delta_{l2} H_1' \right] \\ &- \int_0^t \mathrm{d}t' \int \mathrm{d}^3x'\, G_\eta(\boldsymbol{x}-\boldsymbol{x}',t,t')\, \left[H_{ml}' + S(t-t')\delta_{m2} H_{1l}' \right] \times \\ &\qquad \times \left[u_l' - St'\delta_{l2} u_1' \right] \qquad (5.20)\end{aligned}$$

This gives the magnetic fluctuation to lowest order in Rm.

5.3.2 Explicit expression for the mean EMF

To lowest order in Rm, the mean EMF is given by $\boldsymbol{\mathcal{E}} = \left\langle \boldsymbol{v}\times\boldsymbol{b}^{(0)} \right\rangle = \langle \boldsymbol{u}\times\boldsymbol{h}\rangle$, where Eqn. (5.20) for $\boldsymbol{h}$ should be substituted. The averaging, $\langle\ \rangle$, acts only on the velocity variables but not the mean field; i.e. $\langle \boldsymbol{uuH}\rangle = \langle \boldsymbol{uu}\rangle\, \boldsymbol{H}$ etc. After interchanging the dummy indices (l, m) in the last term, the mean EMF is given in component form as

$$
\begin{aligned}
\mathcal{E}_i(\boldsymbol{x},t) \;=\;& \epsilon_{ijm}\,\langle u_j h_m\rangle \\
=\;& \int_0^t \mathrm{d}t' \int \mathrm{d}^3x'\, G_\eta(\boldsymbol{x}-\boldsymbol{x}',t,t') \left[\widehat{\alpha}_{il}(\boldsymbol{x},t,\boldsymbol{x}',t') \;+\; S(t-t')\widehat{\beta}_{il}(\boldsymbol{x},t,\boldsymbol{x}',t')\right] \times \\
& \qquad \times \left[H'_l \;-\; St'\delta_{l2}\, H'_1\right] \\
-\;& \int_0^t \mathrm{d}t' \int \mathrm{d}^3x'\, G_\eta(\boldsymbol{x}-\boldsymbol{x}',t,t') \left[\,\widehat{\eta}_{iml}(\boldsymbol{x},t,\boldsymbol{x}',t') \;-\; St'\delta_{m2}\,\widehat{\eta}_{i1l}(\boldsymbol{x},t,\boldsymbol{x}',t')\right] \times \\
& \qquad \times \left[H'_{lm} \;+\; S(t-t')\delta_{l2}\, H'_{1m}\right]
\end{aligned}
\tag{5.21}
$$

Here, $(\widehat{\alpha}\,, \widehat{\beta}\,, \widehat{\eta}\,)$, are *transport coefficients*, which are defined in terms of the $\boldsymbol{uu}$ velocity correlators by

$$
\begin{aligned}
\widehat{\alpha}_{il}(\boldsymbol{x},t,\boldsymbol{x}',t') &= \epsilon_{ijm}\,\langle u_j(\boldsymbol{x},t)\, u_{ml}(\boldsymbol{x}',t')\rangle \\
\widehat{\beta}_{il}(\boldsymbol{x},t,\boldsymbol{x}',t') &= \epsilon_{ij2}\,\langle u_j(\boldsymbol{x},t)\, u_{1l}(\boldsymbol{x}',t')\rangle \\
\widehat{\eta}_{iml}(\boldsymbol{x},t,\boldsymbol{x}',t') &= \epsilon_{ijl}\,\langle u_j(\boldsymbol{x},t)\, u_m(\boldsymbol{x}',t')\rangle
\end{aligned}
\tag{5.22}
$$

It is also useful to consider velocity statistics in terms of $\boldsymbol{vv}$ velocity correlators, because this is referred to the lab frame. By definition, from (Eqn. 5.10),

$$u_m(\boldsymbol{x},t) \;=\; v_m(\boldsymbol{X}(\boldsymbol{x},t),t) \tag{5.23}$$

where

$$X_1 \;=\; x_1\,, \qquad X_2 \;=\; x_2 + Stx_1\,, \qquad X_3 \;=\; x_3\,, \qquad \tau \;=\; t \tag{5.24}$$

is the inverse of the shearing transformation given in Eqn. (A.2). Using

$$\frac{\partial}{\partial x_l} \;=\; \frac{\partial}{\partial X_l} \;+\; S\tau\,\delta_{l1}\,\frac{\partial}{\partial X_2} \tag{5.25}$$

the velocity gradient u_{ml} can be written as

$$u_{ml} \;\equiv\; \frac{\partial u_m}{\partial x_l} \;=\; \left(\frac{\partial}{\partial X_l} \;+\; S\tau\,\delta_{l1}\,\frac{\partial}{\partial X_2}\right) v_m \;=\; v_{ml} \;+\; S\tau\,\delta_{l1}\,v_{m2} \tag{5.26}$$

where $v_{ml} = (\partial v_m/\partial X_l)$. Then the transport coefficients are given in terms of the $\boldsymbol{vv}$ velocity correlators by

$$\begin{aligned}
\widehat{\alpha}_{il}(\boldsymbol{x},t,\boldsymbol{x}',t') &= \epsilon_{ijm}\left[\langle v_j(\boldsymbol{X},t)\,v_{ml}(\boldsymbol{X}',t')\rangle \;+\; St'\,\delta_{l1}\,\langle v_j(\boldsymbol{X},t)\,v_{m2}(\boldsymbol{X}',t')\rangle\right] \\
\widehat{\beta}_{il}(\boldsymbol{x},t,\boldsymbol{x}',t') &= \epsilon_{ij2}\left[\langle v_j(\boldsymbol{X},t)\,v_{1l}(\boldsymbol{X}',t')\rangle \;+\; St'\,\delta_{l1}\,\langle v_j(\boldsymbol{X},t)\,v_{12}(\boldsymbol{X}',t')\rangle\right] \\
\widehat{\eta}_{iml}(\boldsymbol{x},t,\boldsymbol{x}',t') &= \epsilon_{ijl}\,\langle v_j(\boldsymbol{X},t)\,v_m(\boldsymbol{X}',t')\rangle
\end{aligned} \tag{5.27}$$

where $\boldsymbol{X}$ and $\boldsymbol{X}'$ are shorthand for

$$\boldsymbol{X} \;=\; (x_1\,, x_2 + Stx_1\,, x_3)\;, \qquad \boldsymbol{X}' \;=\; (x_1'\,, x_2' + St'x_1'\,, x_3') \tag{5.28}$$

Equation (5.21), together with (5.22) or (5.27), gives the mean EMF in general form. $\boldsymbol{X}$ can be thought of as the coordinates of the origin at time t of an observer *comoving* with the background shear flow, who was at $\boldsymbol{x}$ at time equal to zero. Similarly, $\boldsymbol{X}'$ can be thought of as the coordinates of the origin at time t' of an observer *comoving* with

the background shear flow, who was at $\boldsymbol{x}'$ at time equal to zero.

5.4 Galilean–invariant velocity statistics

5.4.1 Galilean invariance of the induction equation

The induction equation, Eqn. (5.1), for the total magnetic field — and also Eqns. (5.3) and (5.4) for the mean and fluctuating components — have a fundamental invariance property relating to measurements made by a special subset of all observers, called *comoving observers* in Sridhar & Subramanian (2009a,b). As this is an important concept with far reaching consequences, we describe it in detail in Appendix B.

Let $\left[\tilde{\boldsymbol{B}^{\rm tot}}(\tilde{\boldsymbol{X}},\tilde{\tau}),\tilde{\boldsymbol{B}}(\tilde{\boldsymbol{X}},\tilde{\tau}),\tilde{\boldsymbol{b}}(\tilde{\boldsymbol{X}},\tilde{\tau}),\tilde{\boldsymbol{v}}(\tilde{\boldsymbol{X}},\tilde{\tau})\right]$ denote the total, the mean, the fluctuating magnetic fields and the fluctuating velocity field, respectively, as measured by the comoving observer. These are all equal to the respective quantities measured in the lab frame:

$$\left[\tilde{\boldsymbol{B}^{\rm tot}}(\tilde{\boldsymbol{X}},\tilde{\tau}),\tilde{\boldsymbol{B}}(\tilde{\boldsymbol{X}},\tilde{\tau}),\tilde{\boldsymbol{b}}(\tilde{\boldsymbol{X}},\tilde{\tau}),\tilde{\boldsymbol{v}}(\tilde{\boldsymbol{X}},\tilde{\tau})\right] \;=\; \left[\boldsymbol{B}^{\rm tot}(\boldsymbol{X},\tau),\boldsymbol{B}(\boldsymbol{X},\tau),\boldsymbol{b}(\boldsymbol{X},\tau),\boldsymbol{v}(\boldsymbol{X},\tau)\right] \tag{5.29}$$

That this must be true may be understood as follows: Magnetic fields are invariant under non–relativistic boosts, so the total, mean and fluctuating components of the magnetic fields must be the same in both frames. To see that the fluctuating velocity fields must be the same, we note from the discussions of the Appendix B that the total fluid velocity measured by the comoving observer is, by definition, equal to $\left(S\tilde{X_1}\boldsymbol{e}_2+\tilde{\boldsymbol{v}}(\tilde{\boldsymbol{X}},\tilde{\tau})\right)$. This must be equal to the difference between the velocity in the lab frame, $(SX_1\boldsymbol{e}_2+\boldsymbol{v}(\boldsymbol{X},\tau))$, and $(S\xi_1\boldsymbol{e}_2)$, which is the velocity of the comoving observer with respect to the lab frame. Using $\tilde{X_1}=X_1-\xi_1$, we see that $\tilde{\boldsymbol{v}}(\tilde{\boldsymbol{X}},\tilde{\tau})=\boldsymbol{v}(\boldsymbol{X},\tau)$.

Using Eqns. (B.2) and (B.3) of the Appendix B, we find that Eqns. (5.1), (5.3) and (5.4) are invariant under the simultaneous transformations given in Eqns. (B.2) and (5.29). This symmetry property is actually an invariance under a subset of the full ten–parameter Galilean group, parametrized by the five quantities $(\xi_1,\xi_2,\xi_3,\tau_0,S)$; for

brevity we will refer to this restricted symmetry as Galilean invariance, or simply GI.

It is important to note that the lab and comoving frames need not constitute inertial coordinate systems. One of the main applications of our theory is to the *shearing sheet*, which is a local description of a differentially rotating disk. In this case the velocity field will be affected by Coriolis forces. The only requirement is that the magnetic field satisfies the induction Eqn. (5.1).

5.4.2 Galilean–invariant velocity correlators

In the low Rm limit, we require only the two–point velocity correlators appearing in Eqn. (5.27). We derive Galilean–invariant expressions for all the relevant velocity correlators. Following the basic ideas of G–invariant velocity correlators discussed in the Appendix B, we rewrite below the statements of Galilean–invariance of unequal time two–point velocity correlator and the correlation between velocities and their gradients (see Eqns. (B.5) and (B.6) given in the Appendix B):

$$\begin{aligned} \langle v_i(\boldsymbol{R},\tau)\, v_j(\boldsymbol{R}',\tau')\rangle &= \langle v_i(\boldsymbol{R}+\boldsymbol{X}_c(\boldsymbol{\xi},\tau),\tau)\, v_j(\boldsymbol{R}'+\boldsymbol{X}_c(\boldsymbol{\xi},\tau'),\tau')\rangle \\ \langle v_i(\boldsymbol{R},\tau)\, v_{jl}(\boldsymbol{R}',\tau')\rangle &= \langle v_i(\boldsymbol{R}+\boldsymbol{X}_c(\boldsymbol{\xi},\tau),\tau)\, v_{jl}(\boldsymbol{R}'+\boldsymbol{X}_c(\boldsymbol{\xi},\tau'),\tau')\rangle \end{aligned} \tag{5.30}$$

for all $(\boldsymbol{R},\boldsymbol{R}',\tau,\tau',\boldsymbol{\xi})$. We want to choose $(\boldsymbol{R},\boldsymbol{R}',\tau,\tau',\boldsymbol{\xi})$ as functions of $(\boldsymbol{x},\boldsymbol{x}',t,t')$ such that we can use Eqn. (5.30) to simplify the velocity correlators in Eqn. (5.27). We note that Eqns. (5.28) and (B.1) give

$$\boldsymbol{X} = \boldsymbol{X}_c(\boldsymbol{x},t)\,, \qquad \boldsymbol{X}' = \boldsymbol{X}_c(\boldsymbol{x}',t') \tag{5.31}$$

It is therefore natural to choose

$$\tau = t\,, \qquad \tau' = t' \tag{5.32}$$

Thus the velocity correlators we require can now be written as

$$\begin{aligned}\langle v_i(\boldsymbol{X},t)\, v_j(\boldsymbol{X}',t')\rangle &= \langle v_i(\boldsymbol{X}_c(\boldsymbol{x},t),t)\, v_j(\boldsymbol{X}_c(\boldsymbol{x}',t'),t')\rangle \\ \langle v_i(\boldsymbol{X},t)\, v_{jl}(\boldsymbol{X}',t')\rangle &= \langle v_i(\boldsymbol{X}_c(\boldsymbol{x},t),t)\, v_{jl}(\boldsymbol{X}_c(\boldsymbol{x}',t'),t')\rangle \end{aligned} \tag{5.33}$$

Comparing Eqn. (5.33) with Eqn. (5.30), we see that if we choose

$$\boldsymbol{R} = \boldsymbol{X}_c(\boldsymbol{x},t), \qquad \boldsymbol{R}' = \boldsymbol{X}_c(\boldsymbol{x}',t') \tag{5.34}$$

then Eqn. (5.33), together with Eqns. (B.1) and (5.30), implies that

$$\begin{aligned}\langle v_i(\boldsymbol{X},t)v_j(\boldsymbol{X}',t')\rangle &= \langle v_i(\boldsymbol{R},\tau)v_j(\boldsymbol{R}',\tau')\rangle \\ &= \langle v_i(\boldsymbol{R}+\boldsymbol{X}_c(\boldsymbol{\xi},\tau),\tau)v_j(\boldsymbol{R}'+\boldsymbol{X}_c(\boldsymbol{\xi},\tau'),\tau')\rangle \\ &= \langle v_i(\boldsymbol{X}_c(\boldsymbol{x}+\boldsymbol{\xi},t),t)v_j(\boldsymbol{X}_c(\boldsymbol{x}'+\boldsymbol{\xi},t'),t')\rangle\end{aligned}$$

Similarly

$$\langle v_i(\boldsymbol{X},t)v_{jl}(\boldsymbol{X}',t')\rangle = \langle v_i(\boldsymbol{X}_c(\boldsymbol{x}+\boldsymbol{\xi},t),t)v_{jl}(\boldsymbol{X}_c(\boldsymbol{x}'+\boldsymbol{\xi},t'),t')\rangle \tag{5.35}$$

Now it is natural to choose

$$\boldsymbol{\xi} = -\frac{1}{2}(\boldsymbol{x}+\boldsymbol{x}') \tag{5.36}$$

Then

$$\begin{aligned}\langle v_i(\boldsymbol{X},\tau)v_j(\boldsymbol{X}',\tau')\rangle &= \left\langle v_i\left(\boldsymbol{X}_c\left(\frac{\boldsymbol{x}-\boldsymbol{x}'}{2},t\right),t\right) v_j\left(\boldsymbol{X}_c\left(\frac{\boldsymbol{x}'-\boldsymbol{x}}{2},t'\right),t'\right)\right\rangle \\ &= R_{ij}(\boldsymbol{x}-\boldsymbol{x}',t,t')\end{aligned} \tag{5.37}$$

Similarly,

$$\begin{aligned}\langle v_i(\boldsymbol{X},\tau)v_{jl}(\boldsymbol{X}',\tau')\rangle &= \left\langle v_i\left(\boldsymbol{X}_c\left(\frac{\boldsymbol{x}-\boldsymbol{x}'}{2},t\right),t\right)v_{jl}\left(\boldsymbol{X}_c\left(\frac{\boldsymbol{x}'-\boldsymbol{x}}{2},t'\right),t'\right)\right\rangle \\ &= Q_{ijl}(\boldsymbol{x}-\boldsymbol{x}',t,t') \end{aligned} \tag{5.38}$$

We note that symmetry and incompressibility imply that

$$\begin{aligned} R_{ij}(\boldsymbol{r},t,t') &= R_{ji}(-\boldsymbol{r},t',t) \\ Q_{ijj}(\boldsymbol{r},t,t') &= 0 \end{aligned} \tag{5.39}$$

5.4.3 Galilean–invariant mean EMF

The transport coefficients are completely determined by the form of the velocity correlator. Using Eqns. (5.37) and (5.38) in Eqns. (5.27) and noting the fact that the velocity correlators defined above are functions only of $(\boldsymbol{x}-\boldsymbol{x}')$, t and t', we can see that the GI transport coefficients,

$$\begin{aligned}\widehat{\alpha}_{il}(\boldsymbol{x},t,\boldsymbol{x}',t') &= \epsilon_{ijm}\left[Q_{jml}(\boldsymbol{x}-\boldsymbol{x}',t,t') \;+\; St'\,\delta_{l1}\,Q_{jm2}(\boldsymbol{x}-\boldsymbol{x}',t,t')\right] \\ \widehat{\beta}_{il}(\boldsymbol{x},t,\boldsymbol{x}',t') &= \epsilon_{ij2}\left[Q_{j1l}(\boldsymbol{x}-\boldsymbol{x}',t,t') \;+\; St'\,\delta_{l1}\,Q_{j12}(\boldsymbol{x}-\boldsymbol{x}',t,t')\right] \\ \widehat{\eta}_{iml}(\boldsymbol{x},t,\boldsymbol{x}',t') &= \epsilon_{ijl}\,R_{jm}(\boldsymbol{x}-\boldsymbol{x}',t,t') \end{aligned} \tag{5.40}$$

The transport coefficients depend on $\boldsymbol{x}$ and $\boldsymbol{x}'$ only through the combination, $(\boldsymbol{x}-\boldsymbol{x}')$, which arises because of Galilean invariance. We can derive an expression for the G–invariant mean EMF by using Eqns. (5.40) for the transport coefficients in Eqn. (5.21). We also change the integration variable in Eqn. (5.21) to $\boldsymbol{r} = \boldsymbol{x}-\boldsymbol{x}'$. The integrands

can be simplified as follows:

$$\begin{aligned}
\widehat{\alpha}_{il}(\boldsymbol{x},t,\boldsymbol{x}',t')\,[H'_l - St'\delta_{l2}H'_1] &= \epsilon_{ijm}\,[Q_{jml} \;+\; St'\,\delta_{l1}\,Q_{jm2}]\,[H'_l - St'\delta_{l2}H'_1] \\
&= \epsilon_{ijm}Q_{jml}(\boldsymbol{r},t,t')H_l(\boldsymbol{x}-\boldsymbol{r},t') \\
\widehat{\beta}_{il}(\boldsymbol{x},t,\boldsymbol{x}',t')\,[H'_l - St'\delta_{l2}H'_1] &= \epsilon_{ij2}\,[Q_{j1l} \;+\; St'\,\delta_{l1}\,Q_{j12}]\,[H'_l - St'\delta_{l2}H'_1] \\
&= \epsilon_{ij2}Q_{j1l}(\boldsymbol{r},t,t')H_l(\boldsymbol{x}-\boldsymbol{r},t')
\end{aligned}$$

$$\begin{aligned}
[\,\widehat{\eta}_{iml} - St'\delta_{m2}\,\widehat{\eta}_{i1l}]\,H'_{lm} &= \epsilon_{ijl}\,[R_{jm}(\boldsymbol{r},t,t') \;-\; St'\delta_{m2}\,R_{j1}(\boldsymbol{r},t,t')]\,H_{lm}(\boldsymbol{x}-\boldsymbol{r},t') \\
[\,\widehat{\eta}_{im2} - St'\delta_{m2}\,\widehat{\eta}_{i12}]\,H'_{1m} &= \epsilon_{ij2}\,\delta_{l1}\,[R_{jm}(\boldsymbol{r},t,t') \;-\; St'\delta_{m2}\,R_{j1}(\boldsymbol{r},t,t')]\,H_{lm}(\boldsymbol{x}-\boldsymbol{r},t')
\end{aligned}$$

Define

$$\begin{aligned}
C_{jml}(\boldsymbol{r},t,t') &= Q_{jml}(\boldsymbol{r},t,t') \;+\; S(t-t')\delta_{m2}\,Q_{j1l}(\boldsymbol{r},t,t') \\
D_{jm}(\boldsymbol{r},t,t') &= R_{jm}(\boldsymbol{r},t,t') \;-\; St'\delta_{m2}\,R_{j1}(\boldsymbol{r},t,t')
\end{aligned} \tag{5.41}$$

The mean EMF can now be written compactly as

$$\begin{aligned}
\mathcal{E}_i(\boldsymbol{x},t) \;=\; & \epsilon_{ijm}\int_0^t \mathrm{d}t' \int \mathrm{d}^3r\; G_\eta(\boldsymbol{r},t,t')\,C_{jml}(\boldsymbol{r},t,t')H_l(\boldsymbol{x}-\boldsymbol{r},t') \\
& - \int_0^t \mathrm{d}t' \int \mathrm{d}^3r\, G_\eta(\boldsymbol{r},t,t')\,[\epsilon_{ijl} + S(t-t')\delta_{l1}\epsilon_{ij2}]\times \\
& \qquad \times D_{jm}(\boldsymbol{r},t,t')H_{lm}(\boldsymbol{x}-\boldsymbol{r},t')
\end{aligned} \tag{5.42}$$

5.5 Mean–field induction equation

5.5.1 Mean–field induction equation in sheared coordinate space

Applying the shearing transformation given in Eqns. (A.2) and (A.3) to the mean–field equation, Eqn. (5.3), we see that the mean–field, $\boldsymbol{H}(\boldsymbol{x},t)$, obeys

$$\frac{\partial H_i}{\partial t} \; - \; S\delta_{i2}H_1 \; = \; (\boldsymbol{\nabla}\times\boldsymbol{\mathcal{E}})_i \; + \; \eta\boldsymbol{\nabla}^2 H_i \tag{5.43}$$

where

$$(\boldsymbol{\nabla})_p \; \equiv \; \frac{\partial}{\partial X_p} \; = \; \frac{\partial}{\partial x_p} \; - \; St\,\delta_{p1}\frac{\partial}{\partial x_2} \tag{5.44}$$

We note that the divergence condition on the mean magnetic field can be written as

$$\boldsymbol{\nabla}\cdot\boldsymbol{H} \; \equiv \; \frac{\partial H_p}{\partial X_p} \; = \; H_{pp} \; - \; StH_{12} \; = \; 0 \tag{5.45}$$

It may be verified that Eqn. (5.43) preserves the condition $\boldsymbol{\nabla}\cdot\boldsymbol{H} = 0$. We now use Eqns. (5.42) and (5.44) to evaluate $\boldsymbol{\nabla}\times\boldsymbol{\mathcal{E}}$.

$$\begin{aligned}
(\boldsymbol{\nabla}\times\boldsymbol{\mathcal{E}})_i \; &= \; \epsilon_{ipq}\frac{\partial \mathcal{E}_q}{\partial X_p} \; = \; \epsilon_{ipq}\left(\frac{\partial}{\partial x_p} \; - \; St\,\delta_{p1}\frac{\partial}{\partial x_2}\right)\mathcal{E}_q \\
&= \; \epsilon_{ipq}\epsilon_{qjm}\int_0^t \mathrm{d}t' \int \mathrm{d}^3r\; G_\eta(\boldsymbol{r},t,t')C_{jml}(\boldsymbol{r},t,t')\left[H'_{lp} - St\,\delta_{p1}H'_{l2}\right] \\
&\quad - \int_0^t \mathrm{d}t' \int \mathrm{d}^3r\, G_\eta(\boldsymbol{r},t,t')D_{jm}(\boldsymbol{r},t,t')\left[\epsilon_{ipq}\epsilon_{qjl} + S(t-t')\delta_{l1}\epsilon_{ipq}\epsilon_{qj2}\right]\times \\
&\qquad \times\left[H'_{lmp} - St\,\delta_{p1}H'_{lm2}\right]
\end{aligned}$$

where $H'_i = H_i(\boldsymbol{x}-\boldsymbol{r},t')$. Expanding $\epsilon_{ipq}\epsilon_{qjm} = (\delta_{ij}\,\delta_{mp} - \delta_{im}\,\delta_{jp})$, the contribution from the C term is

$$\begin{aligned}
(\boldsymbol{\nabla}\times\boldsymbol{\mathcal{E}})_i^C \; = \quad & \int_0^t \mathrm{d}t' \int \mathrm{d}^3r\; G_\eta(\boldsymbol{r},t,t')\left[C_{ipl}(\boldsymbol{r},t,t') - C_{pil}(\boldsymbol{r},t,t')\right]\times \\
& \qquad \times\left[H'_{lp} - St\delta_{p1}H'_{l2}\right]
\end{aligned} \tag{5.46}$$

Evaluating the D term is a bit more involved. Again, we begin by expanding $\epsilon_{ipq}\epsilon_{qjl} = (\delta_{ij}\,\delta_{lp} - \delta_{il}\,\delta_{jp})$. Then we get

$$\begin{aligned}(\boldsymbol{\nabla}\times\boldsymbol{\mathcal{E}})_i^D &= \int_0^t \mathrm{d}t' \int \mathrm{d}^3r\; G_\eta(\boldsymbol{r},t,t')\, D_{pm}(\boldsymbol{r},t,t') \times \\ &\qquad \times \left\{ H'_{ipm} - St\delta_{p1}H'_{i2m} + S(t-t')\delta_{i2}\left[H'_{1pm} - St\delta_{p1}H'_{12m}\right]\right\} \\ &\quad - \int_0^t \mathrm{d}t' \int \mathrm{d}^3r\; G_\eta(\boldsymbol{r},t,t')\, D_{im}(\boldsymbol{r},t,t')\left[H'_{ppm} - St'H'_{12m}\right] \qquad (5.47)\end{aligned}$$

The second integral vanishes because the factor in [ ] multiplying D_{im} is zero: to see this, differentiate the divergence–free condition of Eqn. (5.45) with respect to x_m. We can now use Eqns. (5.46) and (5.47) to write $(\boldsymbol{\nabla}\times\boldsymbol{\mathcal{E}}) = (\boldsymbol{\nabla}\times\boldsymbol{\mathcal{E}})^C + (\boldsymbol{\nabla}\times\boldsymbol{\mathcal{E}})^D$. Substituting this expression in Eqn. (5.43), we obtain a set of integro–differential equation governing the dynamics of the mean–field, $\boldsymbol{H}(\boldsymbol{x},t)$, valid for arbitrary values of the shear strength S:

$$\begin{aligned}\frac{\partial H_i}{\partial t} - S\delta_{i2}H_1 = \eta\boldsymbol{\nabla}^2 H_i &+ \int_0^t \mathrm{d}t' \int \mathrm{d}^3r\; G_\eta(\boldsymbol{r},t,t')\;\left[C_{iml}(\boldsymbol{r},t,t') - C_{mil}(\boldsymbol{r},t,t')\right]\times \\ &\quad \times \left[H_{lm}(\boldsymbol{x}-\boldsymbol{r},t') - St\delta_{m1}H_{l2}(\boldsymbol{x}-\boldsymbol{r},t')\right] \\ &+ \int_0^t \mathrm{d}t' \int \mathrm{d}^3r\; G_\eta(\boldsymbol{r},t,t')\, D_{jm}(\boldsymbol{r},t,t')\times \\ &\quad \times \left[H_{ijm}(\boldsymbol{x}-\boldsymbol{r},t') - St\delta_{j1}H_{i2m}(\boldsymbol{x}-\boldsymbol{r},t') + \right. \\ &\quad \left. + S(t-t')\delta_{i2}\left\{H_{1jm}(\boldsymbol{x}-\boldsymbol{r},t') - St\delta_{j1}H_{12m}(\boldsymbol{x}-\boldsymbol{r},t')\right\}\right] \qquad (5.48)\end{aligned}$$

We note some important properties of the mean–field induction Eqn. (5.48):

1. The $D_{jm}(\boldsymbol{r},t,t')$ terms are such that $(\boldsymbol{\nabla}\times\boldsymbol{\mathcal{E}})_i$ involves only H_i for $i=1$ and $i=3$, whereas $(\boldsymbol{\nabla}\times\boldsymbol{\mathcal{E}})_2$ depends on both H_2 and H_1. The implications for the original field, $\boldsymbol{B}(\boldsymbol{X},\tau)$, can be read off, because it is equal to $\boldsymbol{H}(\boldsymbol{x},t)$ component–wise (i.e

$B_i(\boldsymbol{X},\tau) = H_i(\boldsymbol{x},t)$). Therefore, in the mean–field induction equation, the "D" terms are of such a form that: (i) the equations for B_1 or B_3 involve only B_1 or B_3, respectively; (ii) the equation for B_2 involves both B_1 and B_2.

2. Only the part of $C_{iml}(\boldsymbol{r},t,t')$ that is antisymmetric in the indices (i,m) contributes. We note that it is possible that the "C" terms can lead to a coupling of different components of the mean magnetic field. To investigate this, it is necessary to specify the statistics of the velocity fluctuations.

3. In the formal limit of zero resistivity, $\eta \to 0$, the resistive Green's function, $G(\boldsymbol{x},t,t') \to \delta(\boldsymbol{x})$. Then the mean–field induction equation simplifies to

$$\begin{aligned}\frac{\partial H_i}{\partial t} \; - \; S\delta_{i2}H_1 \; = \qquad & \int_0^t \mathrm{d}t' \; [C_{iml}(\mathbf{0},t,t') - C_{mil}(\mathbf{0},t,t')] \times \\ & \times [H_{lm}(\boldsymbol{x},t') \; - \; St\delta_{m1}H_{l2}(\boldsymbol{x},t')] \\ + \; & \int_0^t \mathrm{d}t' \, D_{jm}(\mathbf{0},t,t') \, [H_{ijm}(\boldsymbol{x},t') \; - \; St\delta_{j1}H_{i2m}(\boldsymbol{x},t') + \\ & + S(t-t')\delta_{i2} \, \{H_{1jm}(\boldsymbol{x},t') - St\delta_{j1}H_{12m}(\boldsymbol{x},t')\}]\end{aligned} \tag{5.49}$$

which is identical to that derived in Sridhar & Subramanian (2009a,b).

5.5.2 Mean–field induction equation in sheared Fourier space

Equation (5.48) governing the time evolution of the mean field may be simplified further by taking a spatial Fourier transform. Let us define

$$\tilde{\boldsymbol{H}}(\boldsymbol{k},t) \; = \; \int \mathrm{d}^3x \, \boldsymbol{H}(\boldsymbol{x},t) \exp\left(-\mathrm{i}\,\boldsymbol{k}\boldsymbol{\cdot}\,\boldsymbol{x}\right) \tag{5.50}$$

and the quantities,

$$\tilde{I}_{iml}(\boldsymbol{k},t,t') = \int \mathrm{d}^3 r\, G_\eta(\boldsymbol{r},t,t') C_{iml}(\boldsymbol{r},t,t') \exp\left(-\mathrm{i}\,\boldsymbol{k}\cdot\boldsymbol{r}\right)$$

$$\tilde{J}_{jm}(\boldsymbol{k},t,t') = \int \mathrm{d}^3 r\, G_\eta(\boldsymbol{r},t,t') D_{jm}(\boldsymbol{r},t,t') \exp\left(-\mathrm{i}\,\boldsymbol{k}\cdot\boldsymbol{r}\right) \tag{5.51}$$

Both $\tilde{I}_{iml}(\boldsymbol{k},t,t')$ and $\tilde{J}_{jm}(\boldsymbol{k},t,t')$ are to be regarded as given quantities, because they are known once the velocity correlators have been specified. Taking the spatial Fourier transform of Eqn. (5.48), we obtain,

$$\begin{aligned}\frac{\partial \tilde{H}_i}{\partial t} - S\delta_{i2}\tilde{H}_1 &= -\eta K^2 \tilde{H}_i + \mathrm{i}\,K_m \int_0^t \mathrm{d}t' \left[\tilde{I}_{iml}(\boldsymbol{k},t,t') - \tilde{I}_{mil}(\boldsymbol{k},t,t')\right] \tilde{H}_l(\boldsymbol{k},t') \\ &\quad - k_m K_j \int_0^t \mathrm{d}t'\, \tilde{J}_{jm}(\boldsymbol{k},t,t') \left[\tilde{H}_i(\boldsymbol{k},t') + S(t-t')\delta_{i2}\tilde{H}_1(\boldsymbol{k},t')\right]\end{aligned} \tag{5.52}$$

where $\boldsymbol{K}(\boldsymbol{k},t) = (k_1 - St\,k_2,\, k_2,\, k_3)$ and $K^2 = |\boldsymbol{K}|^2 = (k_1 - Stk_2)^2 + k_2^2 + k_3^2$. Once the initial data, $\tilde{\boldsymbol{H}}(\boldsymbol{k},0)$, has been specified, Eqns. (5.52) can be integrated in time to determine $\tilde{\boldsymbol{H}}(\boldsymbol{k},t)$. Whereas these equations are not easy to solve, we note some of their important properties:

1. Only the part of $\tilde{I}_{iml}(\boldsymbol{k},t,t')$ that is antisymmetric in the indices (i,m) contributes.

2. The time evolution of $\tilde{\boldsymbol{H}}(\boldsymbol{k},t)$ depends only on $\tilde{\boldsymbol{H}}(\boldsymbol{k},t')$ for $0 \le t' < t$, not on the values of $\tilde{\boldsymbol{H}}$ at other values of $\boldsymbol{k}$. Thus each $\boldsymbol{k}$ labels a *normal mode* whose *amplitude* and *polarization* are given by $\tilde{\boldsymbol{H}}(\boldsymbol{k},t)$, the time evolution of which is independent of all the other normal modes.

3. When we have determined $\tilde{\boldsymbol{H}}(\boldsymbol{k},t)$, the magnetic field in the original variables, $\boldsymbol{B}(\boldsymbol{X},\tau)$, can be recovered by using the shearing transformation, Eqn. (A.2), to

write $(\boldsymbol{x}, t)$ in terms of the lab frame coordinates $(\boldsymbol{X}, \tau)$:

$$\boldsymbol{B}(\boldsymbol{X}, \tau) \;=\; \boldsymbol{H}(\boldsymbol{x}, t) \;=\; \int \frac{\mathrm{d}^3 k}{(2\pi)^3}\, \tilde{\boldsymbol{H}}(\boldsymbol{k}, t) \exp\left(\mathrm{i}\, \boldsymbol{k}\cdot \boldsymbol{x}\right)$$

$$= \int \frac{\mathrm{d}^3 k}{(2\pi)^3}\, \tilde{\boldsymbol{H}}(\boldsymbol{k}, \tau) \exp\left[\mathrm{i}\, \boldsymbol{K}(\boldsymbol{k}, \tau)\cdot \boldsymbol{X}\right] \tag{5.53}$$

where we have used $\boldsymbol{K}\cdot \boldsymbol{X} = \boldsymbol{k}\cdot \boldsymbol{x}$. Thus $\boldsymbol{B}(\boldsymbol{X}, \tau)$ has been expressed as a superposition of the normal modes, each of which is a *shearing wave*, whose spatial structure is given by

$$\exp\left[\mathrm{i}\, \boldsymbol{K}(\boldsymbol{k}, \tau)\cdot \boldsymbol{X}\right] \;=\; \exp\left[\mathrm{i}\, \{(k_1 - Stk_2)X_1 + k_2 X_2 + k_3 X_3\}\right] \tag{5.54}$$

For non–axisymmetric waves, $k_2 \neq 0$ and, as time progresses, the shearing wave develops fine-structure along the X_1–direction with a time–dependent spatial frequency equal to $(k_1 - Stk_2)$.

5.5.3 The integral kernels expressed in terms of the velocity spectrum tensor

We have derived the integral equation satisfied by the mean magnetic field, to lowest order in Rm; in sheared coordinate space it is given by Eqns. (5.48), and in sheared Fourier space it is given by Eqns. (5.52). One can proceed to look for solutions if the integral kernels are known. This means that either the pair $[C_{iml}(\boldsymbol{r}, t, t')\,, D_{jm}(\boldsymbol{r}, t, t')]$ or the pair $\left[\tilde{I}_{iml}(\boldsymbol{k}, t, t')\,, \tilde{J}_{jm}(\boldsymbol{k}, t, t')\right]$ needs to be specified. Here we show that all these integral kernels can be expressed in terms of a single entity, which is the velocity spectrum tensor, $\Pi_{ij}(\boldsymbol{k}, t, t')$, derived earlier in Ch. 3.

It may be noted from the Appendix B that the Galilean invariance of velocity correlators stated in Eqn. (5.30) is most compactly expressed in Fourier–space, where we show that the G–invariant expression for Fourier–space two–point velocity correlator is given by Eqn. (B.7). We first work out $R_{jm}(\boldsymbol{r}, t, t')$ and $Q_{jml}(\boldsymbol{r}, t, t')$ in terms of $\Pi_{jm}(\boldsymbol{k}, t, t')$.

Using the results of the Appendix B, we may write from Eqns. (5.37) & (5.38):

$$\begin{aligned} R_{jm}(\boldsymbol{r},t,t') &= \left\langle v_j\left(\boldsymbol{X}_c\left(\frac{\boldsymbol{r}}{2},t\right),t\right) v_m\left(\boldsymbol{X}_c\left(-\frac{\boldsymbol{r}}{2},t'\right),t'\right)\right\rangle \\ &= \int \frac{\mathrm{d}^3K}{(2\pi)^3}\frac{\mathrm{d}^3K'}{(2\pi)^3}\,\langle\tilde{v}_j\left(\boldsymbol{K},t\right)\tilde{v}_m^*\left(\boldsymbol{K'},t'\right)\rangle\,\times \\ &\qquad \times\exp\left[\mathrm{i}\left(\boldsymbol{K}\boldsymbol{\cdot}\boldsymbol{X}_c\left(\frac{\boldsymbol{r}}{2},t\right)-\boldsymbol{K'}\boldsymbol{\cdot}\boldsymbol{X}_c\left(-\frac{\boldsymbol{r}}{2},t'\right)\right)\right] \end{aligned} \tag{5.55}$$

$$\begin{aligned} Q_{jml}(\boldsymbol{r},t,t') &= \left\langle v_j\left(\boldsymbol{X}_c\left(\frac{\boldsymbol{r}}{2},t\right),t\right) v_{ml}\left(\boldsymbol{X}_c\left(-\frac{\boldsymbol{r}}{2},t'\right),t'\right)\right\rangle \\ &= \int \frac{\mathrm{d}^3K}{(2\pi)^3}\frac{\mathrm{d}^3K'}{(2\pi)^3}\,(-\mathrm{i}\,K'_l)\,\langle\tilde{v}_j\left(\boldsymbol{K},t\right)\tilde{v}_m^*\left(\boldsymbol{K'},t'\right)\rangle\,\times \\ &\qquad \times\exp\left[\mathrm{i}\left(\boldsymbol{K}\boldsymbol{\cdot}\boldsymbol{X}_c\left(\frac{\boldsymbol{r}}{2},t\right)-\boldsymbol{K'}\boldsymbol{\cdot}\boldsymbol{X}_c\left(-\frac{\boldsymbol{r}}{2},t'\right)\right)\right] \end{aligned} \tag{5.56}$$

Substituting for $\boldsymbol{X}_c$ from Eqn. (B.1), we can write the phase

$$\boldsymbol{K}\boldsymbol{\cdot}\boldsymbol{X}_c\left(\frac{\boldsymbol{r}}{2},t\right)-\boldsymbol{K'}\boldsymbol{\cdot}\boldsymbol{X}_c\left(-\frac{\boldsymbol{r}}{2},t'\right) = (\boldsymbol{k}+\boldsymbol{k}')\boldsymbol{\cdot}\frac{\boldsymbol{r}}{2} \tag{5.57}$$

where $\boldsymbol{k}$ and $\boldsymbol{k}'$ are defined in Eqns. (B.12) of the Appendix B. Therefore,

$$\begin{aligned} R_{jm}(\boldsymbol{r},t,t') &= \int \mathrm{d}^3k\,\Pi_{jm}(\boldsymbol{k},t,t')\,\exp\left[\mathrm{i}\,\boldsymbol{k}\boldsymbol{\cdot}\boldsymbol{r}\right] \\ Q_{jml}(\boldsymbol{r},t,t') &= -\mathrm{i}\int \mathrm{d}^3k\,\left[k_l - St'\delta_{l1}k_2\right]\,\Pi_{jm}(\boldsymbol{k},t,t')\,\exp\left[\mathrm{i}\,\boldsymbol{k}\boldsymbol{\cdot}\boldsymbol{r}\right] \end{aligned} \tag{5.58}$$

Using Eqns. (5.41) we can write the real–space integral kernels, $C_{jml}(\boldsymbol{r},t,t')$ and $D_{jm}(\boldsymbol{r},t,t')$,

as

$$
\begin{aligned}
D_{jm}(\boldsymbol{r},t,t') &= R_{jm}(\boldsymbol{r},t,t') \; - \; St'\delta_{m2}\, R_{j1}(\boldsymbol{r},t,t') \\
&= \int \mathrm{d}^3k \; [\Pi_{jm}(\boldsymbol{k},t,t') - St'\delta_{m2}\,\Pi_{j1}(\boldsymbol{k},t,t')] \exp\left[\mathrm{i}\,\boldsymbol{k}\cdot\boldsymbol{r}\right] \\
C_{jml}(\boldsymbol{r},t,t') &= Q_{jml}(\boldsymbol{r},t,t') \; + \; S(t-t')\delta_{m2}\, Q_{j1l}(\boldsymbol{r},t,t') \\
&= -\mathrm{i} \int \mathrm{d}^3k \, [k_l - St'\delta_{l1}k_2] \, [\Pi_{jm}(\boldsymbol{k},t,t') + S(t-t')\delta_{m2}\Pi_{j1}(\boldsymbol{k},t,t')] \exp\left[\mathrm{i}\,\boldsymbol{k}\cdot\boldsymbol{r}\right]
\end{aligned}
\tag{5.59}
$$

Using Eqns. (5.51) we can express the Fourier–space integral kernels, $\tilde{I}_{jml}(\boldsymbol{k},t,t')$ and $\tilde{J}_{jm}(\boldsymbol{k},t,t')$, as

$$
\begin{aligned}
\tilde{J}_{jm}(\boldsymbol{k},t,t') &= \int \mathrm{d}^3k' \, \tilde{G}_\eta(\boldsymbol{k}-\boldsymbol{k}',t,t') \, [\Pi_{jm}(\boldsymbol{k}',t,t') - St'\delta_{m2}\,\Pi_{j1}(\boldsymbol{k}',t,t')] \\
\tilde{I}_{jml}(\boldsymbol{k},t,t') &= -\mathrm{i} \int \mathrm{d}^3k' \, \tilde{G}_\eta(\boldsymbol{k}-\boldsymbol{k}',t,t') \, [k'_l - St'\delta_{l1}k'_2] \; \times \\
&\qquad \times \; [\Pi_{jm}(\boldsymbol{k}',t,t') + S(t-t')\delta_{m2}\Pi_{j1}(\boldsymbol{k}',t,t')]
\end{aligned}
\tag{5.60}
$$

Thus, we have expressed the integral kernels in terms of the velocity spectrum tensor, $\Pi_{jm}(\boldsymbol{k},t,t')$, which is the fundamental dynamical quantity that needs to be known before the integro–differential equation for the mean magnetic field can be solved.

5.6 Conclusions

We have formulated the problem of large–scale kinematic dynamo action due to turbulence in the presence of a linear shear flow, in the limit of small magnetic Reynolds number (Rm) but arbitrary fluid Reynolds number. The mean–field theory we present is non perturbative in the shear parameter, and makes systematic use of the shearing

coordinate transformation and the Galilean invariance of the linear shear flow. Using Reynolds averaging, we split the magnetic field into mean and fluctuating components. The mean magnetic field is driven by the Curl of the mean EMF, which in turn must be determined in terms of the statistics of the velocity fluctuations. In order to do this it is necessary to determine the magnetic fluctuations in terms of the mean magnetic field and the velocity fluctuations. So we develop the equation for the fluctuations perturbatively in the small parameter, Rm. Using the shearing coordinate transformation, we make an explicit calculation of the resistive Green's function for the linear shear flow. From the perturbative scheme it is clear that the fluctuations can be determined to any order in Rm. Here we determine the magnetic fluctuations and the mean EMF to lowest order in Rm. The transport coefficients are given in general form in terms of the two–point correlators of the velocity fluctuations. At this point we make use of Galilean invariance, which is a fundamental symmetry of the problem. For Galilean invariant velocity statistics we prove that the transport coefficients, although space-dependent, possess the property of translational invariance in sheared coordinate space. An explicit expression for the Galilean–invariant mean EMF is derived.

We put together all the results in § 5.5 by deriving the integro–differential equation governing the time evolution of the mean magnetic field. Some important properties of this equation are the following:

1. Velocity fluctuations contribute to two different kinds of terms, the "C" and "D" terms, in which first and second spatial derivatives of the mean magnetic field, respectively, appear inside the spacetime integrals.

2. The "C" terms are a generalization to the case of shear, of the "α" term familiar from mean–field electrodynamics in the absence of shear. However, they can also contribute to "magnetic diffusion"; see discussion below. Likewise, the "D" terms are a generalization to the case of shear, of the "magnetic diffusion" term familiar from mean–field electrodynamics in the absence of shear. It must be noted that the generalization is non perturbative in the shear strength.

3. In the mean–field induction equation, the "D" terms are of such a form that: (i) the equations for B_1 or B_3 involve only B_1 or B_3, respectively; (ii) the equation for B_2 involves both B_1 and B_2. Therefore, to lowest order in Rm but to all orders in the shear strength, the "D" terms cannot give rise to a shear–current assisted dynamo effect.

4. In the formal limit of zero resistivity, the quasilinear theory of Sridhar & Subramanian (2009a,b) is recovered. In this case, the "C" terms vanish when the velocity field is non helical. However, this may not be the case when the resistivity is non zero. Whether the "C" terms give rise to such a shear–current–type effect depends on the form of the velocity correlators, which will be strongly affected by shear and highly anisotropic; hence it is difficult to guess their tensorial forms *a priori* and it is necessary to develop a dynamical theory of velocity correlators – see below for further discussion.

5. Sheared Fourier space is the natural setting for the mean magnetic field; the normal modes of the theory are a set of shearing waves, labelled by their sheared wavevectors.

6. We prove a result (given in the Appendix B) on the form of the two–point velocity correlator in Fourier space; the velocity spectrum tensor and its general properties are discussed. The integral kernels are expressed in terms of the velocity spectrum tensor, which is the fundamental dynamical quantity that needs to be specified to complete the integro–differential equation description of the time evolution of the mean magnetic field.

The physical meaning of the "C" and "D" terms becomes clear in the limit of a slowly varying magnetic field, when the integro–differential equation reduces to a partial differential equation (Singh & Sridhar, 2011). Then we encounter the well–known α–effect and turbulent magnetic diffusion (η), albeit in tensorial form. The "C" terms alone contributes to α, whereas both "C" and "D" terms contribute to magnetic diffusion. When the velocity field is non helical, the velocity spectrum tensor is real, and the tensorial

α coefficient vanishes; this result is true for arbitrary values of the shear parameter. The "C" terms can, in principle, contribute to a shear–current effect, through the off–diagonal components of the diffusivity tensor (which couple the streamwise component of the mean magnetic field with the cross–stream components). It turns out that these off–diagonal components depend on the microscopic resistivity in such a manner that they vanish when the microscopic resistivity vanishes. This result is consistent with the results of Sridhar & Subramanian (2009a,b). To deal with the case when the microscopic resistivity does not vanish, it is necessary to provide our kinematic development with a dynamical model for the velocity field. Singh & Sridhar (2011) show that, for forced non helical driving at low fluid Reynolds number, the sign of the off–diagonal terms of the diffusivity tensor does not favour the shear–current effect. This conclusion agrees with those reported in Rädler & Stepanov (2006); Rüdiger & Kitchatinov (2006); Brandenburg et al. (2008), even if our results are limited to low Reynolds numbers. If we seek a different explanation for the dynamo action seen in numerical simulations, the "fluctuating α–effect" still remains a promising candidate. α itself is described by second–order velocity correlators, so to describe fluctuations of α, it is necessary to deal with either fourth–order velocity correlators or products of two second–order velocity correlators. This requires extending our perturbative calculations by at least two higher orders, a task which, while tractable, is beyond the scope of the present investigation.

Chapter 6

The Shear Dynamo Problem for Small Fluid and Magnetic Reynolds Numbers

6.1 Introduction

In the present chapter, we extend the work presented in previous chapter (Ch. 5) by giving definite form to the statistics of the velocity field; specifically, the velocity field is assumed to obey the forced Navier–Stokes equation, in the absence of Lorentz forces. The dynamics of the stochastic velocity field due to non–helical forcing in the presence of the background linear shear flow has been presented in detail in the Ch. 3. The velocity spectrum tensor (Π_{jm}) and various time correlation properties of the fluctuating velocity field, $\boldsymbol{v}$, which were derived and discussed in detail in Ch. 3 will be extremely useful for the formulation of this chapter. Thus, in the present chapter, our main focus will be to compute various transport coefficients for the shear dynamo problem, by essentially using the formulation developed in Ch. 5. Taking the limit of slowly varying mean magnetic field, together with the definite form of the fluctuating velocity field given in Ch. 3, enables us to determine the transport coefficients for the shear dynamo problem at small Reynolds numbers.

In § 6.2, we derive the expression for the mean EMF for the case of a mean magnetic field that is slowly varying in time. Thus the mean–field induction equation, which is an integro–differential equation in the formulation of Ch. 5 now simplifies to a partial differential equation. This reduction is an essential first step to the later comparison with the numerical experiments of Brandenburg et al. (2008). Explicit expressions for the transport coefficients, α_{il} and η_{iml}, are derived in terms of the two–point velocity correlators. Using results from Ch. 3, we could express the relevant two–point, unequal–time velocity correlators, and hence the transport coefficients, in terms of the velocity spectrum tensor. This tensorial quantity is real when the velocity field is non helical; we are able to prove that, in this case, the transport coefficient α_{il} vanishes. In § 6.3 we specialize to the case when the mean–field is a function only of the spatial coordinate X_3 and time τ ; this reduction is necessary for comparison with the numerical experiments of Brandenburg et al. (2008). Explicit expressions are derived for all four components of the magnetic diffusivity tensor, $\eta_{ij}(\tau)$, in terms of the velocity power spectrum; the late–time saturation values, η_{ij}^{∞} , have direct bearing on the growth (or otherwise) of the mean magnetic field. Comparisons with earlier work—in particular Brandenburg et al. (2008)—are made, and the implications for the shear–current effect are discussed. We then conclude in § 6.4.

6.2 Mean–field electrodynamics in a linear shear flow

Following the same notation as given in Ch. 5, let $(\boldsymbol{e}_1, \boldsymbol{e}_2, \boldsymbol{e}_3)$ be the unit basis vectors of a Cartesian coordinate system in the laboratory frame. Using notation, $\boldsymbol{X} = (X_1, X_2, X_3)$ for the position vector and τ for time, we write the fluid velocity as $(SX_1\boldsymbol{e}_2 + \boldsymbol{v})$, where S is the rate of shear parameter and $\boldsymbol{v}(\boldsymbol{X}, \tau)$ is an incompressible and randomly fluctuating velocity field with zero mean. The mean magnetic field, $\boldsymbol{B}(\boldsymbol{X}, \tau)$, obeys the mean–field induction equation given by Eqn. (5.3) and the fluctuating magnetic field obeys Eqn. (5.4) to lowest order in Rm. In Ch. 5, the general expressions were provided for the fluctuating magnetic field and the mean EMF (see Eqns. (5.20) and (5.42)) under Galilean invariant

formulation, and the implications for the evolution of the mean magnetic field were discussed in § 5.5. Below, we construct a model to study the shear dynamo problem at small Reynolds numbers, in the limit of slowly varying mean magnetic field.

6.2.1 The mean EMF for a slowly varying magnetic field

The mean EMF given in Eqn. (5.42) is a *functional* of H_l and H_{lm}. When the mean–field is slowly varying compared to velocity correlation times, we expect to be able to approximate $\boldsymbol{\mathcal{E}}$ as a *function* of H_l and H_{lm}. In this case, the mean–field induction equation would reduce to a set of coupled partial differential equations, instead of the more formidable set of coupled integro–differential equations given by (5.43) and (5.42). Sheared coordinates are essential for the calculations, but physical interpretation is simplest in the laboratory frame; hence we derive an expression for the mean EMF in terms of $\boldsymbol{B}(\boldsymbol{X},\tau)$.

The first step involves a Taylor expansion of the quantities, H_l and H_{lm}, occurring in Eqn. (5.42) for the mean EMF. Neglecting spacetime derivatives higher than the first order ones, we have

$$\begin{aligned} H_l(\boldsymbol{x}-\boldsymbol{r},t') &= H_l(\boldsymbol{x},t) - r_p H_{lp}(\boldsymbol{x},t) - (t-t')\,\frac{\partial H_l(\boldsymbol{x},t)}{\partial t} + \ldots \\ H_{lm}(\boldsymbol{x}-\boldsymbol{r},t') &= H_{lm}(\boldsymbol{x},t) - (t-t')\,\frac{\partial H_{lm}(\boldsymbol{x},t)}{\partial t} + \ldots \end{aligned} \tag{6.1}$$

We now use the mean–field induction Eqn. (5.43), to express $(\partial\boldsymbol{H}/\partial t)$ in terms of spatial derivatives. Let L be the spatial scale over which the mean–field varies. When the mean–field varies slowly, L is large and the contributions from both the resistive term and the mean EMF are small, as is shown below. Let ℓ and $v_{\rm rms}$ be the spatial scale and root–mean–squared amplitude of the velocity fluctuations. The resistive term makes a contribution of order $(\ell/L)^2\mathrm{Rm}^{-1}$, which we now assume is much less than unity. Using Eqn. (5.42), we can verify that $\boldsymbol{\nabla}\times\boldsymbol{\mathcal{E}}$ contributes terms of five different orders;

(ℓ/L), $(\ell/L)(S\ell/v_{\rm rms})$, $(\ell/L)^2$, $(\ell/L)^2(S\ell/v_{\rm rms})$ and $(\ell/L)^2(S\ell/v_{\rm rms})^2$. These are all small when (ℓ/L) and $(\ell/L)(S\ell/v_{\rm rms})$ are both much smaller than unity. That we must have $(\ell/L) \ll 1$ is natural from the familiar case of zero shear. The presence of shear introduces an additional requirement that $(\ell/L)(S\ell/v_{\rm rms}) \ll 1$. We now define the small parameter, $\mu \ll 1$, to be equal to the largest of the three small quantities, $(\ell/L)^2{\rm Rm}^{-1} \ll 1$, $(\ell/L) \ll 1$ and $(\ell/L)(S\ell/v_{\rm rms}) \ll 1$. Then,

$$\frac{\partial H_l}{\partial t} \;=\; S\delta_{l2}H_1 \;+\; O(\mu) \tag{6.2}$$

and Eqns. (6.1) give,

$$\begin{aligned} H_l(\boldsymbol{x}-\boldsymbol{r},t') \;&=\; H_l(\boldsymbol{x},t) \;-\; r_p H_{lp}(\boldsymbol{x},t) \;-\; S(t-t')\delta_{l2}H_1 \;+\; O(\mu) \\ H_{lm}(\boldsymbol{x}-\boldsymbol{r},t') \;&=\; H_{lm}(\boldsymbol{x},t) \;-\; S(t-t')\delta_{l2}H_{1m} \;+\; O(\mu) \end{aligned} \tag{6.3}$$

We substitute Eqn. (6.3) in (5.42) to get,

$$\begin{aligned} \mathcal{E}_i(\boldsymbol{x},t) \;=\; & \epsilon_{ijm}\, H_l(\boldsymbol{x},t) \int_0^t {\rm d}t' \int {\rm d}^3r\, G_\eta(\boldsymbol{r},t,t') \;[C_{jml}(\boldsymbol{r},t,t') \;-\; S(t-t')\,\delta_{l1}\, C_{jm2}(\boldsymbol{r},t,t')] \\ & - \epsilon_{ijm}\, H_{lp}(\boldsymbol{x},t) \int_0^t {\rm d}t' \int {\rm d}^3r\; r_p\, G_\eta(\boldsymbol{r},t,t')\; C_{jml}(\boldsymbol{r},t,t') \\ & - \epsilon_{ijl}\, H_{lm}(\boldsymbol{x},t) \int_0^t {\rm d}t' \int {\rm d}^3r\, G_\eta(\boldsymbol{r},t,t')\; D_{jm}(\boldsymbol{r},t,t') \;+\; O(\mu^2) \end{aligned} \tag{6.4}$$

The final step is to rewrite the above expression in terms of the original magnetic field variable, using,

$$
\begin{aligned}
H_l(\boldsymbol{x},t) &= B_l(\boldsymbol{X},\tau) \\
H_{lm}(\boldsymbol{x},t) &\equiv \frac{\partial H_l(\boldsymbol{x},t)}{\partial x_m} = \left(\frac{\partial}{\partial X_m} + S\tau\delta_{m1}\frac{\partial}{\partial X_2}\right) B_l(\boldsymbol{X},\tau)
\end{aligned} \tag{6.5}
$$

Therefore, for a slowly varying magnetic field, the mean EMF is given by,

$$
\mathcal{E}_i = \alpha_{il}(\tau) B_l(\boldsymbol{X},\tau) - \eta_{iml}(\tau)\,\frac{\partial B_l(\boldsymbol{X},\tau)}{\partial X_m} \tag{6.6}
$$

where the *transport coefficients* are given by,

$$
\begin{aligned}
\alpha_{il}(\tau) &= \epsilon_{ijm}\int_0^\tau \mathrm{d}\tau' \int \mathrm{d}^3 r\, G_\eta(\boldsymbol{r},\tau,\tau')\,[C_{jml}(\boldsymbol{r},\tau,\tau') - S(\tau-\tau')\,\delta_{l1}\,C_{jm2}(\boldsymbol{r},\tau,\tau')] \\
\eta_{iml}(\tau) &= \epsilon_{ijp}\int_0^\tau \mathrm{d}\tau' \int \mathrm{d}^3 r\,[r_m + S\tau\delta_{m2}r_1]\,G_\eta(\boldsymbol{r},\tau,\tau')\,C_{jpl}(\boldsymbol{r},\tau,\tau') + \\
&\quad + \epsilon_{ijl}\int_0^\tau \mathrm{d}\tau' \int \mathrm{d}^3 r\, G_\eta(\boldsymbol{r},\tau,\tau')\,[D_{jm}(\boldsymbol{r},\tau,\tau') + S\tau\delta_{m2}D_{j1}(\boldsymbol{r},\tau,\tau')]
\end{aligned} \tag{6.7}
$$

Then the mean–field induction equation, Eqn. (5.3), together with Eqns. (6.6) and (6.7), is a closed partial differential equation (which is first order in temporal and second order in spatial derivatives). Now we wish to compute these transport coefficients with the help of techniques and results developed in earlier chapters, which enables us to study the evolution of mean magnetic field.

6.2.2 Transport coefficients expressed in terms of the velocity spectrum tensor

The expressions for the transport coefficients, $\alpha_{il}(\tau)$ and $\eta_{iml}(\tau)$, given in Eqn. (6.7), involve the quantities $C_{jml}(\boldsymbol{r},\tau,\tau')$ and $D_{jm}(\boldsymbol{r},\tau,\tau')$, which have been expressed, in Eqns. (5.59), in terms of a single entity, which is the velocity spectrum tensor, $\Pi_{jm}(\boldsymbol{k},t,t')$.

We rewrite below all the relevant velocity correlators, given before by Eqns. (5.58) and (5.59), in terms of $\Pi_{jm}(\boldsymbol{k}, t, t')$

$$
\begin{aligned}
R_{jm}(\boldsymbol{r}, t, t') &= \int \mathrm{d}^3k\, \Pi_{jm}(\boldsymbol{k}, t, t')\, \exp\left[\mathrm{i}\, \boldsymbol{k}\cdot \boldsymbol{r}\right] \\
Q_{jml}(\boldsymbol{r}, t, t') &= -\mathrm{i} \int \mathrm{d}^3k\, \left[k_l - St'\delta_{l1}k_2\right]\, \Pi_{jm}(\boldsymbol{k}, t, t')\, \exp\left[\mathrm{i}\, \boldsymbol{k}\cdot \boldsymbol{r}\right] \\
D_{jm}(\boldsymbol{r}, t, t') &= \int \mathrm{d}^3k\, \left[\Pi_{jm}(\boldsymbol{k}, t, t') - St'\delta_{m2}\, \Pi_{j1}(\boldsymbol{k}, t, t')\right] \exp\left[\mathrm{i}\, \boldsymbol{k}\cdot \boldsymbol{r}\right] \\
C_{jml}(\boldsymbol{r}, t, t') &= -\mathrm{i} \int \mathrm{d}^3k\, \left[k_l - St'\delta_{l1}k_2\right] \left[\Pi_{jm}(\boldsymbol{k}, t, t') + S(t-t')\delta_{m2}\Pi_{j1}(\boldsymbol{k}, t, t')\right] \exp\left[\mathrm{i}\, \boldsymbol{k}\cdot \boldsymbol{r}\right]
\end{aligned}
\tag{6.8}
$$

Using the above expressions for D_{jm} and C_{jml} in Eqns. (6.7), the transport coefficients $\alpha_{il}(\tau)$ and $\eta_{iml}(\tau)$ can also be written in terms of the velocity spectrum tensor. In Ch. 3 of the thesis, we explicitly determined $\Pi_{ij}(\boldsymbol{k}, t, t')$ by considering non–helical random stirring of an incompressible fluid with background linear shear flow in the absence of the Lorentz forces in the limit of low fluid Reynolds number (Re). We also noted in Eqn. (3.25) and the discussion following Eqn. (3.25) of Ch. 3 that the correlation helicity of the flow due to such a non–helical random forcing *vanishes* in the limit of low Re. From the first of the Eqns. (B.8), we can see that the real part of $\Pi_{jm}(\boldsymbol{k}, t, t')$ is an even function of $\boldsymbol{k}$, whereas the imaginary part is an odd function of $\boldsymbol{k}$. For the non–helical random forcing of our interest, which has been considered in Ch. 3, we find that $\Pi_{jm}(\boldsymbol{k}, t, t')$ is a real quantity; see the discussion following Eqn. (3.24). Therefore in this

case,

$$
\begin{aligned}
Q_{jml}(\boldsymbol{r},t,t') &= \int \mathrm{d}^3k\ [k_l - St'\delta_{l1}k_2]\ \Pi_{jm}(\boldsymbol{k},t,t')\ \sin[\boldsymbol{k}\cdot\boldsymbol{r}] \\
C_{jml}(\boldsymbol{r},t,t') &= \int \mathrm{d}^3k\,[k_l - St'\delta_{l1}k_2]\,[\Pi_{jm}(\boldsymbol{k},t,t') + S(t-t')\delta_{m2}\Pi_{j1}(\boldsymbol{k},t,t')]\sin[\boldsymbol{k}\cdot\boldsymbol{r}]
\end{aligned}
\tag{6.9}
$$

are both *odd* functions of $\boldsymbol{r}$. Since the resistive Green's function, $G_\eta(\boldsymbol{r},t,t')$, is an *even* function of $\boldsymbol{r}$ (as may be seen from Appendix A), we see that the integrand of the expression for $\alpha_{il}(\tau)$, given by first of Eqns. (6.7), is an *odd* function of $\boldsymbol{r}$, and therefore this implies that the *transport coefficient* $\alpha_{il}(\tau)$ *vanishes*.

Also, we note from the analysis of Ch. 3 that the velocity spectrum tensor, Π_{jm}, is given in terms of the forcing spectrum tensor, Φ_{jm}, which requires the knowledge of the forcing power spectrum, $F(K/K_F)$; see Eqns. (3.24) and (3.28). For computation of the transport coefficients, we always choose the form for $F(K/K_F)$ as given in Eqn. (3.35). Few useful dimensionless variables could be defined as: The *fluid Reynolds number*, $\mathrm{Re} = v_{\mathrm{rms}}^{\infty}/(\nu K_F)$; the *magnetic Reynolds number*, $\mathrm{Rm} = v_{\mathrm{rms}}^{\infty}/(\eta K_F)$; the *magnetic Prandtl number*, $\mathrm{Pr} = \nu/\eta$; the dimensionless *Shear parameter*, $\mathrm{S_h} = S/(v_{\mathrm{rms}}^{\infty}K_F)$. The definition of $v_{\mathrm{rms}}^{\infty}$ may be seen from the discussion following Eqn. (3.33) of Ch. 3, and K_F is the wavenumber at which the fluid is stirred.

6.3 Predictions and comparison with numerical experiments

We have already established that the transport coefficient $\alpha_{il} = 0$ when the stirring is non helical. The other transport coefficient η_{iml} can be calculated by the following steps:

(i) Computing the velocity spectrum tensor, Π_{jm}, using Eqns. (3.28) and (3.35).

(ii) Using this in Eqn. (6.8) to compute the velocity correlators C_{jml} and D_{jm}.

(iii) Substituting these correlators in the second of Eqns. (6.7).

We also seek to compare our analytical results with measurements of numerical simulations, which use the test–field method (Brandenburg et al., 2008). In this method, the mean–magnetic field is averaged over the coordinates X_1 and X_2. So we consider the case when the mean magnetic field, $\boldsymbol{B} = \boldsymbol{B}(X_3, \tau)$. The condition $\boldsymbol{\nabla \cdot B} = 0$ implies that B_3 is uniform in space, and it can be set to zero; hence we have $\boldsymbol{B} = (B_1,\, B_2,\, 0)$. Thus, Eqn. (6.6) for the mean EMF gives $\boldsymbol{\mathcal{E}} = (\mathcal{E}_1,\, \mathcal{E}_2,\, 0)$, with

$$\mathcal{E}_i \;=\; -\,\eta_{ij}(\tau)\, J_j\,; \qquad\qquad \boldsymbol{J} \;=\; \boldsymbol{\nabla \times B} \;=\; \left(-\frac{\partial B_2}{\partial X_3},\;\; \frac{\partial B_1}{\partial X_3},\;\; 0\right) \tag{6.10}$$

where 2–indexed magnetic diffusivity tensor η_{ij} has four components, $(\eta_{11},\, \eta_{12},\, \eta_{21},\, \eta_{22})$, which are defined in terms of the 3–indexed object η_{iml} by

$$\eta_{ij}(\tau) \;=\; \epsilon_{lj3}\, \eta_{i3l}(\tau)\,; \quad \text{which implies that} \quad \eta_{i1}(\tau) \;=\; -\,\eta_{i32}(\tau)\,, \quad \eta_{i2}(\tau) \;=\; \eta_{i31}(\tau) \tag{6.11}$$

Equation (6.10) for $\boldsymbol{\mathcal{E}}$ can now be substituted in Eqn. (5.3). Then the mean–field induction becomes,

$$\begin{aligned} \frac{\partial B_1}{\partial \tau} \;&=\; -\,\eta_{21}\,\frac{\partial^2 B_2}{\partial X_3^2} \;+\; (\eta + \eta_{22})\,\frac{\partial^2 B_1}{\partial X_3^2} \\ \frac{\partial B_2}{\partial \tau} \;&=\; S B_1 \;-\; \eta_{12}\,\frac{\partial^2 B_1}{\partial X_3^2} \;+\; (\eta + \eta_{11})\,\frac{\partial^2 B_2}{\partial X_3^2} \end{aligned} \tag{6.12}$$

The diagonal components, $\eta_{11}(\tau)$ and $\eta_{22}(\tau)$, augment the microscopic resistivity, η, whereas the off–diagonal components, $\eta_{12}(\tau)$ and $\eta_{21}(\tau)$, lead to cross–coupling of B_1 and B_2.

6.3.1 The magnetic diffusivity tensor

We now use our dynamical theory to calculate $\eta_{ij}(\tau)$. From Eqns. (6.11) and (6.7), we have

$$\begin{aligned}
\eta_{ij}(\tau) &= \epsilon_{lj3}\,\eta_{i3l}(\tau) \\
&= \epsilon_{lj3}\epsilon_{ipm}\int_0^\tau \mathrm{d}\tau' \int \mathrm{d}^3r\; r_3\, G_\eta(\boldsymbol{r},\tau,\tau')\, C_{pml}(\boldsymbol{r},\tau,\tau') \;+ \\
&\quad + \delta_{ij}\int_0^\tau \mathrm{d}\tau' \int \mathrm{d}^3r\, G_\eta(\boldsymbol{r},\tau,\tau')\; D_{33}(\boldsymbol{r},\tau,\tau') \qquad (6.13)
\end{aligned}$$

Thus the "D" terms contribute only to the diagonal components, η_{11} and η_{22}. This is the expected behaviour of turbulent diffusion, which we now see is true for arbitrary shear. Using Eqn. (6.8), the velocity correlators C_{pml} and D_{33} can now be written in terms of Π_{jm}. After some lengthy calculations, the $\eta_{ij}(\tau)$ can be expressed in terms of the velocity spectrum tensor by,

$$\begin{aligned}
\eta_{ij}(\tau) &= 2\eta\int_0^\tau \mathrm{d}\tau' \int \mathrm{d}^3k\; \widetilde{G}_\eta(\boldsymbol{k},\tau,\tau')\,(\tau-\tau')\,k_3\left[\delta_{j2}(k_1 - S\tau' k_2) \;-\; \delta_{j1}k_2\right]\times \\
&\qquad \times\left[\delta_{i1}\left\{\Pi_{23}-\Pi_{32}-S(\tau-\tau')\Pi_{31}\right\} \;+\; \delta_{i2}\left\{\Pi_{31}-\Pi_{13}\right\}\right] \quad + \\
&+ \quad \delta_{ij}\int_0^\tau \mathrm{d}\tau' \int \mathrm{d}^3k\; \widetilde{G}_\eta(\boldsymbol{k},\tau,\tau')\,\Pi_{33} \qquad (6.14)
\end{aligned}$$

where $\Pi_{lm} = \Pi_{lm}(\boldsymbol{k},\tau,\tau')$, and the indices (i,j) run over values 1 and 2. Here $\widetilde{G}_\eta(\boldsymbol{k},\tau,\tau')$ is the Fourier–space resistive Green's function defined in Eqn. (5.16). The final step in computing $\eta_{ij}(\tau)$ is to use Eqn. (3.28) for the velocity spectrum tensor, Π_{lm} together with Eqn. (3.35). It should be noted that the first term, which is contributed by the "C" terms, vanishes when η vanishes. *Thus the off–diagonal components of the magnetic*

diffusivity tensor, η_{12} and η_{21} are non zero only when the microscopic resistivity, η, is non zero. Using Eqns. (6.14), (5.16), (3.28) and (3.35), together with the definitions of various dimensionless parameters defined below Eqn. (6.9), it can be verified that the functional dependence of $\eta_{ij}(\tau)$ assumes the following general form,

$$\eta_{ij}(\tau) \;=\; \eta^{ZS}\,\frac{\widehat{\eta}_{ij}\,(\nu K_F^2\tau\,;\mathrm{S_h Re}\,;\mathrm{Pr})}{1\,+\,\chi(\mathrm{S_h}\,;\mathrm{Re}\,;\mathrm{Pr})} \tag{6.15}$$

where the constant

$$\eta^{ZS} \;=\; \frac{4\pi}{3}\frac{F_0}{\nu(\eta\,+\,\nu)\,K_F} \tag{6.16}$$

is a typical value of $\eta_{ij}(\tau)$ in the absence of shear. $\widehat{\eta}_{ij}$ are dimensionless functions which depend on the dimensionless variable, $(\nu K_F^2\tau)$, and the two dimensionless parameters, Pr and $\mathrm{S_h Re}$. χ is a dimensionless function of three dimensionless parameters, $\mathrm{S_h}$, Re and Pr. For the case of *zero shear*, Eqn. (6.14) gives,

$$\lim_{S\to 0}\eta_{ij}(\tau) \;=\; \delta_{ij}\,\eta^{ZS}\left\{1\,+\,\frac{2\nu}{\eta-\nu}\exp\left[-(\eta+\nu)K_F^2\tau\right]\,-\,\frac{\eta+\nu}{\eta-\nu}\exp\left[-2\nu K_F^2\tau\right]\right\} \tag{6.17}$$

Panels (a–d) in the Figure (6.1) display plots of $\eta_{ij}(\tau)$ versus $\nu K_F^2\,\tau$ for a range of values of the shear parameter, $\mathrm{S_h}$, and for fixed values, Re = Rm = 0.1. Some noteworthy properties are as follows:

(i) The η_{ij} have been scaled with respect to η^{ZS} of Eqn. (6.16). For comparison, we have plotted in bold lines $\eta_{ij}(\tau)$ for Sh = 0, as given by Eqn. (6.17).

(ii) All the components of η_{ij} are zero at $\tau = 0$, and saturate at finite values at late times.

(iii) The behavior of the diagonal components, η_{11} and η_{22}, is remarkably similar. On the other hand, the off–diagonal components, η_{12} and η_{21}, show very different behavior as functions of τ and Sh.

(iv) When |Sh| is not too large, η_{12} is negative. But at larger |Sh| the behavior of

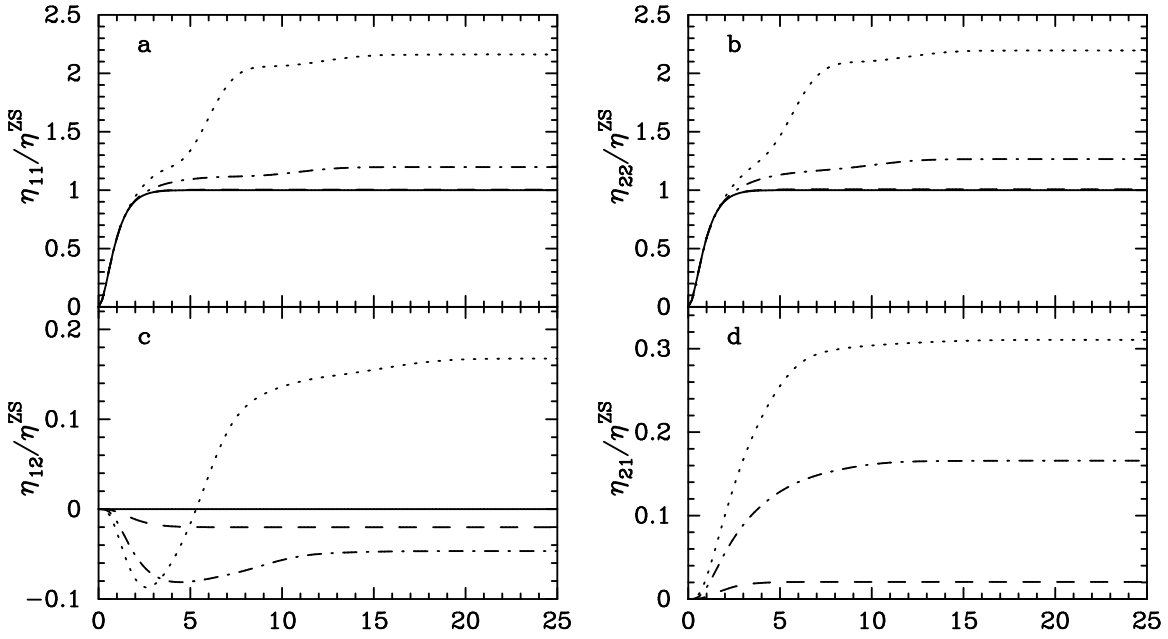

Figure 6.1: Plots of $\eta_{ij}(\tau)$ scaled with respect to η^{ZS}. The abcissa in all figures is the dimensionless time variable $(\nu K_F^2\,\tau)$. Bold line is for Sh $= 0$, Bold–dashed line is for Sh $= -1$, Bold–dotted line is for Sh $= -5$ and the Fine–dotted line is for Sh $= -10$.

$\eta_{12}(\tau)$ is more interesting. It starts at zero for $\tau = 0$, becomes negative, reaches a minimum and begins increasing, ultimately saturating at a positive value.

(v) The behavior of η_{21} is simpler: it seems to be always positive, and saturates at larger values for larger |Sh|.

The $\eta_{ij}(\tau)$ saturate at some constant values at late times; let us denote these constant values by $\eta_{ij}^{\infty} = \eta_{ij}(\tau \to \infty)$. If the mean magnetic field changes over times that are longer than the saturation time, we may use η_{ij}^{∞} instead of the time–varying quantities $\eta_{ij}(\tau)$ in Eqn. (6.12). Looking for solutions $\boldsymbol{B} \propto \exp\left[\lambda\tau + \mathrm{i}K_3X_3\right]$, we obtain the dispersion relation,

$$\frac{\lambda_{\pm}}{\eta_T\,K_3^2} \;=\; -1 \;\pm\; \frac{1}{\eta_T}\sqrt{\eta_{21}^{\infty}\left(\frac{S}{K_3^2} + \eta_{12}^{\infty}\right) \;+\; \epsilon^2} \tag{6.18}$$

given in Brandenburg et al. (2008), where the new constants are defined as,

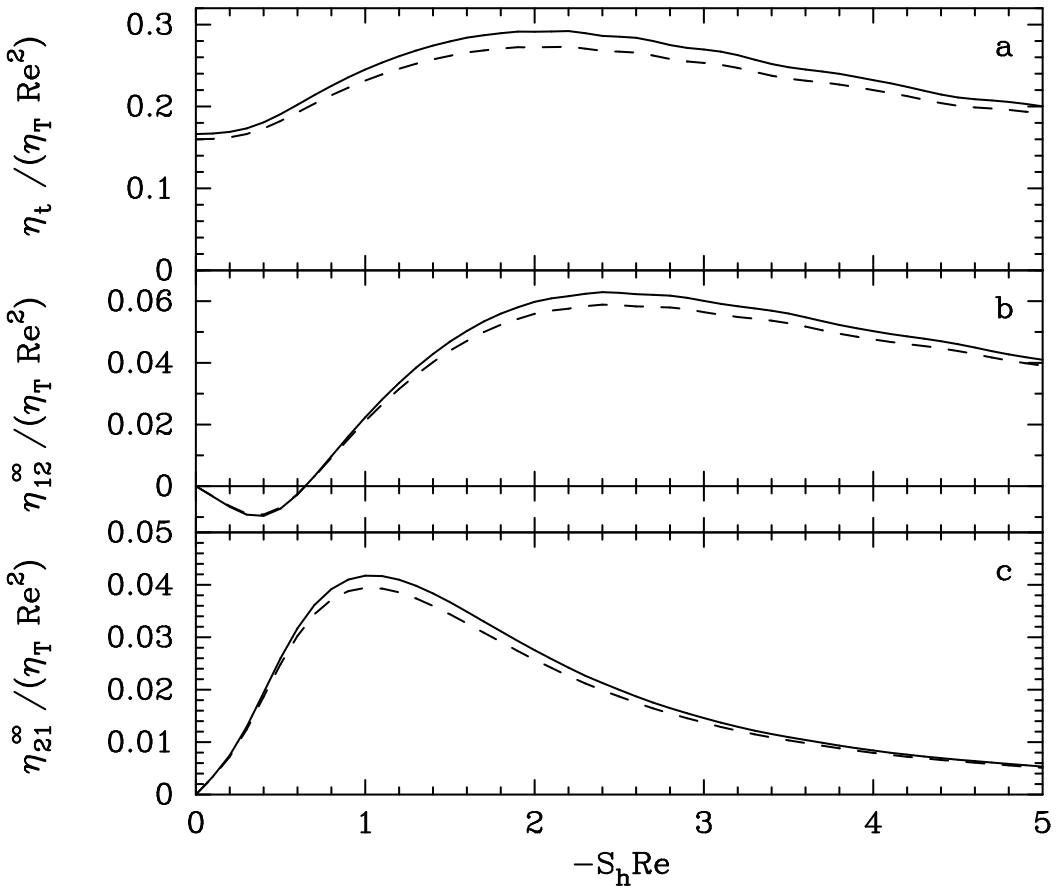

Figure 6.2: Plots of the saturated quantities η_t, η_{12}^∞ and η_{21}^∞ for Re = Rm = 0.1 and Re = Rm = 0.5, corresponding to Pr = 1 , versus the dimensionless parameter $(-\mathrm{S_h Re})$. The bold lines are for Re = Rm = 0.1, and the dashed lines are for Re = Rm = 0.5 .

$$\eta_t \;=\; \frac{1}{2}(\eta_{11}^\infty + \eta_{22}^\infty)\,, \qquad \eta_T \;=\; \eta + \eta_t\,, \qquad \epsilon \;=\; \frac{1}{2}(\eta_{11}^\infty - \eta_{22}^\infty) \tag{6.19}$$

Exponentially growing solutions for the mean magnetic field are obtained when the radicand in Eqn. (6.18) is both positive and exceeds η_T^2 .

From Eqns. (6.14), (5.16), (3.28), (3.34) and (3.35), together with the definitions of various dimensionless parameters defined below Eqn. (6.9), it can be verified that the saturated values of the magnetic diffusivities, η_{ij}^∞, have the following general functional form:

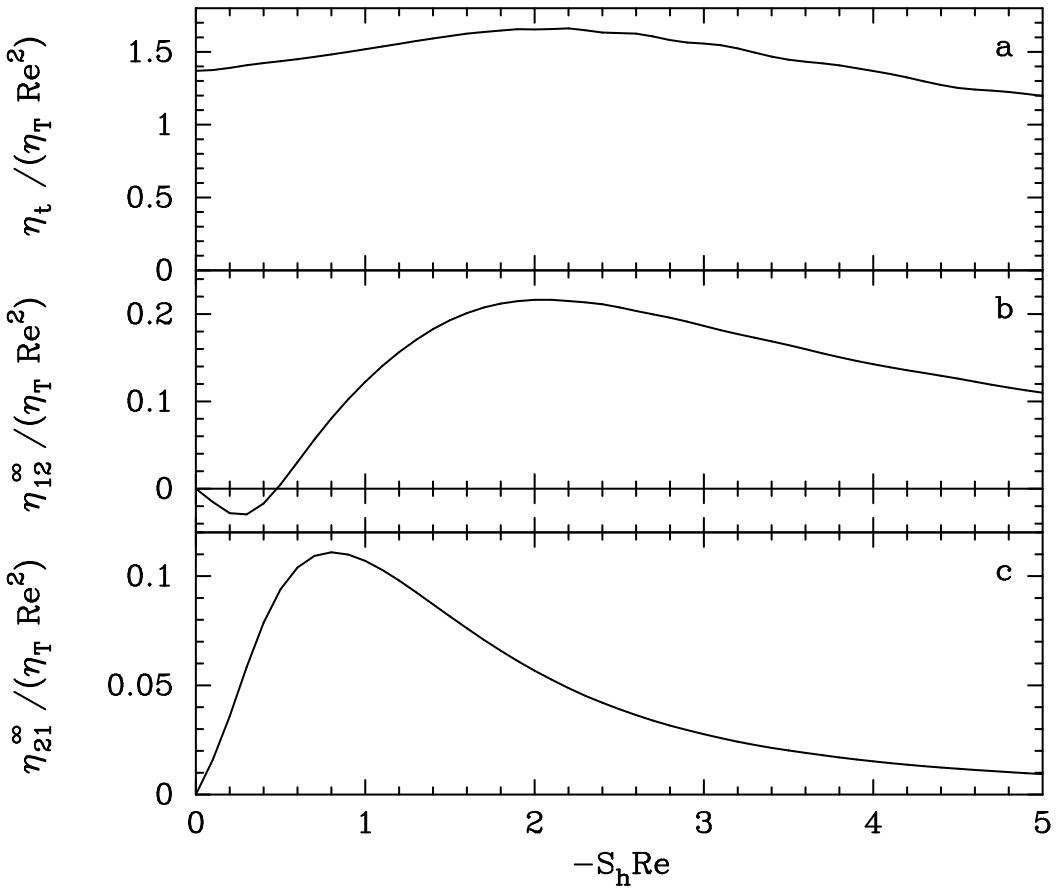

Figure 6.3: Plots of the saturated quantities η_t, η_{12}^∞ and η_{21}^∞ for $\mathrm{Re} = 0.1$ and $\mathrm{Rm} = 0.5$, corresponding to $\mathrm{Pr} = 5$, versus the dimensionless parameter $(-\mathrm{S_h Re})$.

$$\eta_{ij}^\infty \;=\; \eta_T \mathrm{Re}^2 \frac{f_{ij}(\mathrm{S_h Re}\,,\mathrm{Pr})}{1 \,+\, \chi(\mathrm{S_h},\mathrm{Re},\mathrm{Pr})}\,, \tag{6.20}$$

where the f_{ij} are dimensionless functions of two variables, and χ is a dimensionless function of three variables. Figures (6.2–6.4) display plots of η_t, η_{12}^∞ and η_{21}^∞, versus the dimensionless parameter $(-\mathrm{S_h Re})$. The scalings of the ordinates have been chosen for compatibility with the functional form displayed in Eqn. (6.20) above. These plots should be compared with Figure (3) of Brandenburg et al. (2008). However, it should be noted that we operate in quite different parameter regimes; we are able to explore larger values of $|\mathrm{S_h}|$, whereas Brandenburg et al. (2008) have done simulations for larger Re and Rm. The plots in Figure (6.2a–c) are for $\mathrm{Pr} = 1$, but for two sets of values of the Reynolds

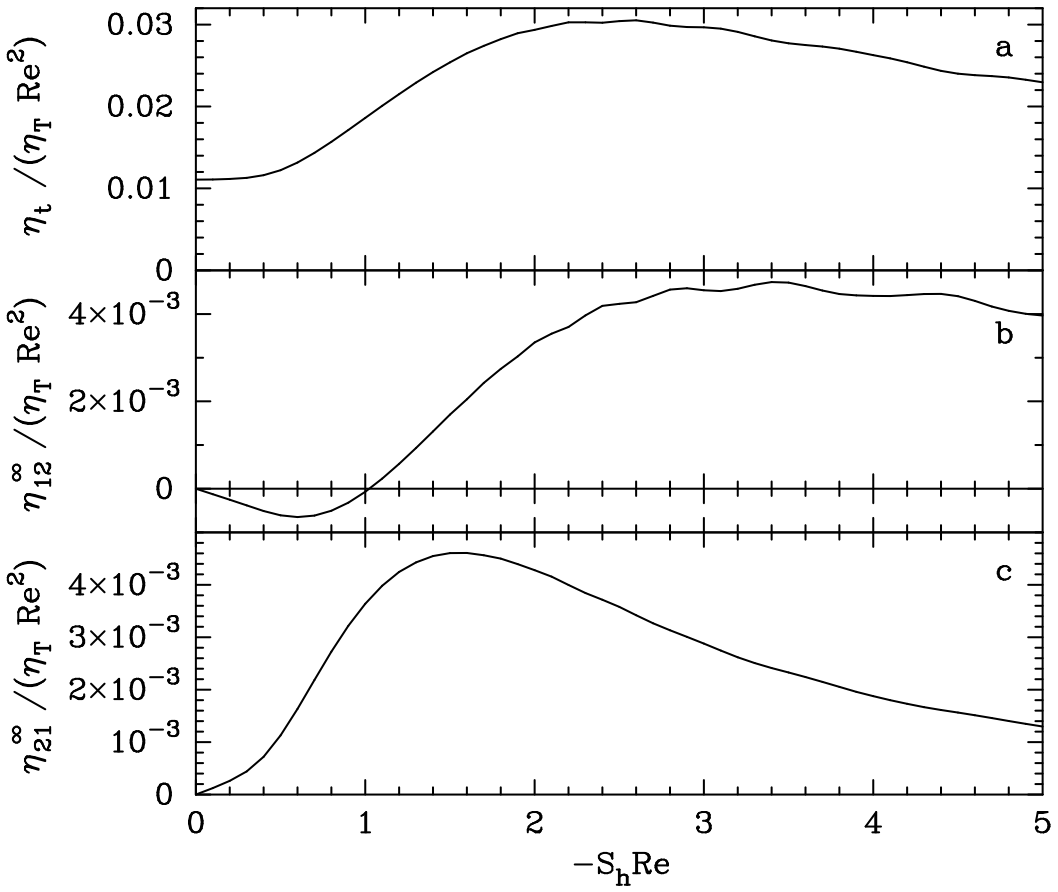

Figure 6.4: Plots of the saturated quantities η_t, η_{12}^∞ and η_{21}^∞ for Re = 0.5 and Rm = 0.1, corresponding to Pr = 0.2, versus the dimensionless parameter $(-\mathrm{S_h Re})$.

numbers; Re = Rm = 0.1, and Re = Rm = 0.5. Figure (6.3a–c) are for Re = 0.1 and Rm = 0.5, corresponding to Pr = 5. Figure (6.4a–c) are for Re = 0.5 and Rm = 0.1, corresponding to Pr = 0.2. As may be seen from Eqn. (6.20), the ratio, $(\eta_{12}^\infty/\eta_{21}^\infty)$, is a function only of the two dimensionless parameters, $(\mathrm{S_h Re})$ and Pr. In Figure (6.5) we plot this ratio versus $(-\mathrm{S_h Re})$ for all the cases considered in Figures (6.2–6.4). Some noteworthy properties are as follows:

(i) We see that η_t is always positive. For a fixed value of $(-\mathrm{S_h Re})$, the quantity $\eta_t/(\eta_T \mathrm{Re}^2)$ increases with Pr and, for a fixed value of Pr, it increases as $(-\mathrm{S_h Re})$ increases from zero (which is consistent with Brandenburg et al. (2008)), attains a maximum value near $(-\mathrm{S_h Re}) \approx 2$, and then decreases while always remaining

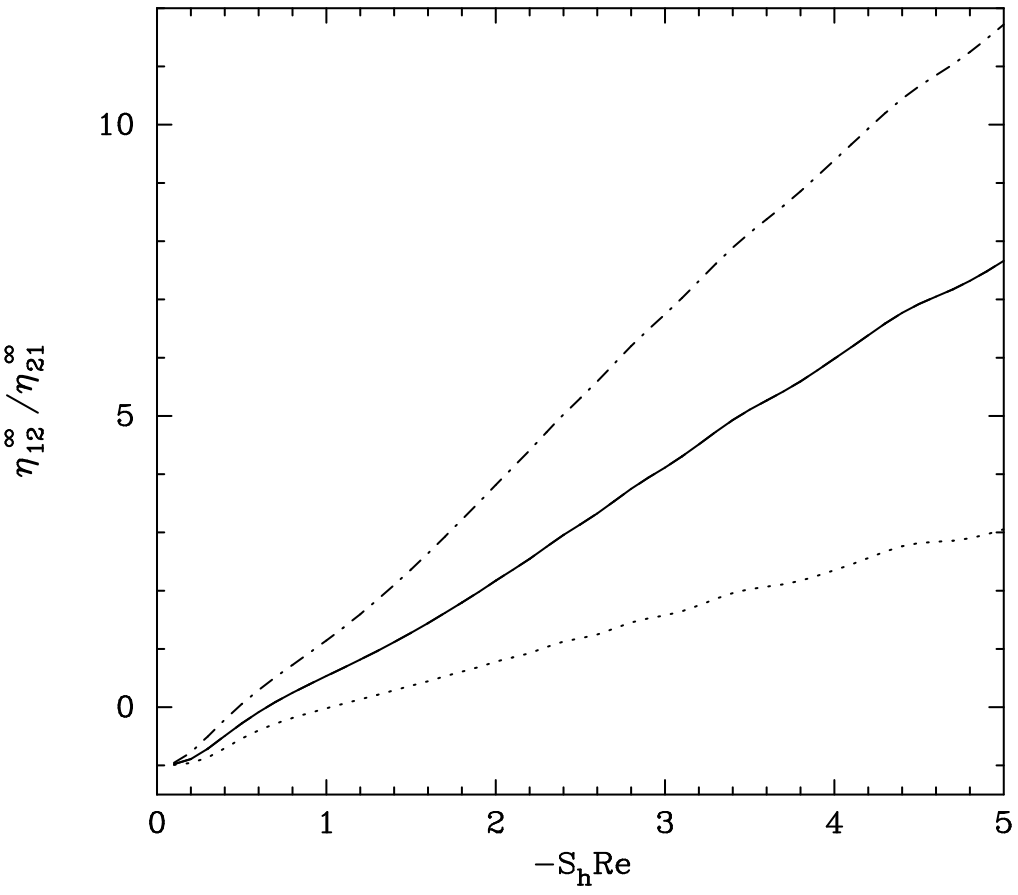

Figure 6.5: Plots of the ratio $(\eta_{12}^{\infty}/\eta_{21}^{\infty})$ versus the dimensionless parameter $(-\mathrm{S_h Re})$ for all the cases considered in Figures (6.2–6.4). The bold line is for the two cases corresponding to $\mathrm{Pr} = 1$, the dashed–dotted line is for $\mathrm{Pr} = 5$, and the dotted line is for $\mathrm{Pr} = 0.2$.

positive.

(ii) As expected, the behaviour of η_{12}^{∞} is more complicated. It is zero for $(-\mathrm{S_h Re}) = 0$, and becomes negative for not too large values of $(-\mathrm{S_h Re})$. After reaching a minimum value, it then becomes an increasing function of $(-\mathrm{S_h Re})$ and attains positive values for large $(-\mathrm{S_h Re})$. Thus the sign of η_{12}^{∞} is sensitive to the values of the control parameters. This may help reconcile, to some extent, the fact that different signs for η_{12}^{∞} are reported in Rüdiger & Kitchatinov (2006) and Brandenburg et al. (2008).

(iii) As may be seen, η_{21}^{∞} is always positive. This agrees with the result obtained in Brandenburg et al. (2008), Rädler & Stepanov (2006) and Rüdiger & Kitchatinov (2006).

(iv) At first sight η_{12}^{∞} and η_{21}^{∞} appear to have quite different behaviour. However, closer inspection reveals certain systematics: as Pr increases, the overall range of values increases, while their shapes shift leftward to smaller values of $(-\mathrm{S_h Re})$. From Eqn. (6.20), it is clear that the ratio $(\eta_{12}^{\infty}/\eta_{21}^{\infty})$ is a function only of the two variables, $(\mathrm{S_h Re})$ and Pr. As Figure (6.5) shows, this ratio is nearly a linear function of $(\mathrm{S_h Re})$, whose slope increases with Pr.

(v) The magnitude of the quantity, $\chi(\mathrm{S_h}, \mathrm{Re}, \mathrm{Pr})$, that appears in Eqn. (6.20), is much smaller than unity. So $\eta_t/(\eta_T \mathrm{Re}^2)$, $\eta_{12}^{\infty}/(\eta_T \mathrm{Re}^2)$ and $\eta_{21}^{\infty}/(\eta_T \mathrm{Re}^2)$ can be thought of (approximately) as functions of $(-\mathrm{S_h Re})$ and Pr. This is the reason why, in Figure (6.2), the bold and dashed lines lie very nearly on top of each other.

6.3.2 Implications for dynamo action & the shear–current effect

The mean magnetic field has a growing mode if the roots of Eqn. (6.18) have a positive real part. It is clear that the real part of λ_- is always negative. So, for the growth of the mean magnetic field, the real part of λ_+ must be positive. Requiring this, we see from Eqn. (6.18) that the condition for dynamo action is,

$$\frac{\eta_{21}^{\infty} S}{\eta_T^2 K_3^2} \; + \; \frac{\eta_{12}^{\infty}\eta_{21}^{\infty}}{\eta_T^2} \; + \; \frac{\epsilon^2}{\eta_T^2} \; > \; 1. \tag{6.21}$$

In Figure (6.6) we plot the last two terms, $(\eta_{12}^{\infty}\eta_{21}^{\infty}/\eta_T^2)$ and (ϵ^2/η_T^2), as functions of $(-\mathrm{S_h Re})$, for all the four cases, $\mathrm{Re} = \mathrm{Rm} = 0.1$; $\mathrm{Re} = \mathrm{Rm} = 0.5$; $\mathrm{Re} = 0.1, \mathrm{Rm} = 0.5$ and $\mathrm{Re} = 0.5, \mathrm{Rm} = 0.1$. As may be seen, the magnitudes of both terms are much smaller than unity, so they are almost irrelevant for dynamo action. Hence, there is growth of the mean magnetic field only when the first term, $(\eta_{21}^{\infty} S/\eta_T^2 K_3^2)$, exceeds unity. This

is possible for small enough K_3^2, so long as $(\eta_{21}^{\infty} S)$ is positive. However, we see from Figures (6.2–6.4) that η_{21}^{∞} is always positive, implying that the product $(\eta_{21}^{\infty} S)$ is always negative. Therefore the inequality of (6.21) cannot be satisfied, and the mean–magnetic field always decays, a conclusion which is in agreement with those of Brandenburg et al. (2008), Rädler & Stepanov (2006) and Rüdiger & Kitchatinov (2006). We can understand the above results more physically. Let us assume that $|K_3|$ is small enough, and keep only the most important terms in Eqn. (6.12). Then we have,

$$\frac{\partial B_1}{\partial \tau} \;=\; -\,\eta_{21}^{\infty}\,\frac{\partial^2 B_2}{\partial X_3^2} \;+\; \ldots\,, \qquad\qquad \frac{\partial B_2}{\partial \tau} \;=\; S B_1 \;+\; \ldots\,, \tag{6.22}$$

where we have used the saturated values of the magnetic diffusivity. If we now look for modes of the form $\boldsymbol{B} \propto \exp\left[\lambda\tau + \mathrm{i}K_3 X_3\right]$, we obtain the dispersion relation, $\lambda_{\pm} = \pm\, K_3 \sqrt{\eta_{21}^{\infty} S}$. So it is immediately obvious that λ_+ is real and positive — i.e. the mean magnetic field grows — only when the product $(\eta_{21}^{\infty} S)$ is positive. However, this product happens to be negative, and the mean magnetic field is a decaying wave.

The above results have direct bearing on the *shear–current effect* (Rogachevskii & Kleeorin, 2003). This effect refers to an extra contribution to the mean EMF which is perpendicular to both the mean vorticity (of the background shear flow) and the mean current. From Eqn. (6.10), we see that, in our case, the relevant term is the contribution, $-\eta_{21}^{\infty} J_1$, to $\mathcal{E}_2$. As Figures (6.2–6.4) show, the diffusivity, η_{21}^{∞} is non zero only in the presence of shear, so the word *shear* refers to this. The word *current* refers to J_1, the cross–field component of the electric current associated with the mean–magnetic field [1]. The shear–current effect would lead to the growth of the mean magnetic field (for small enough K_3), if only the product $(\eta_{21}^{\infty} S)$ is positive. However, as we have demonstrated, this product is negative, so the shear–current effect cannot be responsible for dynamo action, at least for small Re and Rm, but for all values of the shear parameter.

[1] Shear also makes an additional contribution through the SB_1 contribution to $(\partial B_2/\partial\tau)$, which accounts for the product $(\eta_{21}^{\infty} S)$ playing an important role. However, this is just the well–known physical effect of the shearing of cross-shear component of the mean magnetic field to generate a shear–wise component; it does not have any bearing on the word *shear* in the phrase *shear–current effect*.

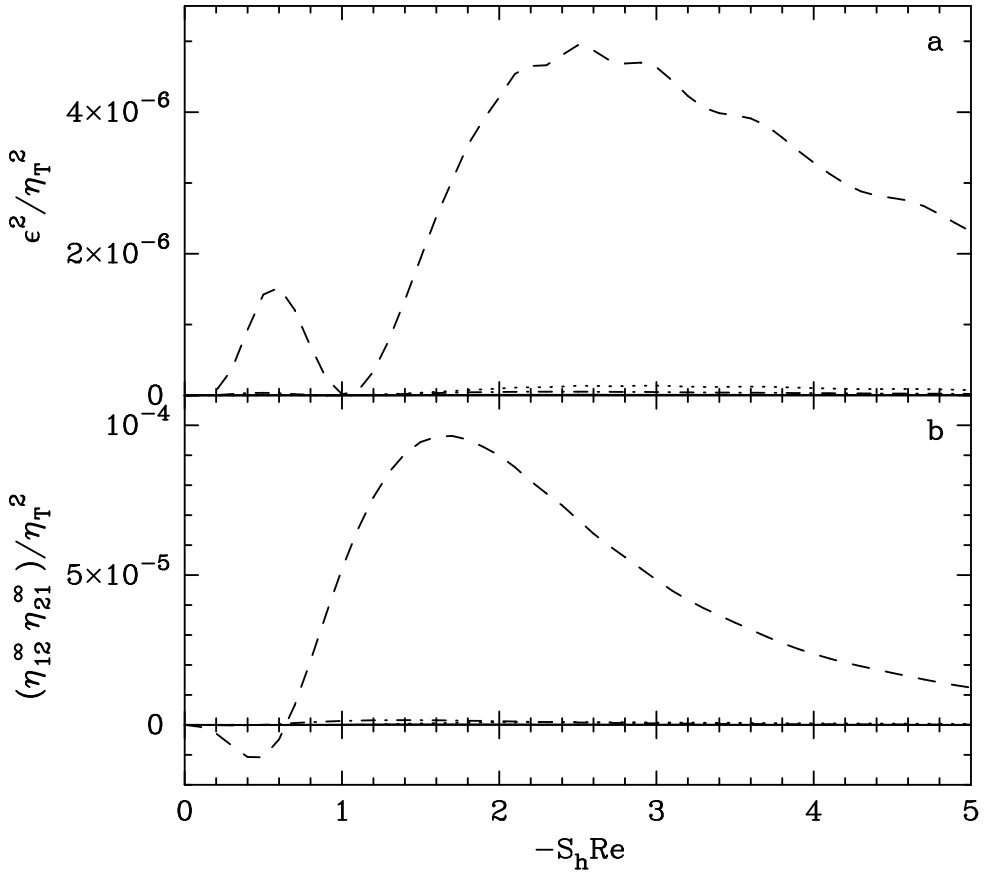

Figure 6.6: Plots of (ϵ^2/η_T^2) and $(\eta_{12}^\infty \eta_{21}^\infty/\eta_T^2)$ versus the dimensionless parameter $(-\mathrm{S_h Re})$ for all the four cases considered in Figures (6.2–6.4). The bold lines are for $\mathrm{Re} = \mathrm{Rm} = 0.1$; the dashed lines are for $\mathrm{Re} = \mathrm{Rm} = 0.5$; the dashed–dotted lines are for $\mathrm{Re} = 0.1, \mathrm{Rm} = 0.5$ and the dotted lines are for $\mathrm{Re} = 0.5, \mathrm{Rm} = 0.1$.

6.4 Conclusions

Building on the formulation of Ch. 3 and 5, we have developed a theory of the *shear dynamo problem* for small magnetic and fluid Reynolds numbers, but for arbitrary values of the shear parameter. Our primary goal is to derive precise analytic results which can serve as benchmarks for comparisons with numerical simulations. A related goal is to resolve the controversy surrounding the nature of the shear–current effect, without treating the shear as a small parameter. We began with the expression for the Galilean–invariant mean EMF derived in Ch. 5, and specialized to the case of a mean magnetic field that

is slowly varying in time. This resulted in the simplification of the mean–field induction equation, from an integro–differential equation to a partial differential equation. This reduction is the first step to the later comparison with the numerical experiments of Brandenburg et al. (2008). Explicit expressions for the transport coefficients, α_{il} and η_{iml}, were derived in terms of the two–point velocity correlators which, using results from Ch. 5, were then expressed in terms of the velocity spectrum tensor. Then we proved that, when the velocity field is non helical, the transport coefficient α_{il} vanishes; just like everything else in our approach, this result is non perturbative in the shear parameter.

Considering the forced, stochastic dynamics for the incompressible velocity field at low Reynolds number, developed in Ch. 3, the velocity spectrum tensor was calculated in terms of the Galilean–invariant forcing statistics. For non helical forcing, the velocity field is also non helical and the transport coefficient α_{il} vanishes, as noted above. We then specialized to the case when the forcing is not only non helical, but isotropic and delta–correlated–in–time as well. We considered the case when the mean–field was a function only of the spatial coordinate X_3 and time τ ; the purpose of this simplification was to facilitate comparison with the numerical experiments of Brandenburg et al. (2008). Explicit expressions were derived for all four components, $\eta_{11}(\tau)$, $\eta_{22}(\tau)$ $\eta_{12}(\tau)$ and $\eta_{21}(\tau)$, of the magnetic diffusivity tensor, in terms of the velocity spectrum tensor. Important properties of this fundamental object are as follows:

1. All the components of η_{ij} are zero at $\tau = 0$, and saturate at finite values at late times, which we denote by η_{ij}^{∞} .

2. The off–diagonal components, η_{12} and η_{21}, vanish when the microscopic resistivity vanishes.

3. The sign of η_{12}^{∞} is sensitive to the values of the control parameters. This may help reconcile, to some extent, the fact that different signs for η_{12}^{∞} are reported in Rüdiger & Kitchatinov (2006) and Brandenburg et al. (2008).

We derived the condition — the inequality (6.21) — required for the growth of the mean magnetic field: the sum of three terms must exceed unity. It was demonstrated that

two of the terms are very small in magnitude, and hence dynamo action was controlled by the behaviour of one term. i.e. the mean magnetic field would grow if $(\eta_{21}^{\infty} S/\eta_T^2 K_3^2)$ exceeds unity. This is possible for small enough K_3^2, so long as $(\eta_{21}^{\infty} S)$ is positive. However, we see from Figures (6.2–6.4) that η_{21}^{∞} is always positive, implying that the product $(\eta_{21}^{\infty} S)$ is always negative. Thus the mean–magnetic field always decays, a conclusion which is in agreement with those of Brandenburg et al. (2008), Rädler & Stepanov (2006) and Rüdiger & Kitchatinov (2006). We then related the above conclusions to the shear–current effect, and demonstrated that the shear–current effect cannot be responsible for dynamo action, at least for small Re and Rm, but for all values of the shear parameter.

Chapter 7

Numerical Studies of Dynamo Action in a Turbulent Shear Flow

7.1 Introduction

This chapter is focussed on various numerical simulations that we have performed to study the shear dynamo problem due to non–helical turbulence. In previous chapters, we have developed a necessary analytical framework for the shear dynamo problem and studied its transport properties in the limit of low Reynolds numbers, but arbitrary shear parameter. Although our results presented so far, resolve some controversies in this field, it is still not established what really causes such a shear dynamo. Some recent works based on the fluctuating alpha effect predict the growth of mean-squared magnetic field, i.e., the second moment, in the limit of small Reynolds numbers (Heinemann, McWilliams & Schekochihin, 2011; Mitra & Brandenburg, 2012; McWilliams, 2011). As our interest has always been focused on the evolution of mean–magnetic field, and not on the mean–squared field, we have not explored the possibility of growth of higher moments of the mean–magnetic field in our analytical calculations. The motivation to study such problems come mainly from numerical simulations, as discussed before. However, it should be noted that all the earlier numerical experiments have been carried out for both the fluid Reynolds number (Re) and the magnetic Reynolds number (Rm)

above unity. Naturally, most of the theoretical studies have focussed their attention in the regime where (Re, Rm) > 1, the limit for which rigorous theory explaining the origin of *the shear dynamo* is yet to come. In Chs. 5 and 6, we make conclusive statements in the limit of Rm < 1, in which Ch. 5 is valid for arbitrary fluid Reynolds number, whereas Ch. 6 also assumes Re < 1. To better understand the shear dynamo problem in non–helical settings, it seems necessary to perform numerical experiments in different parameter regimes; namely, when both (Re, Rm) < 1, when Re > 1 and Rm < 1, when Re < 1 and Rm > 1. Simulations in these limits have never been reported before. Thus, there are two main motivations to perform numerical experiments in these previously unexplored parameter regimes: first, to compare our analytical findings with the results of numerical simulations in similar parameter regimes; and second, to look for the growth of mean magnetic field in the limit when Re < 1. The limit of low Re is particularly interesting, as seeing a dynamo action in this limit would provide enough motivation for further theoretical investigations, which may focus the attention to this analytically more tractable limit of Re < 1, as compared to more formidable limit of Re > 1.

In this chapter, we present numerical simulations for the shear dynamo problem which can be broadly classified in following three categories: (i) The simulations are done when both Re and Rm are less than unity. This is done for comparison with earlier analytical work, presented in Ch. 6; (ii) possibility of dynamo action is explored when Re > 1 and Rm < 1; (iii) finally we perform simulations for the shear dynamo problem in the limit when Re < 1 and Rm > 1. We have used Pencil Code [1] for all the simulations presented in this chapter and followed the method given in Brandenburg et al. (2008). In § 7.2 we begin with the fundamental equations of magnetohydrodynamics in a background linear shear flow. We then consider the case when the mean–magnetic field is a function only of the spatial coordinate x_3 and time t. We briefly describe the transport coefficients and discuss the test field method. Few important details of the simulation have been presented. In § 7.3, we put together all the results in three parts, namely, part A, part B and part C corresponding to the three categories discussed above. We also make

[1] See http://www.nordita.org/software/pencil-code.

comparisons with our analytical works presented in earlier chapters. In § 7.4, we have estimated the fluctuations in the transport coefficients to investigate the reason for the observed dynamo action. In § 7.5, we present our conclusions.

7.2 The model and numerical set up

Let $(\boldsymbol{e}_1, \boldsymbol{e}_2, \boldsymbol{e}_3)$ be the unit basis vectors of a Cartesian coordinate system in the laboratory frame. Using notation $\boldsymbol{x} = (x_1, x_2, x_3)$ for the position vector and t for time, we write the total fluid velocity as $(Sx_1\boldsymbol{e}_2 + \boldsymbol{v})$, where S is the rate of shear parameter and $\boldsymbol{v}(\boldsymbol{x}, t)$ is the velocity deviation from the background shear flow. Let $\boldsymbol{B}^{\rm tot}$ be the total magnetic field which obeys the induction equation. We have performed numerical simulations using the Pencil Code which is a weakly compressible MHD code, so we consider velocity field $\boldsymbol{v}$ to be compressible and write the momentum, continuity and induction equations for a compressible fluid of mass density ρ satisfying the isothermal equation of state as follows:

$$\left(\frac{\partial}{\partial t} + Sx_1\frac{\partial}{\partial x_2}\right)\boldsymbol{v} + Sv_1\boldsymbol{e}_2 + (\boldsymbol{v}\cdot\boldsymbol{\nabla})\boldsymbol{v} = -\frac{1}{\rho}\boldsymbol{\nabla}P + \frac{\boldsymbol{J}^{\rm tot}\times\boldsymbol{B}^{\rm tot}}{\rho} + \boldsymbol{F}_{\rm visc} + \boldsymbol{f} \quad (7.1)$$

$$\left(\frac{\partial}{\partial t} + Sx_1\frac{\partial}{\partial x_2}\right)\rho + (\boldsymbol{v}\cdot\boldsymbol{\nabla})\rho = -\rho\boldsymbol{\nabla}\cdot\boldsymbol{v} \quad (7.2)$$

$$\left(\frac{\partial}{\partial t} + Sx_1\frac{\partial}{\partial x_2}\right)\boldsymbol{B}^{\rm tot} - SB_1^{\rm tot}\boldsymbol{e}_2 = \boldsymbol{\nabla}\times(\boldsymbol{v}\times\boldsymbol{B}^{\rm tot}) + \eta\nabla^2\boldsymbol{B}^{\rm tot} \quad (7.3)$$

where $\boldsymbol{F}_{\rm visc} = \nu\nabla^2\boldsymbol{v} + \left[\frac{\nu}{3} + \frac{\zeta}{\rho}\right]\boldsymbol{\nabla}(\boldsymbol{\nabla}\cdot\boldsymbol{v})$, $\boldsymbol{f}$ is the random stirring force per unit mass and $\boldsymbol{J}^{\rm tot} = (\boldsymbol{\nabla}\times\boldsymbol{B}^{\rm tot})/\mu_0$. ν, ζ, μ_0 and η represent the coefficient of kinematic viscosity, coefficient of bulk viscosity, magnetic permeability and magnetic diffusivity respectively, all assumed to be constant here.

Our aim is to investigate the case of *incompressible* magnetohydrodynamics in a background linear shear flow for a non–helical forcing. In order to do that with Pencil

Code, we limit ourselves to the cases for which the root–mean–squared velocity, $v_{\rm rms}$, is small compared with the sound speed, making the Mach number very small. In this case the solutions of compressible equations approximate the solutions of incompressible equations. When the velocity field $\boldsymbol{v}$ is incompressible (or weakly compressible), the viscous term in Eqn. (7.1) becomes $\boldsymbol{F}_{\rm visc} = \nu\nabla^2\boldsymbol{v}$ (this is true also in the absence of variable compression) and the right hand side of continuity equation vanishes.

7.2.1 Mean–field induction equation

Various transport phenomena have traditionally been studied in the framework of mean–field theory (Moffatt, 1978; Krause & Rädler, 1980; Brandenburg & Subramanian, 2005). Applying Reynolds averaging to the induction Eqn. (7.3) we find that the mean magnetic field, $\boldsymbol{B}(\boldsymbol{x},t)$, obeys the following (mean–field induction) equation:

$$\left(\frac{\partial}{\partial t} \;+\; Sx_1\frac{\partial}{\partial x_2}\right)\boldsymbol{B} \;-\; SB_1\boldsymbol{e}_2 \;=\; \boldsymbol{\nabla}\times\boldsymbol{\mathcal{E}} \;+\; \eta\boldsymbol{\nabla}^2\boldsymbol{B} \tag{7.4}$$

where η is the microscopic resistivity, and $\boldsymbol{\mathcal{E}}$ is the mean electromotive force (EMF), $\boldsymbol{\mathcal{E}} = \langle\boldsymbol{v}\times\boldsymbol{b}\rangle$, where $\boldsymbol{v}$ and $\boldsymbol{b}$ are the fluctuations in the velocity and magnetic fields. The mean EMF is, in general, a *functional* of the mean magnetic field, B_l, and its first spatial derivative, $B_{lm} = (\partial B_l/\partial x_m)$, to the lowest order. For a slowly varying mean magnetic field, the mean EMF can approximately be written as a *function* of B_l and B_{lm}; see (Brandenburg et al., 2008; Singh & Sridhar, 2011):

$$\mathcal{E}_i \;=\; \alpha_{il}(t)B_l(\boldsymbol{x},t) \;-\; \eta_{iml}(t)\,\frac{\partial B_l(\boldsymbol{x},t)}{\partial x_m} \tag{7.5}$$

where $\alpha_{il}(t)$ and $\eta_{iml}(t)$ are the *transport coefficients*.

7.2.2 Transport coefficients

Previous studies have shown that $\alpha_{il} = 0$ so long as the stirring is non–helical (Brandenburg et al., 2008; Sridhar & Subramanian, 2009a,b; Sridhar & Singh, 2010; Singh & Sridhar, 2011). To simplify further, the mean–magnetic field is averaged over the coordinates

x_1 and x_2. So we consider the case when the mean magnetic field, $\boldsymbol{B} = \boldsymbol{B}(x_3, t)$. The condition $\boldsymbol{\nabla \cdot B} = 0$ implies that B_3 is uniform in space, and it can be set to zero; hence we have $\boldsymbol{B} = (B_1,\, B_2,\, 0)$. Thus, Eqn. (7.5) for the mean EMF gives $\boldsymbol{\mathcal{E}} = (\mathcal{E}_1,\, \mathcal{E}_2,\, 0)$, with

$$\mathcal{E}_i \;=\; -\,\eta_{ij}\, J_j\,; \qquad\qquad \boldsymbol{J} \;=\; \boldsymbol{\nabla \times B} \;=\; \left(-\frac{\partial B_2}{\partial x_3},\;\; \frac{\partial B_1}{\partial x_3},\;\; 0\right) \tag{7.6}$$

where 2–indexed magnetic diffusivity tensor η_{ij} has four components, $(\eta_{11},\, \eta_{12},\, \eta_{21},\, \eta_{22})$, which are defined in terms of the 3–indexed object η_{iml} by

$$\eta_{ij} \;=\; \epsilon_{lj3}\, \eta_{i3l}\,; \quad \text{which implies that} \quad \eta_{i1} \;=\; -\,\eta_{i32}\,, \quad \eta_{i2} \;=\; \eta_{i31} \tag{7.7}$$

Equation (7.6) for $\boldsymbol{\mathcal{E}}$ can now be substituted in Eqn. (7.4). Then the mean–field induction equation becomes,

$$\begin{aligned} \frac{\partial B_1}{\partial \tau} \;&=\; -\,\eta_{21}\, \frac{\partial^2 B_2}{\partial x_3^2} \;+\; (\eta + \eta_{22})\, \frac{\partial^2 B_1}{\partial x_3^2} \\ \frac{\partial B_2}{\partial \tau} \;&=\; S B_1 \;-\; \eta_{12}\, \frac{\partial^2 B_1}{\partial x_3^2} \;+\; (\eta + \eta_{11})\, \frac{\partial^2 B_2}{\partial x_3^2} \end{aligned} \tag{7.8}$$

The diagonal components, η_{11} and η_{22}, augment the microscopic resistivity, η, whereas the off–diagonal components, η_{12} and η_{21}, lead to cross–coupling of B_1 and B_2. We note that the η_{ij} are in general time–dependent but we consider here the saturated values denoted by η_{ij}^{∞} in Singh & Sridhar (2011).

7.2.3 Test field method

We use test field method to determine the quantities η_{ij} introduced above. The procedure has been described in detail in Brandenburg et al. (2008) (see also references therein). A brief description of the method is as follows: Let $\boldsymbol{B}^q$ be a set of test–fields and $\boldsymbol{\mathcal{E}}^q$ be the EMF corresponding to the test field $\boldsymbol{B}^q$. Subtracting Eqn. (7.4) from Eqn. (7.3), we get

the evolution equation for the fluctuating field $\boldsymbol{b}$. With properly chosen $\boldsymbol{B}^q$ and the flow $\boldsymbol{v}$, we can numerically solve for the fluctuating field $\boldsymbol{b}^q$. This enables us to determine $\boldsymbol{\mathcal{E}}^q$ which can then be used to find η_{ij} using $\mathcal{E}_i^q = -\,\eta_{ij}\, J_j^q$ where $\boldsymbol{J}^q = \boldsymbol{\nabla}\times\boldsymbol{B}^q$.

There could be various choices for the number and form of the test fields which essentially depends on the problem that one is trying to solve. For our purposes, let us choose the test fields denoted as $\boldsymbol{B}^{qc}$ defined by,

$$\boldsymbol{B}^{1c} \;=\; B\,(\cos[kx_3],0,0)\;; \qquad \boldsymbol{B}^{2c} \;=\; B\,(0,\cos[kx_3],0) \tag{7.9}$$

where B and k are assumed to be constant. Using Eqn. (7.9) in the expression $\mathcal{E}_i^q = -\,\eta_{ij}\, J_j^q$, we find the corresponding mean EMF denoted by $\boldsymbol{\mathcal{E}}^{qc}$ as,

$$\mathcal{E}_i^{1c} \;=\; \eta_{i2}\, Bk\, \sin[kx_3]\,; \qquad \mathcal{E}_i^{2c} \;=\; -\eta_{i1}\, Bk\, \sin[kx_3]\,; \qquad i=1,2 \tag{7.10}$$

Zeros of $\sin[kX_3]$ provide singular solutions for η_{ij} as can be seen from Eqn. (7.10). To avoid this difficulty, we further consider the following set of test field denoted as $\boldsymbol{B}^{qs}$ defined by,

$$\boldsymbol{B}^{1s} \;=\; B\,(\sin[kx_3],0,0)\;; \qquad \boldsymbol{B}^{2s} \;=\; B\,(0,\sin[kx_3],0) \tag{7.11}$$

where B and k are assumed to be constant as before. Using Eqn. (7.11) in the expression $\mathcal{E}_i^q = -\,\eta_{ij}\, J_j^q$, we find the corresponding mean EMF denoted by $\boldsymbol{\mathcal{E}}^{qs}$ as,

$$\mathcal{E}_i^{1s} \;=\; -\eta_{i2}\, Bk\, \cos[kx_3]\,; \qquad \mathcal{E}_i^{2s} \;=\; \eta_{i1}\, Bk\, \cos[kx_3]\,; \qquad i=1,2 \tag{7.12}$$

Using Eqns. (7.10) and (7.12) we can write,

$$\begin{aligned}
\eta_{i1} \;&=\; -\frac{1}{Bk}\left(\mathcal{E}_i^{2c}\sin[kx_3] - \mathcal{E}_i^{2s}\cos[kx_3]\right) \\
\eta_{i2} \;&=\; \frac{1}{Bk}\left(\mathcal{E}_i^{1c}\sin[kx_3] - \mathcal{E}_i^{1s}\cos[kx_3]\right)\;; \qquad i=1,2
\end{aligned} \tag{7.13}$$

Thus from the Eqn. (7.13) we can determine the unknown quantities η_{ij}. For homogeneous turbulence being considered here, η_{ij} need to be independent of x_3, therefore, the apparent dependence on x_3 through the terms $\sin[kx_3]$ and $\cos[kx_3]$ in Eqn. (7.13) have to be compensated by x_3-dependent $\mathcal{E}_i$'s given by Eqns. (7.10) and (7.12).

7.2.4 Boundary conditions

We use "shear–periodic" boundary conditions to solve Eqns. (7.1–7.3) in the same manner as given in Brandenburg et al. (2008). Shear–periodic boundary conditions have been widely used in numerical simulations of a variety of contexts. Simulations of local patch of planetary rings Wisdom & Tremaine (1988), local dynamics of differentially rotating discs in astrophysical systems Balbus & Hawley (1998); Binney & Tremaine (2008), nonlinear evolution of perturbed shear flow in two–dimensions with the ultimate goal to understand the dynamics of accretion disks Lithwick (2007), the shear dynamo Brandenburg et al. (2008); Yousef et al. (2008a,b); Käpylä, Korpi & Brandenburg (2008) etc serve to be few examples. We provide below a brief explanation of shear–periodic boundary conditions. Let us define *sheared coordinates* by

$$x_1^{\rm sh} = x_1\,, \qquad x_2^{\rm sh} = x_2 - St x_1\,, \qquad x_3^{\rm sh} = x_3\,. \tag{7.14}$$

These may be thought of as the Lagrangian coordinates of fluid elements that are carried along by the background shear flow. A function is said to be *shear–periodic* when it is a periodic function of $(x_1^{\rm sh}, x_2^{\rm sh}, x_3^{\rm sh})$ with periodicities (L_1, L_2, L_3), respectively. Specifically, the Eqns. (7.1–7.3) are solved in a box of size $L_1 \times L_2 \times L_3$ which is subjected to periodic boundary conditions in the x_2- and x_3-directions and shear–periodic (or "shifted–periodic") boundary condition in the x_1-direction. Letting f to be a shear–periodic function, we can write explicitly,

$$\begin{aligned} f(x_1, 0, x_3) &= f(x_1, L_2, x_3) \\ f(x_1, x_2, 0) &= f(x_1, x_2, L_3) \\ f(0, x_2, x_3) &= f(L_1, (x_2 + StL_1)_{[modulo\ L_2]}, x_3) \end{aligned} \tag{7.15}$$

where

$$(x_2 + StL_1)_{[modulo\ L_2]} = x_2 + StL_1 + mL_2 \tag{7.16}$$

In Eqn. (7.16) m can take any integer value. This is done to ensure that the right hand side of Eqn. (7.16) always lies inside the box in the direction of shear, i.e., x_2-direction for the present case. Thus the identity $0 \leq (x_2 + StL_1)_{[modulo\ L_2]} \leq L_2$ is satisfied at all times.

7.2.5 Random stirring

The random forcing function $\boldsymbol{f}$ in Eqn. (7.1) is assumed to be *mirror–symmetric*, *homogeneous*, *isotropic* and *delta–correlated–in–time*. Further, we assume that the vector function $\boldsymbol{f}$ is solenoidal and the forcing is confined to a spherical shell of magnitude $|\boldsymbol{k}_f| = k_f$ where the wavevector $\boldsymbol{k}_f$ signifies the energy–injection scale ($l_f = 2\pi/k_f$) of turbulence. This can be *approximately* achieved by following the method described in Brandenburg et al. (2008), which is briefly outlined here. Simulations have been performed in a cubic box of size $L \times L \times L$ (i.e., $L_1 = L_2 = L_3 = L$) in which the forcing $\boldsymbol{f}$ at each time step is a single plane wave proportional $\boldsymbol{k}_f \times \boldsymbol{a}$ where the wavevector $\boldsymbol{k}_f$ is randomly chosen from a set of precalculated vectors, the procedure for which has already been implemented in the code and $\boldsymbol{a}$ is an arbitrary random unit vector not aligned with $\boldsymbol{k}_f$. Average value of moduli of these wavevectors is what we call k_f described above. The properties as described above that $\boldsymbol{f}$ should possess can be achieved if the size of the

box is much larger as compared to the forcing–scale, i.e., $k_f/K \gg 1$ where $K = 2\pi/L$. The background turbulence becomes almost statistically steady for acceptable values of k_f/K if the averaging is done over long times, in which case the quantities which have been averaged over x_1- and x_2-directions show smaller and smaller fluctuations in x_3-direction and t, which would otherwise have shown more pronounced fluctuations.

We note that although the random forcing $\boldsymbol{f}$ is delta–correlated–in–time, the resulting fluctuating velocity field $\boldsymbol{v}$ will *not* be delta–correlated–in–time (this is due to the inertia as has been pointed out in Brandenburg et al. (2008)). This has been rigorously proved in Singh & Sridhar (2011) in the limit of small fluid Reynolds number, the limit which we aim to explore in the present manuscript. Another important fact to note is that in the limit of small Re the non–helical forcing has been shown to give rise to non–helical velocity field in the reference Singh & Sridhar (2011); whether this is true even in the limit of high Re has not been proved yet. Thus performing the simulation in the limit $\mathrm{Re} < 1$ with non–helical forcing guarantees the fact that *the fluctuating velocity field is also non–helical*.

7.3 Results

We have explored following three parameter regimes: (i) $\mathrm{Re} < 1$ and $\mathrm{Rm} < 1$; (ii) $\mathrm{Re} > 1$ and $\mathrm{Rm} < 1$; (iii) $\mathrm{Re} < 1$ and $\mathrm{Rm} > 1$. All the results obtained in numerical simulations for various parameter regimes are being presented. As noted earlier, the η_{ij} are in general time–dependent but we are considering only the saturated values, η_{ij}^{∞}. For discussions concerning η_{ij} we define new quantities as given in earlier works:

$$\eta_t \;=\; \frac{1}{2}(\eta_{11}^{\infty} + \eta_{22}^{\infty})\,, \qquad\qquad \eta_T \;=\; \eta + \eta_t \tag{7.17}$$

We now define various dimensionless quantities: The *fluid Reynolds number*, $\mathrm{Re} = v_{\mathrm{rms}}/(\nu k_F)$; the *magnetic Reynolds number*, $\mathrm{Rm} = v_{\mathrm{rms}}/(\eta k_F)$; the *Prandtl number*, $\mathrm{Pr} = \nu/\eta$; the dimensionless *Shear parameter*, $\mathrm{S_h} = S/(v_{\mathrm{rms}} k_F)$. Symbols used in these definitions have usual meanings.

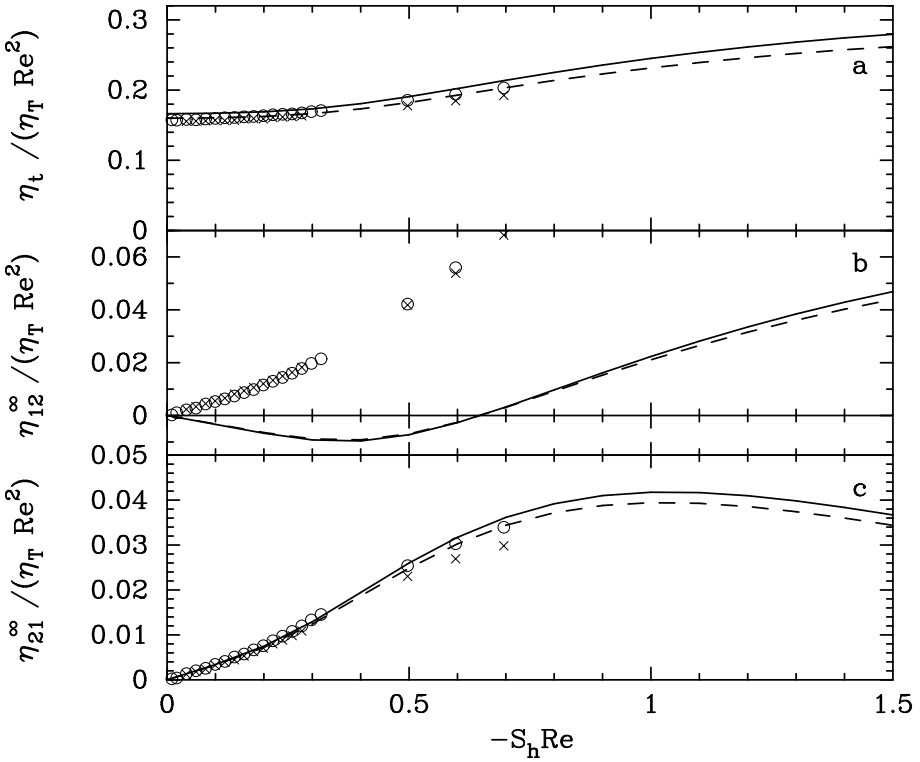

Figure 7.1: Plots, comparing the results of the simulations with our theory presented in Ch. 6, of the saturated quantities η_t, η_{12}^{∞} and η_{21}^{∞} for $\mathrm{Re} = \mathrm{Rm} \approx 0.16$, and $\mathrm{Re} = \mathrm{Rm} \approx 0.46$, corresponding to $\mathrm{Pr} = 1$, versus the dimensionless parameter $(-\mathrm{S_h Re})$. The lines ('bold' and 'dashed') correspond to the theory, whereas the symbols ('$\circ$' and '$\times$') correspond to the simulations. The 'bold' lines and the symbols '$\circ$' are for $\mathrm{Re} = \mathrm{Rm} \approx 0.16$, whereas the 'dashed' lines and the symbol '$\times$' are for $\mathrm{Re} = \mathrm{Rm} \approx 0.46$.

PART A: $\mathrm{Re} < 1$ **and** $\mathrm{Rm} < 1$

It is a necessary step to compare the numerical results obtained in this parameter regime with the earlier analytical work in which the general functional form for the saturated values of magnetic diffusivities, η_{ij}, was predicted (see Eqn. (6.20) and related discussion in Ch. 6).

Figures (7.1–7.3) display plots of η_t, η_{12}^{∞} and η_{21}^{∞}, versus the dimensionless parameter $(-\mathrm{S_h Re})$, which demonstrate the comparison of the results from a direct numerical simulation with 64^3 mesh points with our theoretical results obtained in Ch. 6. The scalings

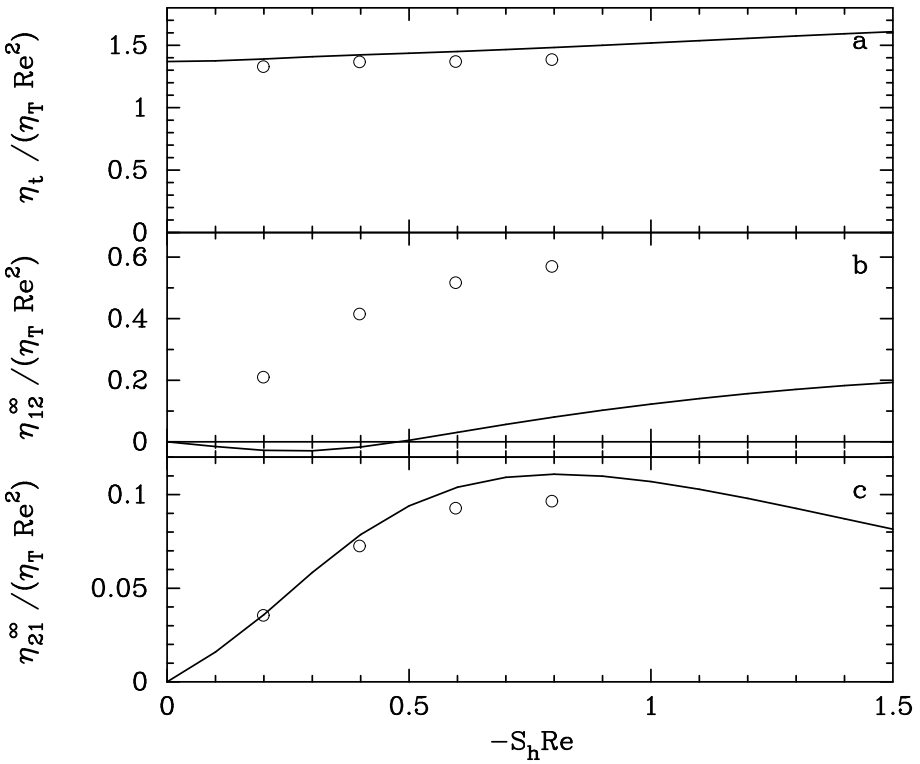

Figure 7.2: Plots, comparing the results of the simulations with our theory presented in Ch. 6, of the saturated quantities η_t, η_{12}^{∞} and η_{21}^{∞} for Re ≈ 0.13 and Rm ≈ 0.64, corresponding to Pr ≈ 5, versus the dimensionless parameter $(-\mathrm{S_h Re})$. The bold lines correspond to the theory, whereas the symbol '$\circ$' correspond to the simulations.

of the ordinates have been chosen for compatibility with the functional form displayed in Eqn. (6.20) of Ch. 6. However, it should be noted that we have performed simulations for values of $(-\mathrm{S_h Re})$ upto about 0.7, whereas we have been able to explore the larger values of $(-\mathrm{S_h Re})$ in our analytical computations, as given in Ch. 6. The plots in Fig. (7.1a–c) are for Pr = 1, but for two sets of values of the Reynolds numbers; Re = Rm ≈ 0.16 (the 'bold' lines represent the theory and the symbols '$\circ$' represent the simulations), and Re = Rm ≈ 0.46 (the 'dashed' lines represent the theory and the symbols '$\times$' represent the simulations). Figure (7.2a–c) are for Re ≈ 0.13 and Rm ≈ 0.64, corresponding to Pr ≈ 5 (the 'bold' lines represent the theory and the symbols '$\circ$' represent the simulations). Figure (7.3a–c) are for Re ≈ 0.13 and Rm ≈ 0.025, corresponding to Pr ≈ 0.2 (the 'bold' lines represent the theory and the symbols '$\circ$' represent the simulations).

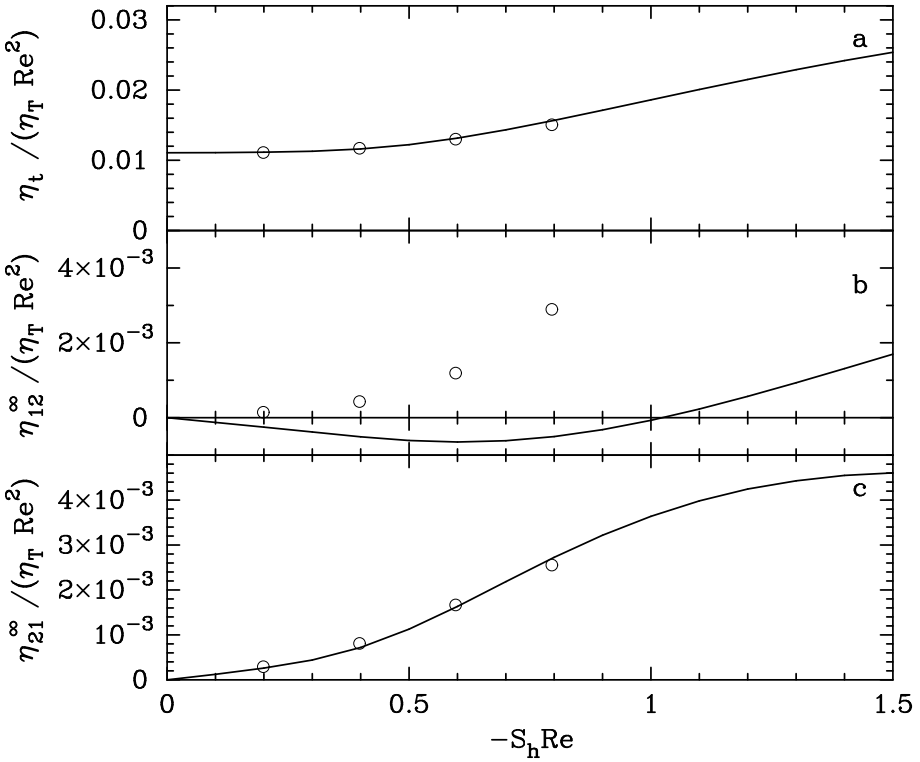

Figure 7.3: Plots, comparing the results of the simulations with our theory presented in Ch. 6, of the saturated quantities η_t, η_{12}^∞ and η_{21}^∞ for $\mathrm{Re} \approx 0.13$ and $\mathrm{Rm} \approx 0.025$, corresponding to $\mathrm{Pr} \approx 0.2$, versus the dimensionless parameter $(-\mathrm{S_h Re})$. The bold lines correspond to the theory, whereas the symbol '$\circ$' correspond to the simulations.

Some noteworthy properties are as follows:

(i) As may be seen from Fig. (7.1), that the symbols '$\circ$' and '$\times$' (also the bold and dashed lines) lie very nearly on top of each other. This implies that $\eta_t/(\eta_T \mathrm{Re}^2)$, $\eta_{12}^\infty/(\eta_T \mathrm{Re}^2)$ and $\eta_{21}^\infty/(\eta_T \mathrm{Re}^2)$ are (approximately) functions of $(-\mathrm{S_h Re})$ and Pr. Therefore the magnitude of χ in Eqn. (6.20) should be much smaller than unity. This was predicted in Ch. 6, and thus our numerical findings are in good agreement with our theoretical investigations.

(ii) We see that η_t is always positive. For a fixed value of $(-\mathrm{S_h Re})$ the quantity $\eta_t/(\eta_T \mathrm{Re}^2)$ increases with Pr, and for a fixed value of Pr, it slowly increases with

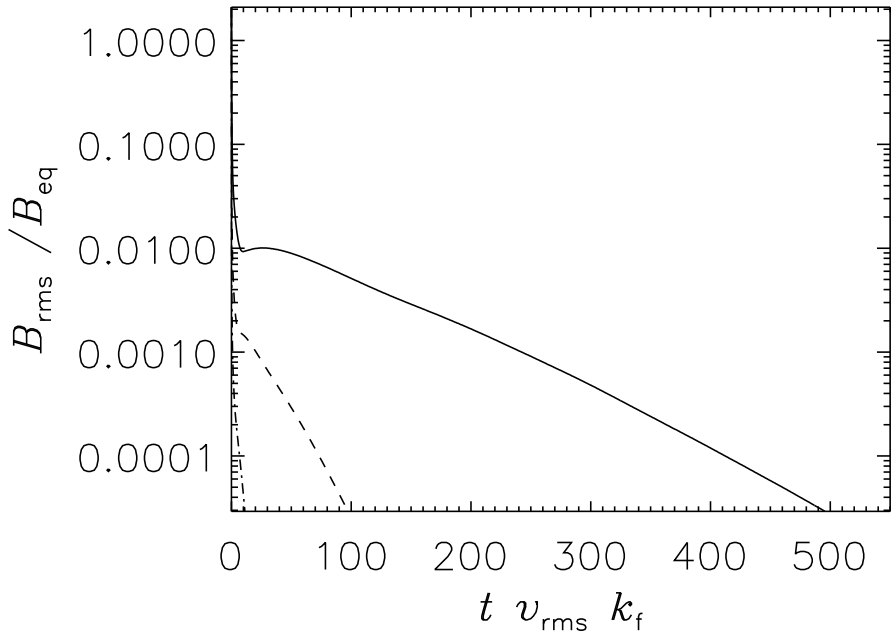

Figure 7.4: Time dependence of the root–mean–squared value of the total magnetic field [scaled with respect to $B_{\rm eq}$] versus the dimensionless parameter $(t\, v_{\rm rms}\, k_f)$. The bold line is for Re ≈ 0.128, Rm ≈ 0.643 (corresponding to Pr ≈ 5.0), $k_f/K = 10.03$ and $\mathrm{S_h} \approx -1.545$; the dashed line is for Re ≈ 0.16, Rm ≈ 0.16 (corresponding to Pr ≈ 1.0), $k_f/K = 10.03$ and $\mathrm{S_h} \approx -1.237$; and the dashed–dotted line is for Re ≈ 0.127, Rm ≈ 0.025 (corresponding to Pr ≈ 0.25), $k_f/K = 10.03$ and $\mathrm{S_h} \approx -1.560$.

$(-\mathrm{S_h Re})$ (which is consistent with Brandenburg et al. (2008)). An excellent agreement between our numerical findings and the theory presented in Ch. 6 may be seen from top panels of Figs. (7.1–7.3).

(iii) The quantity η_{12}^{∞} approaches the value zero in the limit when $(-\mathrm{S_h Re})$ is nearly zero. In the numerical simulation, it is seen to be increasing with $(-\mathrm{S_h Re})$ for a fixed value of Pr, and for a fixed value of $(-\mathrm{S_h Re})$ it increases with Pr. η_{12}^{∞} is expected to behave in a more complicated way. Different signs of η_{12}^{∞} are reported in Brandenburg et al. (2008) and Rüdiger & Kitchatinov (2006), whereas both signs have been predicted in our calculations. The differences between the theory

and the simulations may be inferred from panels (b) of Figs. (7.1–7.3).

(iv) As may be seen from the bottom panels of Figs. (7.1–7.3), that, η_{21}^{∞} is always positive. This agrees with the results obtained in earlier works (Brandenburg et al., 2008; Rädler & Stepanov, 2006; Rüdiger & Kitchatinov, 2006). Once again, the agreement between our numerical findings and our theoretical investigations of Ch. 6, for this *crucial* component of the diffusivity tensor is remarkably good[2].

Further, we show the time dependence of root–mean–squared value of the total magnetic field ($B_{\rm rms}$) in Fig. (7.4), which explicitly demonstrates the *decay* of $B_{\rm rms}$ for following three sets of values of control parameters: (i) Re $\approx$ 0.128, Rm $\approx$ 0.643 (corresponding to Pr $\approx$ 5.0; shown by the bold line), $S_h \approx -1.545$; (ii) Re $\approx$ 0.16, Rm $\approx$ 0.16 (corresponding to Pr $\approx$ 1.0; shown by the dashed line), $S_h \approx -1.237$; and (iii) Re $\approx$ 0.127, Rm $\approx$ 0.025 (corresponding to Pr $\approx$ 0.25; shown by the dashed-dotted line), $S_h \approx -1.560$. Results shown in Fig. (7.4) are from a direct numerical simulation with 64^3 mesh points and $k_f/K = 10.03$.

PART B: Re > 1 **and** Rm < 1

We explored this parameter regime for completeness in order to investigate the dynamo action when Rm < 1 whereas Re > 1. Kinematic theory of shear–dynamo problem (see Ch. 5) was developed which is valid for low magnetic Reynolds number but places no restriction on the fluid Reynolds number. We computed all relevant components of the magnetic diffusivity tensor using test–field method and also investigated the possibility of dynamo action. We summarize all our results for Re > 1 and Rm < 1 in detail in Table I.

We find no evidence of dynamo action in this particular parameter regime where Re > 1 and Rm < 1. This is shown clearly in Fig. (7.5), in which we plot the time dependence of root–mean–squared value of the total magnetic field ($B_{\rm rms}$) and demonstrate

[2]As discussed in Ch. 6, the sign of η_{21}^{∞} has a direct bearing on the shear–current effect, and this being positive suggests that the shear–current effect cannot be responsible for dynamo action, at least in the range of parameters explored.

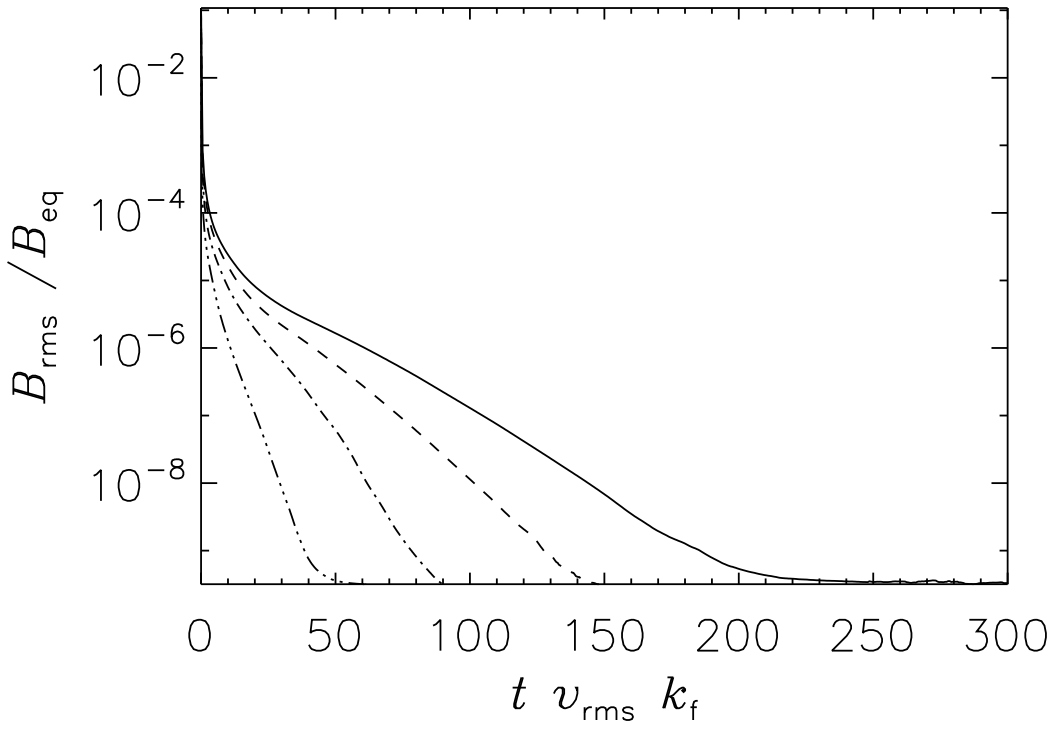

Figure 7.5: Time dependence of the root–mean–squared value of the total magnetic field [scaled with respect to $B_{\rm eq}$] versus the dimensionless parameter $(t\, v_{\rm rms}\, k_f)$. The bold line is for Re ≈ 24.57, Rm ≈ 0.614 (corresponding to Pr ≈ 0.025), $k_f/K = 5.09$ and $\mathrm{S_h} \approx -0.118$; the dashed line is for Re ≈ 22.40, Rm ≈ 0.448 (corresponding to Pr ≈ 0.02), $k_f/K = 5.09$ and $\mathrm{S_h} \approx -0.128$; the dashed–dotted line is for Re ≈ 43.17, Rm ≈ 0.863 (corresponding to Pr ≈ 0.02), $k_f/K = 3.13$ and $\mathrm{S_h} \approx -0.177$; and the dashed–dots line is for Re ≈ 36.54, Rm ≈ 0.365 (corresponding to Pr ≈ 0.009), $k_f/K = 3.13$ and $\mathrm{S_h} \approx -0.209$

.

Table 7.1: Summary of the simulations for Re > 1 and Rm < 1.

Run	Re	Rm	k_f/K	$-\mathrm{S_h}$	Ma^3	Grid	$\eta_t/(\eta_T \mathrm{Re}^2)$	$\eta_{12}/(\eta_T \mathrm{Re}^2)$	$\eta_{21}/(\eta_T \mathrm{Re}^2)$	Comments
A	5.50	0.14	10.03	0.136	0.110	64^3	0.000366	0.000044	0.0000279	No dynamo
B	4.63	0.70	10.03	0.014	0.139	64^3	0.006845	0.000174	0.0000764	No dynamo
C	4.69	0.70	10.03	0.057	0.141	64^3	0.007000	0.000628	0.0003048	No dynamo
D	4.83	0.73	10.03	0.103	0.145	64^3	0.007247	0.001224	0.0005103	No dynamo
E	5.63	0.84	10.03	0.141	0.169	64^3	0.006654	0.002330	0.0006008	No dynamo
F	41.14	0.82	3.13	0.186	0.258	64^3	0.000110	0.000017	0.0000092	No dynamo
G	48.40	0.41	3.13	0.186	0.258	64^3	0.000025	0.000003	0.0000021	No dynamo

the absence of dynamo action in this parameter regime. Figure (7.5) shows results from direct simulation with 64^3 mesh points for the following four sets of parameter values: (i) Re ≈ 24.57, Rm ≈ 0.614, $k_f/K = 5.09$, $\mathrm{S_h} \approx -0.118$ (shown by the bold line); (ii) Re ≈ 22.40, Rm ≈ 0.448, $k_f/K = 5.09$, $\mathrm{S_h} \approx -0.128$ (shown by the dashed line); (iii) Re ≈ 43.17, Rm ≈ 0.863, $k_f/K = 3.13$, $\mathrm{S_h} \approx -0.177$ (shown by the dashed–dotted line); and (iv) Re ≈ 36.54, Rm ≈ 0.365, $k_f/K = 3.13$, $\mathrm{S_h} \approx -0.209$ (shown by the dashed–dots line).

PART C: Re < 1 **and** Rm > 1

We now report our analysis concerning the growth of mean magnetic field in a background linear shear flow, with non–helical forcing at small scale, for the case when Re < 1 and Rm > 1. All the simulations presented in this part are performed with 128^3 mesh points. This is a particularly interesting regime for the following reasons: (i) it is an important fact to note that in the limit of small Re the non–helical forcing has been shown to give rise to non–helical velocity field (see the discussion below Eqn. (3.24) in Ch. 3); whether this is true even in the limit of high Re has not been proved yet. Thus performing the simulation in this limit (i.e., Re < 1) with non–helical forcing guarantees the fact that *the fluctuating velocity field is also non–helical*; (ii) For low Re the Navier–Stokes Eqn. (7.1) can be linearized and thus it becomes analytically more tractable problem, as

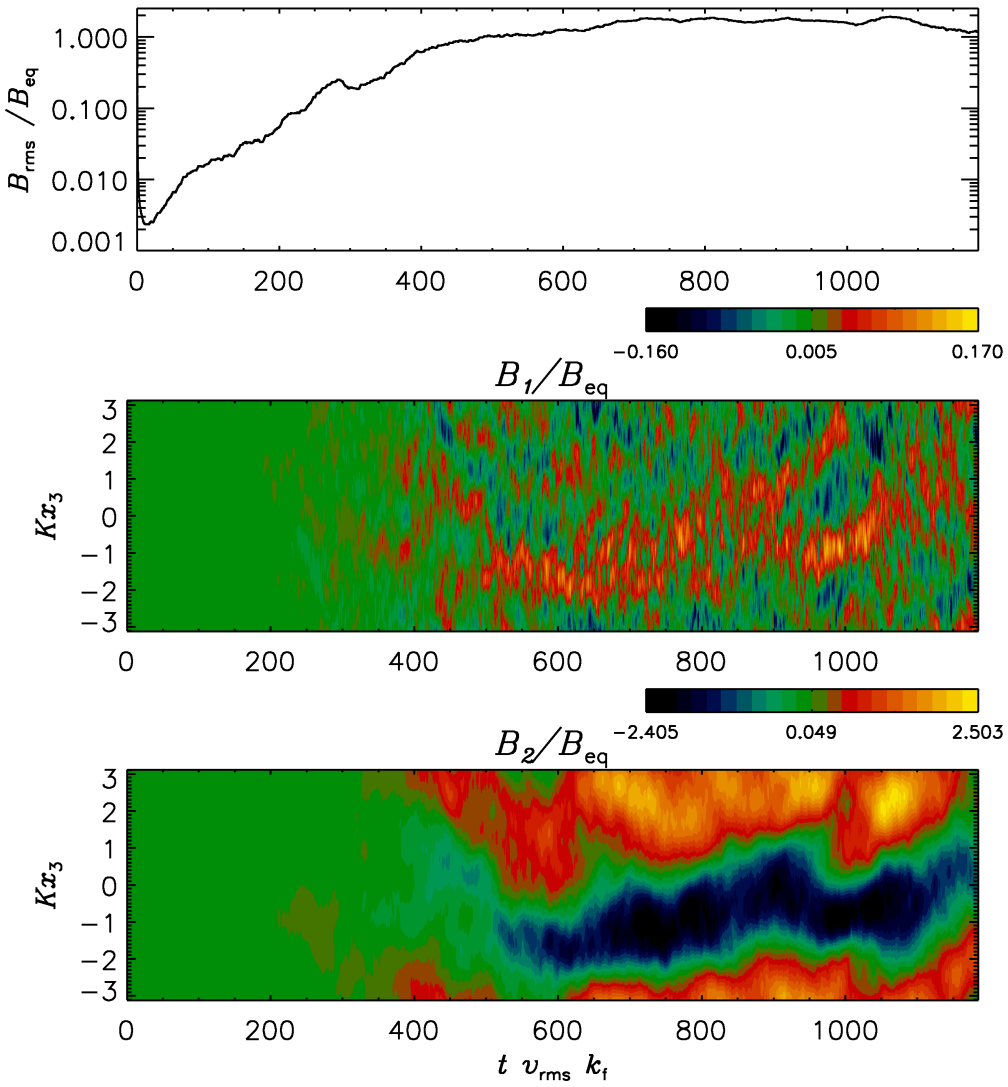

Figure 7.6: Time dependence of the root–mean–squared value of the total magnetic field $\boldsymbol{B}^{\rm tot}$ and spacetime diagrams of $B_1(x_3,t)$ and $B_2(x_3,t)$ [all scaled with respect to $B_{\rm eq}$] from a direct simulation with Re ≈ 0.378, Rm ≈ 15.135 (corresponding to Pr ≈ 40.0), $k_f/K = 3.13$ and $\mathrm{S_h} \approx -1.01$, versus the dimensionless parameter $(t\,v_{\rm rms}\,k_f)$. The top panel shows the initial exponential growth of mean magnetic field which saturates with time. The other two panels demonstrate the episodes of large scale feature in the x_3-direction, especially in the B_2 component.

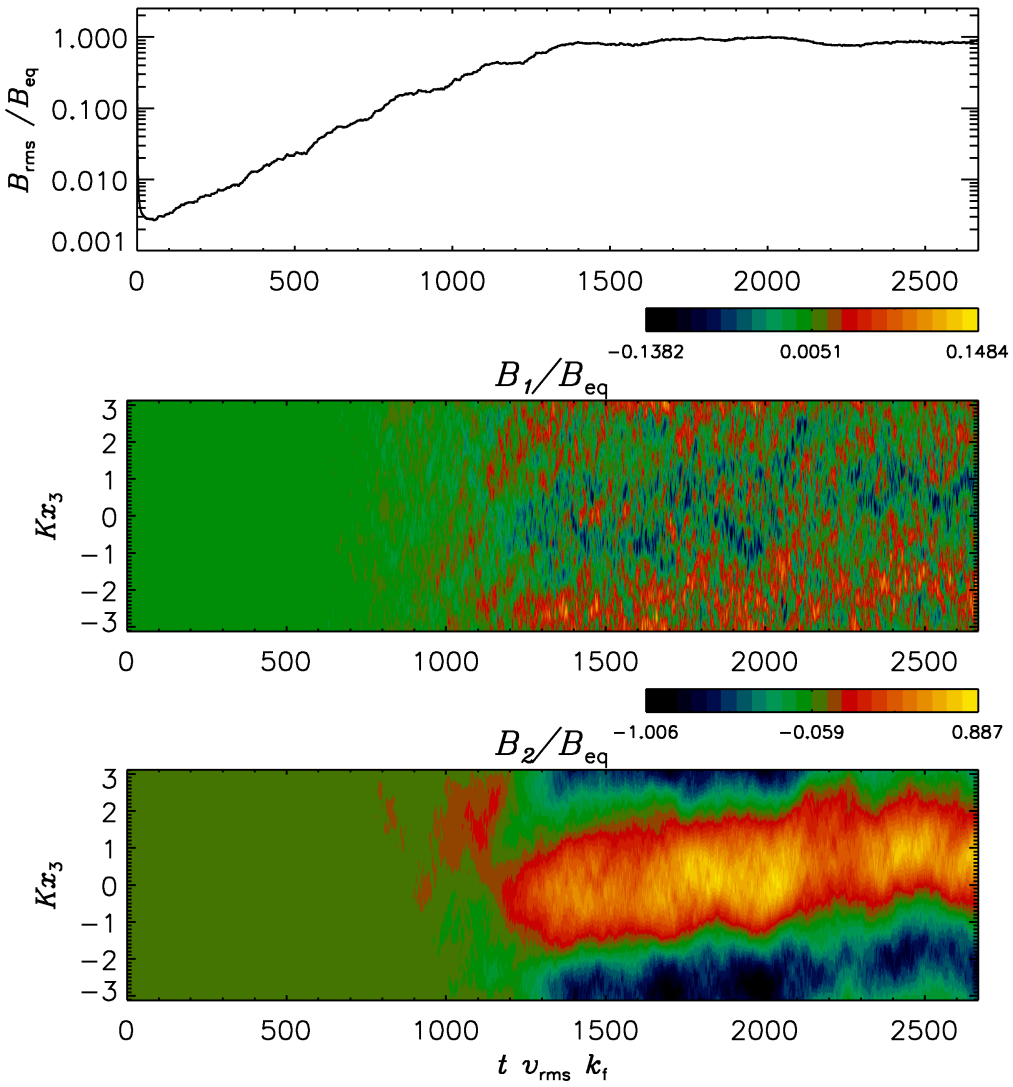

Figure 7.7: Time dependence of the root–mean–squared value of the total magnetic field $\boldsymbol{B}^{\rm tot}$ and spacetime diagrams of $B_1(x_3,t)$ and $B_2(x_3,t)$ [all scaled with respect to $B_{\rm eq}$] from a direct simulation with Re ≈ 0.833, Rm ≈ 24.976 (corresponding to Pr ≈ 30.0), $k_f/K = 3.13$ and $\mathrm{S_h} \approx -0.23$, versus the dimensionless parameter $(t\,v_{\rm rms}\,k_f)$. The top panel shows the initial exponential growth of mean magnetic field which saturates with time. The other two panels demonstrate the episodes of large scale feature in the x_3-direction, especially in the B_2 component.

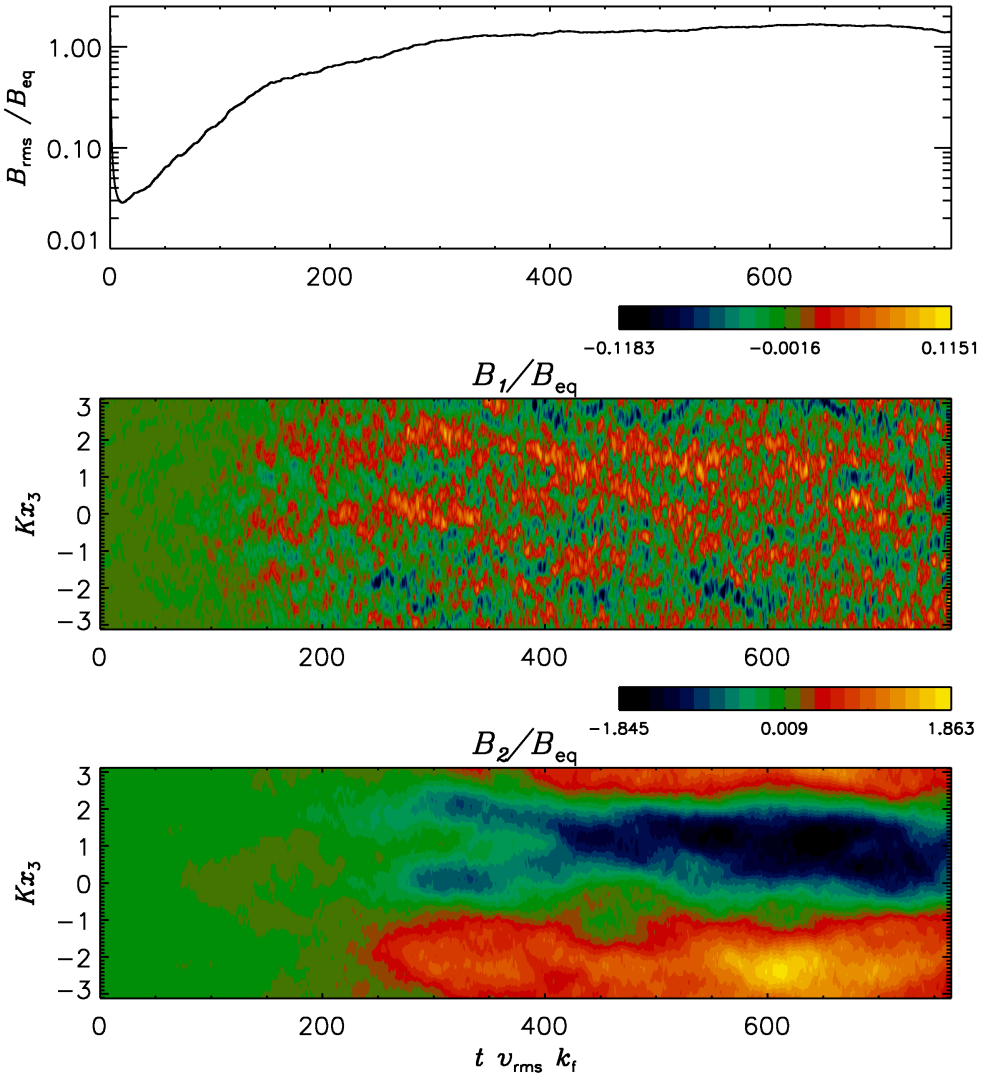

Figure 7.8: Time dependence of the root–mean–squared value of the total magnetic field $\boldsymbol{B}^{\rm tot}$ and spacetime diagrams of $B_1(x_3,t)$ and $B_2(x_3,t)$ [all scaled with respect to $B_{\rm eq}$] from a direct simulation with Re ≈ 0.641, Rm ≈ 32.039 (corresponding to Pr ≈ 50.0), $k_f/K = 5.09$ and $\mathrm{S_h} \approx -0.60$, versus the dimensionless parameter $(t\,v_{\rm rms}\,k_f)$. The top panel shows the initial exponential growth of mean magnetic field which saturates with time. The other two panels demonstrate the episodes of large scale feature in the x_3-direction, especially in the B_2 component.

compared to the case of high Re. Such solutions have been rigorously obtained without the Lorentz forces in Navier–Stokes equation and have been presented in Ch. 3. So it appears more reasonable to develop a theoretical framework in the limit, Re < 1 and Rm > 1 before one aims to have a theory which is valid for both (Re, Rm) > 1. Such thoughts motivated us to perform numerical experiment in this limit to look for the dynamo action. Figures (7.6–7.8) display the time dependence of root–mean–squared value of mean magnetic field $\boldsymbol{B}$ and spacetime diagrams of $B_1(x_3, t)$ and $B_2(x_3, t)$ for three different combinations of Re and Rm. We have scaled the magnetic fields in Figs. (7.6–7.8) with respect to $B_{\rm eq}$ where $B_{\rm eq} = (\mu_0 \langle \rho v_{\rm rms}^2 \rangle)^{1/2}$. Scalings in these Figures have been chosen for compatibility with Figs. (7) and (8) of Brandenburg et al. (2008). Below we list few useful points related to the dynamo action when Re < 1 and Rm > 1 based on careful investigation of Figs. (7.6–7.8):

(i) Top panels of Figs. (7.6–7.8) clearly show the *growth* of $B_{\rm rms}$ demonstrating the shear dynamo due to non–helical forcing ($B_{\rm rms}^2 = \langle B^2 \rangle + \langle b^2 \rangle$, where B and b are the magnitudes of the mean and fluctuating magnetic fields respectively). Thus the $B_{\rm rms}-$field may grow either due to B or b, or due to both B and b.

(ii) Denoting the *magnetic diffusion time scale* as $\tau_\eta = (\eta k_f^2)^{-1}$ and *eddy turn over time scale* as $\tau_{\rm edd} = (v_{\rm rms} k_f)^{-1}$, we write $\tau_\eta = ({\rm Rm})\, \tau_{\rm edd}$. The magnetic fields in these simulations survive for times, say $t = 320\, \tau_{edd}$, which for Rm ≈ 32 (corresponding to Fig. (7.8)) implies, $t = 10\, \tau_\eta$, i.e., ten times the diffusion time scale. This is a clear indication of the dynamo action as the magnetic fields survive much longer than the magnetic diffusion time scale.

(iii) Spacetime diagrams in Figs. (7.6–7.8) reveal that the mean magnetic fields start developing only after times which are few times the magnetic diffusion time scale (τ_η).

(iv) Although the mean magnetic field starts developing at much later times, $B_{\rm rms}$ starts growing at earlier times. The possibility of the growth of mean–squared field, with no net mean magnetic field at these early times, cannot be ruled out.

It is instructive to know the magnitude of magnetic power at different length scales in the simulations and study its evolution in time. Although the forcing is done at a *single* length scale, a typical kinetic energy spectrum has a peak at the stirring scale with significantly less power at other length scales (e.g., see dashed lines in various panels of Fig. (7.9)). We display in Fig. (7.9) the energy spectra obtained in one of the three simulations (for different combinations of the control parameters, all with Re < 1), corresponding to the one shown in Fig. (7.8). Thus Figs. (7.8) and (7.9) show results obtained from one particular simulation with 128^3 mesh points, Re ≈ 0.641, Rm ≈ 32.039, $k_f/K = 5.09$ and $\mathrm{S_h} \approx -0.60$. Few noteworthy points are discussed below in detail:

(i) Initially the magnetic power is very small as compared to the kinetic power and it is mainly concentrated at large $k-$values (i.e. small length scales), as may be seen from panel (a) of Fig. (7.9). Also, there is essentially no magnetic power at large scales at the initial stage of the simulation.

(ii) The strength of the total magnetic field decreases upto certain time due to dissipation (compare panels (a) and (b) of Fig. (7.9)), before it starts building up due to dynamo action.

(iii) From the top panel of Fig. (7.8), we see that the root–mean–squared value of the total magnetic field starts growing due to dynamo action ($B^2_{\rm rms} = \langle B^2 \rangle + \langle b^2 \rangle$, where B and b are the magnitudes of the mean and fluctuating magnetic fields respectively). As the $B_{\rm rms}-$field may grow either due to B or b, or due to both B and b, it seems necessary to understand this in more detail. From Fig. (7.9), it may be seen that the magnetic energy grows at all scales once it starts growing up till it saturates.

(iv) The small scale field grows faster, which averages out to zero, and hence does not show up in the spacetime diagrams of Fig. (7.8). This is generally referred to as *the fluctuation dynamo*. The growth rate changes and becomes smaller after the

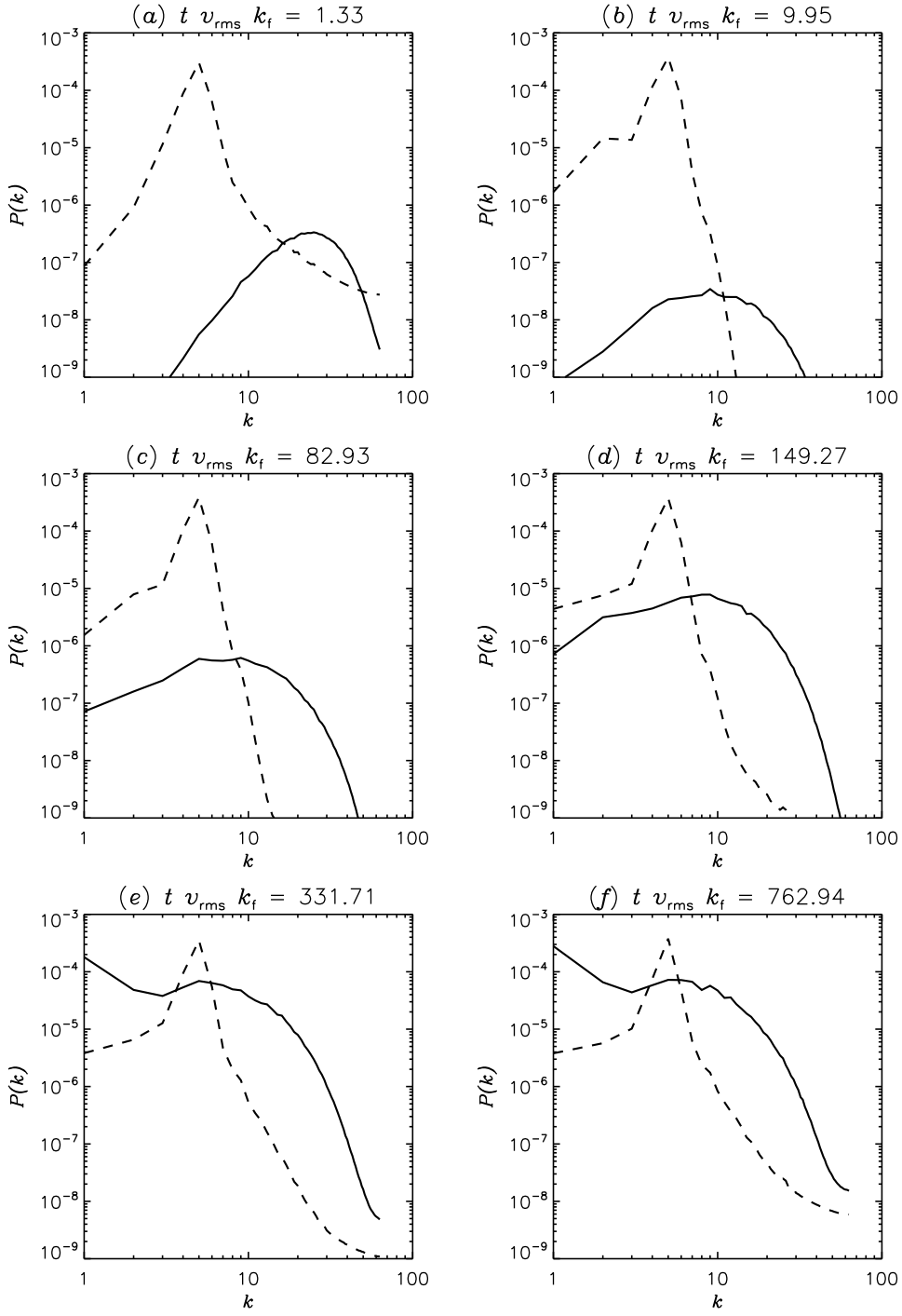

Figure 7.9: Panels (a–f) show magnetic (bold line) and kinetic (dashed line) energy spectra from a direct simulation (presented above in Fig. (7.8), in which the forcing was non–helical with Re ≈ 0.641, Rm ≈ 32.039, $k_f/K = 5.09$ and $\mathrm{S_h} \approx -0.60$) for different values of $(t\, v_{\rm rms}\, k_f)$.

fluctuation dynamo saturates (which happens at $t\, v_{\rm rms}\, k_f \approx 150$ in Fig. (7.8) and the corresponding power spectrum at that time is shown in panel (d) of Fig. (7.9)).

(v) Although there is non–zero magnetic energy in the large scales when $t\, v_{\rm rms}\, k_f \approx 150$ (see panel (d) of Fig. (7.9)), we begin to see some features in the spacetime diagrams of the mean magnetic field (shown in Fig. (7.8)) only beyond $t\, v_{\rm rms}\, k_f \approx 150$. Thus, it is possible that $\boldsymbol{B} = \boldsymbol{0}$ while $\langle B^2 \rangle$ be finite.

(vi) The mean magnetic field starts developing beyond $t\, v_{\rm rms}\, k_f \approx 150$ (*which is about five times the magnetic diffusion time scale*) which saturates at $t\, v_{\rm rms}\, k_f \approx 330$ (see Fig. (7.8)) after which the magnetic energy essentially stops evolving at all length scales, as may be seen from Fig. (7.9).

(vii) When the magnetic energy saturates at some value, we see significant magnetic power at the largest scale.

It may be seen from the top panels of Figs. (7.6–7.8) that $B_{\rm rms}$ shows exponential growth. We denote the initial exponential growth rate of $B_{\rm rms}$ as γ. It is evident from Fig. (7.10) that the dimensionless growth rate ($\gamma^* = \gamma/(v_{\rm rms} k_f)$) appear to scale as $\gamma^* \propto -{\rm S_h}$ in the range of parameters explored in this work. This result is in agreement with (Yousef et al., 2008a; Brandenburg et al., 2008; Heinemann, McWilliams & Schekochihin, 2011; Richardson & Proctor, 2012).

7.4 Investigating the reasons for observed dynamo action

We have demonstrated in the last section that the dynamo action is possible in a background linear shear flow due to non–helical forcing, when the magnetic Reynolds number is above unity, whereas the fluid Reynolds number is below unity (i.e., Re < 1 and Rm > 1). Earlier works have shown dynamo action in such systems when both (Re, Rm) > 1. It is still not clear what causes such shear dynamo to operate due to

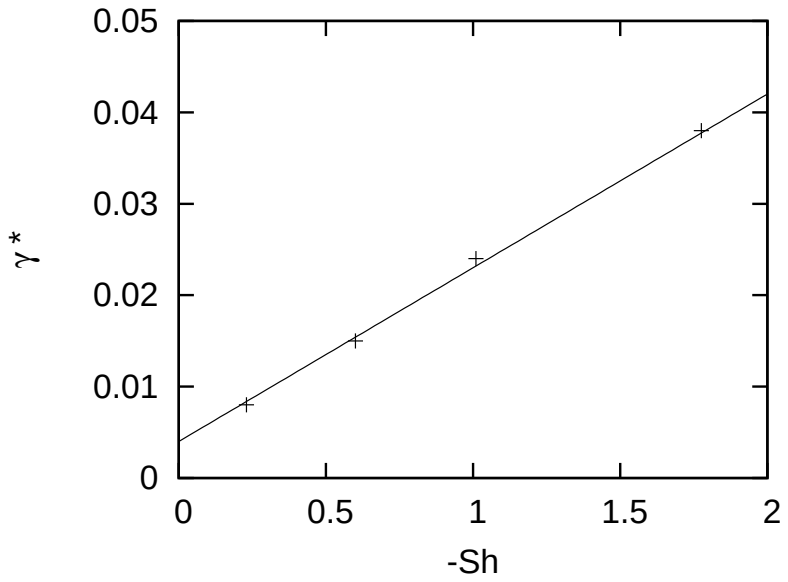

Figure 7.10: Plot of dimensionless initial growth rates, $\gamma^* = \gamma/(v_{\rm rms}k_f)$, of $B_{\rm rms}$ (corresponding to the cases when Re < 1 and Rm > 1) versus $-\mathrm{S_h}$. The '+' symbols denote results from direct simulations whereas the bold line shows the slope of the linear trend corresponding to $\gamma^* \propto -\mathrm{S_h}$.

non–helical turbulence. In this section, we try to estimate the effects of *fluctuations of turbulent transport coefficients*, which might have implications for the observed dynamo action in these numerical simulations. Estimating the magnitude and effects of these fluctuations, which are being presented below, have been motivated by some earlier analytical and numerical works (Kraichnan, 1976; Moffatt, 1978; Vishniac & Brandenburg, 1997; Sokolov, 1997; Silant'ev, 2000; Proctor, 2007; Brandenburg et al., 2008).

7.4.1 Fluctuating $\alpha-$effect & incoherent alpha-shear dynamo

In 1976, Kraichnan discussed the possibility of fluctuations in scalar alpha with zero mean (Kraichnan, 1976), which together with large scale shear could possibly give rise to the dynamo action in the mirror–symmetric turbulence (Vishniac & Brandenburg, 1997; Sokolov, 1997; Silant'ev, 2000; Proctor, 2007). As the coefficient 'α' (which, in

general, is a tensorial quantity α_{il} as may be seen from Eqn. (7.5)) is, by definition, an averaged quantity, it requires some extra care to imagine the fluctuations in such quantities. The $\alpha-$fluctuations should be viewed as the fluctuations in the turbulent helicity, which will be argued and discussed in detail in the next chapter, as we have pursued the problem of fluctuating turbulent helicity in context to the shear dynamo problem, analytically.

Following Brandenburg et al. (2008), we estimate the fluctuations in each component of α_{il} which, together with mean shear, might drive the dynamo action by what is known as *the incoherent alpha–shear* mechanism. The procedure to investigate the incoherent alpha–shear dynamo may be given as follows:

(i) There seem to be a dimensionless parameter, $D_{\alpha S}$, known as *the dynamo number*, which is defined as,

$$D_{\alpha S} \;=\; \frac{\alpha_{22}^{\rm rms}\,|S|}{\eta_T^2\,K^3} \tag{7.18}$$

where η_T has been defined in Eqn. (7.17) and K is the smallest finite wavenumber in the X_3-direction. It has been determined *numerically* in Brandenburg et al. (2008), that the condition for the growth of mean magnetic field is

$$D_{\alpha S} \;>\; D_{\alpha S}^{\rm crit}\;; \qquad \text{where} \quad D_{\alpha S}^{\rm crit} \;\approx\; 2.3 \tag{7.19}$$

(ii) To measure the magnitude of the fluctuations in α_{il} as found in our test–field simulations, in order to estimate $\alpha^{\rm rms}$, we do the following:

(a) A typical time series of transport coefficients shows variations of the quantity around some mean value. These variations are not to be confused with the fluctuating transport coefficients.

(b) The values of each components of α_{il}, when averaged over the whole time series, approach zero for long enough time series, for non–helical turbulence.

(c) The whole time series can be split into multiple bins with suitably chosen width.

(d) Now we find the average value of α_{il} in each bin. If the averages thus computed for each bin take different values, these quantities are understood to be fluctuating, although averaged over some sufficiently long times.

(e) We find the probability density function (PDF) of each component of α_{il} which appears like Gaussian in all the cases we have investigated. The Gaussian nature of the PDFs are also seen in Brandenburg et al. (2008).

(f) $\alpha_{22}^{\rm rms}$ can now be estimated by $\alpha_{22}^{\rm rms} = \sqrt{\langle(\alpha_{22})^2\rangle}$, where $\langle\rangle$ denotes the average of the binned–averaged quantities.

(iii) Our aim now will be to determine $D_{\alpha S}$ corresponding to various simulations we have performed in different regimes of the control parameters, discussed in the last section.

7.4.2 Estimation of the dynamo numbers for variety of simulations

We have computed the dynamo number defined by Eqn. (7.18) using the test–field simulations, which were performed for various regimes of the control parameters, we are interested in. We summarize our results in the Table (7.2).

As may be seen from Table (7.2) that the growth of mean magnetic field is always associated with cases for which the dynamo number exceeds its critical value, i.e., when $D_{\alpha S} > D_{\alpha S}^{\rm crit}$ where, $D_{\alpha S}^{\rm crit} \approx 2.3$. Some noteworthy properties are as follows:

(i) In the cases where both (Re, Rm) < 1 (runs (b), (e) and (f) which are shown in red in Table (7.2)), we do not see the dynamo action, but the corresponding dynamo numbers have been found to be below the critical value. Therefore, we cannot conclude that the dynamo action is impossible in this parameter regime; larger values of the dynamo numbers in this parameter regime need to be explored before reaching any conclusion. We tried to run simulations aiming to explore larger dynamo numbers when both (Re, Rm) < 1, but it could not be done due to limitations of the pencil code.

Table 7.2: Summary of simulations with various dynamo numbers and its implications.

Run	Re	Rm	k_f/K	$-\mathrm{S_h}$	Ma^4	Grid	$D_{\alpha S}$	Comments
(a)	41.20	0.82	3.13	0.186	0.258	64^3	0.0106	No dynamo
(b)	0.76	0.57	1.54	2.78	0.0701	128^3	0.0125	No dynamo
(c)	4.65	0.69	10.03	0.0285	0.139	64^3	0.0207	No dynamo
(d)	4.99	0.75	10.03	0.133	0.150	64^3	0.0827	No dynamo
(e)	0.47	0.47	10.03	1.27	0.0235	64^3	0.2002	No dynamo
(f)	0.73	0.91	10.03	0.41	0.0727	128^3	0.34	No dynamo
(g)	1.04	41.66	3.13	0.367	0.13	128^3	2.341	Dynamo
(h)	1.79	89.51	5.09	0.215	0.0911	128^3	2.443	Dynamo
(i)	0.85	25.50	5.09	0.226	0.129	128^3	3.05	Dynamo
(j)	0.75	33.60	10.03	0.236	0.0674	128^3	11.22	Dynamo
(k)	0.59	29.47	5.09	0.66	0.03	128^3	11.45	Dynamo

(ii) We do not find any evidence of dynamo action for cases when Re > 1 and Rm < 1 (runs (a), (c) and (d) which are shown in red in Table (7.2)), but even in these cases, the corresponding dynamo numbers are below the critical value. So, one needs to explore larger values of $D_{\alpha S}$ before reaching any conclusion, which could not be done using the pencil code.

(iii) Dynamo action was seen when $D_{\alpha S}$ was just above its critical value (see the runs (g) and (h) shown in green in Table (7.2)), for both of which, Re is just above unity whereas Rm is much larger than unity).

(iv) For the cases in which Re < 1 and Rm > 1, we see the growth of large–scale magnetic field (see the runs (i), (j) and (k) shown in green in Table (7.2)), and the corresponding dynamo numbers were always found to be above $D_{\alpha S}^{\mathrm{crit}}$.

(v) To further establish the dependence of observed dynamo action on the dynamo number, $D_{\alpha S}$, we investigated a particular case more carefully. We chose the run (k)

of Table (7.2), in which we see the growth of mean magnetic field, and $D_{\alpha S} = 11.45$. Keeping everything else same, we changed the value of the shear parameter, which in turn affects the value of $D_{\alpha S}$ through the linear dependence of $D_{\alpha S}$ on $|S|$ (see Eqn. (7.18)). First, we reduce $|S|$ by a factor 10, which makes $D_{\alpha S}$ ten times smaller, and it becomes *subcritical*. In this case, the $B_{\rm rms}$ just decays in time. Second, we reduce $|S|$ by a factor 4 compared to its original value of case (k). In this case, $D_{\alpha S}$ becomes *marginally supercritical* ($D_{\alpha S} \approx 2.86$), and we see the dynamo action in the simulation. This particular investigation seems to strengthen the idea that $D_{\alpha S}$ plays a crucial role in determining whether the dynamo action is going to operate or fail.

7.5 Conclusions

Motivated by theoretical investigations of the shear dynamo problem due to non–helical stirring of an incompressible fluid, we performed variety of numerical simulations exploring different regimes of the control parameters. The simulations were done for the following three parameter regimes: (i) both (Re, Rm) < 1; (ii) Re > 1 and Rm < 1; and (iii) Re < 1 and Rm > 1. These limits, which were never explored in any earlier works, appeared interesting to us for following reasons: first, to compare our analytical findings with the results of numerical simulations in the similar parameter regimes; and second, to look for the growth of mean magnetic field in the limit when Re < 1. Exploring the possibility of dynamo action when Re < 1 seems particularly interesting, as, in the limit of small Re, the non–helical forcing has been shown to give rise to non–helical velocity field (see the discussion below Eqn. (3.24) in Ch. 3); whether this is true even in the limit of high Re has not been proved yet. Thus performing the simulation in this limit (i.e., Re < 1) with non–helical forcing guarantees the fact that *the fluctuating velocity field is also non–helical*. Also, for low Re, the Navier–Stokes Eqn. (7.1) can be linearized and thus it becomes analytically more tractable problem, as compared to the case of high Re. Such solutions have been rigorously obtained without the Lorentz forces in

Navier–Stokes equation, and have been presented in Ch. 3.

In the present chapter, we successfully demonstrated that the dynamo action is possible in a background linear shear flow due to non–helical forcing when the magnetic Reynolds number is above unity whereas the fluid Reynolds number is below unity, i.e., when Re $<$ 1 and Rm $>$ 1 (see Figs. (7.6–7.9)). To investigate the reasons for the observed dynamo action (or otherwise), we computed the dynamo number, $D_{\alpha S}$, corresponding to the incoherent alpha–shear mechanism, by estimating the fluctuations in the turbulent transport coefficients. The simulations, where we see the growth of mean magnetic field, are the ones, in which the dynamo number exceeds its critical value, i.e., when $D_{\alpha S} > D_{\alpha S}^{\rm crit}$ where, $D_{\alpha S}^{\rm crit} \approx 2.3$ (see Table (7.2)). Few important conclusions may be given as follows:

1. We did not find any dynamo action in the limit when both (Re, Rm) $<$ 1 (see Fig. (7.4)). We computed all the transport coefficients by test–field simulations and compared with our theoretical work of Ch. 6 (see Figs. (7.1–7.3)). A good agreement between the theory and the simulations was found for all components of the magnetic diffusivity tensor, η_{ij}^{∞}, except for η_{12}^{∞}, which is expected to behave in a complicated fashion (Brandenburg et al., 2008; Rüdiger & Kitchatinov, 2006; Singh & Sridhar, 2011).

2. η_{21}^{∞} was always found to be positive in all the simulations performed in different parameter regimes. This is in agreement with our earlier conclusion that the shear–current effect cannot be responsible for dynamo action, at least for all the cases we have studied in different parameter regimes.

3. There was no evidence of dynamo action in the limit when Re $>$ 1 and Rm $<$ 1 (see Fig. (7.5)).

4. We demonstrated the dynamo action when Re $<$ 1 and Rm $>$ 1, for the first time (see Figs. (7.6–7.9)). The initial exponential growth rate of $B_{\rm rms}$, γ, seems to scale *linearly* with the rate of shear, $|S|$, in the range of parameters explored in this chapter (see Fig. (7.10)); a result which is in agreement with Yousef et

al. (2008a); Brandenburg et al. (2008); Heinemann, McWilliams & Schekochihin (2011); Richardson & Proctor (2012).

5. It is important to note that the dynamo number, $D_{\alpha S}$, corresponding to the incoherent alpha–shear mechanism, was computed for all the simulations performed in different parameter regimes, and the results have been presented in Table (7.2). Interestingly, those simulations, where we see the growth of mean magnetic field, are the ones, in which the dynamo number exceeds its critical value, i.e., when $D_{\alpha S} > D_{\alpha S}^{\rm crit}$ where, $D_{\alpha S}^{\rm crit} \approx 2.3$, whereas for all the other cases, in which we do not find the dynamo action, the corresponding dynamo number is always subcritical.

The hypothesis, that the fluctuations in the α_{ij} with zero mean, together with the mean shear (which is known as the incoherent alpha–shear mechanism) might drive the dynamo, seems a promising candidate for the observed dynamo action in linear shear flow, with no net helicity. We find that the dynamo action seems to crucially depend on the quantity, $D_{\alpha S}$, with its critical value $D_{\alpha S}^{\rm crit} \approx 2.3$, which was determined by Brandenburg et al. (2008), and supported by our numerical simulations presented in this chapter; see Table (7.2). We note that $D_{\alpha S}$ is an empirically constructed quantity and our goal in the next chapter is to construct a theory of dynamo action due to the combined effects of $\alpha-$fluctuations and shear.

Chapter 8

Dynamo Action due to $\alpha-$Fluctuations in a Linear Shear Flow

8.1 Introduction

The mechanism, by which the large–scale cosmic magnetic fields could be generated due to mirror–symmetric turbulence (i.e., in the absence of usual $\alpha-$effect) in a background linear shear flow, remains to be understood. In the framework of the classical mean–field theory (Moffatt, 1978; Krause & Rädler, 1980; Brandenburg & Subramanian, 2005), which may also be viewed as a two–scale approach, one has not yet been able to construct a rigorous theory explaining the origin of the shear dynamo problem due to non–helical turbulence. It has been argued in previous works that the fluctuations in the turbulent helicity in such systems with no net helicity, together with differential rotation, might be able to generate the observed large–scale magnetic field (see e.g., Vishniac & Brandenburg (1997); Sokolov (1997); Silant'ev (2000); Proctor (2007); Brandenburg et al. (2008); Sur & Subramanian (2009)). It will be quite a challenging task to study the effects of the turbulent helicity fluctuations in traditional mean–field approach, for reasons that will be described later. A slight revision of the usual mean–field theory might

be useful to study and understand the effects of the turbulent helicity fluctuations. The aim of the present chapter is to explore the possibility of such revision based on some arguments and suggestions which appeared in earlier works (Kraichnan, 1976; Hoyng, 1987a,b, 1988; Sokolov, 1997).

The *helicity* (or chirality or screwness) at each spacetime point is given by, $\boldsymbol{v}\cdot(\boldsymbol{\nabla}\times\boldsymbol{v})$, where $\boldsymbol{v}$ denotes the turbulent flow. The helicity is a pseudo–scalar (non mirror–symmetric) quantity which is also turbulent due to the turbulent nature of the flow. The net helicity in a perfectly mirror–symmetric turbulence is expected to vanish, but the correlation of helicities at different spacetime points need not be zero. In other words, the ensemble average of $\boldsymbol{v}\cdot(\boldsymbol{\nabla}\times\boldsymbol{v})$ contributing to usual $\alpha-$effect vanishes identically for perfectly mirror–symmetric turbulence, while the net helicity fluctuations, characterized by $\langle(\,\boldsymbol{v}\cdot(\boldsymbol{\nabla}\times\boldsymbol{v})\,)^2\rangle$ in the single averaging scheme, need not be zero. Thus a rigorous theory, aiming to address issues related to the turbulent helicity fluctuations in a non–helical turbulence, would inevitably require the computation of four–point unequal time velocity correlator in the single averaging scheme, a task which although is of great importance, would be quite challenging in practice. In order to study the effects of fluctuations of the turbulent helicity in an analytically simpler way, the concept of *double averaging* seems reasonably useful (Kraichnan, 1976). As argued in Kraichnan (1976), both the turbulent field variables, $\boldsymbol{v}$ and $\boldsymbol{v}\cdot(\boldsymbol{\nabla}\times\boldsymbol{v})$, have correlation times τ_v and τ_h, respectively[1], with $\tau_v \neq \tau_h$, in general. Following the arguments of Kraichnan (1976) and Sokolov (1997), where the mathematical aspects of double averaging have been given, we consider an *ensemble*, in which, each member of the ensemble corresponds to a different realization of the fluctuating velocity field, $\boldsymbol{v}$. The ensemble average of $\boldsymbol{v}$ is strictly zero, i.e., $\langle\boldsymbol{v}\rangle = \boldsymbol{0}$, where $\langle Q\rangle$ denotes the ensemble average of some quantity Q. The ensemble average of the quantity $\boldsymbol{v}\cdot(\boldsymbol{\nabla}\times\boldsymbol{v})$ (over different realizations of velocity field) need not be strictly zero in the perfectly mirror–symmetric turbulence, and it can be a stochastic variable. Thus

[1]The correlation time of a turbulent field may be thought of as the time scale over which the fluctuating quantity, at a particular spatial location, does not vary appreciably. Similarly one may define the correlation length of the turbulent field.

$\langle \boldsymbol{v}\cdot(\boldsymbol{\nabla}\times\boldsymbol{v})\rangle$ which contributes to $\alpha-$effect does not vanish even in the perfectly mirror–symmetric turbulence and α may be viewed as a fluctuating quantity. Now we construct a *superensemble*, in which, each member of the superensemble corresponds to a different realization of the fluctuating $\alpha \propto \langle \boldsymbol{v}\cdot(\boldsymbol{\nabla}\times\boldsymbol{v})\rangle$. For a perfectly mirror–symmetric turbulence, the *net* helicity is expected to vanish, i.e., the superensemble–average of the *ensemble–averaged–helicity* (over different realizations of α) vanishes. In other words, $\overline{\alpha} \propto \overline{\langle \boldsymbol{v}\cdot(\boldsymbol{\nabla}\times\boldsymbol{v})\rangle} = 0$, where $\overline{Q}$ denotes the superensemble–average of some quantity Q.

In § 8.2 we formulate the shear dynamo problem by considering temporal fluctuations in the quantity α. Using Reynolds averaging, we split the magnetic field into mean and fluctuating components and note that the mean field is driven by mean electromotive force (EMF) due to $\alpha-$fluctuations. We develop the equation for fluctuating magnetic field and ignore the term which is non–linear in fluctuations. Making use of the shearing coordinate transformation and the Green's function for linear shear, which is derived in the Appendix A, we write an explicit solution for the magnetic fluctuations. Thus we determine the mean EMF due to $\alpha-$fluctuations. In § 8.3 we derive explicit expressions for mean EMF and transport coefficients for the case when the mean magnetic field is a slowly varying function of spacetime. In § 8.4 we specialize to the case when the mean–field is a function only of the spatial coordinate X_3 and time τ; this reduction is necessary for comparison with some earlier works. We derive explicit expressions for all components of magnetic diffusivity tensor, which depend on the two–time correlator of fluctuating α. General expression for the dispersion relation is derived, which could be expressed as a function of three dimensionless parameters. Comparisons with earlier works are made and the implications for the dynamo action are discussed. We provide the conclusions in § 8.5.

8.2 The shear dynamo problem due to fluctuating $\alpha-$effect

8.2.1 The basic equations

Let $(\boldsymbol{e}_1, \boldsymbol{e}_2, \boldsymbol{e}_3)$ be the unit vectors of a Cartesian coordinate system which we refer as a lab frame, and we use the notation $\boldsymbol{X} = (X_1, X_2, X_3)$ for the position vector, and τ for time. The evolution of *once-averaged* magnetic field, denoted as $\boldsymbol{B}(\boldsymbol{X}, \tau)$, is given by

$$\frac{\partial \boldsymbol{B}}{\partial \tau} = \boldsymbol{\nabla} \times [\boldsymbol{V} \times \boldsymbol{B} + \alpha \boldsymbol{B} - (\eta + \eta_t) \boldsymbol{\nabla} \times \boldsymbol{B}] \tag{8.1}$$

where α and η_t depend on the kinetic helicity and the energy density of the *turbulence* (prescribed by the turbulent flow, denoted as $\boldsymbol{v}$), respectively. Both, α and η_t are, by definition, quantities which are suitably averaged over the same ensemble over which we have averaged the total magnetic field, $\boldsymbol{B}^{\rm tot}(\boldsymbol{X}, \tau)$, to define once-averaged magnetic field, $\boldsymbol{B}(\boldsymbol{X}, \tau)$. Denoting this ensemble average as $\langle\ \rangle$, we write explicitly,

$$\left\langle \boldsymbol{B}^{\rm tot} \right\rangle \ = \ \boldsymbol{B}\ ; \qquad \alpha \approx -\frac{1}{3}\,\tau_v \langle \boldsymbol{v} \cdot (\boldsymbol{\nabla} \times \boldsymbol{v}) \rangle\ ; \qquad \eta_t \approx \frac{1}{3}\,\tau_v \langle \boldsymbol{v} \cdot \boldsymbol{v} \rangle\ ; \qquad \langle \boldsymbol{v} \rangle \ = \ \boldsymbol{0} \tag{8.2}$$

$\boldsymbol{V}$ in Eq. (8.1) is the background mean flow, which we assume, in our case, to be of the form $SX_1\boldsymbol{e}_2$, where S is the rate of shear parameter. We recall from Chapter (1) that the Eq. (8.1) is valid under what is famously known as the "first order smoothing approximation" (FOSA) or "second order correlation approximation" (SOCA). As mentioned in the introduction of this chapter that, in the usual single averaging schemes, α and η_t cannot be fluctuating quantities, as all the fluctuations have been averaged out while taking the ensemble average, but by using the scheme of double averaging (Kraichnan, 1976; Sokolov, 1997), we may study the effects of fluctuations in the helicity by considering the fluctuations in α. The fluctuations in α have been considered in various earlier works (Silant'ev, 2000; Proctor, 2007; Sur & Subramanian, 2009; Richardson & Proctor, 2012).

In this chapter, we study a problem where α is prescribed in Eqn. (8.1). It is assumed that α is independent of spatial coordinates, i.e., it is a homogeneous quantity, and it shows temporal fluctuations which have zero mean. Symbolically, $\alpha = \alpha(\tau)$ and $\overline{\alpha} = 0$, where $\overline{Q}$ denotes an average of an arbitrary quantity Q over the superensmeble discussed above. The action of fluctuations in α on some given initial magnetic field is assumed to produce $\boldsymbol{B}$ (discussed above) with well–defined *mean–field* ($\overline{\boldsymbol{B}}$) and *fluctuating–field* ($\boldsymbol{b}^{\alpha}$):

$$\boldsymbol{B} \;=\; \overline{\boldsymbol{B}} + \boldsymbol{b}^{\alpha}\;, \qquad\qquad \overline{\boldsymbol{b}^{\alpha}} = 0 \tag{8.3}$$

Taking average of Eqn. (8.1) and following Reynolds rules, we obtain the equations governing the dynamics of the mean and fluctuating magnetic fields:

$$\left(\frac{\partial}{\partial\tau} + SX_1\frac{\partial}{\partial X_2}\right)\overline{\boldsymbol{B}} - S\overline{B_1}\boldsymbol{e}_2 \;=\; \boldsymbol{\nabla}\times\boldsymbol{\mathcal{E}}^{\alpha} + \eta_T\boldsymbol{\nabla}^2\overline{\boldsymbol{B}} \tag{8.4}$$

$$\left(\frac{\partial}{\partial\tau} + SX_1\frac{\partial}{\partial X_2}\right)\boldsymbol{b}^{\alpha} - Sb_1^{\alpha}\boldsymbol{e}_2 \;=\; \boldsymbol{\nabla}\times\left(\alpha\overline{\boldsymbol{B}}\right) + \boldsymbol{\nabla}\times\left(\alpha\,\boldsymbol{b}^{\alpha} - \overline{\alpha\,\boldsymbol{b}^{\alpha}}\right) + \eta_T\boldsymbol{\nabla}^2\boldsymbol{b}^{\alpha} \tag{8.5}$$

where $\eta_T = \eta + \eta_t$ and $\boldsymbol{\mathcal{E}}^{\alpha} = \overline{\alpha\,\boldsymbol{b}^{\alpha}}$ is the mean electromotive force (EMF) due to $\alpha-$fluctuations. Ignoring the term which is non–linear in fluctuations in Eqn. (8.5) by FOSA–like approximation, we can write the evolution equation of $\boldsymbol{b}^{\alpha}$ as,

$$\left(\frac{\partial}{\partial\tau} + SX_1\frac{\partial}{\partial X_2}\right)\boldsymbol{b}^{\alpha} - Sb_1^{\alpha}\boldsymbol{e}_2 \;=\; \boldsymbol{\nabla}\times\left(\alpha\overline{\boldsymbol{B}}\right) + \eta_T\boldsymbol{\nabla}^2\boldsymbol{b}^{\alpha}, \tag{8.6}$$

We note that $\boldsymbol{\nabla}\times\left(\alpha\overline{\boldsymbol{B}}\right)$ acts as a source term for $\boldsymbol{b}^{\alpha}$. Once $\boldsymbol{b}^{\alpha}$ has been determined, the mean EMF due to $\alpha-$fluctuations may be calculated directly by, $\boldsymbol{\mathcal{E}}^{\alpha}(\boldsymbol{X},\tau) = \overline{\alpha(\tau)\;\boldsymbol{b}^{\alpha}(\boldsymbol{X},\tau)}$, as $\alpha(\tau)$ is being assumed to be prescribed.

8.2.2 The shearing coordinate transformation

Eqn. (8.6) is similar to the Eqn. (5.9) of Ch. 5, in which the $(X_1\partial/\partial X_2)$ term makes Eqn. (8.6) inhomogeneous in the coordinate X_1. This term can be eliminated through

a shearing transformation to new spacetime variables, as was done in Ch. 5. We follow a similar technique here. We use Eqns. (A.2) and (A.3), given in the Appendix A, and define new variables, which are component–wise equal to the old variables:

$$\overline{\boldsymbol{H}}(\boldsymbol{x},t) \;=\; \overline{\boldsymbol{B}}(\boldsymbol{X},\tau)\,, \qquad\qquad \boldsymbol{h}^{\alpha}(\boldsymbol{x},t) \;=\; \boldsymbol{b}^{\alpha}(\boldsymbol{X},\tau) \tag{8.7}$$

Note that, just like the old variables, the new variables are expanded in the fixed Cartesian basis of the lab frame. For example, $\overline{\boldsymbol{H}} \;=\; \overline{H_1}\boldsymbol{e}_1 + \overline{H_2}\boldsymbol{e}_2 + \overline{H_3}\boldsymbol{e}_3$, where $\overline{H_i}(\boldsymbol{x},t) = \overline{B_i}(\boldsymbol{X},\tau)$, and similarly for the other variables. In the new variables, Eqn. (8.6) becomes,

$$\frac{\partial \boldsymbol{h}^{\alpha}}{\partial t} \;-\; Sh_1^{\alpha}\boldsymbol{e}_2 \;=\; \alpha(\tau)\,\left(\boldsymbol{\nabla}\times\overline{\boldsymbol{H}}\right) \;+\; \eta_T\boldsymbol{\nabla}^2\boldsymbol{h}^{\alpha} \tag{8.8}$$

where $\boldsymbol{\nabla}$ is given, in terms of shearing coordinates, by

$$\boldsymbol{\nabla} \equiv \boldsymbol{e}_1\frac{\partial}{\partial X_1} + \boldsymbol{e}_2\frac{\partial}{\partial X_2} + \boldsymbol{e}_3\frac{\partial}{\partial X_3} = \boldsymbol{e}_1\left(\frac{\partial}{\partial x_1} - St\frac{\partial}{\partial x_2}\right) + \boldsymbol{e}_2\frac{\partial}{\partial x_2} + \boldsymbol{e}_3\frac{\partial}{\partial x_3} \tag{8.9}$$

$\boldsymbol{\nabla}^2$ is given by Eqn. (A.4). Work out,

$$\left(\boldsymbol{\nabla}\times\overline{\boldsymbol{B}}\right)_i \;=\; \epsilon_{ijk}\frac{\partial\overline{B_k}}{\partial X_j} \;=\; \epsilon_{ijk}\left(\frac{\partial}{\partial x_j} - \delta_{j1}St\frac{\partial}{\partial x_2}\right)\overline{H_k} \;=\; \left(\epsilon_{ijk} - \epsilon_{i1k}\,\delta_{j2}\,St\right)\overline{H_{kj}} \tag{8.10}$$

where we have used the notation $\overline{H_{kj}} \;=\; (\partial\overline{H_k}/\partial x_j)$. Eqn. (8.9) may be expressed in component form using Eqn. (8.10) as,

$$\left(\frac{\partial}{\partial t} \;-\; \eta_T\boldsymbol{\nabla}^2\right)h_m^{\alpha}(\boldsymbol{x},t) \;=\; q_m^{\alpha}(\boldsymbol{x},t) \tag{8.11}$$

where $\boldsymbol{\nabla}^2$ is given by Eqn. (A.4), and

$$q_m^{\alpha}(\boldsymbol{x},t) \;=\; \alpha(t)\,\left[\epsilon_{mjk} - \epsilon_{m1k}\,\delta_{j2}\,St\right]\overline{H_{kj}} \;+\; S\delta_{m2}h_1^{\alpha} \tag{8.12}$$

Below we obtain a particular (i.e. *forced*) solution to Eqn. (8.11) following the methods described in Ch. 5 and the Appendix A.

8.2.3 Explicit solution for $\boldsymbol{h}^{\alpha}(\boldsymbol{x},t)$

As may be seen from Eqn. (A.1) of Appendix A that Eqn. (8.11) is exactly of similar form. The general method to construct the Green's function solution has been discussed in detail in Ch. 5 and Appendix A. We are interested in the particular solution to Eqn. (8.11) (i.e. the *forced solution*) which vanishes at $t = 0$. This can be written as

$$h_m^{\alpha}(\boldsymbol{x},t) \;=\; \int_0^t \mathrm{d}t' \int \mathrm{d}^3x'\, G_{\eta_T}(\boldsymbol{x}-\boldsymbol{x}',t,t')\; q_m^{\alpha}(\boldsymbol{x}',t') \tag{8.13}$$

where $G_{\eta_T}(\boldsymbol{x},t,t')$ is the resistive Green's function for linear shear flows whose derivation and properties are given in the Appendix A (see Eqn. (A.16) where μ signifies the role of η_T). Substituting the expression for q_m^{α} from Eqn. (8.12) in Eqn. (8.13), we have

$$\begin{aligned} h_m^{\alpha}(\boldsymbol{x},t) \;=\; & \int_0^t \mathrm{d}t' \int \mathrm{d}^3x'\; G_{\eta_T}(\boldsymbol{x}-\boldsymbol{x}',t,t')\; \alpha(t')\; [\epsilon_{mjk} - \epsilon_{m1k}\,\delta_{j2}\,St']\,\overline{H'_{kj}} \\ & + S\delta_{m2} \int_0^t \mathrm{d}t' \int \mathrm{d}^3x'\, G_{\eta_T}(\boldsymbol{x}-\boldsymbol{x}',t,t')\; h_1^{\alpha}(\boldsymbol{x}',t') \end{aligned} \tag{8.14}$$

where primes denote evaluation at spacetime point $(\boldsymbol{x}',t')$. The solution is not yet in explicit form because the last term on the right side contains the unknown quantity $h_1^{\alpha}(\boldsymbol{x}',t')$. Thus we need to work out the integral

$$\begin{aligned} \int_0^t \mathrm{d}t' \int \mathrm{d}^3x'\, G_{\eta_T}(\boldsymbol{x}-\boldsymbol{x}',t,t')\; h_1^{\alpha}(\boldsymbol{x}',t') \;=\; & \int_0^t \mathrm{d}t' \int \mathrm{d}^3x'\, G_{\eta_T}(\boldsymbol{x}-\boldsymbol{x}',t,t') \times \\ & \times \int_0^{t'} \mathrm{d}t'' \int \mathrm{d}^3x''\, G_{\eta_T}(\boldsymbol{x}'-\boldsymbol{x}'',t',t'')\; \alpha(t'')\, \epsilon_{1jk}\overline{H''_{kj}} \end{aligned}$$

where $''$ means evaluation at spacetime point $(\boldsymbol{x}'',t'')$. Note that, on the right side, $\boldsymbol{x}'$ occurs only in the Green's functions. So, by using the property given in Eqn. (A.7d), the integral over $\boldsymbol{x}'$ can be performed. Then

$$\int_0^t \mathrm{d}t' \int \mathrm{d}^3x' G_{\eta_T}(\boldsymbol{x}-\boldsymbol{x}',t,t')\; h_1^{\alpha}(\boldsymbol{x}',t') = \int_0^t \mathrm{d}t' \int_0^{t'} \mathrm{d}t'' \int \mathrm{d}^3x'' G_{\eta_T}(\boldsymbol{x}-\boldsymbol{x}'',t,t'')\alpha(t'')\, \epsilon_{1jk}\overline{H''_{kj}}$$

The double–time integrals can be reduced to single–time integrals because of the following simple identity. For any function $f(\boldsymbol{x},t)$, we have

$$\begin{aligned}\int_0^t \mathrm{d}t' \int_0^{t'} \mathrm{d}t'' \int \mathrm{d}^3x''\, f(\boldsymbol{x}'',t'') &= \int_0^t \mathrm{d}t'' \int \mathrm{d}^3x''\, f(\boldsymbol{x}'',t'') \int_{t''}^t \mathrm{d}t' \\ &= \int_0^t \mathrm{d}t''\,(t-t'') \int \mathrm{d}^3x''\, f(\boldsymbol{x}'',t'') \\ &= \int_0^t \mathrm{d}t'\,(t-t') \int \mathrm{d}^3x'\, f(\boldsymbol{x}',t')\end{aligned}$$

where in the last equality we have merely replaced the dummy integration variables $(\boldsymbol{x}'',t'')$ by $(\boldsymbol{x}',t')$. Then we have

$$\int_0^t \mathrm{d}t' \int \mathrm{d}^3x' G_{\eta_T}(\boldsymbol{x}-\boldsymbol{x}',t,t')\; h_1^\alpha(\boldsymbol{x}',t') = \int_0^t \mathrm{d}t'\,(t-t')\,\alpha(t') \int \mathrm{d}^3x'\, G_{\eta_T}(\boldsymbol{x}-\boldsymbol{x}',t,t')\;\epsilon_{1jk}\overline{H'_{kj}}$$

Therefore the forced solution to Eqn. (8.11) can finally be written in explicit form as

$$\begin{aligned}h_m^\alpha(\boldsymbol{x},t) &= \int_0^t \mathrm{d}t'\,\alpha(t')\,[\epsilon_{mjk} - \epsilon_{m1k}\,\delta_{j2}\,St' + \epsilon_{1jk}\,\delta_{m2}S(t-t')] \times \\ &\quad \times \int \mathrm{d}^3x'\, G_{\eta_T}(\boldsymbol{x}-\boldsymbol{x}',t,t')\,\overline{H'_{kj}} \qquad (8.15)\end{aligned}$$

Eqn. (8.15) gives the magnetic fluctuations due to fluctuating α.

8.2.4 Explicit expression for the mean EMF ($\boldsymbol{\mathcal{E}}^\alpha$)

The mean EMF is given by $\boldsymbol{\mathcal{E}} = \overline{\alpha\,\boldsymbol{b}} = \overline{\alpha\,\boldsymbol{h}}$, where Eqn. (8.15) for $\boldsymbol{h}$ should be substituted. We note that the averaging acts only on the alpha variables but not on the mean field,

i.e., $\overline{\alpha\alpha\,\overline{\boldsymbol{H}}} = \overline{\alpha\alpha}\,\overline{\boldsymbol{H}}$. Thus the mean EMF in component form may be written as

$$\begin{aligned}\mathcal{E}^{\alpha}_{m}(\boldsymbol{x},t) &= \int_0^t \mathrm{d}t'\ \overline{\alpha(t)\,\alpha(t')}\ [\epsilon_{mjk} - \epsilon_{m1k}\,\delta_{j2}\,St' + \epsilon_{1jk}\,\delta_{m2}S(t-t')] \times \\ &\quad \times \int \mathrm{d}^3x'\, G_{\eta_T}(\boldsymbol{x}-\boldsymbol{x}',t,t')\,\overline{H'_{kj}} \end{aligned} \tag{8.16}$$

Changing the integration variable to $\boldsymbol{r} = \boldsymbol{x} - \boldsymbol{x}'$, we may write,

$$\begin{aligned}\mathcal{E}^{\alpha}_{m}(\boldsymbol{x},t) &= \int_0^t \mathrm{d}t'\ \overline{\alpha(t)\,\alpha(t')}\ [\epsilon_{mjk} - \epsilon_{m1k}\,\delta_{j2}\,St' + \epsilon_{1jk}\,\delta_{m2}S(t-t')] \times \\ &\quad \times \int \mathrm{d}^3r\, G_{\eta_T}(\boldsymbol{r},t,t')\,\overline{H_{kj}}(\boldsymbol{x}-\boldsymbol{r},t') \end{aligned} \tag{8.17}$$

where

$$\overline{H'_{kj}} = \frac{\partial\overline{H_k}(\boldsymbol{x}',t')}{\partial x'_j} = \frac{\partial\overline{H_k}(\boldsymbol{x}-\boldsymbol{r},t')}{\partial(x_j-r_j)} = \frac{\partial\overline{H_k}(\boldsymbol{x}-\boldsymbol{r},t')}{\partial x_j} = \overline{H_{kj}}(\boldsymbol{x}-\boldsymbol{r},t')$$

We note that the mean EMF depends only on the first spatial derivative of the mean magnetic field.

8.3 The mean EMF ($\boldsymbol{\mathcal{E}}^{\alpha}$) for a slowly varying magnetic field

Eqn. (8.4) describing the evolution of mean magnetic field may be written in shearing coordinates as,

$$\frac{\partial\overline{\boldsymbol{H}}}{\partial t} = S\overline{H_1}\boldsymbol{e}_2 + \boldsymbol{\nabla}\times\boldsymbol{\mathcal{E}}^{\alpha} + \eta_T\boldsymbol{\nabla}^2\overline{\boldsymbol{H}} \tag{8.18}$$

where $\boldsymbol{\nabla}$ and $\boldsymbol{\nabla}^2$ are given by Eqns. (8.9) and (A.4) respectively. The term $\boldsymbol{\nabla}\times\boldsymbol{\mathcal{E}}^{\alpha}$ in Eqn. (8.18) may be readily determined using Eqn. (8.17). While taking curl of Eqn. (8.17), it may be noted that the curl operates only on $\overline{H_{kj}}(\boldsymbol{x}-\boldsymbol{r},t')$ inside the integral sign. Thus the term $\boldsymbol{\nabla}\times\boldsymbol{\mathcal{E}}^{\alpha}$ is contributed only by the second order spatial derivative of the mean magnetic field. Eqn. (8.18) together with curl of Eqn. (8.17)

completely specifies the evolution of mean magnetic field in terms of a set of coupled integro–differential equations, assuming the nature of alpha fluctuation is known.

The mean EMF given in Eqn. (8.17) is a *functional* of $\overline{H_{kj}}$. When the mean–field is slowly varying compared to correlation time of alpha fluctuations, we expect to be able to approximate $\boldsymbol{\mathcal{E}}^{\alpha}$ as a *function* of $\overline{H_{kj}}$. In this case, the mean–field evolution equation would reduce to a set of coupled partial differential equations, instead of the more formidable set of coupled integro–differential given above.

The first step involves a Taylor expansion of the quantities, $\overline{H_k}$ and $\overline{H_{kj}}$. Neglecting spacetime derivatives higher than the first order ones, we have

$$\begin{aligned}
\overline{H_k}(\boldsymbol{x}-\boldsymbol{r},t') &= \overline{H_k}(\boldsymbol{x},t) - r_p\overline{H_{kp}}(\boldsymbol{x},t) - (t-t')\frac{\partial\overline{H_k}(\boldsymbol{x},t)}{\partial t} + \ldots \\
\overline{H_{kj}}(\boldsymbol{x}-\boldsymbol{r},t') &= \overline{H_{kj}}(\boldsymbol{x},t) - (t-t')\frac{\partial\overline{H_{kj}}(\boldsymbol{x},t)}{\partial t} + \ldots
\end{aligned} \tag{8.19}$$

We now use the equation for mean–field, Eqn. (8.18), to express $\left(\partial\overline{H_k}/\partial t\right)$ and $\left(\partial\overline{H_{kj}}/\partial t\right)$, appearing in Eqn. (8.19), in terms of spatial derivatives. Assuming that the terms involving second order spatial derivatives are of order μ, where $\mu \ll 1$, we may write

$$\begin{aligned}
\frac{\partial\overline{H_k}}{\partial t} &= S\delta_{k2}\overline{H_1} + \mathcal{O}(\mu) \\
\frac{\partial\overline{H_{kj}}}{\partial t} &= S\delta_{k2}\overline{H_{1j}} + \mathcal{O}(\mu)
\end{aligned} \tag{8.20}$$

Using Eqn. (8.20) in the Eqn. (8.19), we write

$$\overline{H_{kj}}(\boldsymbol{x}-\boldsymbol{r},t') = \overline{H_{kj}}(\boldsymbol{x},t) - S(t-t')\delta_{k2}\,\overline{H_{1j}}(\boldsymbol{x},t) + \mathcal{O}(\mu) \tag{8.21}$$

Substituting Eqn. (8.21) in Eqn. (8.17), we write the following expression for mean EMF

for slowly varying mean magnetic field:

$$\mathcal{E}_m^{\alpha}(\boldsymbol{x},t) \;=\; \int_0^t \mathrm{d}t'\; \overline{\alpha(t)\,\alpha(t')}\; [\epsilon_{mjk} - \epsilon_{m1k}\,\delta_{j2}\,St' + \epsilon_{1jk}\,\delta_{m2} S(t-t')] \times$$

$$\times \left[\; \overline{H_{kj}}(\boldsymbol{x},t) \;-\; S(t-t')\delta_{k2}\; \overline{H_{1j}}(\boldsymbol{x},t)\right] \int \mathrm{d}^3 r\, G_{\eta_T}(\boldsymbol{r},t,t') \qquad (8.22)$$

From Eqn. (A.17) of Appendix A, we note that

$$\int \mathrm{d}^3 r\, G_{\eta_T}(\boldsymbol{r},t,t') \;=\; 1 \qquad (8.23)$$

Using Eqn. (8.23) in Eqn. (8.22), we may write after some straightforward algebra

$$\mathcal{E}_m^{\alpha}(\boldsymbol{x},t) \;=\; \overline{H_{kj}}(\boldsymbol{x},t) \int_0^t \mathrm{d}t'\; \overline{\alpha(t)\,\alpha(t')}\; [\Gamma_{mjk}(t,t') - S(t-t')\delta_{k1}\Gamma_{mj2}(t,t')] \qquad (8.24)$$

where

$$\Gamma_{mjk}(t,t') \;=\; \epsilon_{mjk} - \epsilon_{m1k}\,\delta_{j2}\,St' + \epsilon_{1jk}\,\delta_{m2} S(t-t') \qquad (8.25)$$

Although the sheared coordinates are essential for the calculations, but physical interpretation is simplest in the laboratory frame; hence we derive an expression for the mean EMF in terms of $\overline{\boldsymbol{B}}(\boldsymbol{X},\tau)$ by using,

$$\overline{H_{kj}}(\boldsymbol{x},t) \equiv \frac{\partial \overline{H_k}(\boldsymbol{x},t)}{\partial x_j} \;=\; \left(\frac{\partial}{\partial X_j} \;+\; S\tau\delta_{j1}\frac{\partial}{\partial X_2}\right) \overline{B_k}(\boldsymbol{X},\tau), \qquad (8.26)$$

and working out

$$\overline{H_{kj}}\; [\Gamma_{mjk} - S(t-t')\delta_{k1}\Gamma_{mj2}] \;=\; -\overline{B_{kj}} \left\{ -\Gamma_{mjk} + S(\tau-\tau')\Gamma_{mj2}\delta_{k1} - \right.$$

$$\left. -S\tau\Gamma_{m1k}\delta_{j2} + S^2\tau(\tau-\tau')\Gamma_{m12}\delta_{k1}\delta_{j2} \right\},$$

we can write the following expression for mean EMF for a slowly varying magnetic field:

$$\mathcal{E}_m^{\alpha}(\boldsymbol{X},\tau) \;=\; -\beta_{mjk}(\tau)\,\frac{\partial\overline{B_k}(\boldsymbol{X},\tau)}{\partial X_j} \tag{8.27}$$

where the *transport coefficient*, $\beta_{mjk}(\tau)$, is given by

$$\begin{aligned}\beta_{mjk}(\tau) \;&=\; \int_0^{\tau} \mathrm{d}\tau' \;\; \overline{\alpha(\tau)\,\alpha(\tau')} \;\;\times \\ &\times \;\; \left\{ -\Gamma_{mjk} + S(\tau-\tau')\Gamma_{mj2}\delta_{k1} - S\tau\Gamma_{m1k}\delta_{j2} + S^2\tau(\tau-\tau')\Gamma_{m12}\delta_{k1}\delta_{j2} \right\}\end{aligned} \tag{8.28}$$

Thus the evolution equation for mean–field, Eqn. (8.4), together with Eqns. (8.27) and (8.28) is a closed partial differential equation (which is first order in temporal and second order in spatial derivatives).

8.4 Predictions and comparisons with earlier works

We wish to compare our analytical results with measurements of numerical simulations, which use the test–field method to compute the transport coefficients (cf. Brandenburg et al. (2008) and Ch. 7). In this method, the mean–magnetic field is averaged over the coordinates X_1 and X_2. So we consider the case when the mean magnetic field, $\overline{\boldsymbol{B}} = \overline{\boldsymbol{B}}(X_3,\tau)$. The condition $\boldsymbol{\nabla}\cdot\overline{\boldsymbol{B}} = 0$ implies that $\overline{B_3}$ is uniform in space, and it can be set to zero; hence we have $\overline{\boldsymbol{B}} = (\overline{B_1}, \overline{B_2}, 0)$. In this case, we can write from Eqns. (8.27) and (8.28)

$$\mathcal{E}_m^{\alpha}(\boldsymbol{X},\tau) \;=\; -\beta_{m3k}(\tau)\,\frac{\partial\overline{B_k}(\boldsymbol{X},\tau)}{\partial X_3} \tag{8.29}$$

$$\beta_{m3k}(\tau) = \int_0^{\tau} \mathrm{d}\tau' \;\; \overline{\alpha(\tau)\,\alpha(\tau')} \;\; [-\Gamma_{m3k} + S(\tau-\tau')\Gamma_{m32}\delta_{k1}] \tag{8.30}$$

where Γ_{mjk} is given by Eqn. (8.25). Now, we can express the mean EMF as $\boldsymbol{\mathcal{E}}^{\alpha} = (\mathcal{E}_1,\, \mathcal{E}_2,\, 0)$, with

$$\mathcal{E}^{\alpha}_{m} \;=\; -\,\beta_{mp}(\tau)\,\overline{J_p}\,; \qquad\qquad \overline{\boldsymbol{J}} \;=\; \boldsymbol{\nabla}\times\overline{\boldsymbol{B}} \;=\; \left(-\frac{\partial\overline{B_2}}{\partial X_3},\;\; \frac{\partial\overline{B_1}}{\partial X_3},\;\; 0\right) \tag{8.31}$$

where 2–indexed magnetic diffusivity tensor due to $\alpha-$fluctuations β_{mp} has four components, $(\beta_{11},\, \beta_{12},\, \beta_{21},\, \beta_{22})$, which are defined in terms of the 3–indexed object β_{mjk} by

$$\beta_{mp}(\tau) \;=\; \epsilon_{kp3}\,\beta_{m3k}(\tau)\,;\ \text{implying} \quad \beta_{m1}(\tau) \;=\; -\,\beta_{m32}(\tau)\,,\;\; \beta_{m2}(\tau) \;=\; \beta_{m31}(\tau) \tag{8.32}$$

Eqn. (8.31) for $\boldsymbol{\mathcal{E}}^{\alpha}$ can now be substituted in Eqn. (8.4). Then the mean–field evolves as,

$$\begin{aligned}
\frac{\partial\overline{B_1}}{\partial\tau} \;&=\; -\,\beta_{21}\,\frac{\partial^2\overline{B_2}}{\partial X_3^2} \;+\; (\eta_T+\beta_{22})\,\frac{\partial^2\overline{B_1}}{\partial X_3^2} \\
\frac{\partial\overline{B_2}}{\partial\tau} \;&=\; S\overline{B_1} \;-\; \beta_{12}\,\frac{\partial^2\overline{B_1}}{\partial X_3^2} \;+\; (\eta_T+\beta_{11})\,\frac{\partial^2\overline{B_2}}{\partial X_3^2}
\end{aligned} \tag{8.33}$$

The diagonal components, $\beta_{11}(\tau)$ and $\beta_{22}(\tau)$, augment the resistivity, η_T, whereas the off–diagonal components, $\beta_{12}(\tau)$ and $\beta_{21}(\tau)$, lead to cross–coupling of $\overline{B_1}$ and $\overline{B_2}$.

8.4.1 Magnetic diffusivity tensor (β_{mp}) due to $\alpha-$fluctuations

We can write the following simplified expression for $\beta_{mp}(\tau)$ after doing some calculations by using Eqns. (8.32), (8.30) and (8.25):

$$\beta_{mp}(\tau) \;=\; \int_0^\tau \mathrm{d}\tau' \;\overline{\alpha(\tau)\,\alpha(\tau')} \;\times$$

$$\times\Bigg\{-\delta_{pm} + S(\tau-\tau')\,[\epsilon_{1p3}\,\epsilon_{m32} \;-\; \delta_{p1}\,\delta_{m2}] - S^2(\tau-\tau')^2\,\epsilon_{1p3}\,\delta_{m2}\Bigg\} \tag{8.34}$$

It is useful to display all four components of $\beta_{mp}(\tau)$:

$$\begin{aligned}
\beta_{11}(\tau) &= -\int_0^\tau \mathrm{d}\tau' \;\overline{\alpha(\tau)\,\alpha(\tau')} \\
\beta_{22}(\tau) &= -\int_0^\tau \mathrm{d}\tau' \;\overline{\alpha(\tau)\,\alpha(\tau')}\;\left[1 + S^2(\tau-\tau')^2\right] \\
\beta_{12}(\tau) &= -\int_0^\tau \mathrm{d}\tau' \;\overline{\alpha(\tau)\,\alpha(\tau')}\;S(\tau-\tau') \\
\beta_{21}(\tau) &= \beta_{12}(\tau) \;=\; -\int_0^\tau \mathrm{d}\tau' \;\overline{\alpha(\tau)\,\alpha(\tau')}\;S(\tau-\tau')
\end{aligned} \tag{8.35}$$

The correlation function of the $\alpha-$fluctuations, denoted as $\overline{\alpha(\tau)\,\alpha(\tau')}$, is expected to be function of the difference of times $\tau-\tau'$ alone, in the steady state. Therefore, we consider it to be of the form

$$\overline{\alpha(\tau)\,\alpha(\tau')} \;=\; \alpha_{\rm rms}^2\,\mathcal{D}(\tau-\tau') \tag{8.36}$$

where $\mathcal{D}(\tau-\tau')$ is a dimensionless function characterizing the profile of the correlation function of fluctuating α. As may be seen from Eqn. (8.36) that $\mathcal{D}(0)=1$, as the root–mean–squared value of alpha at any arbitrary time τ is defined by, $\alpha_{\rm rms}^2(\tau) = \overline{\alpha(\tau)\,\alpha(\tau)}$. Let us assume that the *correlation time* of alpha fluctuations is denoted by τ_α.

The $\beta_{mp}(\tau)$ saturate at some constant value at late times; let us denote these constant values by $\beta_{mp}^\infty = \beta_{mp}(\tau\to\infty)$. If the mean magnetic field changes over times that are longer than the saturation time, we may use β_{mp}^∞ instead of the time–varying quantities $\beta_{mp}(\tau)$ in Eqn. (8.33). In this case, we can write the following expressions for

all components of β^{∞}_{mp} using Eqns. (8.35) and (8.36):

$$\begin{aligned} \beta^{\infty}_{11} &= -\alpha^2_{\rm rms}\,\tau_\alpha \ ; & \beta^{\infty}_{22} &= -\alpha^2_{\rm rms}\,\tau_\alpha\left[1+2n(S\tau_\alpha)^2\right] \\ \beta^{\infty}_{12} &= -\alpha^2_{\rm rms}\,\tau_\alpha\, m(S\tau_\alpha) \ ; & \beta^{\infty}_{21} &= \beta^{\infty}_{12} \end{aligned} \tag{8.37}$$

where τ_α, m and n have been defined to be of the form

$$\tau_\alpha = \int_0^\infty {\rm d}\tau'\ \mathcal{D}(\tau')\ ; \quad m = \frac{1}{\tau_\alpha^2}\int_0^\infty {\rm d}\tau'\ \tau'\ \mathcal{D}(\tau')\ ; \quad n = \frac{1}{2\tau_\alpha^3}\int_0^\infty {\rm d}\tau'\ \tau'^2\ \mathcal{D}(\tau') \tag{8.38}$$

m and n defined above are just the numbers characterizing the profile of the correlation function of the $\alpha-$fluctuations. By choosing some form for $\mathcal{D}(\tau')$, m and n may be determined by using Eqn. (8.38). Few important properties of β^{∞}_{mp} are as follows:

(i) We see that β^{∞}_{11} is always negative and is independent of shear. This leads to the negative diffusion of $\overline{B_2}$ as may be seen from Eqns. (8.33).

(ii) β^{∞}_{22}, which is also always negative, is contributed by two terms, one of which depends on the shear. Shear adds to the negative diffusion, and if strong enough, it might lead to self–excitation of $\overline{B_1}$. For zero shear, $\lim_{S\to 0}\beta^{\infty}_{22} = \beta^{\infty}_{11}$.

(iii) We find that β^{∞}_{12}, which is equal to β^{∞}_{21}, is a positive quantity for negative values of the shear parameter, S. These components vanish in the limit of zero shear.

(iv) Negative diffusion of mean magnetic field in the absence of shear was first noted by Kraichnan in 1976 (see Kraichnan (1976)). This was called an α^2-effect. Our results obtained above reduce in agreement to the results of Kraichnan in the limit of zero shear.

(v) All four components of β^{∞}_{mp} depend on $\alpha^2_{\rm rms}$ and the correlation time of $\alpha-$fluctuations, τ_α.

Looking for solutions $\boldsymbol{B} \propto \exp\left[\lambda\tau + {\rm i}K_3X_3\right]$ and substituting it in Eqn. (8.33), we obtain the dispersion relation,

$$\frac{\lambda_\pm}{\eta_{T\beta}\,K_3^2} \;=\; -1 \;\pm\; \frac{1}{\eta_{T\beta}}\sqrt{\beta_{21}^{\infty}\left(\frac{S}{K_3^2}+\beta_{12}^{\infty}\right)\;+\;\epsilon_\beta^2} \tag{8.39}$$

where the new constants are defined as,

$$\eta_{T\beta} \;=\; \eta_T + \frac{1}{2}(\beta_{11}^{\infty}\;+\;\beta_{22}^{\infty})\;, \qquad \epsilon_\beta \;=\; \frac{1}{2}(\beta_{11}^{\infty}\;-\;\beta_{22}^{\infty}) \tag{8.40}$$

Before examining various conditions for exponentially growing solutions of the mean magnetic field, we wish to rewrite Eqn. (8.39) in more useful form. To do that, we define few dimensionless control parameters which may be identified as *dynamo numbers*:

$$\mathcal{D}_K \;=\; \frac{\alpha_{\rm rms}^2\,\tau_\alpha}{\eta_T}\;; \qquad \mathcal{T}_\alpha \;=\; \tau_\alpha\,\eta_T\,K_3^2\;; \qquad \mathcal{S}_\alpha \;=\; |S|\,\tau_\alpha \tag{8.41}$$

With the help of Eqns. (8.37), (8.40) and (8.41), the dispersion relation given in Eqn. (8.39) may be expressed as

$$\frac{\lambda_\pm}{\eta_T\,K_3^2} \;=\; -1+\mathcal{D}_K\left[1+n\,\mathcal{S}_\alpha^2\right] \;\pm\; \mathcal{D}_K^{1/2}\,\mathcal{S}_\alpha\left(\frac{-m}{\mathcal{T}_\alpha}\;+\;m^2\,\mathcal{D}_K\;+\;n^2\,\mathcal{D}_K\,\mathcal{S}_\alpha^2\right)^{1/2} \tag{8.42}$$

As the modes were sought in the form of $\boldsymbol{B}\propto\exp\left[\lambda\tau+{\rm i}K_3X_3\right]$, we note that the *positive real roots* of Eqn. (8.42) admit exponentially growing solutions for the mean magnetic field. Defining a quantity,

$$\mathcal{T}_\alpha^{\rm crit} \;=\; \frac{m}{m^2\,\mathcal{D}_K\;+\;n^2\,\mathcal{D}_K\,\mathcal{S}_\alpha^2}\;, \tag{8.43}$$

we may write the Eqn. (8.42) as,

$$\frac{\lambda_\pm}{\eta_T\,K_3^2} \;=\; -1+\mathcal{D}_K\left[1+n\,\mathcal{S}_\alpha^2\right] \;\pm\; m^{1/2}\,\mathcal{D}_K^{1/2}\,\mathcal{S}_\alpha\sqrt{\frac{1}{\mathcal{T}_\alpha^{\rm crit}}\;-\;\frac{1}{\mathcal{T}_\alpha}} \tag{8.44}$$

8.4.2 Implications for dynamo action

Our aim is to find various conditions for the dynamo action by analyzing Eqn. (8.42) in detail. Below, we first consider the following limiting cases before discussing various conditions for dynamo action in greater detail:

- The case of zero shear (i.e., $\mathcal{S}_\alpha = 0$): Substituting $\mathcal{S}_\alpha = 0$ in Eqn. (8.42), we find

$$\frac{\lambda_\pm}{\eta_T\, K_3^2} \;=\; -1 + \mathcal{D}_K \;; \quad \text{Condition for dynamo action}: \; \mathcal{D}_K > 1 \tag{8.45}$$

  This case was first discussed by Kraichnan (1976) where it was noted that the fluctuations in α lead to the negative diffusion of mean magnetic field, in other words, its effect is to diminish the decay of mean magnetic field due to positive diffusion (through the η_T-term, where η_T is assumed to be positive), and if the fluctuations in α be strong enough, it might lead to the growth of mean magnetic field.

- A sufficient condition for dynamo action: In the case of *non–zero* shear, a *sufficient* condition for dynamo action may be given by $\mathcal{D}_K\,[1 + n\,\mathcal{S}_\alpha^2] > 1$, as may be seen from Eqn. (8.42).

- Negative radicand in Eqn. (8.44), i.e., when $0 < \mathcal{T}_\alpha \leq \mathcal{T}_\alpha^{\rm crit}$: In this case the radicand in Eqn. (8.44) becomes negative and does not exhibit growing modes. The condition for growth of mean magnetic field in this case is, $\mathcal{D}_K\,[1 + n\,\mathcal{S}_\alpha^2] > 1$.

- Positive radicand in Eqn. (8.44), i.e., when $\mathcal{T}_\alpha > \mathcal{T}_\alpha^{\rm crit}$: In this case λ_+ seems to be the favourable root for dynamo action if the first two terms on the right hand side of Eqn. (8.44) be subcritical.

- Growth rate in the limit when, $\mathcal{S}_\alpha \ll 1$ and $\mathcal{D}_K < 1$: In this limit, it may be shown from Eqn. (8.42) that

$$\frac{\lambda_\pm}{\eta_T\, K_3^2} \;=\; -1 + \mathcal{D}_K \;\pm\; \mathcal{D}_K^{1/2}\,\mathcal{S}_\alpha \left(\frac{-m}{\mathcal{T}_\alpha} \;+\; m^2\,\mathcal{D}_K\right)^{1/2} \;+\; \mathcal{O}(\mathcal{S}_\alpha^2) \tag{8.46}$$

It may be seen from above equation that λ_+ is favourable for the dynamo action. We note from Eqn. (8.46) that the growth rate varies *linearly* with shear, i.e., $\lambda_+ \propto |S|$. This scaling has been observed and discussed in various earlier works (Yousef et al., 2008a,b; Brandenburg et al., 2008; Hughes & Proctor, 2009; Heinemann, McWilliams & Schekochihin, 2011; Mitra & Brandenburg, 2012; Richardson & Proctor, 2012). *This linear scaling was also observed in our simulations presented in Ch. 7 (see Fig. (7.10)).*

- Growth rate in the limit when, $\mathcal{S}_\alpha \gg 1$: In this limit, the terms of order $\mathcal{S}_\alpha^2$ dominate, as may be seen from Eqn. (8.42). Thus for sufficiently large shear, we may write by ignoring the first two terms of the radicand given in Eqn. (8.42),

$$\frac{\lambda_+}{\eta_T K_3^2} \approx -1 + \mathcal{D}_K \left[1 + 2n\,\mathcal{S}_\alpha^2\right] ; \qquad \frac{\lambda_-}{\eta_T K_3^2} \approx -1 + \mathcal{D}_K \tag{8.47}$$

We see that λ_+ shows strong dependence on shear and seem to scale with shear as, $\lambda_+ \propto |S|^2$. The root λ_- seem to be approximately independent of shear in this limit. Thus, in the limit of small $\mathcal{D}_K$, only λ_+ may be responsible for dynamo action with growth rate scaling as, $\lambda_+ \propto |S|^2$, for large values of $\mathcal{S}_\alpha$.

Having discussed some of the asymptotic limits of Eqn. (8.42), we now wish to demonstrate some general conditions for dynamo action by exploring range of values of the three dynamo numbers, $\mathcal{D}_K$, $\mathcal{T}_\alpha$ and $\mathcal{S}_\alpha$ defined above in Eqn. (8.41). First, we need to choose some form for the profile function of $\alpha\,\alpha$ correlation, $\mathcal{D}(\tau')$, given in Eqn. (8.36), in order to compute the values of the quantities m and n defined in Eqn. (8.38). Out of many possible choices for $\mathcal{D}(\tau')$, let us choose it to be of the form

$$\mathcal{D}(\tau') = \exp\left(-\frac{\tau'}{\tau_\alpha}\right) ; \text{ which implies from Eqn. (8.38), } m = 1 ; \; n = 1 \tag{8.48}$$

As an illustrative example, we wish to choose some parameter values which are typical to the interstellar medium of our Galaxy. Let us choose following typical values of some parameters: Supernovae (SNe) inject energy in the interstellar medium (ISM) with a

typical stirring scale of order, $\ell_{\rm stir} \sim 100\,{\rm pc}$; the turbulent velocity field caused due to SNe stirring is typically of order, $v_{\rm turb} \sim 10\,{\rm km/s}$ at the disc mid–plane; a typical scale over which the mean magnetic field varies ($L_{\overline{B}}$) may be taken to be of the order of the scale height of the ionized gas, thus $L_{\overline{B}} \sim 500\,{\rm pc}$; and, the observed value of the rate of shear for the Milky Way gives the shearing time scale, $|S|^{-1} \sim 10^8\,{\rm yr}$. Using these values, we estimate: (i) the turbulent diffusivity, $\eta_t \sim (v_{\rm turb}\ell_{\rm stir})/3 \sim 10^{26}\,{\rm cm^2/s}$; (ii) the turbulent diffusion time scale (or the decay time scale) of the "large–scale" magnetic field, $t_{\rm decay} \sim L^2_{\overline{B}}/\eta_t \sim 5 \times 10^8{\rm yr}$; [2] and (iii) the stirring time scale due to the SNe, $t_{\rm stir} \sim \ell_{\rm stir}/v_{\rm turb} \sim 10^7\,{\rm yr}$. Although $\eta_T = \eta + \eta_t$, the microscopic resistivity (η) in the ISM being extremely small ($\eta \sim 10^7\,{\rm cm^2/s}$) as compared to the turbulent diffusivity, η_t ($\sim 10^{26}\,{\rm cm^2/s}$ estimated above), we can take $\eta_T \approx \eta_t$ (see Shukurov & Sokoloff (2008) for a detailed introduction to the "Galactic Dynamos"). We note from Eqn. (8.41) that $\mathcal{T}_\alpha$ is an estimate of the ratio of the correlation time of the fluctuating α (τ_α) and the turbulent diffusion time scale of the large–scale magnetic field ($t_{\rm decay}$), and $\mathcal{S}_\alpha$ measures the ratio between τ_α and the shearing time scale given by $|S|^{-1}$. Assuming τ_α to lie between $t_{\rm stir}$ and the galactic life time (which is twenty times larger than $t_{\rm decay}$), i.e., $10^7\,{\rm yr} < \tau_\alpha < 10^{10}\,{\rm yr}$, we can see that $2 \times 10^{-2} < \mathcal{T}_\alpha < 20$ and $10^{-1} < \mathcal{S}_\alpha < 100$.

As we saw in the expression for the dispersion relation of the form given in Eqn. (8.42) that there are three different dimensionless parameters, $\mathcal{D}_K$, $\mathcal{T}_\alpha$ and $\mathcal{S}_\alpha$ defined in Eqn. (8.41), which can be varied to explore the possibility of the dynamo action. It is helpful to fix the value of one of the parameters and vary the remaining two to look for the real positive roots of the dispersion relation (Eqn. (8.42)) which are responsible for the dynamo growth. Figs. (8.1–8.3) display the *region plots*, demonstrating the *dynamo region*, as a function of two dimensionless parameters while the remaining third one is kept constant. Various combinations of these dynamo numbers have been explored to look for the conditions for the growth of large–scale magnetic field. In Fig. (8.1) we plot the dynamo region as a function of $\mathcal{D}_K$ and $\mathcal{S}_\alpha$ for fixed values of $\mathcal{T}_\alpha$. The three panels

[2] Note that this decay time of "large–scale" magnetic field is a small fraction of the Galactic lifetime ($\sim 10^{10}\,{\rm yr}$), and hence the observed magnetic field needs to be maintained by the dynamo action

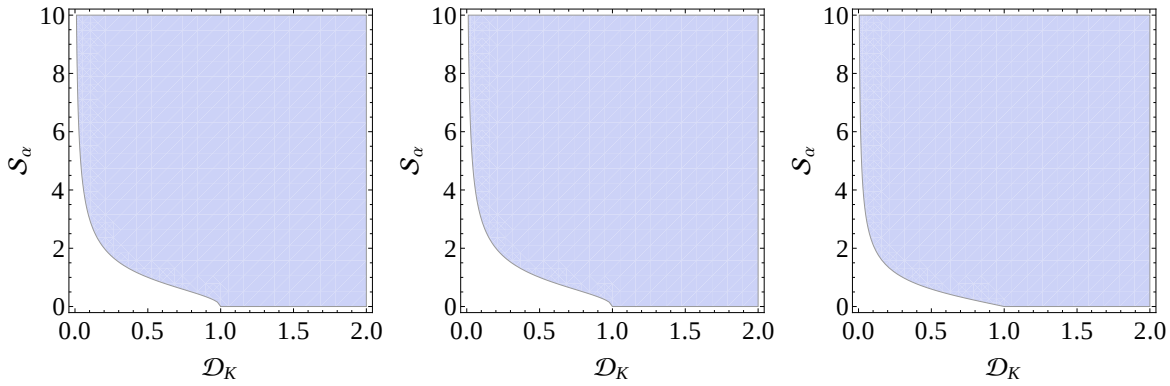

Figure 8.1: Region plots of the growth rate as a function of $\mathcal{D}_K$ and $\mathcal{S}_\alpha$ for three different values of $\mathcal{T}_\alpha$. These figures demonstrate the shaded region (shown in sky blue colour) in which the dynamo action is possible. The left panel corresponds to $\mathcal{T}_\alpha = 0.1$; the middle panel corresponds to $\mathcal{T}_\alpha = 1.0$; and the right panel corresponds to $\mathcal{T}_\alpha = 10.0$.

in Fig. (8.1) correspond to three different values of $\mathcal{T}_\alpha$, namely $\mathcal{T}_\alpha = 0.1, 1.0$ and 10.0 corresponding to the left, middle and the right panels respectively. In Fig. (8.2) we plot the dynamo region as a function of $\mathcal{D}_K$ and $\mathcal{T}_\alpha$ for fixed values of $\mathcal{S}_\alpha$. The three panels in Fig. (8.2) correspond to three different values of $\mathcal{S}_\alpha$, namely $\mathcal{S}_\alpha = 0.1, 1.0$ and 10.0 corresponding to the left, middle and the right panels respectively. Fig. (8.3) displays the dynamo region as a function of $\mathcal{T}_\alpha$ and $\mathcal{S}_\alpha$ for fixed values of $\mathcal{D}_K$. The two panels in Fig. (8.3) correspond to the two values of $\mathcal{D}_K$, namely $\mathcal{D}_K = 0.1$ for the left panel and $\mathcal{D}_K = 1.0$ for the right panel. The interfaces between the shaded (sky blue) and the blank (white) regions in various panels of Figs. (8.1–8.5) define the *threshold* or the *criticality* for the dynamo action. As may be seen from these figures that the critical condition for the dynamo action is a function of the parameters being explored. As noted before, $\mathcal{D}_K$ is a measure of alpha fluctuations; $\mathcal{T}_\alpha$ is an estimate of the ratio of the correlation time of the fluctuating α (τ_α) and the turbulent diffusion time scale of the large–scale magnetic field ($t_{\rm decay}$); and $\mathcal{S}_\alpha$ measures the ratio between τ_α and the shearing time scale given by $|S|^{-1}$. Some noteworthy properties are as follows:

(i) If $\mathcal{D}_K$ exceeds unity, we see dynamo action even when $\mathcal{S}_\alpha = 0$, whereas for smaller

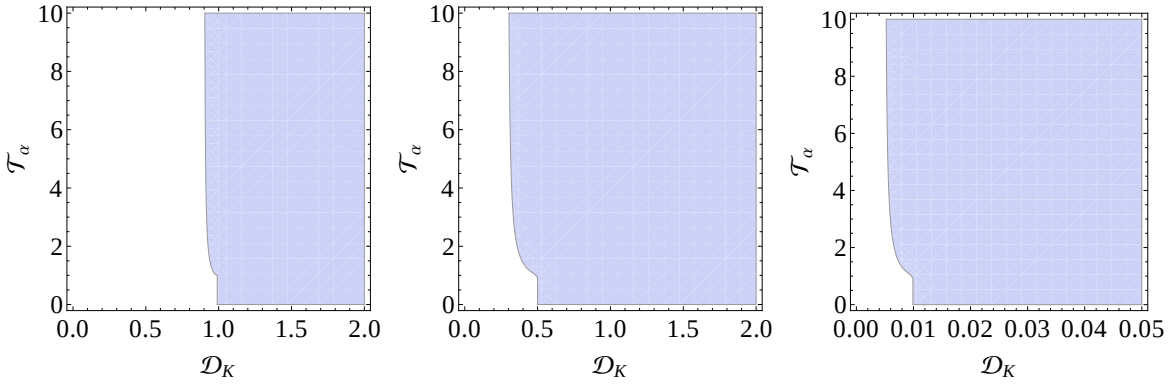

Figure 8.2: Region plots of the growth rate as a function of $\mathcal{D}_K$ and $\mathcal{T}_\alpha$ for three different values of $\mathcal{S}_\alpha$. These figures demonstrate the shaded region (shown in sky blue colour) in which the dynamo action is possible. The left panel corresponds to $\mathcal{S}_\alpha = 0.1$; the middle panel corresponds to $\mathcal{S}_\alpha = 1.0$; and the right panel corresponds to $\mathcal{S}_\alpha = 10.0$.

values of $\mathcal{D}_K$, we need some minimum values of $\mathcal{S}_\alpha$ defining the threshold above which there is dynamo action and below which there is no dynamo action; see Fig. (8.1).

(ii) For larger values of $\mathcal{S}_\alpha$ we see that it is easy to excite dynamo for even smaller values of $\mathcal{D}_K$. The critical value of $\mathcal{T}_\alpha$ is a strong function of $\mathcal{D}_K$. If the value of $\mathcal{D}_K$ falls below a certain value for fixed $\mathcal{S}_\alpha$, the critical value of $\mathcal{T}_\alpha$ approach extremely large values; see Fig. (8.2).

(iii) For a fixed $\mathcal{D}_K$, there is a minimum value of $\mathcal{S}_\alpha$ which is needed to excite the dynamo. This minimum value of $\mathcal{S}_\alpha$ as a function of $\mathcal{T}_\alpha$ is insensitive upto certain value of $\mathcal{T}_\alpha$, and falls below once $\mathcal{T}_\alpha$ is increased further; see Fig. (8.3).

We saw in § 7.4 of Ch. 7 of this thesis that there is a dimensionless parameter, $D_{\alpha S}$, defined in Eqn. (7.18) with respect to $\alpha_{22}^{\rm rms}$, which, when exceeds the value 2.3, gives rise to the dynamo action ($D_{\alpha S}^{\rm crit} \approx 2.3$ was first determined numerically in Brandenburg et al. (2008)). To explore the dynamo regime as a function of $D_{\alpha S}$, we define the dimensionless parameter corresponding to the incoherent alpha–shear mechanism considering

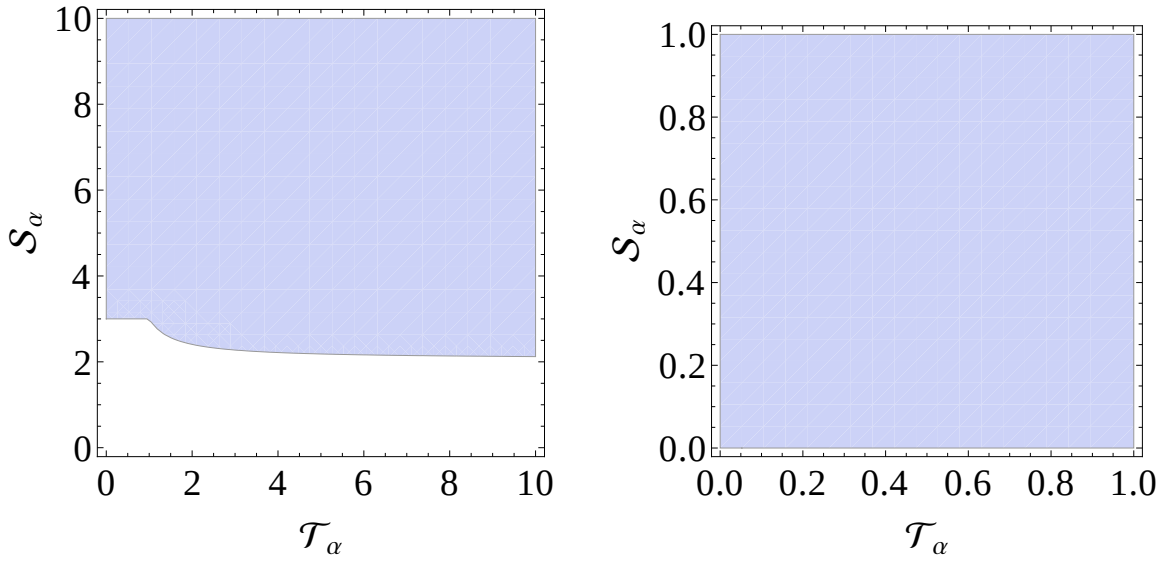

Figure 8.3: Region plots of the growth rate as a function of $\mathcal{T}_\alpha$ and $\mathcal{S}_\alpha$ for tow different values of $\mathcal{D}_K$. These figures demonstrate the shaded region (shown in sky blue colour) in which the dynamo action is possible. The left panel corresponds to $\mathcal{D}_K = 0.1$; and the right panel corresponds to $\mathcal{D}_K = 1.0$.

fluctuations in isotropic alpha. The new dynamo parameter is related to $\mathcal{D}_K$, $\mathcal{T}_\alpha$ and $\mathcal{S}_\alpha$ by,

$$\mathcal{D}_{S\alpha} \;=\; \frac{\alpha_{\rm rms}|S|}{\eta_T^2 K_3^3} \;=\; \frac{\mathcal{D}_K^{1/2}\mathcal{S}_\alpha}{\mathcal{T}_\alpha^{3/2}} \tag{8.49}$$

Using Eqn. (8.49) we can write any one of the parameters $\mathcal{D}_K$, $\mathcal{T}_\alpha$ or $\mathcal{S}_\alpha$ in terms of $\mathcal{D}_{S\alpha}$. Thus we can always express the dispersion relation given in Eqn. (8.42) in terms of $\mathcal{D}_{S\alpha}$ and any two of the three known parameters, $\mathcal{D}_K$, $\mathcal{T}_\alpha$ and $\mathcal{S}_\alpha$. In Fig. (8.4) we display the dynamo region as a function of $\mathcal{D}_K$ and $\mathcal{D}_{S\alpha}$ for fixed values of $\mathcal{T}_\alpha$. The left panel corresponds to $\mathcal{T}_\alpha = 0.5$ and the right panel corresponds to $\mathcal{T}_\alpha = 1.0$. A careful investigation of Fig. (8.4) reveals:

(i) If $\mathcal{T}_\alpha = 1.0$ (right panel), the critical value of $\mathcal{D}_{S\alpha}$, which is understood to be a function of $\mathcal{D}_K$, never exceeds unity.

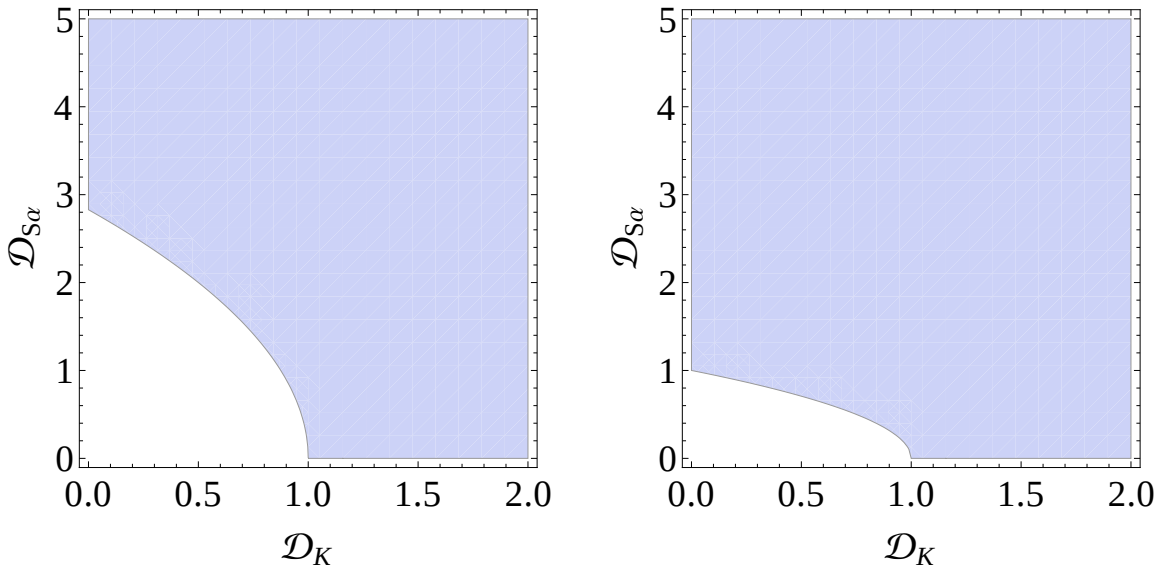

Figure 8.4: Region plots of the growth rate as a function of $\mathcal{D}_K$ and $\mathcal{D}_{S\alpha}$ for tow different values of $\mathcal{T}_\alpha$. These figures demonstrate the shaded region (shown in sky blue colour) in which the dynamo action is possible. The left panel corresponds to $\mathcal{T}_\alpha = 0.5$; and the right panel corresponds to $\mathcal{T}_\alpha = 1.0$.

(ii) While it is understood that the value $\mathcal{D}_{S\alpha}^{\rm crit} = 2.3$ has nothing special in terms of exciting the dynamo, it may be noted from the left panel that it can be satisfied for the chosen values of parameters $(\mathcal{T}_\alpha, m, n)$ when the value of $\mathcal{D}_K$ is very small, as may be the case in most numerical simulations (of Brandenburg et al. (2008) and Ch. 7 of this thesis).

To further comment on $\mathcal{D}_{S\alpha}$, we plot in Fig. (8.5) the dynamo region as a function of $\mathcal{D}_K$ and $\mathcal{T}_\alpha$ for $\mathcal{D}_{S\alpha} = 2.3$. We note that the smaller values of $\mathcal{D}_K$ would require larger values of critical values of $\mathcal{T}_\alpha$ and vice versa to trigger the dynamo action.

It is important to realize that the dispersion relation, which we explore to find various dynamo conditions, is a function of three dimensionless parameters and it can be expressed in terms of different sets of three dimensionless parameters by constructing more dimensionless numbers. The real positive roots of the dispersion relation are responsible for dynamo action. Thus the critical condition for the dynamo action is essentially given

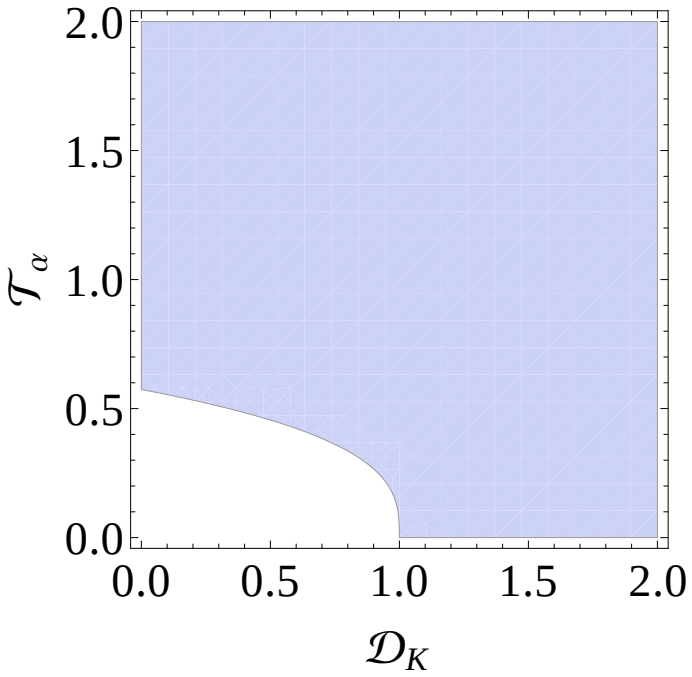

Figure 8.5: Region plot of the growth rate as a function of $\mathcal{D}_K$ and $\mathcal{T}_\alpha$ for $\mathcal{D}_{S\alpha} = 2.3$, demonstrating the dynamo region (shown in sky blue colour). Compare Brandenburg et al. (2008).

by a surface in three dimensional parameter space at which the real part of the dispersion relation vanishes.

8.5 Conclusions

In this chapter we have formulated the shear dynamo problem by considering fluctuations in α which have zero mean. In Chs. 5 and 6 we studied the shear dynamo problem due to non–helical flows in the limit of small Rm, where the analysis of Ch. 5 was valid for arbitrary values of Re, whereas the analysis of Ch. 6 also assumed the small Re limit. Our theoretical investigations were always non–perturbative in the shear parameter. The main conclusion of Chs. 5 and 6 was that there is no dynamo action in the limits explored. Results of Ch. 7 motivated us to study this problem in the light of fluctuating

helicity in a mirror–symmetric turbulence. This problem may be studied by using the concept of double averaging in which any quantity may be first averaged over an ensemble (defined by the different realizations of the velocity field) and then one can take another average over the superensemble (defined by different realization of the fluctuating $\alpha \propto \langle \boldsymbol{v} \cdot (\boldsymbol{\nabla} \times \boldsymbol{v}) \rangle$). Thus, we modelled the usual "alpha square–omega" dynamo equation and considered that the quantity α is a stochastic variable.

We start with the usual $\alpha^2 - \Omega$ dynamo equation for the once–averaged (or ensemble–averaged) magnetic field. The quantity α is assumed to fluctuate in time whose average over the superensemble vanishes. Using Reynolds averaging, we split the magnetic field into mean and fluctuating components. The mean magnetic field is driven by the curl of mean EMF due to fluctuating α, denoted as $\boldsymbol{\mathcal{E}}^{\alpha}$, which may be determined by solving the equation for fluctuating magnetic field. We write the equation for fluctuating magnetic field by ignoring the term which is non–linear in fluctuations; this may be thought of as FOSA–like approximation. Using the shearing coordinate transformation and the various properties of the Resistive Green's function discussed in the Appendix A, we write explicit solution of the fluctuating magnetic field. We then determine $\boldsymbol{\mathcal{E}}^{\alpha}$ in terms of two–point correlation function of random alpha and the first spatial derivative of mean magnetic field, suggesting that the fluctuating α lead to diffusive–like effect. We considered the case of slowly varying mean magnetic field and wrote explicit expressions for the mean EMF due to alpha fluctuations and the transport coefficient. The transport coefficient could be expressed in terms of two–time correlator of random alpha. For comparative purposes, we considered the case when the mean–field is a function only of the spatial coordinate X_3 and time τ. We derived explicit expressions for all four components of the transport coefficient, which is also called 'the turbulent diffusivity tensor due to alpha fluctuations', $\beta_{mp}(\tau)$. As $\beta_{mp}(\tau)$ saturate at finite values at late times, we consider the saturated values of $\beta_{mp}(\tau)$ denoted by β^{∞}_{mp} in our analysis. Few important properties of β^{∞}_{mp} are as follows:

1. In the limit of zero shear, only the diagonal components, β^{∞}_{11} and β^{∞}_{22}, survive and the off–diagonal components vanish.

2. Both β_{11}^{∞} and β_{22}^{∞} are negative, in which β_{11}^{∞} is independent of shear and β_{22}^{∞} is contributed by two terms, one of which depends on shear. The shear makes β_{22}^{∞} more negative.

3. The negative values of β_{11}^{∞} and β_{22}^{∞} lead to the *negative diffusion* of mean magnetic field giving rise to self–excited dynamo without any cross–coupling between different components of mean magnetic field.

4. Our results reduce in agreement to the results of Kraichnan (1976) in the limit of zero shear, who did similar analysis in the absence of shear and reported the negative diffusion of mean magnetic field.

5. Both β_{12}^{∞} and β_{21}^{∞}, which lead to the coupling of different components of mean magnetic field, are positive for negative values of the rate of shear which we assume. Also $\beta_{12}^{\infty} = \beta_{21}^{\infty}$.

We derive the dispersion relation, Eqn. (8.39), and write it in convenient form, Eqn. (8.42), by defining three dimensionless parameters, $\mathcal{D}_K$, $\mathcal{T}_\alpha$ and $\mathcal{S}_\alpha$, which are given in Eqn. (8.41). We study various situations in which the mean magnetic field could grow by exploring range of values of the three dimensionless parameters. The main conclusion may be stated as: *the fluctuations in α with zero mean in conjunction with background shear flow can give rise to the growth of large–scale magnetic field.*

Below we summarize some of the key results related to the dynamo action:

- The dispersion relation, which we explore to find various dynamo conditions, is a function of three dimensionless parameters and it can be expressed in terms of different sets of three dimensionless parameters by constructing more dimensionless numbers. The real positive roots of the dispersion relation are responsible for dynamo action. Thus the critical condition for the dynamo action is essentially given by a surface in three dimensional parameter space at which the real part of the dispersion relation vanishes.

- The critical value required by one of the parameters for dynamo action is a function of the remaining two dimensionless parameters, e.g., $D_{\alpha S}^{\rm crit}$ varies as a function of two other dimensionless parameters, and hence is not a unique number; see Figs. (8.1)–(8.5).

- Sufficiently strong $\alpha-$fluctuations may lead to the growth of mean magnetic field by the process of negative diffusion, even in the absence of shear; see Eqn. (8.45).

- Assuming that the fluctuations in α be small such that $\mathcal{D}_K < 1$, we find that the growth rate varies linearly with shear in the limit of small $\mathcal{S}_\alpha$; see Eqn. (8.46). This linear scaling has been observed and discussed in various earlier works (Yousef et al., 2008a,b; Brandenburg et al., 2008; Hughes & Proctor, 2009; Heinemann, McWilliams & Schekochihin, 2011; Mitra & Brandenburg, 2012; Richardson & Proctor, 2012). This linear scaling is also observed in our simulations presented in Ch. 7; see Fig. (7.10).

- For large values of $\mathcal{S}_\alpha$, the growth rate varies as $|S|^2$. This scaling has also been reported in Richardson & Proctor (2012).

- By analyzing the conditions for dynamo action as a function of three dimensionless parameters, we find that the shear helps in the generation of large–scale magnetic field in the presence of $\alpha-$fluctuations. If the fluctuations in α are extremely small, one can still find growing solutions for the mean magnetic field for sufficiently large values of shear; see Figs. (8.1)–(8.5).

- In most numerical simulations that we perform, the fluctuations in α are not too strong, and hence these alone may not give rise to the dynamo action, unless supported by the shear.

It is routinely found in the numerical simulations of the shear dynamo that the quantity α fluctuates in time without having any net value, even when the random forcing at small scales in these simulations was non–helical, therefore, it seems plausible that these observed $\alpha-$fluctuations together with background shear flow could have led

to the growth of large–scale magnetic fields in these simulations, by the mechanisms described in our analytical calculations of fluctuating α discussed above.

Chapter 9

Conclusions & Outlook

In this chapter we present some of the broad conclusions of different problems that were studied in this thesis. The conclusions for each chapter are also separately given at the end of every chapter, and therefore here we highlight only the main conclusions. We briefly mention below the central topic of the thesis and its basic motivation:

- **The main question that was considered:** We studied *the shear dynamo problem* which may be stated as: Under what conditions does the large–scale magnetic field grow due to the mirror–symmetric (i.e. non–helical) turbulence at small scales, in the background linear shear flow ?

  This problem may be viewed in the following way: In a given background mean shear flow, the kinetic energy is being supplied by stirring the electrically conducting incompressible fluid in a non–helical fashion, as a result of which, the magnetic energy at large–scale is seen to grow in time due to the large–scale dynamo action. This is clearly a process of inverse–cascade in which the energy is being transferred from small scale to larger scales. Our aim is to understand the reason for this shear dynamo action in the absence of usual $\alpha-$effect.

- **The motivation to pursue this problem:** We mention the following two main motivations to study this problem:

(i) From observations: Astrophysical systems possess ordered magnetic field in addition to a random component which survive for time scales much larger than the diffusion time scales in those systems, and therefore are thought to be self–sustained by the turbulent dynamo action. The mean differential rotation is common in these systems, e.g., the Sun, the disc galaxies, the accretion discs etc. The standard paradigm involves amplification of seed magnetic fields, due to non mirror–symmetric (i.e. helical) turbulent flows through the $\alpha-$effect (Moffatt, 1978; Parker, 1979). Only recently the role of mean shear in the turbulent flow is beginning to be appreciated. Dynamo action due to shear and turbulence received some attention in the astrophysical contexts of accretion discs (Vishniac & Brandenburg, 1997) and galactic discs (Blackman, 1998; Sur & Subramanian, 2009). The natural question to be addressed may be posed as: In the absence of usual $\alpha-$ effect, will it be possible to generate large–scale magnetic field just due to the action of mirror–symmetric turbulence in background shear flow on the seed magnetic field ?

(ii) From simulations: The question posed just above were simulated in the recent past by Yousef et al. (2008a,b); Brandenburg et al. (2008). These simulations clearly demonstrated the growth of large–scale magnetic field due to non–helical stirring at small scale in the background linear shear flow.

This forms the basic motivation for our interest in the study of *the shear dynamo problem* in the absence of usual $\alpha-$effect. It is realized that this problem of the shear dynamo is quite difficult in nature and therefore we first develop the necessary techniques, which is then applied to a simpler problem of passive scalar mixing, before pursuing the main problem concerning the shear dynamos. In the problems studied in this thesis, we assumed a *linear* shear flow, and throughout this thesis, we dealt with the shear parameter *non–perturbatively*. We derived the resistive Green's function for a linear shear flow, which is equivalent to the one first derived by Krause & Rädler (1980). Using the Galilean invariance of linear shear flows, which is a statement of homogeneity in the sheared coordinate frame, we proved a result on the Galilean invariant form of the

unequal–time two–point velocity correlators in Fourier space, and demonstrated that any general second order correlator of random velocity field, in terms of which various transport coefficients of different transport phenomena (of passive scalar or the magnetic field) could be expressed, can entirely be written in terms of a single entity which we called the *velocity spectrum tensor*. Below we present broad conclusions together with statements of different problems in the sequence of their appearance in the thesis:

1. **Shearing waves:** Shear flows are common and seen in a variety of astrophysical contexts; like differential rotation in disc galaxies, accretion discs around compact objects etc. The shearing waves are excited in such systems by some random stirring in the medium, e.g., in disc galaxies the random supernovae (SNe) events stir the differentially rotating disc and excite shearing waves. These shearing waves tend to mix passive scalar and the magnetic fields in the medium. Our aim is to understand the large–scale dynamo action in systems which possess mean shear, and therefore a necessary understanding of waves in such shearing systems is quite useful in our studies related to the large–scale dynamo action. We studied the *free* and *non–helically forced* shearing waves in background linear shear.

- Exact solutions of the Navier–Stokes equations: By studying the incompressible Navier–Stokes equations in a background linear shear flow *in the absence of any external forcing*, we have constructed a plane shearing wave solution for the Navier–Stokes equations in linear shear flows. These solutions are also the *exact solutions* and we have presented explicit expressions for all three components of the velocity field in the real form. We demonstrate that, when these shearing modes, also known as the Kelvin modes, with parallel wavevectors are superposed, they remain exact solutions. We give, in explicit form, the most general plane transverse shearing wave solution, with any specified initial orientation, profile and polarization structure, with either unbounded or shear–periodic boundary conditions. This was presented in Ch. 2.

- Forced stochastic velocity dynamics: In Ch. 3 we studied the stochastically forced

incompressible shear flows by solving the Navier–Stokes equations with a background linear shear flow with external random forcing in the limit of small fluid Reynolds numbers. The forcing was assumed to be non–helical (mirror–symmetric), as our aim was to model the non–helical random flow in linear shear flows. It was shown that the non–helical forcing of an incompressible fluid at low Re, in the absence of Lorentz forces, gives rise to a non–helical velocity field. We determined the velocity spectrum tensor which was later used to compute various transport coefficients.

2. **Passive scalar mixing in shear flows:** A passive scalar evolves according to an advection–diffusion equation, which is much simpler than the induction equation governing the evolution of magnetic field, and therefore provides a simpler situation where we could quickly apply our techniques to understand the large–scale mixing of the passive scalar. As we have developed stochastic forced shearing wave solutions which are non–helical, because of our ultimate interest in the shear dynamos, we applied the same solutions of non–helical turbulent flows in background linear shear flows to study the mixing of passive scalars. We found the possibility of transient amplification of mean concentration of the passive scalar. Just like everything else in the thesis, this result is non–perturbative in the shear parameter.

3. **The shear dynamo problem:** The problem of the shear dynamo was first analytically studied in the limit of low Reynolds numbers and *the $\alpha-$effect was strictly absent*. These investigations motivated us to look for the dynamo action in such systems in the limit when at least the fluid Reynolds number be below unity, and we performed numerical simulations using the Pencil Code[1] in previously unexplored parameter regimes. Results of our numerical simulations and the simulations of Brandenburg et al. (2008) in different parameter regimes provided strong evidence for the non–trivial role of fluctuations in α, which have zero mean, in the presence of background linear shear flow. This led us to analytically study the shear dynamo problem where α could

[1]See http://www.nordita.org/software/pencil-code.

be considered as a fluctuating quantity with zero mean. As argued before by Kraichnan (1976), these fluctuations in α may be understood in terms of helicity fluctuations. We show analytically that the fluctuations in α with zero mean together with mean background shear can drive the large–scale dynamo action. The main results may be given as follows:

(i) When $\alpha-$effect is strictly zero: Some earlier works on the similar problem proposed that the origin of the large–scale magnetic field in such systems may be explained by an effect known as the shear–current effect (Rogachevskii & Kleeorin 2003, 2004, 2008).

We formulated the problem of the shear dynamo in the limit of low Reynolds numbers and concluded that the shear–current effect cannot be responsible for dynamo action. Our theory is found to be in good agreement with some other works, esp., with Brandenburg et al. (2008) who computed the magnetic diffusivity tensor and concluded that the relevant component responsible for the shear–current effect (η_{21}^{∞}) is of wrong sign and hence cannot give rise to the dynamo action. This was the natural prediction of our theory.

Thus the main contribution of our studies, in which α was strictly zero, may be stated as follows: The mean magnetic field cannot grow due to mirror–symmetric turbulence in the background linear shear flow, at least in the limit when: (a) both fluid and magnetic Reynolds numbers are below unity; (b) $\alpha-$effect is strictly absent (without considering any fluctuations in α); but (c) the shear parameter can take arbitrary values.

This negative result of no dynamo action prompted us to carry out various numerical simulations when at least one of Re, Rm is below unity.

(ii) Results of numerical studies of the shear dynamo: We demonstrated the large–scale dynamo action in the limit when $\mathrm{Re} < 1$ and $\mathrm{Rm} > 1$. We performed simulations in the regime when both $(\mathrm{Re}, \mathrm{Rm}) < 1$ to compare the results with our analytical calculations done in the similar regime and found a reasonably good agreement. We

also estimated the dynamo number ($D_{\alpha S}$), which was empirically defined in Brandenburg et al. (2008) corresponding to the *incoherent alpha–shear mechanism*[2], for many simulations, and found that the dynamo number ($D_{\alpha S}$) is always *supercritical* for cases, in which, we see dynamo growth, a result which is in agreement with Brandenburg et al. (2008)[3]. This suggested that the incoherent alpha–shear mechanism could plausibly be the reason for observed shear dynamo due to non–helical random stirring in these simulations. Thus our numerical investigations, together with those of Brandenburg et al. (2008) in different parameter regime, motivated us to analytically study the problem of dynamo action by assuming fluctuations in α *with no net value* in the presence of background linear shear flow.

(iii) When α is a fluctuating quantity with zero mean: By considering temporal fluctuations in the quantity α, with its mean value zero, we demonstrated that *the fluctuations in α with zero mean in conjunction with background shear flow can give rise to the growth of large–scale magnetic field.* Some other conclusions of this analysis could be stated as:

(a) In the limit of zero shear, we find that only the diagonal components of the turbulent diffusivity tensor (β^{∞}_{mp}) survive, which are *negative*. This leads to the *negative turbulent diffusion* of mean magnetic field, which in case of sufficiently strong $\alpha-$fluctuations may give rise to the self–excited dynamo action. This result was first obtained by Kraichnan (1976) who did a similar analysis in the absence of shear.

(b) The shear leads to cross–coupling of different components of mean magnetic field with each other through the off–diagonal components of β^{∞}_{mp}. The diagonal components couple each component of mean magnetic field with itself.

[2]A mechanism by which the fluctuations in α with no net value in conjunction with mean shear might give rise to the large–scale dynamo action in such systems.

[3]Critical value of $D_{\alpha S}$ ($D^{\rm crit}_{\alpha S} \approx 2.3$), above which the dynamo is seen, was empirically determined in Brandenburg et al. (2008). We show by our analytical investigation of fluctuating α with background mean shear that this number 2.3 is not unique; we describe it later.

The shear makes one of the diagonal components β_{22}^{∞} more negative whereas β_{11}^{∞} is independent of the shear.

(c) By deriving the dispersion relation and putting it in a useful form in terms of three dimensionless parameters, we explored various conditions for the dynamo action, and found that the critical conditions could be given by a surface in three dimensional parameter space. Therefore, the critical value required by one of the parameters for dynamo action is a function of the remaining two dimensionless parameters (e.g., $D_{\alpha S}^{\rm crit}$ varies as a function of two other dimensionless parameters, and hence is not a unique number).

(d) We find that the shear helps in the generation of large–scale magnetic field in the presence of $\alpha-$fluctuations. If the fluctuations in α are extremely small, one can still find growing solutions for the mean magnetic field for sufficiently large values of shear.

(e) In most numerical simulations that we perform, the fluctuations in α are not too strong, and hence these alone may not give rise to the dynamo action, unless supported by the shear.

It is routinely found in the numerical simulations of the shear dynamo that the quantity α fluctuates in time without having any net value, even when the random forcing at small scales in these simulations was non–helical, therefore, it seems plausible that these observed $\alpha-$fluctuations together with background shear flow could have led to the growth of large–scale magnetic fields in these simulations, by the mechanisms described in our analytical calculations of fluctuating α discussed above. The natural scope for future works related to this problem could be to perform numerical experiments exploring conditions for the dynamo action, as predicted in our analytical calculation of $\alpha-$fluctuations, in which, we suggested that there are three dimensionless parameters, which, if tuned suitably, can always give rise to the dynamo action.

Appendix A

The Resistive Green's Function for a Linear Shear Flow

The Green's function for linear shear flows was first derived by Krause & Rädler (1971). Here, we derive an expression of the resistive Green's function for a linear shear flow, in the coordinate system which is suitable for our purposes. Equations (4.10), (5.12) and (8.11) are of the following form:

$$\left(\frac{\partial}{\partial t} \; - \; \mu \boldsymbol{\nabla}^2\right) \varphi(\boldsymbol{x}, t) \; = \; \zeta(\boldsymbol{x}, t) \tag{A.1}$$

where μ takes the role, for example, of molecular diffusivity (κ) for the problem of passive scalar mixing and microscopic resistivity (η) for the shear dynamo problem. $\zeta(\boldsymbol{x}, t)$ in the Eqn. (A.1) may be thought of as the source term, which is different for various problems we have studied. The spacetime coordinates in the *sheared frame*, denoted as $(\boldsymbol{x}, t)$, and in the laboratory frame, denoted as $(\boldsymbol{X}, \tau)$, are related by the following *shearing transformation*:

$$x_1 = X_1 \,, \qquad x_2 = X_2 - S\tau X_1 \,, \qquad x_3 = X_3 \,, \qquad t = \tau \tag{A.2}$$

Partial derivatives transform as

$$\frac{\partial}{\partial\tau} = \frac{\partial}{\partial t} - Sx_1\frac{\partial}{\partial x_2}\,, \quad \frac{\partial}{\partial X_1} = \frac{\partial}{\partial x_1} - St\frac{\partial}{\partial x_2}\,, \quad \frac{\partial}{\partial X_2} = \frac{\partial}{\partial x_2}\,, \quad \frac{\partial}{\partial X_3} = \frac{\partial}{\partial x_3} \tag{A.3}$$

Therefore $\boldsymbol{\nabla}^2$ in Eqn. (A.1) is given by

$$\begin{aligned} \boldsymbol{\nabla}^2 \equiv \frac{\partial^2}{\partial X_p \partial X_p} &= \left(\frac{\partial}{\partial x_p} - St\delta_{p1}\frac{\partial}{\partial x_2}\right)^2 \\ &= \frac{\partial^2}{\partial x_p \partial x_p} - 2St\frac{\partial^2}{\partial x_1 \partial x_2} + S^2t^2\frac{\partial^2}{\partial x_2^2} \end{aligned} \tag{A.4}$$

Equation (A.1) is linear, homogeneous in $\boldsymbol{x}$ and inhomogeneous in t. Therefore, the general solution can be written in the form,

$$\begin{aligned} \varphi(\boldsymbol{x},t) \;=\; & \int \mathrm{d}^3x'\, G_\mu(\boldsymbol{x}-\boldsymbol{x}',t,s)\;\varphi(\boldsymbol{x}',s) \\ & + \int_s^t \mathrm{d}t' \int \mathrm{d}^3x'\, G_\mu(\boldsymbol{x}-\boldsymbol{x}',t,t')\;\zeta(\boldsymbol{x}',t')\;; \qquad \text{for any } s<t\,, \end{aligned} \tag{A.5}$$

where $G_\mu(\boldsymbol{x},t,t')$ is the *resistive Green's function* for the linear shear flow. Allowing $\left(\partial/\partial t - \mu\boldsymbol{\nabla}^2\right)$ to act on both sides, we have

$$\begin{aligned} \left(\frac{\partial}{\partial t} - \mu\boldsymbol{\nabla}^2\right)\varphi \;=\; & \int \mathrm{d}^3x'\,\varphi(\boldsymbol{x}',s)\left(\frac{\partial}{\partial t} - \mu\boldsymbol{\nabla}^2\right) G_\mu(\boldsymbol{x}-\boldsymbol{x}',t,s) \\ & + \int_s^t \mathrm{d}t' \int \mathrm{d}^3\boldsymbol{x}'\,\zeta(\boldsymbol{x}',t')\left(\frac{\partial}{\partial t} - \mu\boldsymbol{\nabla}^2\right) G_\mu(\boldsymbol{x}-\boldsymbol{x}',t,t') \\ & + \int \mathrm{d}^3x'\,\zeta(\boldsymbol{x}',t)\lim_{t'\to t_-} G_\mu(\boldsymbol{x}-\boldsymbol{x}',t,t') \end{aligned} \tag{A.6}$$

From Eqn. (A.1), we note that the right side of Eqn. (A.6) must be equal to $\zeta(\boldsymbol{x},t)$. Therefore the Green's function must satisfy the following properties:

$$G_\mu(\boldsymbol{x},t,t') \quad \text{is non–zero only when} \quad 0 \le t' < t. \tag{A.7a}$$

$$\lim_{t' \to t_-} G_\mu(\boldsymbol{x}, t, t') \;=\; \delta^3(\boldsymbol{x}) \tag{A.7b}$$

$$\left(\frac{\partial}{\partial t} - \mu \boldsymbol{\nabla}^2\right) G_\mu(\boldsymbol{x}, t, t') \;=\; 0 \tag{A.7c}$$

By iterating Eqn. (A.5), we have

$$\begin{aligned}
\varphi(\boldsymbol{x}, t) \;=\; & \int \mathrm{d}^3x' \, \varphi(\boldsymbol{x}', t_0) \int \mathrm{d}^3x'' \, G_\mu(\boldsymbol{x} - \boldsymbol{x}'', t, s) \, G_\mu(\boldsymbol{x}'' - \boldsymbol{x}', s, t_0) \\
+ \; & \int_{t_0}^{s} \mathrm{d}t' \int \mathrm{d}^3x' \, \zeta(\boldsymbol{x}', t') \int \mathrm{d}^3x'' \, G_\mu(\boldsymbol{x} - \boldsymbol{x}'', t, s) \, G_\mu(\boldsymbol{x}'' - \boldsymbol{x}', s, t') \\
+ \; & \int_{s}^{t} \mathrm{d}t' \int \mathrm{d}^3x' \, \zeta(\boldsymbol{x}', t') \, G_\mu(\boldsymbol{x} - \boldsymbol{x}', t, t') \,; \quad \text{for } t_0 < s < t \,.
\end{aligned}$$

Comparing this with Eqn. (A.5), we obtain another property of the Green's function, namely,

$$G_\mu(\boldsymbol{x} - \boldsymbol{x}', t, t_0) \;=\; \int \mathrm{d}^3x'' \, G_\mu(\boldsymbol{x} - \boldsymbol{x}'', t, s) \, G_\mu(\boldsymbol{x}'' - \boldsymbol{x}', s, t_0) \,; \quad \text{for } t_0 < s < t \,. \tag{A.7d}$$

Let us define the spatial Fourier transform of the Green's function as,

$$\widetilde{G}_\mu(\boldsymbol{k}, t, t') \;=\; \int \mathrm{d}^3x \, \exp\left(-\mathrm{i}\, \boldsymbol{k} \boldsymbol{\cdot} \boldsymbol{x}\right) G_\mu(\boldsymbol{x}, t, t') \tag{A.8}$$

where $\boldsymbol{k}$, being conjugate to the sheared coordinate vector $\boldsymbol{x}$, can be regarded as a *sheared wavevector*. Then Eqns. (A.7a)–(A.7d) imply that

$$\widetilde{G}_\mu(\boldsymbol{k}, t, t') \quad \text{is non–zero only when} \quad 0 \le t' < t. \tag{A.9a}$$

$$\lim_{t' \to t_-} \widetilde{G}_\mu(\boldsymbol{k}, t, t') \;=\; 1 \tag{A.9b}$$

$$\frac{\partial \widetilde{G}_\mu}{\partial t} \;+\; \mu \, K^2(\boldsymbol{k}, t) \, \widetilde{G}_\mu \;=\; 0 \tag{A.9c}$$

$$\widetilde{G}_\mu(\boldsymbol{k}, t, t_0) \;=\; \widetilde{G}_\mu(\boldsymbol{k}, t, s) \, \widetilde{G}_\mu(\boldsymbol{k}, s, t_0) \,; \quad \text{for } t_0 < s < t \,. \tag{A.9d}$$

where, in Eqn. (A.9c), $K^2(\boldsymbol{k},t) = (k_1 - Stk_2)^2 + k_2^2 + k_3^2$. It is now straightforward to write down the solution:

$$\begin{aligned}\widetilde{G}_\mu(\boldsymbol{k},t,t') &= \exp\left[-\mu\int_{t'}^{t}\mathrm{d}s\, K^2(\boldsymbol{k},s)\right] \\ &= \exp\left[-\mu\left(k^2(t-t') - S\,k_1\,k_2(t^2-t'^2) + \frac{S^2}{3}\,k_2^2(t^3-t'^3)\right)\right] \qquad \text{(A.10)}\end{aligned}$$

Note also that $\widetilde{G}_\mu(\boldsymbol{k},t,t')$ is a positive quantity which takes values between 0 and 1, and that it is an even function of $\boldsymbol{k}$ and k_3.

We now take the inverse Fourier transform of Eqn. (A.10) to get $G_\mu(\boldsymbol{x},t,t')$. It is convenient to write this as

$$G_\mu(\boldsymbol{x},t,t') = \int\frac{\mathrm{d}^3k}{(2\pi)^3}\exp\left[\mathrm{i}\,\boldsymbol{k}\cdot\boldsymbol{x} - \mu(t-t')\{k^2 + T_{ij}\,k_i\,k_j\}\right] \qquad \text{(A.11)}$$

where T_{ij} is a 2×2 symmetric matrix whose elements are given by,

$$T_{11} = 0, \quad T_{12} = T_{21} = -\frac{S}{2}(t+t'), \quad T_{22} = \frac{S^2}{3}(t^2+tt'+t'^2) \qquad \text{(A.12)}$$

The integral in Eqn. (A.11) can be evaluated by diagonalising the matrix T_{ij}. It proves useful to express $G_\mu(\boldsymbol{x},t,t')$ in terms of the principal–axes coordiates, $\overline{\boldsymbol{x}} = (\overline{x}_1, \overline{x}_2, \overline{x}_3)$. These are defined by the orthogonal transformation,

$$\begin{pmatrix}\overline{x}_1\\ \overline{x}_2\\ \overline{x}_3\end{pmatrix} = \begin{pmatrix}\cos\theta & \sin\theta & 0\\ -\sin\theta & \cos\theta & 0\\ 0 & 0 & 1\end{pmatrix}\begin{pmatrix}x_1\\ x_2\\ x_3\end{pmatrix} \qquad \text{(A.13)}$$

which is a time–dependent rotation of the coordinate axes in the x_1–x_2 plane. The angle

of rotation, θ, is determined by

$$\begin{aligned} \tan\theta &= f + \sqrt{1+f^2} \\ f &= -\frac{1}{3}\frac{S(t^2+tt'+t'^2)}{(t+t')} \end{aligned} \tag{A.14}$$

Note that θ depends on the shear parameter, S, and the times, t and t'. Let us define the dimensionless quantitites,

$$\begin{aligned} \sigma_1 &= \left[1 - \frac{S}{2}(t+t')\,\tan\theta\right]^{1/2} \\ \sigma_2 &= \left[1 + \frac{S}{2}(t+t')\,\cot\theta\right]^{1/2} \end{aligned} \tag{A.15}$$

Now we can write the Green's function as a *sheared heat kernel*,

$$\begin{aligned} G_\mu(\boldsymbol{x},t,t') = {} & [4\pi\mu(t-t')]^{-3/2}\left[1 + \frac{S^2}{12}(t-t')^2\right]^{-1/2} \times \\ & \times \exp\left[-\frac{1}{4\mu(t-t')}\left(\frac{\overline{x}_1^2}{\sigma_1^2} + \frac{\overline{x}_2^2}{\sigma_2^2} + \overline{x}_3^2\right)\right], \end{aligned} \tag{A.16}$$

which is equivalent to the one first derived in Krause & Rädler (1971). Properties of the Green's function have also been discussed in Ch. 5; see Fig. (5.1). It is useful to note that the Green's function $G_\mu(\boldsymbol{x},t,t')$ is *an even function of* $\boldsymbol{x}$.

Also, substituting $\boldsymbol{k}=\boldsymbol{0}$ in Eqns. (A.8) and (A.10), we find

$$\int \mathrm{d}^3x\, G_\mu(\boldsymbol{x},t,t') = \widetilde{G}_\mu(\boldsymbol{0},t,t') = 1 \tag{A.17}$$

Appendix B

Galilean Invariance & A Result on G–invariant Velocity Correlators

The linear shear flow has a basic symmetry relating to measurements made by a special subset of all observers. These special observers are termed as the *comoving observers* in Sridhar & Subramanian (2009a,b). A comoving observer is defined to be the one whose velocity with respect to the laboratory frame is equal to the velocity of the background shear flow, and whose cartesian axes are aligned with those of the laboratory frame. In the laboratory frame, a comoving observer can be labelled by the coordinates, $\boldsymbol{\xi} = (\xi_1, \xi_2, \xi_3)$, of her origin at time $\tau = 0$. Different labels identify different comoving observers and vice versa. As the labels run over all possible values, they exhaust the set of all comoving observers. At any time τ, the origin of the comoving observer with respect to the laboratory frame is given by,

$$\boldsymbol{X}_c(\boldsymbol{\xi}, \tau) \;=\; (\xi_1\,, \xi_2 + S\tau\xi_1\,, \xi_3) \tag{B.1}$$

An event with spacetime coordinates $(\boldsymbol{X}, \tau)$ in the lab frame has spacetime coordinates $(\tilde{\boldsymbol{X}}, \tilde{\tau})$ with respect to the comoving observer, given by

$$\tilde{\boldsymbol{X}} \;=\; \boldsymbol{X} \;-\; \boldsymbol{X}_c(\boldsymbol{\xi}, \tau)\,, \qquad \tilde{\tau} \;=\; \tau - \tau_0 \tag{B.2}$$

where the arbitrary constant τ_0 allows for translation in time as well. The coordinate transformation given in Eqn. (B.2) implies that partial derivatives are related through

$$\frac{\partial}{\partial \tau} \;=\; \frac{\partial}{\partial \tilde{\tau}} \;-\; S\xi_1 \frac{\partial}{\partial \tilde{X}_2}\,, \qquad \frac{\partial}{\partial \boldsymbol{X}} \;=\; \frac{\partial}{\partial \tilde{\boldsymbol{X}}} \tag{B.3}$$

We note that the combination $(\partial/\partial\tau + SX_1\partial/\partial X_2) = \left(\partial/\partial\tilde{\tau} + S\tilde{X}_1\partial/\partial\tilde{X}_2\right)$ is invariant in form. There is a fundamental difference between the coordinate transformations associated with Galilean invariance (Eqn. B.2) and the shearing transformation (Eqn. A.2). The former relates different comoving observers, whereas the latter describes a time–dependent distortion of the coordinates axes of one observer. Comparing Eqn. (B.3) with (A.3), we note that the relationship between old and new variables is homogeneous for the Galilean transformation, whereas it is inhomogeneous for the shearing transformation.

B.1 Galilean–invariant velocity correlators

We now explore the consequences of requiring that the statistics of the velocity fluctuations be Galilean–invariant. We consider the n–point velocity correlator measured by the observer in the lab frame. Let this observer correlate v_{j_1} at spacetime location $(\boldsymbol{R}_1, \tau_1)$, with v_{j_2} at spacetime location $(\boldsymbol{R}_2, \tau_2)$, and so on upto v_{j_n} at spacetime location $(\boldsymbol{R}_n, \tau_n)$. Now consider a comoving observer, the position vector of whose origin is given by $\boldsymbol{X}_c(\boldsymbol{\xi}, \tau)$ of Eqn. (B.1). An identical experiment performed by this observer must yield the same results, the measurements now made at the spacetime points denoted by $(\boldsymbol{R}_1 + \boldsymbol{X}_c(\boldsymbol{\xi}, \tau_1), \tau_1)\,; (\boldsymbol{R}_2 + \boldsymbol{X}_c(\boldsymbol{\xi}, \tau_2), \tau_2)\,; \ldots\,;\, (\boldsymbol{R}_n + \boldsymbol{X}_c(\boldsymbol{\xi}, \tau_n), \tau_n)$. If the velocity statistics is GI, the n–point velocity correlator must satisfy the condition

$$\langle v_{j_1}(\boldsymbol{R}_1, \tau_1) \ldots v_{j_n}(\boldsymbol{R}_n, \tau_n)\rangle \;=\; \langle v_{j_1}(\boldsymbol{R}_1 + \boldsymbol{X}_c(\boldsymbol{\xi}, \tau_1), \tau_1) \ldots v_{j_n}(\boldsymbol{R}_n + \boldsymbol{X}_c(\boldsymbol{\xi}, \tau_n), \tau_n)\rangle \tag{B.4}$$

for all $(\boldsymbol{R}_1, \ldots \boldsymbol{R}_n\,; \tau_1, \ldots \tau_n\,; \boldsymbol{\xi})$.

We find that the transport coefficients of different transport phenomena (of passive

scalars or magnetic fields), within the framework of FOSA, are given in terms of second order correlator of random velocity field (see e.g. Eqns. (4.19) and (5.27)), for which

$$\langle v_i(\boldsymbol{R},\tau)\, v_j(\boldsymbol{R}',\tau')\rangle \;=\; \langle v_i(\boldsymbol{R}+\boldsymbol{X}_c(\boldsymbol{\xi},\tau),\tau)\, v_j(\boldsymbol{R}'+\boldsymbol{X}_c(\boldsymbol{\xi},\tau'),\tau')\rangle \tag{B.5}$$

for all $(\boldsymbol{R},\boldsymbol{R}',\tau,\tau',\boldsymbol{\xi})$. We also need to work out the correlation between velocities and their gradients:

$$\begin{aligned}
\langle v_i(\boldsymbol{R},\tau)\, v_{jl}(\boldsymbol{R}',\tau')\rangle &= \frac{\partial}{\partial R'_l}\,\langle v_i(\boldsymbol{R},\tau)\, v_j(\boldsymbol{R}',\tau')\rangle \\
&= \frac{\partial}{\partial R'_l}\,\langle v_i(\boldsymbol{R}+\boldsymbol{X}_c(\boldsymbol{\xi},\tau),\tau)\, v_j(\boldsymbol{R}'+\boldsymbol{X}_c(\boldsymbol{\xi},\tau'),\tau')\rangle \\
&= \langle v_i(\boldsymbol{R}+\boldsymbol{X}_c(\boldsymbol{\xi},\tau),\tau)\, v_{jl}(\boldsymbol{R}'+\boldsymbol{X}_c(\boldsymbol{\xi},\tau'),\tau')\rangle
\end{aligned} \tag{B.6}$$

The Galilean–invariance of velocity correlators stated in Eqn. (B.5) is most compactly expressed in Fourier–space, which will be shown below. Let $\tilde{\boldsymbol{v}}(\boldsymbol{K},\tau)$ be the spatial Fourier transform of $\boldsymbol{v}(\boldsymbol{X},\tau)$, defined by Eqn. (3.3). As may be seen from Eqns. (3.18) and (3.19) that the quantity to be determined, in order to find various real–space correlators between velocities and their gradients, is Fourier–space two–point unequal–time velocity correlator, $\left\langle \tilde{v}_i\left(\boldsymbol{K},t\right)\tilde{v}_j^*\left(\boldsymbol{K}',t'\right)\right\rangle$.

We prove below that *a G–invariant Fourier–space two–point velocity correlator must be of the form*

$$\left\langle \tilde{v}_i(\boldsymbol{K},\tau)\,\tilde{v}_j^*(\boldsymbol{K}',\tau')\right\rangle \;=\; (2\pi)^6\,\delta(\boldsymbol{k}-\boldsymbol{k}')\,\Pi_{ij}(\boldsymbol{k},t,t') \tag{B.7}$$

where Π_{ij} is the *velocity spectrum tensor*, which must possess the following properties:

$$\begin{aligned}
\Pi_{ij}(\boldsymbol{k},t,t') &= \Pi_{ij}^*(-\boldsymbol{k},t,t') \;=\; \Pi_{ji}(-\boldsymbol{k},t',t) \\
K_i\,\Pi_{ij}(\boldsymbol{k},t,t') &= (k_i - St\,\delta_{i1}k_2)\,\Pi_{ij}(\boldsymbol{k},t,t') \;=\; 0 \\
K'_j\,\Pi_{ij}(\boldsymbol{k},t,t') &= (k_j - St'\,\delta_{j1}k_2)\,\Pi_{ij}(\boldsymbol{k},t,t') \;=\; 0
\end{aligned} \tag{B.8}$$

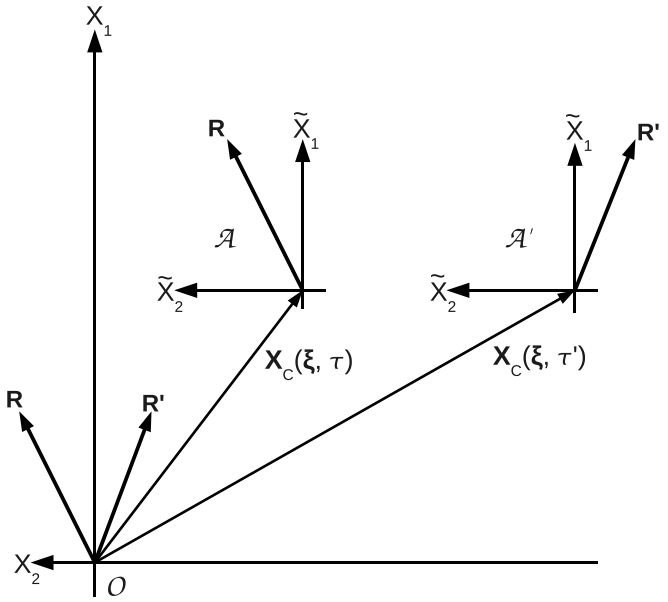

Figure B.1: Galilean invariance of the two–point velocity correlator given in Eqn. (B.5). O labels the observer in the laboratory frame who correlates the velocity fluctuation at location $\boldsymbol{R}$ at time τ with the velocity fluctuation at location $\boldsymbol{R}'$ at a later time τ'. $\mathcal{A}$ and $\mathcal{A}'$ label a comoving observer the origin of whose cooordinate axes is at $\boldsymbol{\xi}$ at the initial time, and who makes an equivalent measurement at the times τ and τ'.

Proof The velocity correlator in Fourier–space is

$$\begin{aligned}\left\langle \tilde{v}_i(\boldsymbol{K},\tau)\,\tilde{v}_j^*(\boldsymbol{K}',\tau')\right\rangle &= \int \mathrm{d}^3X\,\mathrm{d}^3X'\,\exp\left[\mathrm{i}\,(\boldsymbol{K}'\boldsymbol{\cdot}\,\boldsymbol{X}'-\boldsymbol{K}\boldsymbol{\cdot}\,\boldsymbol{X})\right]\left\langle v_i(\boldsymbol{X},\tau)\,v_j(\boldsymbol{X}',\tau')\right\rangle \\ &= \int \mathrm{d}^3X\,\mathrm{d}^3X'\,\exp\left[\mathrm{i}\,(\boldsymbol{K}'\boldsymbol{\cdot}\,\boldsymbol{X}'-\boldsymbol{K}\boldsymbol{\cdot}\,\boldsymbol{X})\right]\times \\ &\qquad \times\left\langle v_i(\boldsymbol{X}+\boldsymbol{X}_c(\boldsymbol{\xi},\tau),\tau)\,v_j(\boldsymbol{X}'+\boldsymbol{X}_c(\boldsymbol{\xi},\tau'),\tau')\right\rangle \qquad \text{(B.9)}\end{aligned}$$

where Eqn. (B.5) has been used. Using new dummy variables of integration, $\boldsymbol{X} \rightarrow$

$\boldsymbol{X} - \boldsymbol{X}_c(\boldsymbol{\xi},\tau)$ and $\boldsymbol{X}' \to \boldsymbol{X}' - \boldsymbol{X}_c(\boldsymbol{\xi},\tau')$, we write

$$\begin{aligned}\left\langle \tilde{v}_i(\boldsymbol{K},\tau)\,\tilde{v}_j^*(\boldsymbol{K}',\tau')\right\rangle &= \exp\left[\mathrm{i}\ (\boldsymbol{K}\cdot\boldsymbol{X}_c(\boldsymbol{\xi},\tau) - \boldsymbol{K}'\cdot\boldsymbol{X}_c(\boldsymbol{\xi},\tau'))\right]\ \times \\ &\quad \times \int \mathrm{d}^3X\,\mathrm{d}^3X'\,\exp\left[\mathrm{i}\ (\boldsymbol{K}'\cdot\boldsymbol{X}' - \boldsymbol{K}\cdot\boldsymbol{X})\right]\left\langle v_i(\boldsymbol{X},\tau)\,v_j(\boldsymbol{X}',\tau')\right\rangle \\ &= \exp\left[\mathrm{i}\ (\boldsymbol{K}\cdot\boldsymbol{X}_c(\boldsymbol{\xi},\tau) - \boldsymbol{K}'\cdot\boldsymbol{X}_c(\boldsymbol{\xi},\tau'))\right]\ \times\ \left\langle \tilde{v}_i(\boldsymbol{K},\tau)\,\tilde{v}_j^*(\boldsymbol{K}',\tau')\right\rangle \end{aligned} \tag{B.10}$$

Comparing the left and right sides, we conclude that the phase,$[\boldsymbol{K}\cdot\boldsymbol{X}_c(\boldsymbol{\xi},\tau) - \boldsymbol{K}'\cdot\boldsymbol{X}_c(\boldsymbol{\xi},\tau')]$, must vanish. Substituting for $\boldsymbol{X}_c$ from Eqn. (B.1), the condition of zero phase implies that

$$(k_1 - k_1')\xi_1 \ +\ (k_2 - k_2')\xi_2 \ +\ (k_3 - k_3')\xi_3 \ =\ 0 \tag{B.11}$$

where $\boldsymbol{k} \equiv (k_1,k_2,k_3)$ and $\boldsymbol{k}' \equiv (k_1',k_2',k_3')$ are sheared wavevectors which are related to $\boldsymbol{K}$ and $\boldsymbol{K}'$ through the Fourier–space shearing transformation

$$\begin{aligned} k_1 &= K_1 + S\tau K_2\,, \qquad k_2 \ =\ K_2\,, \qquad k_3 \ =\ K_3\,, \qquad t \ =\ \tau \\ k_1' &= K_1' + S\tau' K_2'\,, \qquad k_2' \ =\ K_2'\,, \qquad k_3' \ =\ K_3'\,, \qquad t' \ =\ \tau' \end{aligned} \tag{B.12}$$

Since Eqn. (B.11) must be valid for arbitrary (ξ_1,ξ_2,ξ_3), we must have $\boldsymbol{k} = \boldsymbol{k}'$. In other words, the G–invariant Fourier–space velocity correlator must be of the general form stated in Eqn. (B.7). Moreover the listed properties of the velocity spectrum tensor, Π_{ij}, given in Eqns. (B.8) follow from the reality of $\boldsymbol{v}(\boldsymbol{X},\tau)$, symmetry with respect to simultaneous interchange of (i,j) and (t,t'), and incompressibility.

Bibliography

[1] Acheson, D. J. 1990 *Elementary Fluid Dynamics*. Oxford University Press, Oxford.

[2] Balbus, S. A. & Hawley, J. F. 1998 *Reviews of Modern Physics*, **70**, 1.

[3] Binney, J. & Tremaine, S. 2008 *Galactic Dynamics: Second Edition*. Princeton University Press.

[4] Blackman, E. G. 1998 *Astrophys. J.* **496**, L17–L20.

[5] Blackman, E. G. & Field, G. B. 2003 *Physics of Fluids* **15**, L73.

[6] Brandenburg, A. 2005 *Astrophysical Journal* **625**, 539.

[7] Brandenburg, A., Rädler, K.-H., Rheinhardt, M., & Käpylä, P. J. 2008 *Astrophys. J.* **676**, 740–751

[8] Brandenburg, A., Sokoloff, D. & Subramanian, K. 2012 arXiv:1203.6195.

[9] Brandenburg, A. & Subramanian, K. 2005 *Phys. Rep.* **417**, 1–209.

[10] Brandenburg, A. & Subramanian, K. 2005 *Astronomische Nachrichten* **326**, 400.

[11] Choudhuri, A. R. 1998 *The Physics of Fluids and Plasmas*. Cambridge University Press, Cambridge.

[12] Craik, A. D. D. & Criminale, W. O. 1986 *Proc. R. Soc. Lond. A* **406**, 13.

[13] Deshpande, A. A. & Kumar, N. 2012 arXiv:1206.3440

[14] Drazin, P. G. & Riley, N. 2006 *The Navier–Stokes equations: a classification of flows and exact solutions*. London Mathematical Society Lecture Note Series. 334, Cambridge University Press.

[15] Eckhardt, B. & Yao, D. 1995 *Chaos, Solitons and Fractals*, **5**, 2073.

[16] Elperin, T., Kleeorin N., Rogachevskii, I. & Sokoloff, D. 2000 *Physical Review E* **61**, 2617.

[17] Falkovich, G., Gawedzki, K. & Vergassola, M. 2001 *Reviews of Modern Physics*, **73**, 913.

[18] Fedotov, S., Bashkirtseva, I. & Ryashko, L. 2006 *Physical Review E* **73**, 066307.

[19] Hale, G. E. 1908 *Astrophys. J.* **28**, 315–343.

[20] Heinemann, T., McWilliams, J. C. & Schekochihin, A. A. 2011 *Physical Review Letters* **107**, 255004.

[21] Hoyng, P. 1987a *Astronomy & Astrophysics* **171**, 348.

[22] Hoyng, P. 1987b *Astronomy & Astrophysics* **171**, 357.

[23] Hoyng, P. 1988 *Astrophysical Journal* **332**, 857.

[24] Hughes, D. W. & Proctor, M. R. E. 2009 *Physical Review Letters* **102**, 044501(1)–044501(4).

[25] Käpylä, P. J., Korpi, M. J. & Brandenburg, A. 2008 *Astron. Astrophys.* **491**, 353–362.

[26] Thomson, W. (Lord Kelvin) 1887 *Philosophical Magazine*, **24** (5), 188.

[27] Kleeorin, N. & Rogachevskii, I. 2008 *Physical Review E* **77**, 036307.

[28] Korycansky, D. G. 1992 *Astrophysical Journal*, **399**, 176.

[29] Kraichnan, R. H. 1976 *Journal of Fluid Mechanics*, **75**, 657.

[30] Krause, F. & Rädler, K.-H. 1971 *Elektrodynamik der mittleren Felder in turbulenten leitenden Medien und Dynamotheorie, in Ergebnisse der Plasmaphysik und der Gaselektronik - Band 2*, Akademie-Verlag Berlin 1971, pp. 2–154

[31] Krause, F. & Rädler, K.-H. 1980 *Mean-field magnetohydrodynamics and dynamo theory*. Pergamon, Oxford.

[32] Kulsrud, R. M. 2005 *Plasma Physics for Astrophysics*. Princeton University Press, Princeton.

[33] Landau, L. D. & Lifshitz, E. M. 1975 *The Classical Theory of Fields*. 4th edn. Pergamon.

[34] Landau, L. D. & Lifshitz, E. M. 1987 *Fluid Mechanics*. 2nd edn. Pergamon.

[35] Larmor, J. 1919 *Rep. Brit. Assoc. Adv. Sci.* 159–160.

[36] Leprovost, N. & Kim, E.-j. 2009 *Astrophysical Journal*, **696**, L125.

[37] Lifschitz, A. & Hameiri, E. 1991 *Physics of Fluids A*, **3**, 2644.

[38] Lithwick, Y. 2007 *Astrophysical Journal* **670**, 789.

[39] Madarassy, E. J. M. & Brandenburg, A. 2010 *Physical Review E*, **82**, 016304.

[40] Marcus, P. S. & Press, W. H. 1977 *Journal of Fluid Mechanics*, **79**, 525.

[41] McWilliams, J. C. 2011 arXiv:1109.0289 (2011).

[42] Mitra, D. & Brandenburg, A. 2012 *Mon. Not. R. Astr. Soc.* **420**, 2170.

[43] Moffatt, H. K. 1978 *Magnetic Field Generation in Electrically Conducting Fluids*. Cambridge University Press, Cambridge.

[44] Monin, A. S. & Yaglom, A. M. 1971 *Statistical Fluid Mechanics, Vol. I.* The M. I. T. Press.

[45] Monin, A. S. & Yaglom, A. M. 1975 *Statistical Fluid Mechanics, Vol. II.* The M. I. T. Press.

[46] Parker, E. N. 1979 *Cosmical magnetic fields: Their origin and their activity* Clarendon Press; New York, Oxford University Press, Oxford.

[47] Pedlosky, J. 1987 *Geophysical Fluid Dynamics.* 2nd edn. Springer.

[48] Proctor, M. R. E. 2007 *Mon. Not. R. Astr. Soc.* **382**, L39–L42

[49] Rädler, K.-H. & Stepanov, R. 2006 *Phys. Rev E* **73**, 056311(1)–056311(15).

[50] Richardson, K. J. & Proctor, M. R. E. 2012 *Mon. Not. R. Astr. Soc.* **422**, L53R.

[51] Rincon, F., Ogilvie, G. I., Proctor, M. R. E., & Cossu, C. 2008 *Astron. Nach.* **329**, 750–762

[52] Rogachevskii, I. & Kleeorin, N. 2003 *Phys. Rev. E* **68**, 036301(1)–036301(12).

[53] Rogachevskii, I. & Kleeorin, N. 2004 *Phys. Rev. E* **70**, 046310(1)–046310(15).

[54] Rogachevskii, I. & Kleeorin, N. 2008 *Astron. Nachr.* **329**, 732–736.

[55] Rüdiger, G. & Kitchatinov L. L. 2006 *Astron. Nachr.* **327**, 298–303.

[56] Shapovalov, D. S. & Vishniac, E. T. 2011 *Astrophysical Journal* **738**, 66.

[57] Shraiman, B. I. & Siggia, E. D. 2000 *Nature* **405**, 639.

[58] Silant'ev, N. A. 2000 *Astronomy & Astrophysics* **364**, 339.

[59] Singh, N. K., & Sridhar, S. 2011 *Physical Review E* **83**, 056309.

[60] Sokolov, D. D. 1997 *Astronomy Reports* **41**, 68–72.

[61] Sridhar, S. & Singh, N. K. 2010 *Journal of Fluid Mechanics*, **664**, 265.

[62] Sridhar, S. & Subramanian, K. 2009a *Physical Review E* **79**, 045305(R1)–045305(R4).

[63] Sridhar, S. & Subramanian, K. 2009b *Phys. Rev E* **80**, 066315(1)–066315(13).

[64] Shukurov, A. & Sokoloff, D. 2008 *Les Houches, Session LXXXVIII, 2007, Dynamos. Editors: Ph. Cardin & L. F. Cugliandolo* Elsevier, pg. 251–299.

[65] Sur, S. & Subramanian, K. 2009 *Mon. Not. R. Astr. Soc.* **392**, L6.

[66] Tung, K. K. 1983 *Journal of Fluid Mechanics*, **133**, 443.

[67] Urpin, V. 1999 *Mon. Not. R. Astr. Soc.* **308**, 741.

[68] Urpin, V. 2002 *Physical Review E* **65**, 026301.

[69] Vishniac, E. T. & Brandenburg, A. 1997 *Astrophysical Journal* **475**, 263–274.

[70] Vishniac, E. T. & Cho, J. 2001 *Astrophysical Journal* **550**, 752.

[71] Wang, C. Y. 1991 *Annual Reviews of Fluid Mechanics*, **23**, 159.

[72] Warhaft, Z. 2000 *Annual Reviews of Fluid Mechanics*, **32**, 203.

[73] Widrow, L. M. 2002 *Reviews of Modern Physics*, **74**, 775.

[74] Wisdom, J. & Tremaine, S. 1988 *Astronomical Journal*, **95**, 925.

[75] Yousef, T. A., Heinemann, T., Schekochihin, A. A., Kleeorin, N., Rogachevskii, I., Iskakov, A. B., Cowley, S. C. & McWilliams, J. C. 2008a *Phys. Rev. Lett.* **100**, 184501(1)–184501(4).

[76] Yousef, T. A., Heinemann, T., Rincon, F., Schekochihin, A. A., Kleeorin, N., Rogachevskii, I., Cowley, S. C. & McWilliams, J. C. 2008b *Astron. Nachr.* **329**, 737–749.

List of Publications

1. The shear dynamo problem for small magnetic Reynolds numbers

   S. Sridhar and Nishant K. Singh (*Journal of Fluid Mechanics,* **664***, 265, 2010*)

2. Transport coefficients for the shear dynamo problem at small Reynolds numbers

   Nishant K. Singh and S. Sridhar (*Physical Review E* **83***, 056309, 2011*)

3. Shearing waves of arbitrary planform: exact solutions of the Navier-Stokes equations

   Nishant K. Singh and S. Sridhar (arXiv:1101.5507v1)

4. Passive scalar mixing due to turbulence in linear shear flows

   manuscript in preparation

5. Numerical studies of dynamo action in a turbulent shear flow

   manuscript in preparation

6. Dynamo action due to $\alpha-$fluctuations in a linear shear flow

   manuscript in preparation

Work not presented in the Thesis:

Binary systems: implications for outflows & periodicities relevant to masers

Nishant K. Singh and Avinash A. Deshpande (arXiv:1203.3427v1)

Proceedings IAU Symposium No. 287, 2012, Cosmic masers